UNIVERSIDAD DE GRANADA

Environmental changes across the Cretaceous/Palaeogene boundary: a high resolution approach for reconstructing eco-sedimentary conditions

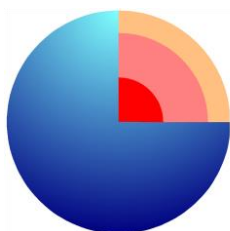**CLAUDIA SOSA MONTES DE OCA**

PhD Thesis

Departamento de Estratigrafía y Paleontología

Universidad de Granada

2018

Programa Doctorado
Ciencias de la Tierra

Dr. Francisco Javier Rodríguez Tovar, Catedrático del Departamento de Estratigrafía y Paleontología de la Universidad de Granada y **Dra. Francisca Martínez Ruiz,** Investigadora Científica del CSIC, ambos co-directores de la presente Tesis Doctoral.

HACEN CONSTAR:

Que la presente tesis titulada ***Environmental changes across the Cretaceous/Palaeogene boundary: a high resolution approach for reconstructing eco-sedimentary conditions*** ha sido realizada bajo su dirección y cumple las condiciones necesarias para que su autora, **Claudia Sosa Montes de Oca**, opte al grado de Doctora en Ciencias Geológicas por la Universidad de Granada.

Granada, Mayo de 2018

VºBº del Director   **VºBº de la Directora**

Dr. Francisco Javier Rodríguez Tovar   **Dra. Francisca Martínez Ruiz**

Doctoranda

Claudia Sosa Montes de Oca

The doctoral candidate **Claudia Sosa Montes de Oca** and thesis supervisors **Prof. Francisco Javier Rodríguez Tovar** and **Prof. Francisca Martínez Ruiz**

Guarantee, by signing this doctoral thesis, that the work has been done by the doctoral candidate under the direction of the thesis supervisors and, as far as our knowledge reaches, in the performance of the work, the rights of other authors to be cited (when their results or publications have been used) have been respected.

Granada, May 2018

Francisco Javier Rodríguez Tovar   Francisca Martínez Ruiz

Thesis supervisor   **Thesis supervisor**

Signed   **Signed**

Claudia Sosa Montes de Oca

Doctoral candidate

Signed

A mis padres, Julio y Elisa

A mi marido David

A mis hijos Ariadna y Daniel

"No te rindas, por favor no cedas, aunque el frío queme, aunque el miedo muerda, aunque el sol se esconda, y se calle el viento, aún hay fuego en tu alma, aún hay vida en tus sueños. Porque la vida es tuya y tuyo también el deseo, porque cada día es un comienzo nuevo, porque esta es la hora y el mejor momento, porque no estás solo…"

— Mario Benedetti (1920-2009)

"La vida no se cuenta por minutos, sino por sueños"

— Joaquin Sabina (1949-)

"Occasionally there is a question that offers an opportunity for a really major discovery"

— Walter Alvarez (1955-)

"Most of the fundamental ideas of science are essentially simple, and may, as a rule, be expresed in a lenguaje comprehensible to everyone"

— Albert Einstein (1879-1955)

Acknowledgements/Agradecimientos

Numerous people and institutions have supported me during these years. Many of them do not understand both English and Spanish, so both languages, and also a little bit of Italian, are used in the present section to express my gratitude and acknowledgements.

Also, I would like to thank all those reviewers who provided useful comments and suggestions for the research papers developed during this period. Moreover, the editors who have contributed to publishing these results with their constructive comments and suggestions in the editorial process are gratefully acknowledged (*Dr. Lorenzo Rook; Dr. Eduardo Koutsoukos; Dr. Tomas Algeo*).

This volume benefited from comments of external referees Dr. Daniel Ariztegui (Geneve University) and Dr. Paolo Monaco (Perugia University).

Finally, I would like to express my thanks to…/**Finalmente**, me gustaria agradecer a…

A todos mis compañeros del Departamento de Estratigrafía y Paleontología de la Universidad de Granada (Mª Jose, Jon, Paola, Saturnina). En especial a Socorro Aranda por su gran ayuda con todo el trabajo administrativo y a Javier Dorador por tener tiempo siempre para compartir un café y escucharme.

A todos mis compañeros del Instituto Andaluz de Ciencias de la Tierra (IACT) (Adrián, Alberto, Álvaro, Ariadna, Manuel, Marga, Mary, Nicole, Rubén…) por compartir comida, risas y muchas conversaciones durante todos estos años. A mis compis de desayuno (Alejandro, Amparo, Carolina, Ignacio, Manolo y Marta), juntos habéis hecho, que ese pequeño ratito del desayuno sea una alegría diaria.... A Elisa, la mejor técnica de laboratorio, por tu inestimable ayuda, por facilitarme el trabajo y sobre todo, por las numerosas charlas que hemos compartido. A mis "hermanos científicos" y compañeros de becaria 029 (Bob, Carmina, Luis, Meri y Rita), juntos hemos pasado innumerables momentos…de decepciones y alegrías, pero sobre todo, en estos años, hemos crecido juntos y eso nos quedará para siempre. En especial a Nieves y a Laura por compartir nuestra "becaria psicológica" sin la cual no habría sobrevivido todo este tiempo… ¡¡¡Sois maravillosas!!!

To Amalia Fillipidi to holding me and made my stays in Utrecht University easier and to the rest of students and staffs from department of Earth Sciences and Geochemistry (UU), especially to Alejandra, Anne, Itzel, Jose, Mary, Mattias, Niels, Peter, among others...

A mis amigas Sonia e Isa porque son mis compañeras de vida. Aunque el trabajo y este loco ritmo de vida no nos deja mucho tiempo libre, siempre nos reencontramos y creamos momentos especiales. Por supuesto también, a sus estupendos maridos Roberto y Santi por estar siempre dispuestos a compartir juntos un "Fragolino Rosso" o mejor aún algún que otro "macetero"…

A mi amiga Lucia, porque un día entraste en mi vida y te quedaste…Por estar siempre cerca y entenderme. Pero además, por compartir esta etapa del doctorado, aunque sea en diferentes universidades.

A mi hermana Adriana y mi cuñado Gabriel porque aunque nos separen muchos kilómetros siempre os siento cerca. A mis sobrinos Joaquín, Sofía y Rodrigo por estar siempre pendientes de su "tita guapa" que los adora y a partir de ahora promete dedicaros más tiempo.

A mi Padre, Julio Néstor Sosa Benia, por estar siempre pendiente de mi trabajo y alentarme. Por venir en pleno junio a coger muestras conmigo al campo, a 40 grados a la sombra…y sin quejarte…también por ayudarme en Utrecht con los niños y por acompañarme en el coche durante los más de 2000 kilómetros de vuelta a casa…

A mi Madre; Elisa Mabel Montes de Oca, por estar pendiente de todo y simplemente por ser tú… eres todo lo que una hija puede desear, tu entrega constante es mi ejemplo en la vida. Sin tu ayuda diaria, sobre todo durante mis estancias, me hubiera sido imposible finalizar con éxito este trabajo, así que esta tesis es también un poco tuya…

Finalmente, a mi pequeña familia, que sois todo lo que necesito en la vida, mi marido David y mis dos "angelitos" Ariadna y Daniel. Os pido disculpas por tener que aguantar mis ausencias y mis nervios. Pero sobre todo, os doy las gracias por no hacerme sentir nunca sola, por acompañarme en mis estancias y así conocer mundo juntos… Al final…¡¡¡lo hemos conseguido!!!

CONTENTS

ABSTRACT

The mass extinction marking the Cretaceous/Palaeogene boundary (KPgB), ≈66.04 ± 0.02 million years ago, was one of the most devastating events in the history of life, being the most recent and the best studied of the 'big five' mass extinctions that occurred during the Phanerozoic eon. At present, the relationship between the Cretaceous/Palaeogene mass extinction and a meteorite impact is broadly accepted. The impact crater, discovered at the begining of the nineties on the Yucatan peninsula in Mexico (called Chicxulub structure), as well as the size of the meteorite (with a diameter of ≈10 km), are essential data to interpret the environmental consequences of this event. An ejecta layer was deposited worldwide, which at distal sites is characterized by the presence of spherules, anomalous concentrations of Iridium and other platinum group elements, the existence of spinels rich in Ni, and changes in the isotopic composition of certain elements, in particular C and O. After decades of research, one persistent challenge is to understand the effects of this impact on the global environmental system, including the re-establishement of pre-impact environmental conditions and marine biological productivity after such a major environmental crisis. This PhD Thesis focuses on characterizing palaeoenvironmental conditions (oxygenation and productivity), including the response of the macrobenthic tracemaker community, prior to, during and after the KPgB impact. With this aim, several KPgB distal sections located over 5000 km from Chicxulub impact site were studied: the Agost and the Caravaca sections, from the Betic Cordillera (Southeast Spain), and the classical Gubbio sections (Bottaccione Gorge and Contessa Highway) located within the Umbria-Marche Basin, in the Apennines (Northeast Italy). A high-resolution sampling was carried out across the KPgB in the studied sections, along with a detailed sampling of trace fossils, differentiating between biogenic structures and host sediment. Geochemical and isotopic analyses were also performed both on the infilled material of the trace fossils and on the host sediment. The obtained results support that anoxic conditions are restricted to the deposit of the ejecta layer, and that oxygen levels similar to those of pre-impact times were re-established shortly after the impact. The rapid re-establishment of the pre-impact conditions (i.e., oxygenation and nutrient availability) is further supported by the tracemaker community recovery, which was favoured by the opportunistic behaviour of some macrobenthic organisms.

RESUMEN

La extinción masiva que marcó el límite entre los periodos Cretácico y Paleógeno (KPgB), ocurrida hace ≈66.04 ± 0.02 millones años, es uno de los eventos más devastadores acaecidos a lo largo de la historia de la vida, siendo la más reciente y mejor estudiada de las "cinco grandes" extinciones en masa que se han producido a lo largo del Fanerozoico. En la actualidad, la relación entre la extinción en masa del Cretácico/Paleógeno y el impacto meteorítico está ampliamente aceptada. Tanto el cráter del impacto, localizado a principios de los años noventa en la península de Yucatán, México (denominado estructura Chicxulub), como el tamaño del meteorito (con un diámetro de ≈10 km), son datos fundamentales para poder interpretar las consecuencias ambientales de este impacto. A nivel mundial, el depósito de una lámina de sedimento (ejecta layer) marca el KPgB, caraterizada, en las secciones distales, por la presencia esférulas, concentraciones anómalas de Iridio y otros elementos del grupo del platino, así como por la existencia de espinelas ricas en Ni y por importantes cambios en la composición isotópica de algunos elementos como C y O. Después de décadas de investigación, uno de los principales retos es conocer los efectos que tuvo este impacto a nivel global, cómo se produjo el restablecimiento de las condiciones paleoambientales previas al impacto, y como fue la recuperación biológica después de la crisis ambiental generada. Así, esta Tesis Doctoral se centra en caracterizar las condiciones paleoambientales (oxigenación y productividad), antes, durante y después del impacto, utilizando un enfoque multidisciplinar, que incluye el estudio de la respuesta de la comunidad macrobentónica generadora de trazas a la crisis ambiental. Con este objetivo, se han estudiado varias secciones distales del KPgB, ubicadas a más de 5000 km del cráter de Chicxulub, en las que el límite aparece marcado por una lámica de unos pocos milímetros (≈2 mm) de espesor que contiene las evidencias del impacto; las secciones de Agost y Caravaca, en la Cordillera Bética (sureste de España), y las clásicas secciones de Gubbio (Bottaccione Gorge y Contessa Highway), en la cuenca de Umbría-Marche, dentro los Apeninos (noreste de Italia). Se ha llevado a cabo un muestreo a muy alta resolución, atendiendo también a las estructuras biogénicas y al material encajante. En este último caso, se han realizado, además, análisis geoquímicos e isotópicos tanto del material relleno de las trazas fósiles como en la roca encajante. Los resultados obtenidos demuestran que las condiciones anóxicas están restringidas únicamente al depósito de la lámina que marca límite y que rápidamente se restablecieron niveles de oxígeno similares a los existentes antes del impacto. Además, asociada al restablecimiento de las condiciones pre-impacto (oxigenación y disponibilidad de nutrientes), tuvo lugar la rápida recuperación de la comunidad generadora de trazas, favorecido por el comportamiento oportunista de algunos organismos macrobentónicos.

Chapter 1

INTRODUCTION AND SCOPE

"The beginning is the most important part of the work"

— Plato (387-347 B.C)

1.1. Introduction

The **Cretaceous/Palaeogene boundary (KPgB**) mass extinction, dated at ≈66.04 ± 0.02 Ma (Renne et al., 2013), was one of the most devastating events in the history of the planet Earth. It is generally considered as the most recent of the "Big five" mass extinctions occurring during the Phanerozoic (Sepkoski, 1996). This led to 40% of extinction at the genus level (Bambach, 2006) and the disappearance of about 70% of the marine and continental species existing at that time (D'Hondt, 2005) (Fig. 1.1). Entire categories of organisms completely disappeared at that time. In the marine realm, mosasaurs, sauropterygians (plesiosaurs and pliosaurs), ammonites and heterohelicid planktic foraminifera became extinct; in the terrestrial realm, all forms of nonavian dinosaurs disappeared. This mass extinction marks the end of the Mesozoic Era, which has been the focus of intensive research during the last few decades (Goderis et al., 2013; Schulte et al., 2010a and references therein).
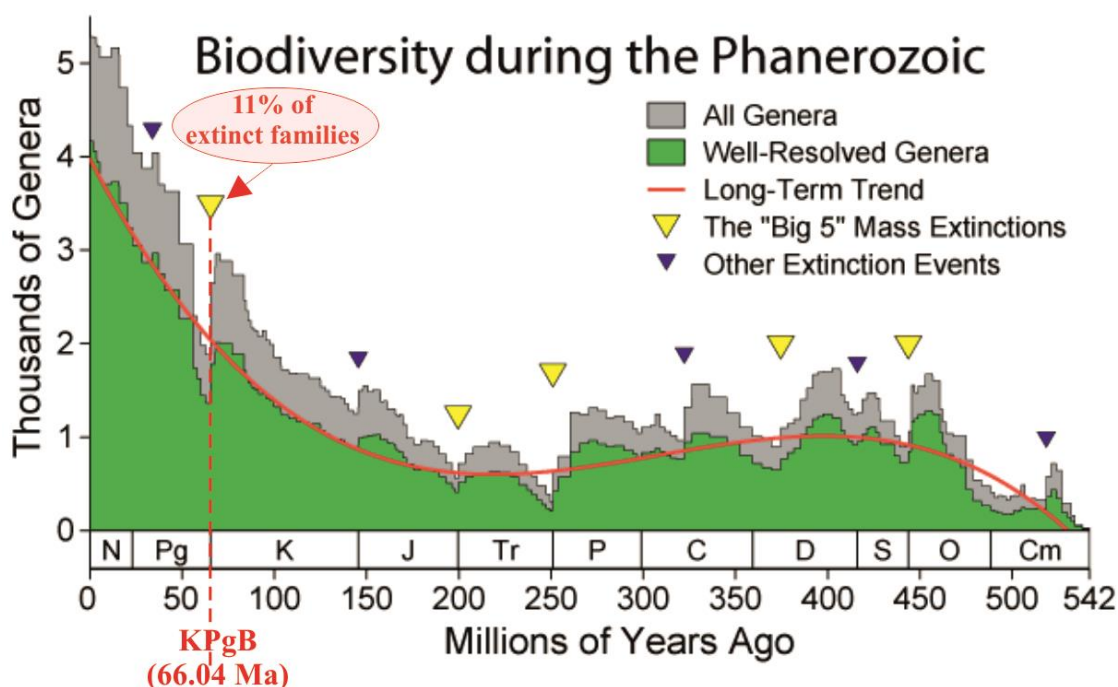
Fig. 1.1. The genus extinction intensity. Numbers of genera as a function of geologic time, showing the five major extinction events marked by sharp biodiversity decreases. Adapted from Rohde and Muller (2005), in turn based on Raup and Sepkoski (1982).

During the late **seventies**, Walter Alvarez studied the Upper Cretaceous-Palaeogene section at Bottaccione Gorge, near Gubbio, which had been biostratigraphically described by Luterbacher and Premoli-Silva (1962). At that time Alvarez and collaborators attempted to estimate the timing of deposition of the KPgB succession, assuming a constant sedimentation rate of cosmic material onto the surface of the Earth (Lowrie and Alvarez, 1977). Surprisingly, they recognized a large Iridium anomaly (Ir enrichment over 4 orders of magnitude) in the sediments marking the end of the Cretaceous and the beginning of the Palaeogene. Following this finding, other sections were analyzed and the team leading this discovery proposed the well-known extraterrestrial hypothesis to explain the faunal extinction at the end of the Cretaceous. The authors proposed that the impact of a large

meteorite would have been responsible for the environmental perturbations that caused the mass extinction that occurred at this time (Alvarez et al., 1980). Other evidences were provided simultaneously to support the extraterrestrial hypothesis. By the late seventies Jan Smit was also studying the KPgB interval at the Barranco del Gredero, near Caravaca (Southeast Spain), and analyses of the thin layer that marks the boundary showed anomalous concentrations of Ni, Cr, Co, As and Sb, as well as Iridium (Smit and Hertogen, 1980). Smit moreover reported the existence of spherules (Fig. 1.2) in the sediments of the KPgB at this section (Smit and Klaver, 1981). The spherules were interpreted as droplets of melt that had travelled ballistically from the impact site and rapidly quenched (Smit, 1999). These spherules, restricted to the thin ejecta layer, were designated microkrystites; and though they are morphologically similar to microtektites, they present crystalline textures (Glass and Burns, 1987),

Also about this time, an alternative extraterrestrial hypothesis was proposed by Ken Hsü, who considered the impact of a comet as an explanation for the mass extinction (Hsü, 1980).
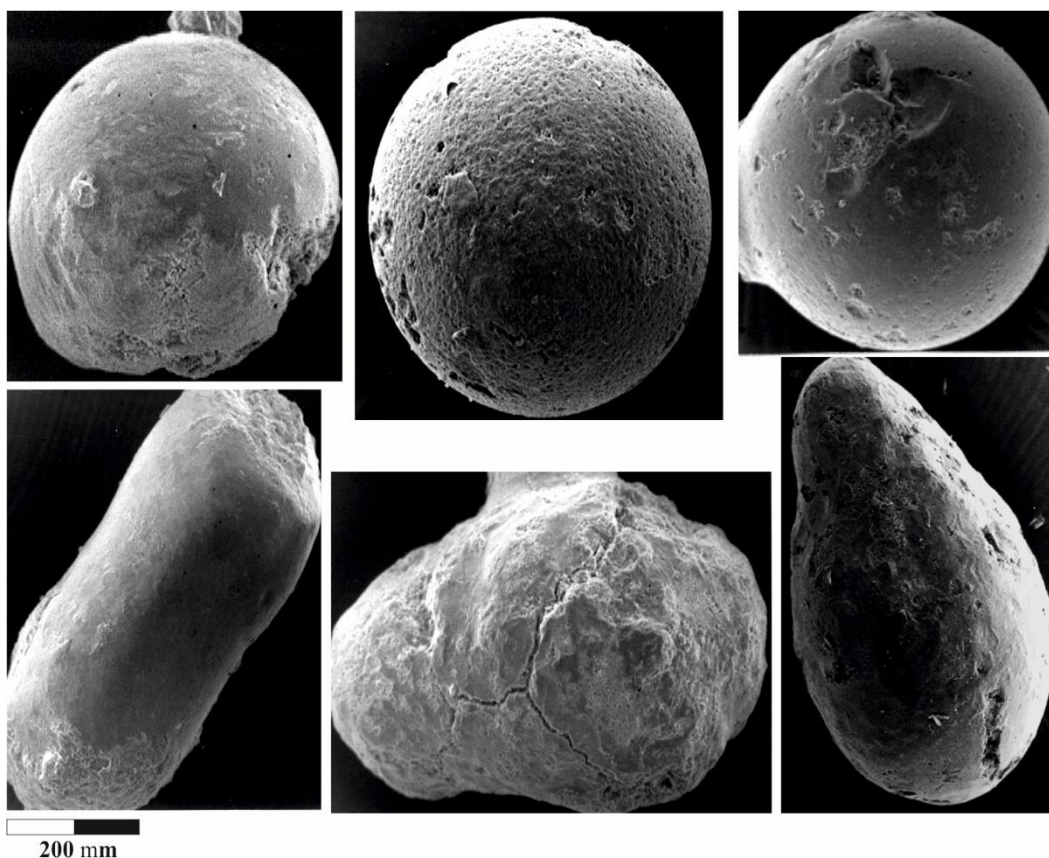
Fig. 1.2. Spherules at KPgB. SEM Photos taken from Martínez-Ruiz (1994).

Then, in the **eighties**, the meteoric impact hypothesis to explain the Ir anomaly and mass extinctions was subjected to intense debate. Alternative hypotheses were formulated, such as generalized volcanism. In particular, the *"Deccan trap"* was cited as responsible for the environmental crisis at the end of the Cretaceous (Courtillot et al., 1986, 1988; Officer and Drake, 1985).

Throughout the eighties diverse sections of the boundary clay of the KPgB were analyzed, and and new evidence supporting an extraterrestrial source was put forth: the existence of shock metamorphism (Bohor et al., 1984, 1987), the presence of metamorphosed zircons with planar features (Bohor, 1990), the record of impact glasses at the KPgB section of Haiti (Blum et al., 1993; Koeberl and Sigurdsson, 1992; Sigurdsson et al., 1991), the presence of nano and micro diamonds (Hough et al., 1997), the existence of spinels rich in Ni in the KPgB (Bohor, 1990; Kyte and Smit, 1986), and changes in the isotopic composition of elements such as C, O and Sr (Hsü and McKenzie, 1985).

In the **nineties,** the debate surrounding the meteorite impact resurged when a crater structure was recognized in the Yucatan Peninsula (N 21° 20' W 89° 30') by the Gulf of Mexico (Hildebrand et al., 1991). The so-called "Chicxulub structur", with a diameter of some 180 km, led researchers to estimate a meteorite size of 10 ± 4 km in diameter (Fig. 1.3).
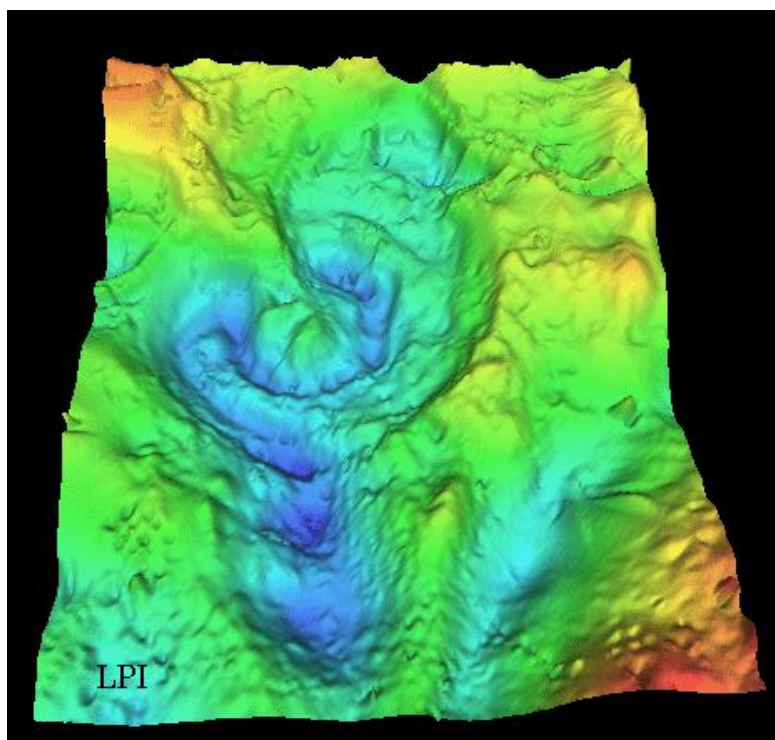
Fig. 1.3. Three-dimensional map of the gravity and magnetic field variations of the Chicxulub structure, from V.L. Sharpton (www.axxon.com).

In the late nineties a possible relict of the meteorite was also reported at DSDP Hole 576 (Kyte, 1998), mixed with the dark-brown oxidized pelagic clays typical of deep-ocean sediments in the North Pacific. Geochemical and petrographic analyses of this meteorite indicated that it most likely derived from a typical metal and sulphide-rich carbonaceous chondrite rather than from the porous aggregate type of interplanetary dust typical of cometary materials. This is further supported by the chromium isotopic signature of several KPgB sites, and consistent with a carbonaceous chondrite-type impactor (Shukolyukov and Lugmair, 1998). Some C-rich cores identified in KPgB spherules and enriched in Ir also support a carbonaceous chondrite composition (Martínez-Ruiz et al., 1997). Although such

meteorites constitute only a small percentage of the observed meteorite falls, they may be an important component of the asteroid belt, which has been considered as the probable source of the KPgB impactor (Bottke et al., 2007).

At present the relationship between the Cretaceous/Palaeogene mass extinction and the impact of a meteorite is broadly accepted (Schulte et al., 2010). The impact site, as well as, the size of the meteorite are essential to interpret the environmental consequences of this event.

Specifically, this impact can be regarded as one of the most rapid events in the history of life on Earth, involving a sequence of regional catastrophes, including earthquakes of magnitude >10 causing continental and marine landslides, tsunamis 100-300 m in height that swept over 300 km onshore and carried continental debris basin-ward to deep-marine sequences, shock waves and air blasts that radiated across the landscape, and high temperatures that generated fires as far as 1,500 to 4,000 km from the crater (e.g., Kring, 2007; Wilf et al., 2003). But the event was also responsible for global catastrophes such as nitric and sulfuric acid rain, widespread dust and blackout, destruction of the stratospheric ozone layer, and an enhancement of the greenhouse effect due to an increase in atmospheric concentrations of greenhouse gases (e.g., Kring, 2007 and references therein). Furthermore, these disturbances gave rise to secondary effects that included an impact winter (Brugger et al., 2017; Vellekoop et al., 2014; Woelders et al., 2017), an increase in oceanic acidification (e.g., Alegret and Thomas, 2005; Alegret et al., 2012; Peryt et al., 2002), and finally, a decrease in the sea surface temperature (Coccioni and Galeotti, 1994; Kaiho et al., 1999; Vellekoop et al., 2015). Consequently, the reestablishment of palaeoenvironmental conditions after the KPgB event is held to be a key point in the context of evolutionary and ecological dynamics of present biota (e.g., Hull, 2015; Labandeira et al., 2016).

Recently, Expedition 364 of the European Consortium for Ocean Research Drilling (ECORD), conducted as part of the International Ocean Discovery Program (IODP) and supported by the International Continental Scientific Drilling Programme (ICDP), drilled during April–May 2016 into the peak-ring of the Chicxulub structure, in order to understand: i) how hypervelocity impacts temporarily change rock behaviour in a way that allows materials to flow large distances and form features such as peak rings; ii) how the impact hypothesis may be beneficial to some life forms; and iii) how ocean life recovered after this event (Chen and Sun, 2017; Kring et al., 2017; Morgan et al., 2016).

The global consequences of the impact event are proven by the numerous deposits of the KPgB worldwide (Goderis et al., 2013; Smit, 1999; Urrutia-Fucugauchi and Pérez-Cruz, 2016) (Fig. 1.4). Such deposits constitute a global stratigraphic marker permitting temporal resolution and lateral correlation, and they show variable features depending on the distance from the Chicxulub crater. Four types of ejecta deposits have been distinguished (Fig. 1.4 and Tables 1.1-1.4):
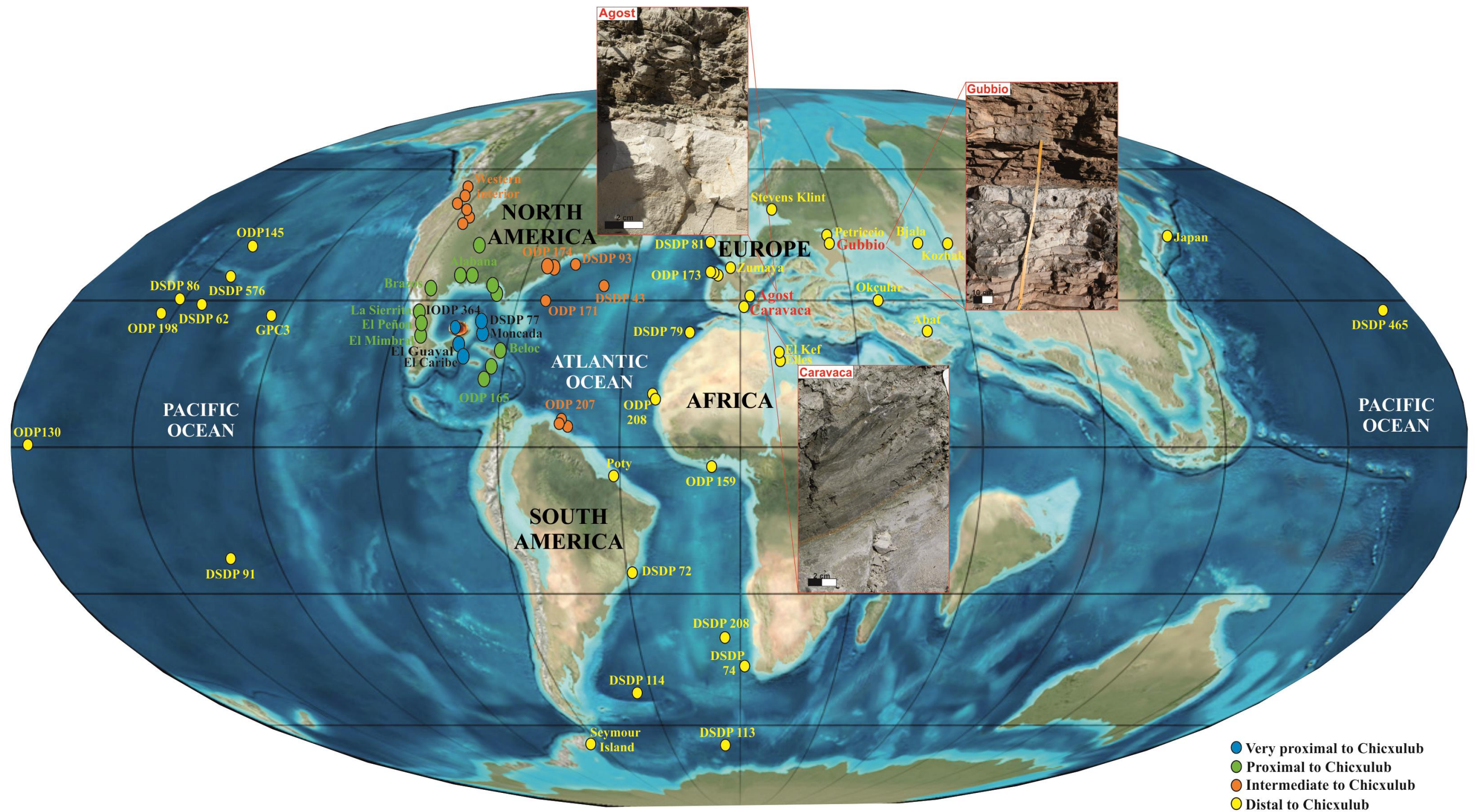
Fig. 1.4. Main global distribution of KPgB sites ubicated in a palaeogeographic map from end-Cretaceous. Deep sea drill sites are referred to by the corresponding Deep Sea Drilling Project (DSDP), Ocean Drilling Program (ODP) and recently to International Ocean Discovery Program (IODP) Leg numbers. Red colour corresponds to the outcrops studied in this Thesis, showing close photographs of each one. Map based on Goderis et al. (2013) and Urrutia-Fucugauchi and Pérez-Cruz (2016).

i. **Very proximal to Chicxulub**: Less than 500 km from Chicxulub impact site. Relatively thick ejecta layer. Cores recovered close to the crater rim inside the Chicxulub impact structure include a more than 100-m-thick impact-breccia sequence, while 1-m- to more than 80-m-thick ejecta rich deposits are present in the surrounding Central American region (e.g., Alegret et al., 2005; Arenillas et al., 2006; Fouke et al., 2002; Goto et al., 2008; Grajales-Nishimura et al., 2003; Izett, 1991; Kiyokawa et al., 2002; Kring et al., 2017; Morgan et al., 2016; Murillo-Muñeton and Dorobek, 2003; Pope et al., 2005, 1999; Tada et al., 2002).

Table 1.1. Main locations of KPgB very proximal sites. *Estimated palaeodistance to the center of the Chicxulub crater structure. **SP, spherules; SQ, shocked quartz; NI, Ni-rich spinel; FS, fern spore spike. ***Bathymetric division defined in Van Morkhoven et al. (1986): neritic (0-200 m), upper bathyal (200-600 m), middle bathyal (600-1000 m), lower bathyal (1000-2000 m), upper abyssal (2000-3000 m), lower abyssal (>3000 m). Modified from Schulte et al. (2010b). Supplementary material.

Region and KPgB sites	Distance* (km)	Impact ejecta**	Max. Iridium concentration (ppb)	Setting***
Very proximal to Chicxulub				
Southern Mexico and Cuba				
Guayal, Tabasco	300	SP, SQ, NI	0.8	Bathyal
Bochil, Chiapas	300	SP, SQ, NI	1.5	Bathyal
Albion Island, Belize	300	SP, SQ	n.a.	Terrestrial
Moncada, Cuba	400	SP, SQ	0.5	Bathyal
Loma Capiro, Santa Isabel, Peñalver, Cacarajícara, and Cidra, Cuba	400	SP, SQ	n.a.	Bathyal

ii. **Proximal to Chicxulub:** Between 500 to 1,000 km from Chicxulub impact site (Northwestern Gulf of Mexico), the KPgB is associated with high-energy clastic deposits, and characterized by a series of cm- to m-thick spherule rich, clastic event beds, indicative of high-energy sediment transport by, for example, tsunamis and gravity flows (e.g., Alegret et al., 2001; Aschoff and Giles, 2005; Bohor and Glass, 1995; Bralower et al., 2010; Campbell et al., 2007; Izett, 1991; Keller et al., 2003; King et al., 2007; Lawton et al., 2005; Leroux et al., 1995; Molina et al., 2009; Schulte et al., 2006; Schulte and Kontny, 2005; Schulte and Speijer, 2009; Sigurdsson and Leckie, 1997; Smit et al., 1996; Soria et al., 2001; Ward et al., 1995; Yancey and Guillemette, 2008).

Table 1.2. Main locations of KPgB proximal sites. Modified from Schulte et al. (2010b). Supplementary material. Legend as in Table 1.1.

Region and KPgB sites	Distance* (km)	Impact ejecta**	Max. Iridium concentration (ppb)	Setting***
Proximal to Chicxulub				
Gulf of Mexico				
Beloc, Haiti	500	SP, SQ, NI	8	Bathyal
La Ceiba, Mexico	700	SP, SQ, NI	n.a.	Lower bathyal
El Mimbral, Mexico	700	SP, SQ, NI	.5	Lower bathyal
La Lajilla, Mexico	750	SP, AC	0.25	Lower bathyal
El Mulato, Mexico	780	SP, AC	1	Lower bathyal
El Peñón, Mexico	800	SP, AC	n.a.	Middle bathyal
La Sierrita, Mexico	800	SP, AC	0.3	Middle bathyal
La Popa Basin, Mexico	800	SP, AC	n.a.	Inner neritic
Brazos River, Texas	900	SP, AC	n.a.	Neritic
Stoddard County, Missouri	900	SP	n.a.	Neritic
Mussel Creek, Shell Creek, Antioch Church Core, Millers Ferry, Alabama	900	SP, AC	n.a.	Neritic
Caribbean Sea				
ODP Leg 165: Site 999 and 1001	600	SP	n.a.	Bathyal

iii. **Intermediate**: Between 2,000 to 3,000 km from Chicxulub impact site. Representative examples are located at continental sections from the US Western Interior and at Northwest Atlantic Ocean as part of the Ocean Drilling Program (i.e., ODP 171, 174, 207) and Deep Sea Drilling Projects (i.e., DSDP 93). The KPgB deposits consist of a 2- to 10-cm-thick spherule layer topped by a 0.2- to 0.5-cm-thick layer that is characterized by a PGE anomaly and abundant shock minerals, granitic clasts, Ni-rich spinel and coals wamp deposits (e.g., Barclay and Johnson, 2002; Bohor et al., 1987; Bohor and Izett, 1986; Izett, 1990; Klaver et al., 1987; Kring, 1995; Kring and Durda, 2002; MacLeod et al., 2007; Martínez-Ruiz et al., 2002, 2001; Morgan et al., 2006; Nichols and Johnson, 2008; Nichols et al., 2002, 1992, 1986; Olsson et al., 1997; Pillmore et al., 1984; Schulte and Speijer, 2009; Sweet et al., 1999; Sweet and Braman, 1992; Tschudy et al., 1984; Wolfe, 1991).

Table 1.3. Main locations of KPgB intermediate sites. Modified from Schulte et al. (2010b). Supplementary material. Legend as in Table 1.1.

Region and KPgB sites	Distance* (km)	Impact ejecta**	Max. Iridium concentration (ppb)	Setting***
Intermediate to Chicxulub				
Western Interior (USA and Canada)				
Sugarite, Raton Basin, New Mexico	2100	SP, SQ (FS)	2.7	Terrestrial
Starkville South, Raton Basin, Colorado	2250	SP, SQ (FS)	56	Terrestrial
Starkville North, Raton Basin, Colorado	2250	SP, SQ (FS)	6	Terrestrial
Long Canyon, Raton Basin, Colorado	2250	SQ (FS)	8.2	Terrestrial
Berwind Canyon, Raton Basin, Colorado	2250	SP, SQ (FS)	27	Terrestrial
West Bijou Site, Denver Basin, Colorado	2250	SQ (FS)	0.68	Terrestrial
Dogie Creek, Powder River Basin, Wyoming	2500	SP, SQ (FS)	20.8	Terrestrial
Sussex, Powder River Basin, Wyoming	2500	SQ (FS)	26	Terrestrial
Sussex, Powder River Basin, Wyoming	2500	SQ (FS)	26	Terrestrial
Mud Buttes, Williston Basin, SW North Dakota	2700	SP, SQ (FS)	1.36	Terrestrial
Brownie Butte, Hell Creek area, Montana	3100	SP, SQ (FS)	1.04	Terrestrial
Knudsen's Farm, Western Canada	3400	SQ (FS)	3.4	Terrestrial
Morgan Creek, Saskatchewan, Western Canada	3400	SQ (FS)	3	Terrestrial
Frenchman River, Saskatchewan	3400	SP	1.35	Terrestrial
Northwest Atlantic Ocean				
DSDP Leg 93 Site 603	2600	SP, SQ	n.a.	Bathyal
ODP Leg 171 Sit1049, 1050, 1052	2400	SP, SQ	1.3	Lower bathyal
ODP Leg 174AX Bass River	2500	SP, SQ, AC	n.a.	Neritic
ODP Leg 207 Site 1258, 1259, 1260	4500	SP, SQ, AC	1.5	Bathyal

iv. **Distal to Chicxulub**: More than 5000 km from Chicxulub impact site, where a few millimeters (≈2 mm thick) of ejecta layer marks the KPgB (Fig. 1.5) (e.g., Abrajevitch and Kodama, 2009; Alegret et al., 2004, 2003, 2002; Alegret and Thomas, 2007, 2005; Bostwick and Kyte, 1996; Brooks et al., 1986, 1985, 1984; Corfield and Cartlidge, 1993; Frei and Frei, 2002; Gallala et al., 2009; Hollis et al., 2003; Hollis and Strong, 2003; Hsü et al., 1982; Ingram, 1992; Kaiho et al., 1999; Kyte et al., 1996, 1980; Martínez-Ruiz et al., 1992; Michel et al., 1990; Molina et al., 2004; Montanari, 1991; Preisinger et al., 2002; Rodríguez-Tovar, 2005; Rodríguez-Tovar et al., 2011; Rodríguez-Tovar and Uchman, 2006, 2004; Schmitz et al., 1991, 1988; Smit, 1999; Smit and Ten Kate, 1982; Sosa-Montes de Oca et al., 2018, 2017, 2013; Stott and Kennett, 1989; Trinquier et al., 2006; Vajda et al., 2003; Vajda and Raine, 2003; Willumsen, 2004, 2012, 2000). A reddish clay layer contains the impact ejecta material (e.g., Smit, 1999). Among distal sections, the El Kef section in Tunisia represents the boundary stratotype and point for the base of the Danian Stage (Molina et al., 2006).

Table 1.4. Main locations of KPgB distal sites. In red are indicated the outcrops studied in this thesis. Modified from Schulte et al. (2010b). Supplementary material. Legend as in Table 1.1.

Region and KPgB sites	Distance* (km)	Impact ejecta**	Max. Iridium concentration	Setting***
Distal to Chicxulub				
South Atlantic Ocean				
DSDP Leg 75 Site 524	9600	n.a.	3	Abyssal
ODP Leg 113 Site 690	11000	n.a.	1.5	Abyssal
ODP Leg 208 Site 1262, 1267	9400	SP, SQ	n.a.	Abyssal
Europe, Africa, Asia				
Gubbio and Petriccio, **Italy**	9200	SP, SQ, NI	8	Bathyal
Stevns Klint and Nye Kløv, Denmark	10200	SP, SQ, NI	48	Neritic
Bidart, France	9500	NI	6	Upper-middle bathyal
Caravaca, Spain	8200	SP, SQ, NI	56	Bathyal
Agost, Spain	8300	SP, SQ, NI	24.4	Upper-middle bathyal
Bjala, Bulgaria	9500	SP, SQ, NI	6.1	Bathyal
El Kef, Ellés, Tunisia	9100	SP, NI	18	Outer neritic – upper bathyal
Aïn Settara, Tunisia	9100	SP, SQ, NI	11	Outer neritic – upper bathyal
Pacific Ocean				
LL44-GPC 3	7200	SP, SQ, NI	12	Abyssal
DSDP Leg 62 Site 465	7900	SP, SQ, NI	54	Lower bathyal
DSDP Leg 86 Site 576, 577	9300	SP, SQ, NI	13.4	Abyssal
DSDP Leg 91 Site 596	9700	SP, SQ, NI	10.8	Abyssal
ODP Leg 119 Site 738	10500	-	18	Abyssal
ODP Leg 130 Site 803, 807	11000	SP, SQ, NI	10.8	Abyssal
ODP Leg 145 Site 886	6450	SP, SQ, NI	3.6	Abyssal
ODP Leg 198 Site 1209 to 1212	11400	-	n.a.	Abyssal
Woodside Creek, New Zealand	10500	SP, SQ, NI (FS)	70	Bathyal
Mid-Waipara, New Zealand	10500	SP, (FS)	0.49	Neritic
Flaxbourne River, New Zealand	10500	SP	21	Upper-Middle bathyal
Moody Creek Mine, New Zealand	10500	SP, (FS)	4.1	Terrestrial

In general, the distance to the impact site determines the thickness, lithology, and the mineralogical and geochemical composition of the different KPgB records. In distal sections (as those studied in this thesis), four possible components are differentiated within the ejecta layer: **Chondritic material**, from the meteorite itself; **material of the target rocks**, also vaporized and distributed globally; **local input**, subsequently different in each section; and **authigenic minerals** formed during of postdepositional alteration of original material.
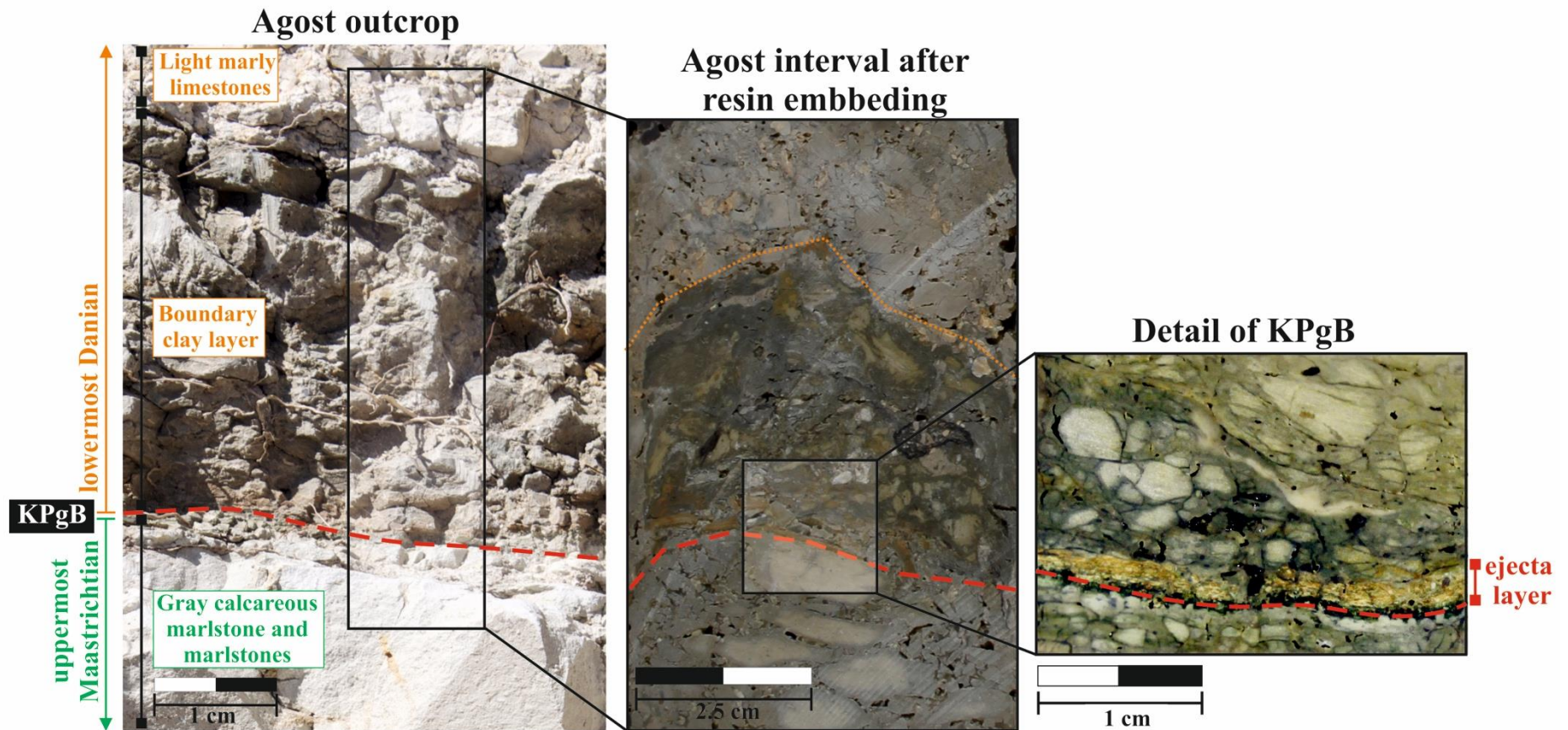
Fig. 1.5. Photos from outcrop and laboratory showing the main lithological components in the distal section of Agost. In ascending order, the Agost Cretaceous-Palaeogene transition comprises Cretaceous sediments that consist of gray calcareous marlstones and marlstones from uppermost Maastrichtian, overlain by Palaeogene sediments that include the 2-3-mm-thick red clay (the ejecta layer), and a blackish-gray clay layer (the boundary clay) that has gradually increasing carbonate content, giving way to the typically light marly limestones from the lowermost Danian.

1.2. Scope of this thesis

Even though a consensus now exists as to the impact of a large meteorite in the Yucatan Peninsula that was responsible for all the environmental perturbations occurring at the end of the Cretaceous, questions remain regarding the patterns of extinction, how this impact affected the different sedimentary basins, and how the recovery of biological productivity took place. The effects of the meteor impact drastically transformed the depositional environments, especially in marine sedimentary basins where severe extinctions occurred and a high input of metals, both of terrestrial and extraterrestrial origin, led to a significant alteration of seawater composition. Enhanced chemical alteration, due to the acid rain conditions generated by the impact, also contributed to higher metal fluxes and extremely reducing conditions. The distribution of trace elements is crucial for a reconstruction of the conditions during the KPgB itsels and during the re-establishment of pre-impact conditions.

In this sense, the present PhD Thesis focuses on characterizing palaeoenvironmental conditions (oxygenation and productivity), prior to, during and after the KPgB impact, by using a multiproxy approach that also includes a study of the response of the macrobenthic tracemaker community to the environmental crisis. Four distal sections of the KPgB were selected to this end: the Agost and Caravaca sections, from the Betic Cordillera (Southeast Spain), and the classic Gubbio sections (Bottaccione Gorge and Contessa Highway) located within the Umbria-Marche Basin, in the Apennines (Northeast Italy).

The specific objectives are:

1. To analyze geochemical processes controlling trace and major element distribution in the boundary sediments. Special attention is devoted to:

    ✓ Ultra high resolution analysis of redox geochemical proxies to reconstruct oxygenation conditions.

    ✓ Assessment of the contribution of extraterrestrial vs. terrestrial material.

2. Ichnological analysis of the boundary sediments, in order to evaluate the effect of the environmental crisis on the macrobentic trace makers.

3. Characterizing the pre, syn- and post-impact environmental conditions to evaluate variations as a consequence of the impact.

4. Constraining the timing of the re-establishment of productivity and the recovery of pre-impact conditions.

To achieve these objectives, a high-resolution sampling was carried out in the studied sections of Agost, Caravaca and Gubbio.

The results of this PhD Thesis have been published in scientific journals included in the Science Citation Index. Thus, the content and structure of some chapters correspond to the original source. The results obtained have also been divulged in the form of oral

presentations or posters, in national (SEM, EJIP) and international meetings (TREMP 2014, ASLO 2015, ICP 2016 and GOLDSCHMIDT 2017).

This PhD Thesis volume is organized as follows:

Chapter 1: Introduction.

Chapter 2: Bottom-water conditions in a marine basin after the Cretaceous-Paleogene impact event: Timing the recovery of oxygen levels and productivity. *doi:10.1371/journal.pone.0082242 (Plos One)*

Chapter 3: Geochemical and isotopic characterization of trace fossil infillings: New insights on tracemaker activity after the K/Pg impact event. *doi: 10.1016/j.cretres.2015.03.003 (Cretaceous Research)*

Chapter 4: Paleoenvironmental conditions across the Cretaceous-Paleogene transition at the Apennines sections (Italy): An integrated geochemical and ichnological approach. *doi: 10.1016/j.cretres.2016.11.005 (Cretaceous Research)*

Chapter 5: Application of laser ablation-ICP-MS to determine high-resolution elemental profiles across the Cretaceous/Paleogene boundary at Agost (Spain). *doi.org/10.1016/j.palaeo.2018.02.012 (Palaeogeography, Palaeoclimatology, Palaeoecology)*

Chapter 6: Microscale trace element distribution across the Cretaceous/Palaeogene ejecta layer at Agost section: Constraining the recovery of preimpact conditions. (*to be submitted*).

Chapter 7: Conclusions.

Chapter 8: Perspectives and future research.

Some data appear in a brief paper titled "High-resolution data from Laser Ablation-ICP-MS and by ICP-OES analyses at the Cretaceous/Paleogene boundary section at Agost (SE Spain)", *doi: 10.1016/j.dib.2018.04.118*. It contains data from Chapter 5, describing the coring, resin embedding methodology and laser ablation data treatment has been included as an **Appendix**.

Note that to obtain International Mention, the use of both English and Spanish language is mandatory. For this reason, the Abstract, Conclusions and Forthcoming research sections are included in both languages.

Chapter 2

BOTTOM-WATER CONDITIONS IN A MARINE BASIN AFTER THE CRETACEOUS–PALEOGENE IMPACT EVENT: TIMING THE RECOVERY OF OXYGEN LEVELS AND PRODUCTIVITY

Claudia Sosa-Montes de Oca[1], Francisca Martínez-Ruiz[1], Francisco Javier Rodríguez-Tovar[2]*

[1]Instituto Andaluz de Ciencias de la Tierra, Consejo Superior de Investigaciones Científicas-Universidad de Granada, Armilla, Granada, Spain.

[2]Departamento de Estratigrafía y Paleontología, Universidad de Granada, 18002 Granada, Spain.

"Have no fear of perfection, you will never reach it"

— Marie Curie (1867-1934)

ABSTRACT

An ultra-high-resolution analysis of major and trace element contents from the Cretaceous–Paleogene boundary interval in the Caravaca section, southeast Spain, reveals a quick recovery of depositional conditions after the impact event. Enrichment/depletion profiles of redox sensitive elements indicate significant geochemical anomalies just within the boundary ejecta layer, supporting an instantaneous recovery —some 10^2 years— of pre-impact conditions in terms of oxygenation. Geochemical redox proxies point to oxygen levels comparable to those at the end of the Cretaceous shortly after impact, which is further evidenced by the contemporary macrobenthic colonization of opportunistic tracemakers. Recovery of the oxygen conditions was therefore several orders shorter than traditional proposals (10^4-10^5 years), suggesting a probable rapid recovery of deep-sea ecosystems at bottom and in intermediate waters.

2.1. Introduction

The Cretaceous–Paleogene boundary (K/Pg), ≈ 65.95 Ma ago, is marked by one of the major faunal extinctions during the Phanerozoic, which led to the disappearance of about 70% of existing marine and continental species (D'Hondt, 2005). In particular, more than 90% of Maastrichtian planktic species of foraminifera disappeared abruptly at this boundary (Arenillas et al., 2006; Smit, 1982). The hypothesis of an extraterrestrial impact (Alvarez et al., 1980; Smit and Hertogen, 1980) to explain the extinction has been widely accepted (Schulte et al., 2010), though some authors also relate this mass extinction event with the activity of the large igneous province of the Deccan Traps (Chenet et al., 2009; Courtillot et al., 1999; Keller et al., 2011), and debate goes on in the literature regarding volcanism, impacts and mass extinctions (Keller, 2013). However, the synchroneity of a bolide impact and the associated mass extinction has been demonstrated (Renne et al., 2013). Despite intensive research, many open questions remain; how and when biological productivity recovered after the impact, and how different ecosystems responded to such environmental changes are still controversial matters. Further understanding of the response of marine ecosystems to global catastrophes calls for deeper study of environmental conditions across this boundary.

The Chicxulub impact (Hildebrand et al., 1991; Smit, 1999) involved a large bolide, about 10 ± 4 km in diameter, that produced severe effects at the local and regional scale (Kring, 2007), including earthquakes of magnitude >11 causing continental and marine landslides, tsunamis of 100-300 m in height that swept more than 300 km onshore and carried continental debris basin-ward to deep-marine sequences, shock waves and air blasts that radiated across the landscape, and high temperatures that generated fires within distances of 1,500 to 4,000 km from the crater. It is estimated that instantaneous combustions of 18%-24% of the terrestrial biomass existed at that time (Arinobu et al., 1999). Other global effects were nitric and sulfuric acid rain, widespread dust and blackout that prevented sunlight from reaching the surface of the Earth and lowered its temperature, and destruction of the stratospheric ozone layer, with a greenhouse effect that led to a temperature increase of 1.5° to 7.5° C. Hence, the impact generated an initial brief warming, followed by a short cooling period (≈ 2 kyr) and then a warm phase (Kring, 2007).

In addition to the major extinction, these environmental changes led to severe changes in depositional conditions, particularly in marine basins. Constraining how fast such conditions recovered is essential to further understand the recovery of ocean productivity, and how ecosystems adapt to major environmental changes. As a result of organic matter and metal accumulations, bottom waters underwent severe oxygen depletion. Trace metal anomalies point to major changes in redox conditions across the boundary (Martínez-Ruiz et al., 1999), also indicated by biomarkers (Mizukami et al., 2013). In this regard, the basal 3-mm-thick K/Pg layer at Caravaca section (Southeast Spain) shows a rapid increase in terrestrial long-chain n-alkanes and dibenzofuran, signaling a greater supply of terrestrial organic matter as well as a rapid increase in the concentration of dibenzothiophenes, evidencing a change from oxic to anoxic/euxinic conditions in the intermediate water

above the seafloor (Mizukami et al., 2013). Similarly, inorganic redox (Calvert and Pedersen, 2007; Tribovillard et al., 2006) allow us to reconstruct the evolution of oxygen conditions.

This study focuses on the Caravaca section, one of the best-preserved sections worldwide, well exposed and continuous (Smit, 2004). It has been extensively studied during the last three decades (Coccioni and Galeotti, 1994; Kaiho et al., 1999; Mizukami et al., 2013; Smit and Hertogen, 1980; Smit and Ten Kate, 1982), and can be considered a highly representative distal section for analysis of the K/Pg impact event. Selection of the sampling interval based on absence of mixing and traces fossils across the boundary to ensure that sampling at a millimetric scale records the original distribution of geochemical signatures. Hence, we present a mm-scale resolution approach, based on geochemical proxies in combination with icnological data, to gain insight into the timing of oxygen recovery and the recovery of biological productivity after the impact event.

2.2. Geologic Setting

The K/Pg boundary section at Caravaca (38°04´36.39´´N, 1°52´41.45´´W) is located on the NW side of road C-336, about 4 km southwest of the town of Caravaca (Murcia, Spain), in the Barranco del Gredero (Fig. 2.1).
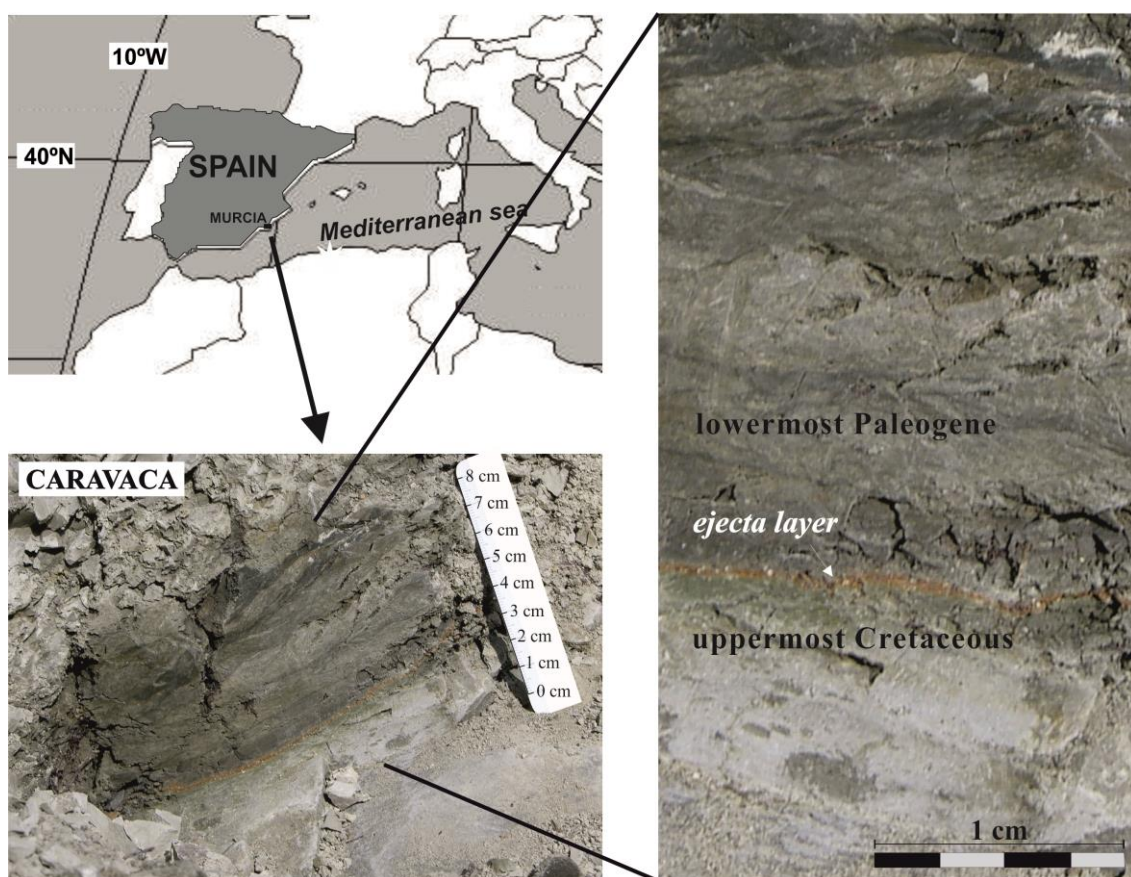
Fig. 2.1. Caravaca outcrop. Location and close-up photographs of the Cretaceous–Paleogene (K/Pg) boundary section at Caravaca (Southeast Spain).

The studied section belongs to the external Subbetic of the Betic Cordillera. Lithology consists of light marls in the upper levels of the Maastrichtian sediments (uppermost Cretaceous), followed by 7-10 cm of a lower Danian (lowermost Paleogene) blackish gray clay layer (the so-called boundary clay layer) with a 2-3 mm thick reddish brown layer at the base (ejecta layer) containing spherules and platinum group element (PGE) anomalies (Martínez-Ruiz et al., 2006, 1999; Smit, 1990; Smit and Klaver, 1981). The 7-10 cm lower Danian clay layer gradually increases its carbonate content to a gray argillaceous marl similar to that of the upper Cretaceous (Fig. 2.1). The Caravaca section, like the nearby Agost section (115 km away, in Alicante, Spain) and the El Kef section (Tunisia), is one of the best-preserved distal sections in the world (Molina et al., 2006). It is thought to represent deposition at paleowater depths of ~200 to 1,000 m (Macleod and Keller, 1994; Smith et al., 1981) and at around 27-30° N paleolatitude (Macleod and Keller, 1991; MacLeod and Keller, 1991; Smith et al., 1981).

2.3. Materials and Methods

In the framework of mm-scale resolution analysis across the K/Pg boundary, we focused on a 4.20 cm interval, from 1.20 cm below the K/Pg boundary to 3.0 cm above it, recording depositional conditions at the Latest Cretaceous, those of the ejecta layer, and the Earliest Danian. The fieldwork was carried out in public land and no specific permission was required. Samples were taken in continuous sampling every 0.2 cm. Ichnological analysis revealed a well-developed lowermost Danian trace fossil assemblage, even penetrating vertically into the Cretaceous sediments. Nonetheless, a careful selection of sampled intervals was done to avoid disturbance across the boundary. Thus, this highly detailed sampling involved materials showing no evidence of discrete trace fossils and without any mixing by bioturbation. According to the sedimentation rates of 3.1 cm Kyr^{-1} estimated for the Maastrichtian sediments, and that of 0.8 cm Kyr^{-1} calculated for the boundary clay layer (Kaiho et al., 1999), the studied material would span a time interval from 400 years prior to the K/Pg boundary to 3,750 years afterward.

Major and trace element concentrations were respectively obtained by Atomic Absorption Spectrometry (AAS) and Inductively Coupled Plasma Mass Spectrometry (ICP-mass), at the Centre for Scientific Instrumentation (CIC), University of Granada, Spain. All samples were crushed in an agate mortar and digested with HNO3 + HF (Bea, 1996).

We used Al-normalized concentrations of redox sensitive elements (V/Al, Mo/Al, U/Al, Pb/Al, Ni/Al, Co/Al, Cu/Al, Zn/Al and Cr/Al ratios), the U/Mo ratio, authigenic factors (Aut), and enrichment factors (EFs) of U and Mo for the reconstruction of redox conditions.

Enrichment factors (EF) were calculated as:

$$X_{EF} = \left[\frac{\left(\dfrac{X}{Al} \right)_{sample}}{\left(\dfrac{X}{Al} \right)_{PAAS}} \right]$$

Authigenic factors (aut) were calculated as:

$$X_{aut} = \left[\frac{(X)_{sample} - (X)_{PAAS}}{(Al)_{PAAS} * (Al)_{sample}} \right]$$

where X and Al represent the weight percentage concentrations of elements X and Al, respectively. Samples were normalized using post-Archean average shale (PAAS) compositions (Taylor and McLennan, 1985).

Rare earth element (REE) concentrations were also determined in order to show the nature of the ejecta layer regarding sediments deposited above and below the K/Pg boundary (Martínez-Ruiz et al., 1999).

2.4. Results and Discussion

It is well known that the K/Pg boundary marks major changes in the chemical composition of sediments deposited across it. Some changes can be expected as a consequence of the sudden drop in carbonate production, and the subsequent change in sediment lithology. Geochemical changes across the boundary are particularly evident in distal sections where a significant extraterrestrial metal contribution is recognized. In contrast, at sections located closer to the impact site, such as Blake Nose (Martínez-Ruiz et al., 2001) or Demerara Rise (Berndt et al., 2011) in the Western Atlantic, the extraterrestrial metal contribution is highly diluted by target rocks.

In distal sections, as the one here studied, the bolide contribution together with the enhanced chemical alteration in emerged areas produced a high metal supply. Additionally, reduced oxygen levels, due to the greater input of organic matter (both terrestrial and marine), also promoted anomalous concentrations of trace elements across the K/Pg boundary (Martínez-Ruiz et al., 1999; Smit, 1999; Smit and Ten Kate, 1982). Despite diagenesis and potential remobilization, original signatures are preserved, evidenced by PGE anomalies (Martínez-Ruiz et al., 2006, 1999; Smit, 1990; Smit and Klaver, 1981) and the extraterrestrial nature of trace elements such as Cr (Shukolyukov and Lugmair, 1998) within the ejecta layer. After the ejecta deposition, the autochthonous terrigenous supply led to the deposition of the boundary clay; primarily as a consequence of the reduced carbonate production. Therefore, the ejecta layer and this clay layer record the impact and post-impact depositional conditions, respectively. Impact evidence at Caravaca section also includes diagenetically altered spherules, largely composed of smectites and K-feldspar (Martínez-Ruiz et al., 1997).
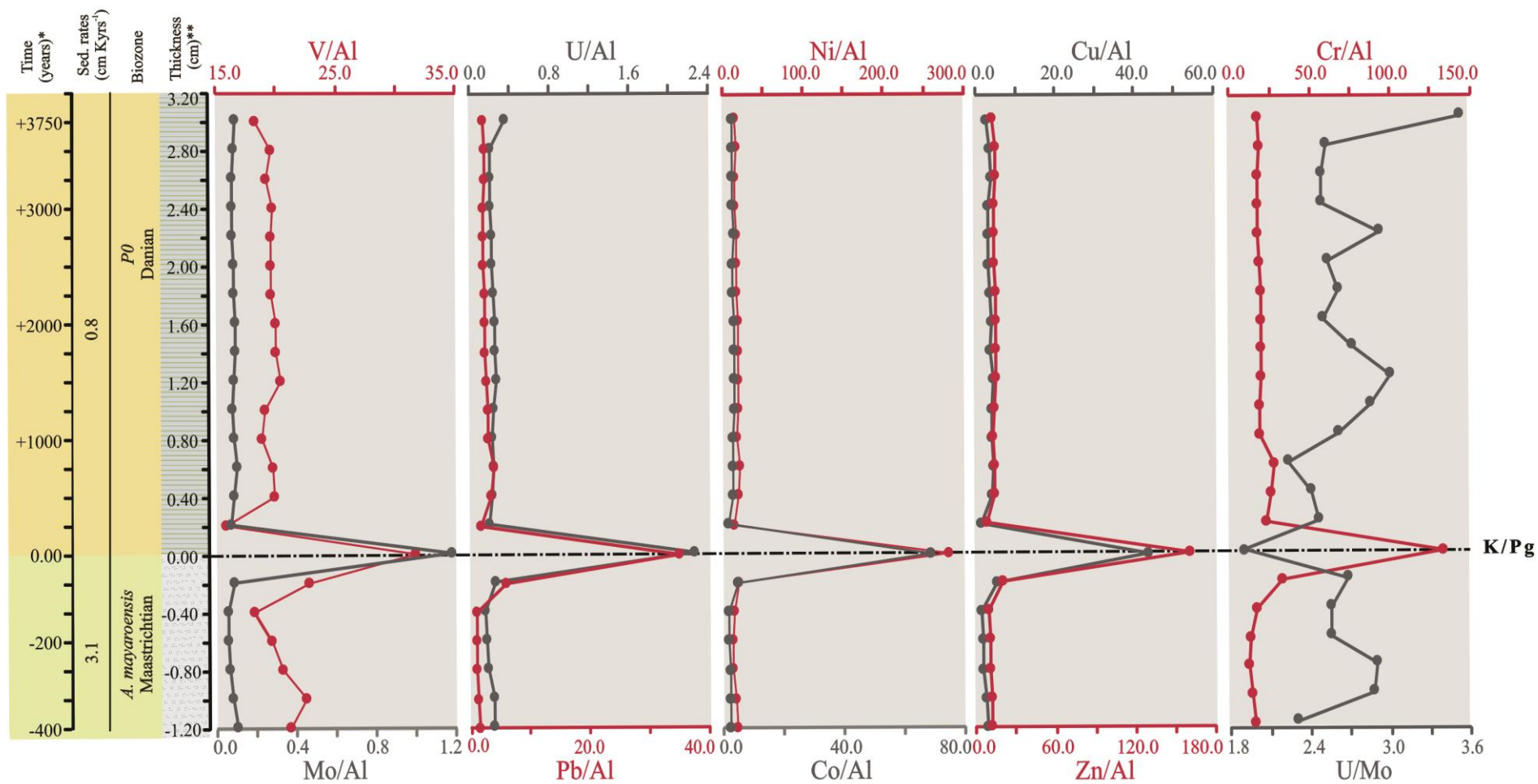
Fig. 2.2. Paleoredox proxy ratios. Enrichment/depletion profiles of redox-sensitive elements across the Cretaceous–Paleogene (K/Pg) boundary at Caravaca section (Al normalized concentrations *10⁻⁴). * The time (years) was calculated base on sedimentation rates in Kaiho et al. (1999), before and after K/Pg event. **'Thickness (cm) from K/Pg event.

Our mm-scale resolution analysis of trace metal concentrations and elemental ratios (V/Al, Cr/Al, Co/Al, Ni/Al, U/Al, Cu/Al, Zn/Al, Mo/Al, Pb/Al, and U/Mo) support the significant geochemical anomalies of the ejecta layer (Fig. 2.2). These ratios sharply peak just within the ejecta layer, with values ($*10^{-4}$) of 31.65 for the V/Al ratio, 1.18 for the Mo/Al ratio, 2.25 for the U/Al ratio, 280.50 for the Ni/Al ratio, 34.98 for the Pb/Al ratio, 69.02 for the Co/Al ratio, 42.95 for the Cu/Al ratio, 160.70 for the Zn/Al ratio, and 132.16 for the Cr/Al ratio; in contrast, the U/Mo ratio (1.91) (Table 2.1.) (Zhou et al., 2012) shows a noteworthy depletion. The abundance of U and Mo is a particularly useful proxy for paleoredox conditions (Algeo and Tribovillard, 2009; Tribovillard et al., 2012). Significant enrichments of U and Mo in marine sediments may generally be imputed to authigenic uptake of these elements from seawater in suboxic (for U) or euxinic conditions (for Mo) (Fig. 2.3). The decrease in the U/Mo ratio thus suggests that sulfidic conditions at this time may have favored a major Mo uptake. The U_{FE} vs Mo_{FE} covariation (Fig. 2.4) also indicates a change in redox conditions just within the K/Pg boundary, which implies a quick return to previous Cretaceous oxygen levels after the impact. Yet a comparison of redox proxies (Fig. 2.2) between Late Cretaceous sediments and those deposited during the very Early Danian showed no major changes, which suggests that oxygenation conditions during the Early Danian were not dramatically different from pre-impact conditions. On a global scale, no evidence of global hypoxia is reported, only rather low oxygen conditions at a local scale for certain outcrops (Alegret and Thomas, 2005). Our data therefore support that lower oxygenation was mostly restricted to the deposition of the ejecta layer, that was settled down instantly on a geological time scale (Artemieva and Morgan, 2009), while sediments from the Early Danian and the Late Cretaceous are similar in terms of oxygenation. The distinct nature of the ejecta layer is moreover supported by the REE depletion (Fig. 2.5), derived not only from the diagenetic alteration of the impact glass and subsequent loss of REE, but also from the relatively high contribution of REE-depleted extraterrestrial material (Martínez-Ruiz et al., 1999; Smit and Ten Kate, 1982).
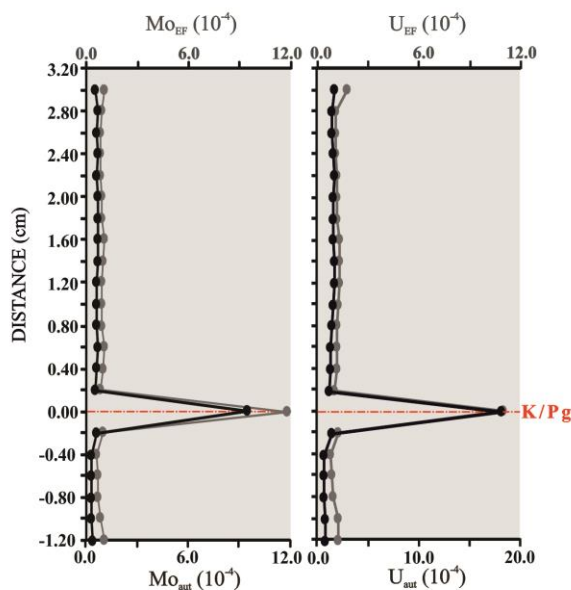
Fig. 2.3. Mo_{EF}-aut and U_{EF}-aut variations. Profiles Mo_{EF}-aut and U_{EF}-aut for the Cretaceous–Paleogene (K/Pg) boundary section at Caravaca (Southeast Spain).

Table 2.1. Element content and elemental ratios. Al and Ca concentrations (%), and elemental ratios (*10^{-4}) across the Cretaceous–Paleogene (K/Pg) boundary at the Caravaca section.

Sample	Distance (cm)	Al	Ca	V/Al	Mo/Al	U/Al	Pb/Al	Ni/Al	Co/Al	Cu/Al	Zn/Al	Cr/Al	REE/Al	U/Mo	Mo$_{EF}$	U$_{EF}$	Mo$_{aut}$	U$_{aut}$
CA +2.8 +3.0	3.00	5.25	18.94	18.31	0.10	0.36	2.34	15.29	3.45	3.20	14.37	17.39	21.57	3.53	1.01	1.15	0.48	1.71
CA +2.6 +2.8	2.80	8.17	6.16	19.56	0.09	0.22	2.62	17.47	3.71	4.17	16.03	18.81	17.78	2.52	0.87	0.71	0.63	1.54
CA +2.4 +2.6	2.60	8.40	6.13	19.21	0.08	0.21	2.50	16.13	3.50	4.55	16.44	17.58	17.49	2.49	0.84	0.68	0.63	1.51
CA +2.2 +2.4	2.40	8.69	5.67	19.72	0.09	0.21	2.19	16.32	3.57	3.73	15.31	17.48	17.28	2.49	0.85	0.68	0.65	1.57
CA +2.0 +2.2	2.20	8.50	6.59	19.57	0.08	0.23	2.36	16.92	3.74	3.67	15.31	17.99	17.36	2.93	0.79	0.74	0.59	1.70
CA +1.8 +2.0	2.00	8.37	6.99	19.58	0.09	0.23	2.36	16.87	3.65	3.84	15.44	18.51	17.29	2.53	0.90	0.73	0.67	1.64
CA +1.6 +1.8	1.80	8.22	7.28	19.59	0.09	0.24	2.54	18.09	3.59	4.25	15.74	19.06	17.28	2.62	0.90	0.76	0.66	1.69
CA +1.4 +1.6	1.60	7.40	8.31	19.92	0.10	0.25	2.65	19.03	3.91	4.43	16.26	19.96	18.58	2.51	1.01	0.82	0.68	1.65
CA +1.2 +1.4	1.40	7.50	7.74	19.90	0.10	0.26	2.62	18.29	3.81	4.30	15.83	19.92	19.30	2.72	0.96	0.84	0.65	1.73
CA +1.0 +1.2	1.20	7.56	8.51	20.36	0.09	0.27	2.88	19.22	3.86	4.75	15.90	19.99	18.76	3.00	0.89	0.86	0.59	1.78
CA +0.8 +1.0	1.00	7.56	8.01	19.03	0.09	0.25	3.02	18.20	4.07	4.55	14.94	18.88	16.36	2.86	0.86	0.79	0.57	1.63
CA +0.6 +0.8	0.80	7.69	7.31	18.78	0.09	0.23	3.13	16.49	3.56	4.53	14.34	18.26	14.70	2.61	0.87	0.73	0.59	1.51
CA +0.4 +0.6	0.60	6.95	7.38	19.69	0.11	0.24	3.89	20.40	3.61	4.88	14.79	27.77	15.17	2.25	1.05	0.76	0.66	1.42
CA +0.2 +0.4	0.40	6.95	8.84	19.84	0.09	0.23	3.63	18.33	3.45	4.68	15.57	25.24	13.76	2.42	0.93	0.73	0.58	1.35
CA +0.0 +0.2	0.20	7.44	6.78	15.70	0.08	0.19	1.75	13.35	1.95	1.73	9.07	22.78	6.25	2.47	0.78	0.62	0.51	1.20
CA K/Pg	**0.00**	**8.11**	**6.57**	**31.65**	**1.18**	**2.25**	**34.98**	**280.50**	**69.02**	**42.95**	**160.70**	**132.16**	**3.02**	**1.91**	**11.80**	**7.25**	**9.49**	**17.99**
CA 0.0 -0.2	-0.20	6.70	12.52	22.76	0.09	0.25	6.08	19.12	4.78	5.71	21.46	31.97	14.43	2.68	0.94	0.81	0.56	1.48
CA -0.2 -0.4	-0.40	5.95	13.38	18.13	0.06	0.15	1.17	12.95	2.10	1.91	10.41	16.53	8.63	2.56	0.60	0.50	0.30	0.74
CA -0.4 -0.6	-0.60	5.38	23.48	19.60	0.06	0.16	1.07	12.32	2.08	2.15	11.53	12.59	10.58	2.56	0.63	0.52	0.29	0.70
CA -0.6 -0.8	-0.80	4.67	21.78	20.49	0.06	0.19	1.06	12.41	2.18	2.35	11.91	11.14	13.15	2.90	0.64	0.60	0.25	0.73
CA -0.8 -1.0	-1.00	4.12	23.95	22.42	0.08	0.24	1.31	15.76	2.51	2.81	12.10	13.82	16.28	2.88	0.83	0.77	0.30	0.85
CA -1.0 -1.2	-1.20	3.89	24.40	21.07	0.11	0.25	1.56	18.06	2.55	3.36	12.66	15.59	16.49	2.31	1.08	0.80	0.38	0.85

In view of the distribution profiles of trace metals in terms of timing, and the interval where pre-impact concentrations were reached (occurring at a distance between 0.2 and 0.3 cm above the K/Pg boundary), as well the sedimentation rates of the first centimeters of the Danian clay —0.8 cm kyr^{-1} in Caravaca (Kaiho et al., 1999)— we infer that oxygenation conditions were recovered in less than 375 years (in the order of 10^2 years). This value is several orders less than intervals traditionally proposed (10^4-10^5 years) (Coccioni and Galeotti, 1994; Kaiho et al., 1999). Such timing differences with respect to previous works may derive from a much higher resolution sampling. Furthermore, the reconstruction of oxygen conditions was based on recently developed geochemical redox proxies that have proven to be reliable (Martínez-Ruiz et al., 1997; Shukolyukov and Lugmair, 1998; Zhou et al., 2012). Accordingly, our data support that oxygenation conditions recovered very quickly, almost instantly on a geological time scale (Artemieva and Morgan, 2009).
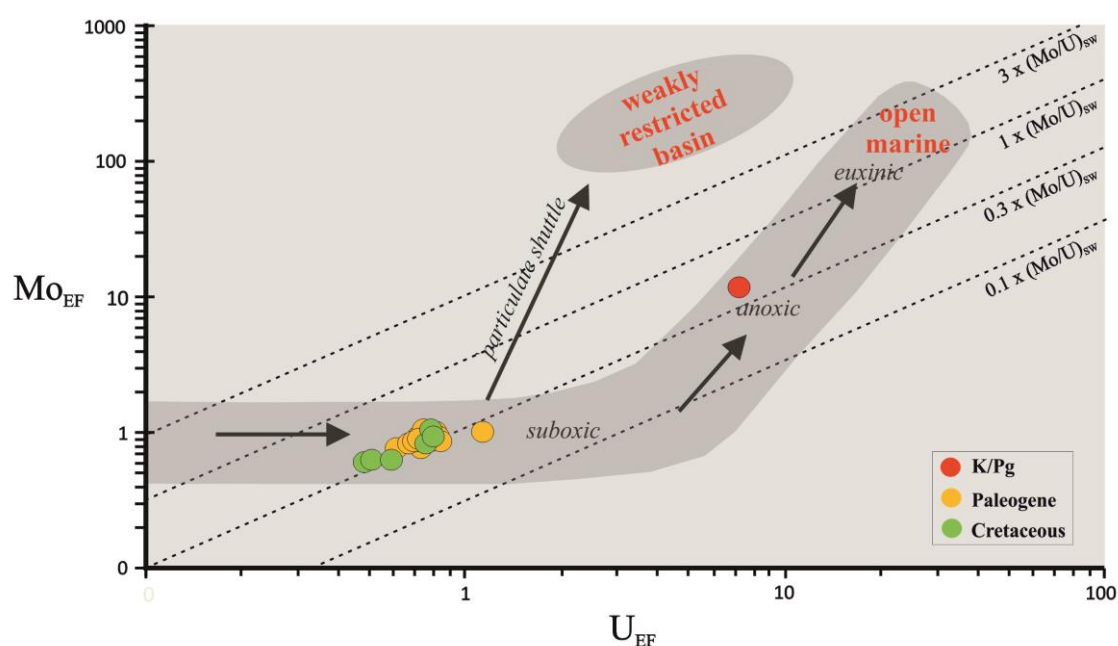
Fig. 2.4. Mo_{EF} vs U_{EF} covariation. Mo_{EF} vs U_{EF} covariation for the Cretaceous–Paleogene (K/Pg) boundary section at Caravaca (Southeast Spain).

Such a conclusion is also in agreement with the rapid recovery interpreted for the macrobenthic tracemaker community based on the presence of Fe-oxide spherules in the infilling of Thalassinoides in the Agost section (Rodríguez-Tovar, 2005), and with the bioturbational disturbance of the 2-3-mm-thick K/Pg red boundary layer at the Caravaca section (Rodríguez-Tovar and Uchman, 2008). In the latter case, the bioturbational disturbance is produced by Chondrites and Zoophycos tracemakers, favored by their relative independence from substrate features, together with an opportunistic behavior allowing colonization of sediment poor in oxygenated pore waters and food (Rodríguez-Tovar and Martín-Peinado, 2011, 2009; Rodríguez-Tovar and Uchman, 2008). Therefore, the geochemical results reported here and previous ichnological data both support that the recovery to normal levels of seafloor oxygenation was almost instantaneous, with absolute values lower than 10^2 years.

The recovery of planktic foraminifera has been linked to that of the marine carbon system. The evolutionary recovery and biogeochemical recovery occurred in two stages, up to four million years after the extinction (Coxall et al., 2006). This is conditioned by the extremely long time (millions of years) required to repair food chains and to reestablish an integrated ecosystem (Adams, 2004).
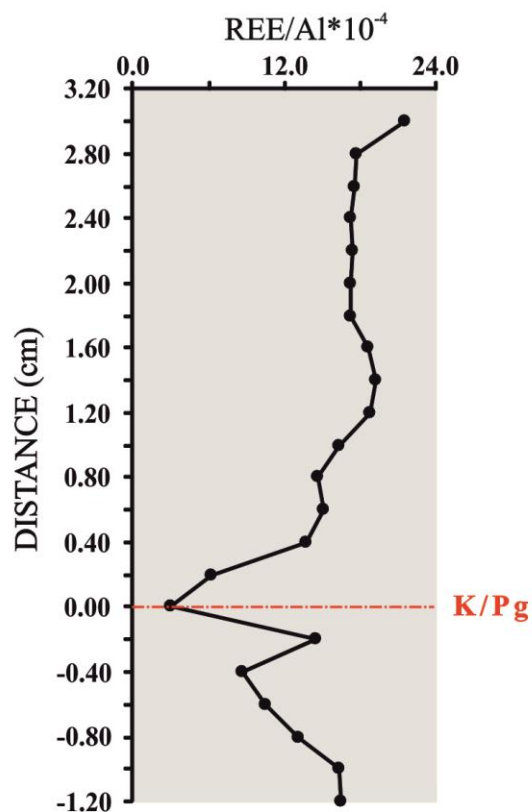
Fig. 2.5. REE variation profile. REE/Al ratio (Al normalized concentrations $*10^{-4}$) for the Cretaceous–Paleogene (K/Pg) boundary section at Caravaca (Southeast Spain).

In the benthic environment, benthic foraminifera reflect no major extinction at the K/Pg boundary, regardless of whether they were shallow or deep dwellers, high or low latitude forms, or infaunal or epifaunal inhabitants (Culver, 2003). However, diversity of the assemblages and number of infaunal morphogroups decreased severely (Alegret and Thomas, 2005). The recovery of these benthic foraminifera assemblages took a few thousand to a few hundred thousand years, suggesting the inhabitability of the benthic foraminifera habitat, and that their food supply likewise did not fully recover during the first few hundred thousand years after impact (Culver, 2003). In the macrobenthic habitat, however, we surmise that macrobenthic opportunist taxa could have initiated a very quick recovery, since low oxygen and adverse environmental conditions were reinstated shortly after the impact. Although full faunal recovery to pre-extinction abundances and the complete recovery of the marine carbon system occurred over a much longer period (Adams, 2004), the earliest response of oceanic ecosystems to the largest biotic disturbance of the Cenozoic in terms of timing was most likely very rapid.

2.5. Conclusions

A mm-scale resolution geochemical analysis across the K/Pg boundary at the Caravaca section evidences a rapid return to pre-impact conditions in terms of oxygenation after this major catastrophe. According to the estimated sedimentation rates for this section, oxygen levels at bottom and intermediate waters recovered at a very fast rate, in a range of few hundred years after the K/Pg boundary event. Depositional conditions for the ejecta layer were highly anoxic, as a consequence of the enhanced contribution of metals to the basins, accompanied by a greater supply of terrestrial and marine organic material. However, shortly after the impact, oxygen levels rapidly recovered, favoring the earliest macrobenthic opportunist colonization.

Acknowledgments

Chapter 3

GEOCHEMICAL AND ISOTOPIC CHARACTERIZATION OF TRACE FOSSIL INFILLINGS: NEW INSIGHTS ON TRACEMAKER ACTIVITY AFTER THE K/PG IMPACT EVENT

Claudia Sosa-Montes de Oca [a,] Francisco J. Rodríguez-Tovar [a], Francisca Martínez-Ruiz [b]*

[a] Departamento de Estratigrafía y Paleontología, Universidad de Granada, Avda. Fuentenueva s/n, 18002 Granada, Spain

[b] Instituto Andaluz de Ciencias de la Tierra, IACT (CSIC-Universidad de Granada), Avda. Las Palmeras 4, 18100 Armilla, Granada, Spain
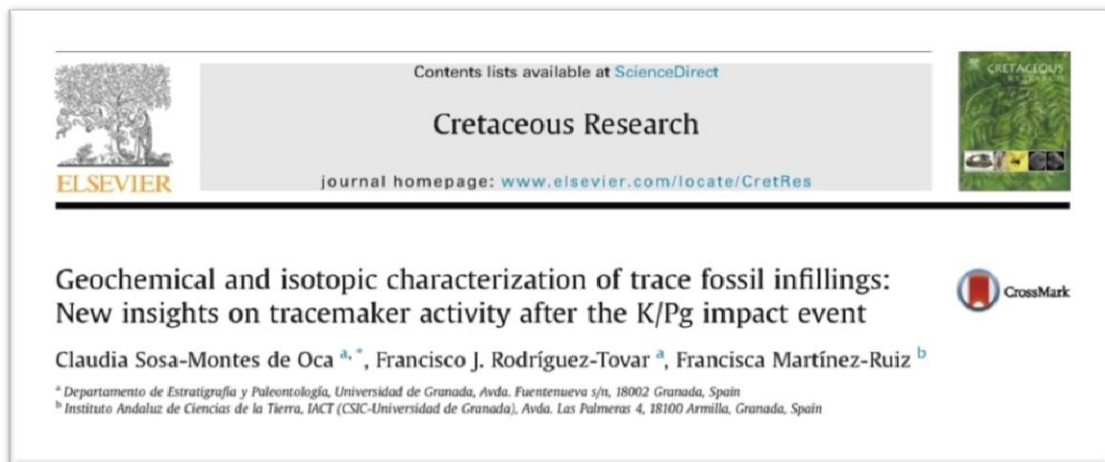
"Look up at the stars and not down at your feet"

— Stephen Hawking (1942-2018)

ABSTRACT

Geochemical and isotopic analyses of the Cretaceous-Paleogene (K/Pg) boundary sediments were conducted at the Caravaca section (External Subbetic, southeast of Spain) in order to evaluate the recovery of the macrobenthic tracemaker community and the bioturbational disturbance. Samples from the infilling material of several lower Danian dark-colored trace fossils (*Chondrites*, *Planolites*, *Thalassinoides* and *Zoophycos*) located in the uppermost 8-cm of the light upper Maastrichtian sediment, as well as samples from the host sediment of these trace fossils, were analyzed and compared with data from the lower Danian sediments. The values of element ratios indicative of extraterrestrial contamination (Cr/Al, Co/Al and Ni/Al) are higher in the infilling trace fossil material than in the upper Maastrichtian and lower Danian sediments, which suggests a contribution of the ejecta layer. Regarding the isotope composition, the δ^{13}C values are lower in the infilling material than in the Maastrichtian host sediments surrounding the traces, while the δ^{18}O are higher in the infilling material. The geochemical and isotopic compositions of the infilling material evidence the unconsolidated character of the sediment, including the red boundary layer. Softground conditions confirm a relatively rapid recovery by the macrobenthic tracemaker community, starting a few millimeters above the K/Pg boundary layer. The mixture of the infilling material of the trace fossils moreover reveals a significant macrobenthic tracemaker activity affecting K-Pg boundary transition sediments that may have significantly altered original signatures.

Keywords: K/Pg boundary, Caravaca section, geochemical anomalies, trace fossils, tracemarker recovery, bioturbational disturbance

3.1. Introduction

The Cretaceous-Paleogene (K/Pg) boundary, recently dated as ≈ 66.04 Ma ago (Husson et al., 2014; Vandenberghe et al., 2012), is associated with the second most relevant mass extinction taking place during the Phanerozoic, with 40% of genus extinction (Bambach, 2006) and the disappearance of about 70% of the marine and continental species existing at this time (D'Hondt, 2005). Currently, the hypothesis of an extraterrestrial impact (Alvarez et al., 1980; Smit and Hertogen, 1980) causing the end-Cretaceous mass extinction is widely accepted (Molina, 2015; Schulte et al., 2010b). The synchronicity of the Chicxulub impact and the mass extinction at the K/Pg boundary has also been widely demonstrated (e.g., Pälike, 2013; Renne et al., 2013 and references therein).

Over recent decades numerous literature on this topic has provided details about the impact site on the Yucatan peninsula in Mexico (Hildebrand et al., 1991); the size of the meteorite, around 10±4 km in diameter (Donaldson and Hildebrand, 2001; Kyte and Wasson, 1982); its nature, of carbonaceous chondritic type CM or CO (Goderis et al., 2013; Kyte, 1998; Shukolyukov and Lugmair, 1998); and the amount and nature of debris ejected to the atmosphere that led to major environmental perturbations (Kring, 2007 and reference therein).

The impact event also resulted in geochemical anomalies worldwide, recognized both in marine and continental depositional environments. The extraterrestrial effects are particularly evident in marine distal sections, located further than 7,000 km from the Chicxulub crater (Smit, 1999). In these sections, trace metals of extraterrestrial origin show higher concentrations than in proximal and intermediate sections, wherein the extraterrestrial contribution is highly diluted by target rocks (Berndt et al., 2011; Martínez-Ruiz et al., 2001).

Major environmental perturbations (i.e., nitric and sulfuric acid rain, widespread dust and blackout, destruction of the stratospheric ozone layer, greenhouse effect, temperature increase), followed the K/Pg event (Alegret and Thomas, 2005; Peryt et al., 2002). Diverse geochemical redox proxies, commonly used to reconstruct paleo-oxygen conditions (e.g., Calvert and Pedersen, 2007; Tribovillard et al., 2006), indicate anoxic conditions across the K/Pg boundary sediments, mostly promoted by the enhanced contribution of metals to the basins (extraterrestrial contamination and terrestrial elements derived from increasing chemical alteration in emerged areas), as well as a higher input of both terrestrial and marine organic material. An abrupt spike in biomarkers such as dibenzofuran, biphenyl and cadalene evidences the increasing input of terrestrial organic material (Mizukami et al., 2014).

The biotic response to the K/Pg impact event, including the post-event recovery, is still a matter of debate. Several contradictory hypotheses postulate the effects on planktonic vs. benthic organisms, k- vs. r-strategists, or deposit vs. suspension feeders (Labandeira et al., 2016; Molina, 2015; Powell and Macgregor, 2011; Schulte et al., 2010). In the past decade, relevant information has been provided by ichnological data. The trace fossil analysis of K/Pg boundary sections reveals a minor impact of K/Pg environmental changes on the

deep-sea macrobenthic tracemaker community, as well as its rapid recovery (Molina, 2015; Rodríguez-Tovar, 2005; Rodríguez-Tovar et al., 2011, 2006, 2004, Rodríguez-Tovar and Uchman, 2008, 2006). As pointed out by Sosa-Montes de Oca et al. (2013), this unusual biotic recovery could be explained by a rapid response (some few hundred years) of bottom water oxygenation that reestablished shortly after the K/Pg event. Ichnological analyses furthermore revealed the importance of the bioturbational redistribution by tracemakers, which may have affected original signatures and therefore should be considered so as to prevent possible misinterpretations (Kędzierski et al., 2011; Rodriguez-Tovar et al., 2010).

In order to evaluate and corroborate the hypothesis of the rapid recovery of the macrobenthic tracemaker community and the bioturbational disturbance, further analyses have been performed. In particular, geochemical and isotopic analyses of the K/Pg boundary sediments at the Caravaca section (southeast of Spain) included the infilling material of trace fossils as well as the upper Maastrichtian and lower Danian host sediments.

3.2. Geological setting and the study section

The K/Pg boundary section at Caravaca (38º04´36.39´´N, 1º52´41.45´´W) is located on the NW side of road C-336, in the Barranco del Gredero, about 4 km southwest of the town of Caravaca (Murcia, Spain) (Fig. 3.1). It belongs to the Jorquera Formation (lower Maastrichtian-lower Eocene), around 225 m-thick, which consists of intercalated marls, marly limestones and occasional turbidites. Geologically, this outcrop belongs to the External Subbetic of the Betic Cordillera, corresponding to a comparatively distal setting mainly composed by pelagic/hemipelagic mid-Lower Jurassic-Upper Cretaceous deposits. Cretaceous-Paleoegene transition sediments were deposited in a middle-bathyal environment, at a variable depth of 200 to 1000 m, according to previous reports (see Rodríguez-Tovar and Uchman, 2006 for review).

The K-Pg sediments at the Caravaca section have also been profusely studied in terms of mineralogical, geochemical and isotopic composition (i.e., Arinobu et al., 1999; Kaiho et al., 1999; Martínez-Ruiz, 1994; Ortega-Huertas et al., 1998, 1995; Smit, 2004; Smit and Hertogen, 1980; Sosa-Montes de Oca et al., 2013). Intensive research focuses on the exceptional record of the K-Pg boundary transition at this section; It shows a continuous succession that allows for a detailed, high-resolution biostratigraphy of the uppermost Maastrichtian to the lowermost Danian sediments based on planktonic foraminifers, as occurs with the close Agost section in Alicante (i.e., Arenillas et al., 2004; Arz et al., 2000; Canudo et al., 1991; Molina et al., 2005, 2001, 1996 and references therein).

The K-Pg transition at the Caravaca section is mainly composed by light-grey marls and marly limestones. The topmost Maastrichtian (uppermost Cretaceous) consists of light-grey marls that grade into a 3 mm-thick green transitional layer (Rodríguez-Tovar and Uchman, 2006). Upper Maastrichtian sediments are capped by a 2-3-mm thick reddish brown layer (ejecta layer) that marks the K/Pg boundary and contains impact evidence such as spherules and platinum group element (PGE) anomalies (Martínez-Ruiz et al., 2006, 1999;

Smit, 1990; Smit and Klaver, 1981) Above the ejecta layer, a 7-10-cm-thick blackish-grey clay layer (the dark boundary clay layer) deposited in the Early Danian gradually increases its carbonate content to a grey argillaceous marl similar to that of the Late Cretaceous (Fig. 3.1). The dark boundary clay layer shows alternating laminated and bioturbated horizons: at the bottom a 14-mm-thick laminated unit, more argillaceous and dark gray in color, is overlain by a 26-mm-thick horizon, light grey and bioturbated; above it lies a 35-mm-thick unit of more argillaceous sediment, lighter colored and with convolute laminae; while the upper part exhibits a 25-mm-thick greenish-grey non-laminated horizon (Rodríguez-Tovar and Uchman, 2006).
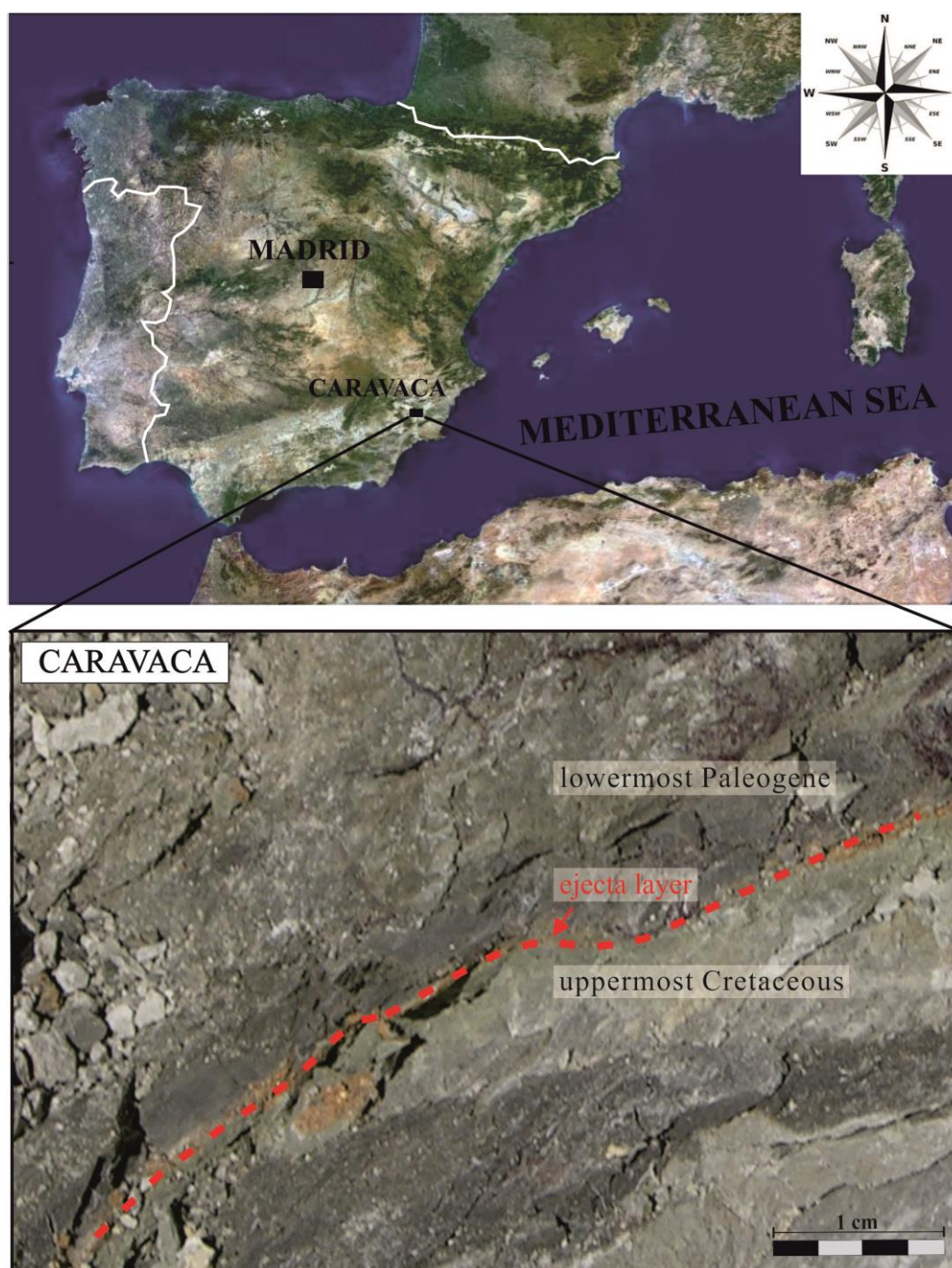
Fig. 3.1. Caravaca outcrop. Location and close-up photographs of the Cretaceous–Paleogene (K-Pg) boundary section at Caravaca (Southeast Spain).

3.3. Materials and methods

For this study we selected a 11-cm-thick interval, involving Maastrichtian materials from 8.0-cm below the K/Pg boundary, and Danian sediments to 3.0-cm above the boundary. According to the sedimentation rate of 3.1 cm Kyr-1 estimated for the Maastrichtian sediments, and of 0.8 cm Kyr-1 calculated for the boundary clay layer (Kaiho et al., 1999), the studied transition would span a time interval of around 6,330 years —from 2,580 years prior to the K/Pg boundary to 3,750 years afterward. Deposition of the ejecta layer at the K/Pg boundary can be considered instantaneous in the geological scale, roughly several weeks after the impact event (Artemieva and Morgan, 2009).

Geochemical and isotopic analyses were conducted on samples from the infilling material of several lower Danian dark-colored trace fossils located in the uppermost 8-cm of the light upper Maastrichtian sediment (see Rodríguez-Tovar and Uchman, 2006 for detailed ichnological information), as well as on samples from the host sediments of these trace fossils. Several specimens of dark-filled trace fossils were analyzed, belonging to *Chondrites*, *Planolites*, *Thalassinoides* and *Zoophycos*. *Thalassinoides* is commonly interpreted as having been passively filled (Bromley, 1996), as are some *Planolites* (Locklair and Savrda, 1998), while the interpretation of *Chondrites* and *Zoophycos* is not yet definitive. Thus, we analyzed samples from i) large *Chondrites* (sample CA-93 Ch) and the corresponding host sediment (CA-93-HS), at 1-cm below the K/Pg boundary, and ii) small *Chondrites* (samples CA-32 Ch, CA-135 Ch, CA-192 Ch,), *Planolites* (samples CA-9 Pl, CA-152 Pl), *Thalassinoides* (samples CA-135 Th1, CA-135 Th2, CA-180 Th), and *Zoophycos* (samples CA-180 Zo1, CA-180 Zo2, CA-180 Zo3), and the host sediment of each trace fossil (CA-9-HS, CA-32-HS, CA-152-HS, CA-135-HS, CA-180-HS, CA-192-HS), from 2 to 8 cm below the K/Pg boundary. Selected specimens were sampled using a Dremmel tool fitted with a fine tip diamond studded drill bit, allowing sampling even the smaller burrows.

Moreover, isotopic analyses of $\delta^{13}C$ and $\delta^{18}O$ on samples from the lowermost Danian (CA+0.0+0.2, CA+0.6+08, CA+0.8+1.0, CA+1.0+1.2, CA+1.8+2.0, CA +2.8+3.0) were integrated with previous geochemical data from these samples (Sosa-Montes de Oca et al., 2013).

As proxies for extraterrestrial contribution we selected Cr, Co and Ni, which are typically enriched within the ejecta layer (Goderis et al., 2013). We used the Al-normalized concentrations of these elements (Cr/Al, Co/Al and Ni/Al) to avoid a lithological effect on trace element contents.

Inductively Coupled Plasma Optical Emission Spectroscopy (ICP-OES) and Inductively Coupled Plasma-Mass Spectroscopy (ICP-MS) were used for major and trace element analyses, and Mass Spectrometry (IRMS) for isotope analyses. All were performed at the Center for Scientific Instrumentation (CIC), University of Granada, Spain.

3.4. Results

3.4.1. Geochemical analysis

Geochemical data are presented in Table 3.1. The normalized concentrations of Cr, Co and Ni are plotted in Figure 3.2, in which the diverse sediment intervals are marked: i) the ejecta layer (CA K-Pg) (data from Sosa-Montes de Oca et al., 2013), ii) the host sediment from the lower Paleogene, at 2.8-3.0-cm above the K/Pg boundary (previous data from Sosa-Montes de Oca et al., 2013), iii) the infilling material of several trace fossils analyzed, and iv) the Cretaceous sediments hosting trace fossils (Fig. 3.2).

3.4.1.1. Lower Danian

To compare the Cr/Al, Co/Al and Ni/Al ratios in the diverse sediment materials, previous data from this section were considered (Sosa-Montes de Oca et al., 2013). According to the lithological differentiation of the dark boundary clay layer (Rodríguez-Tovar and Uchman, 2006), four selected samples (CA+0.0+0.2, CA+0.6+08, CA+0.8+1.0, CA+1.0+1.2) belong to the lower 14-mm-thick laminated unit and two (CA+1.8+2.0, CA+2.8+3.0) to the overlying 26-mm-thick bioturbated horizon. Samples from the laminated unit are in the range of ($*10^{-4}$) 18.26-22.78 (mean 19.98) for the Cr/Al ratio, 1.95-4.07 (mean 3.36) for the Co/Al ratio and 13.35-19.22 (mean 16.81) for the Ni/Al ratio. Samples from the overlying bioturbated interval show values of ($*10^{-4}$) 17.39-18.51 (mean 17.95) for the Cr/Al ratio, 3.45-3.65 (mean 3.55) for the Co/Al ratio and 15.29-16.87 (mean 16.08) for the Ni/Al ratio.

The ejecta layer (lowermost Danian) presents concentrations with values ($*10^{-4}$) of 132.16 for the Cr/Al ratio, 69.02 for the Co/Al ratio and 280.50 for the Ni/Al ratio (Table 3.1; Sosa-Montes de Oca et al., 2013).
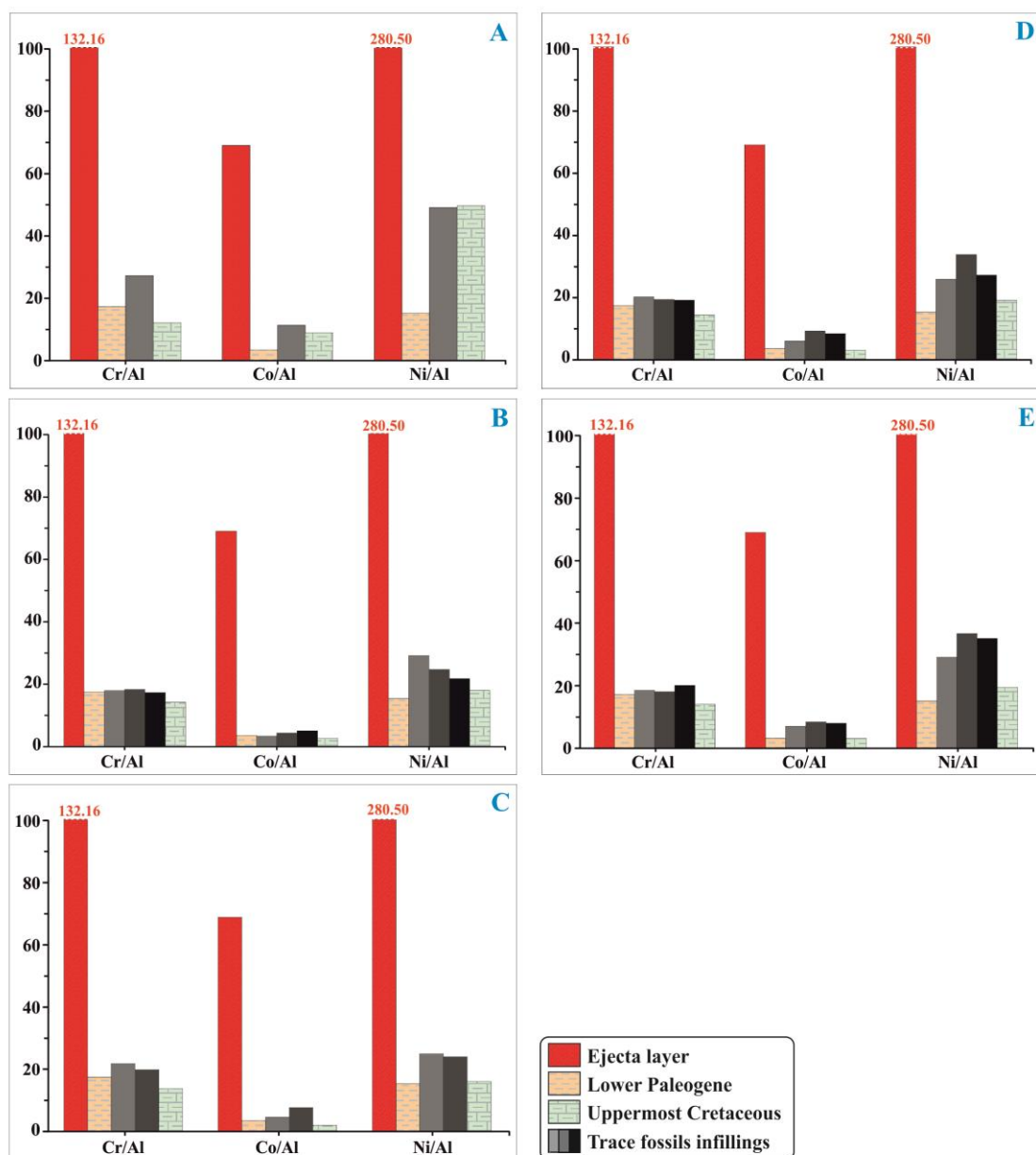
Fig. 3.2. Geochemical graphics. Compared the concentrations of Cr/Al, Co/Al and Ni/Al ratios (data from Table 3.1). i) In the ejecta layer; ii) in the host sediment from the lower Paleogene; iii) in the trace fossils: at 1 cm bellow K-Pg boundary we found (A) large *Chondrites* (sample CA-93 Ch); between 2-4-8 cm bellow K-Pg boundary, we found (B) *Chondrites* (samples CA-192 Ch, CA-32 Ch, CA-135 Ch), (C) *Planolites* (samples CA-9 Pl, CA-152 Pl), (D) *Thalassinoides* (samples CA-135 Th1, CA-135 Th2, CA-180 Th) and E) *Zoophycos* (sample CA-180 Zo1, CA-180 Zo2, CA-180 Zo3); iv) and finally, in the host sediment from Cretaceous nearby to each trace fossils.

Table 3.1. Element content (major and trace), elemental ratios and isotopic values. Al, Ca and $CaCO_2$ concentrations (%), Cr/ Al, Co/Al, Ni/Al ratios (*10^{-4}), and isotopic values (‰) measured across the Cretaceous–Paleogene (K-Pg) boundary at the Caravaca section i) in the ejecta layer, ii) in the host sediment from the lower Paleogene, iii) in the traces fossils infillings and in iv) the host sediment from upper Maastrichtian nearby each trace fossil. The geochemical data from the ejecta layer (CA K-Pg) and from lowermost Paleogene (CA+0.0+0.2, CA+0.6+08, CA+0.8+1.0, CA+1.0+1.2, CA+1.8+2.0, CA +2.8+3.0) were taken from Sosa-Montes de Oca et al. (2013). The isotopic data from the ejecta layer (CA K-Pg) were taken from Martínez-Ruiz (1994).

Sample	Distance (cm)	Age	Al	Ca	CaCO₃	Cr	Co	Ni	Cr/Al	Co/Al	Ni/Al	δ¹³C	δ¹⁸O
CA +2.8 +3.0	3.0		5.25	18.94	47.34	91.23	18.11	80,23	17.39	3.45	15.29	0.45	-2.48
CA +1.8 +2.0	2.0		8.37	6.99	17.49	154.99	30.54	141.26	18.51	3.65	16.87	0.07	-2.75
CA +1.0 +1.2	1.2	Early Danian	7.56	8.51	21.28	151.09	29.17	145.22	19.99	3.86	19.22	0.12	-4.00
CA +0.8 +1.0	1.0	host sediments	7.56	8.01	20.02	142.74	30.77	137.63	18.88	4.07	18.20	0.13	-3.53
CA +0.6 +0.8	0.8		7.69	7.31	18.27	140.44	27.36	126.80	18.26	3.56	16.49	-0.02	-3.97
CA +0.0 +0.2	0.2		7.44	6.78	16.95	169.46	14.49	99.32	22.78	1.95	13.35	0.02	-3.73
CA K-Pg	K-Pg	K/Pg boundary	8.11	6.57	16.42	1071.94	559.76	2275.07	132.16	69.02	280.50	**1.14**	**-2.43**
CA-93 Ch	-1.0		6.56	14.13	35.33	178.73	74.43	322.14	27.27	11.35	49.14	1.86	-2.28
CA-32 Ch	-2.0-8.0		3.20	24.23	60.58	57.08	10.38	93.03	17.85	3.25	29.10	1.92	-2.04
CA-192 Ch	-2.0-8.0		4.23	22.66	56.65	72.92	20.78	91.72	17.25	4.91	21.69	1.41	-2.97
CA-135 Ch	-2.0-8.0		4.19	22.27	55.68	76.04	17.61	103.13	18.17	4.21	24.64	1.85	-1.88
CA-135 Th2	-2.0-8.0		3.66	21.58	53.95	70.74	33.55	123.60	19.32	9.16	33.76	1.67	-2.30
CA-135 Th1	-2.0-8.0	Trace fossils	4.60	19.33	48.33	92.39	27.50	118.61	20.11	5.98	25.81	1.59	-2.01
CA-180 Th	-2.0-8.0	infilling material	4.97	18.36	45.90	94.76	41.40	134.87	19.09	8.34	27.16	1.49	-2.15
CA-180 Zo3	-2.0-8.0		4.76	17.70	44.25	96.26	38.80	167.46	20.24	8.16	35.22	1.23	-2.77
CA-180 Zo2	-2.0-8.0		4.72	20.00	50.00	86.12	40.47	173.60	18.25	8.58	36.79	1.32	-2.65
CA-180 Zo1	-2.0-8.0		4.92	19.67	49.18	91.57	35.17	143.90	18.60	7.15	29.24	1.19	-2.48
CA-152 Pl	-4.0-8.0		4.91	16.74	41.85	96.89	37.38	117.23	19.73	7.61	23.88	1.25	-2.05
CA-9 Pl	-4.0-8.0		5.04	18.28	45.70	109.14	23.07	125.12	21.66	4.58	24.84	1.16	-2.55
CA-93 HS	-1.0		6.74	20.80	52.00	81.86	60.61	335.10	12.15	9.00	49.73	2.19	-1.92
CA-32 HS	-2.0-8.0	Upper	3.34	30.29	75.73	46.30	8.20	65.46	13.86	2.45	19.59	2.02	-1.91
CA-192 HS	-2.0-8.0	Maastrichtian	3.50	30.48	76.20	49.35	7.89	54.33	14.08	2.25	15.51	2.24	-1.51
CA-135 HS	-2.0-8.0	host sediments	3.22	31.35	78.38	46.07	8.91	59.94	14.32	2.77	18.63	2.06	-1.82
CA-180 HS	-2.0-8.0	nearby each trace	3.12	30.78	76.95	44.37	10.14	61.05	14.23	3.25	19.58	2.12	-1.97
CA-152 HS	-4.0-8.0	fossil	3.16	31.39	78.48	43.63	7.93	56.96	13.83	2.51	18.05	2.04	-2.00
CA-9 HS	-4.0-8.0		3.52	30.71	76.78	47.91	6.34	53.77	13.63	1.80	15.29	1.99	-1.92

Standart desviation obtained with NBS 19, NBS18 is ≤ 0,05 ‰ for δ¹³C and ≤ 0,08 ‰ for δ¹⁸O

3.4.1.2. Upper Maastrichtian

In the uppermost Maastrichtian, at 1.0-cm below the ejecta layer, the infilling of large *Chondrites* (sample CA-93 Ch) shows values (*10^{-4}) of 27.27 for the Cr/Al ratio, 11.35 for the Co/Al ratio and 49.14 for the Ni/Al ratio. The uppermost Maastrichtian host sediments nearby this trace (CA-93 HS) show values (*10^{-4}) of 12.15 for the Cr/Al ratio, 9.00 for the Co/Al ratio and 49.73 for the Ni/Al ratio (Fig. 3.2A).

The infilling of trace fossils and the corresponding upper Maastrichtian host sediments from between 2 to 8 cm below the ejecta layer give the following results:

- The three specimens of small *Chondrites* (samples CA-32 Ch, CA-135 Ch, and CA-192 Ch) present values for the infilling material in the range of (*10^{-4}) 17.25-18.17 (mean 17.75) for the Cr/Al ratio, 3.25-4.91 (mean 4.12) for the Co/Al ratio and 21.69-29.10 (mean 25.14) for the Ni/Al ratio (Fig. 3.2B).

- The host sediments close to these trace fossils (samples CA-135 HS, CA-192 HS, CA-32 HS) show values in the range of 13.86-14.32 (mean 14.09) for the Cr/Al ratio, 2.25-2.77 (mean 2.49) for the Co/Al ratio and 15.51-19.59 (mean 17.91) for the Ni/Al ratio.

- The two specimens of *Planolites* (samples CA-9 Pl and CA-152 Pl) show values in the infilling material (*10^{-4}) of 19.73-21.66 (mean 20.69) for the Cr/Al ratio, 4.58-7.61 (mean 6.09) for the Co/Al ratio and 23.88-24.84 (mean 24.36) for the Ni/Al ratio (Fig. 3.2C). The host upper Maastrichtian sediments near *Planolites* (samples CA-9 HS and CA-152 HS) present values (*10^{-4}) of 13.63-13.83 (mean 13.73) for the Cr/Al ratio, 1.80-2.51 (mean 2.16) for the Co/Al and 15.29-18.05 (mean 16.67) for the Ni/Al ratio.

- Specimens of *Thalassinoides* (samples CA-135 Th1, CA-135 Th2, and CA-180 Th) register infilling material values (*10^{-4}) in the range of 19.09-20.11 (mean 19.50) for the Cr/Al ratio, 5.98-9.16 (mean 7.82) for the Co/Al ratio and 25.81-33.76 (mean 28.29) for the Ni/Al ratio (Fig. 3.2D). The host sediments nearby these trace fossils (samples CA-135 HS, CA-180 HS) show values (*10^{-4}) of 14.23-14.32 (mean 14.27) for the Cr/Al ratio, 2.77-3.25 (mean 3.01) for the Co/Al ratio and 18.63-19.58 (mean 19.10) for the Ni/Al ratio.

- *Zoophycos* (samples CA-180 Zo1, CA-180 Zo2, CA-180 Zo3) present values regarding the infilling material (*10^{-4}) in the range of 18.25-20.24 (mean 19.03) for the Cr/Al ratio, 7.15-8.58 (mean 7.76) for the Co/Al ratio, and 29.24-36.79 (mean 33.75) for the Ni/Al ratio (Fig. 3.2E). The host sediments near the analyzed *Zoophycos* (sample CA-180 HS) present values (*10^{-4}) of 14.23 for the Cr/Al ratio, 3.25 for the Co/Al ratio and 19.58 for the Ni/Al ratio.

3.4.2. Isotope composition

Isotope data are presented in Fig. 3.3, Fig. 3.4 and Table 3.1. Moreover, the isotopic data from the K/Pg boundary layer were taken from Martínez-Ruiz (1994) in the case of $\delta^{18}O$.

3.4.2.1. Lower Danian

Isotopic data from the selected samples belonging to the lower 14-mm-thick laminated unit at the bottom of the dark boundary clay layer are in the range of -0.02‰-0.13‰ for the $\delta^{13}C$ (mean of 0.06‰) and from -4.00‰ to -3.53‰ for $\delta^{18}O$ (mean -3.01‰) (Fig. 3.3 and Table 3.1). Samples from the overlying bioturbated interval show values of 0.07‰-0.45‰ for $\delta^{13}C$ (mean 0.26‰), and of -2.48‰ and -2.75‰ for $\delta^{18}O$ (mean -2.61‰).

The K/Pg boundary layer gives isotopic values of 1.14‰ for $\delta^{13}C$ and of -2.43‰ for $\delta^{18}O$ (Martínez-Ruiz, 1994). We cannot discard the possibility of a slightly altered isotopic value for $\delta^{13}C$, considering the global average value of -0.40‰ obtained by Ivany and Salawitch (1993).
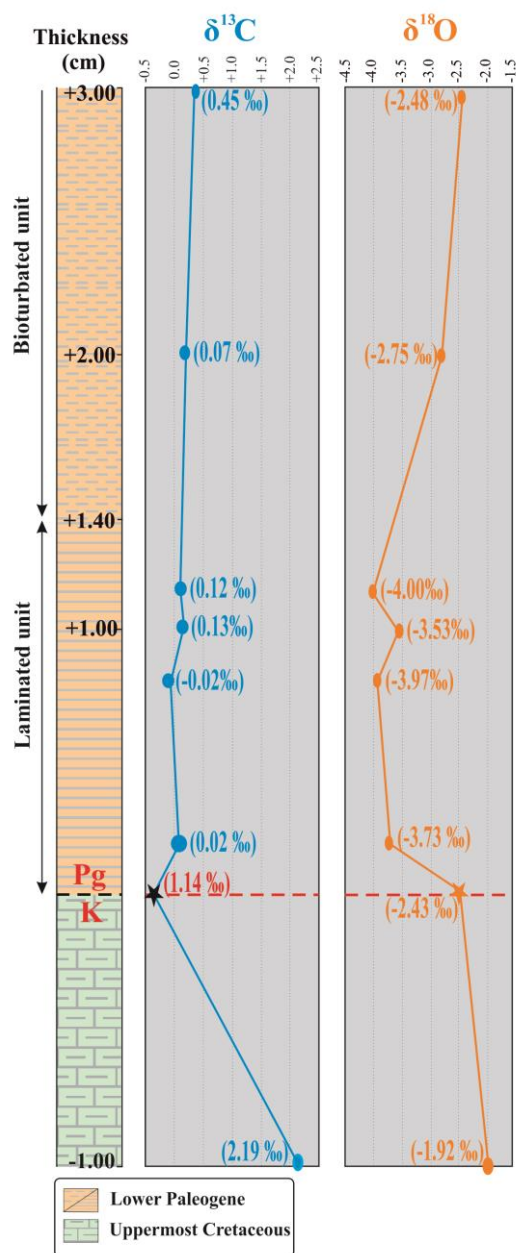
Fig. 3.3. Isotopic composition of Caravaca section. Isotopic composition of carbonate ($\delta^{13}C$, $\delta^{18}O$) for the Cretaceous–Paleogene (K-Pg) boundary at Caravaca section (Southeast Spain). The isotopic data ($\delta^{13}C$, $\delta^{18}O$) from the K-Pg boundary layer were taken from Martínez-Ruiz (1994).
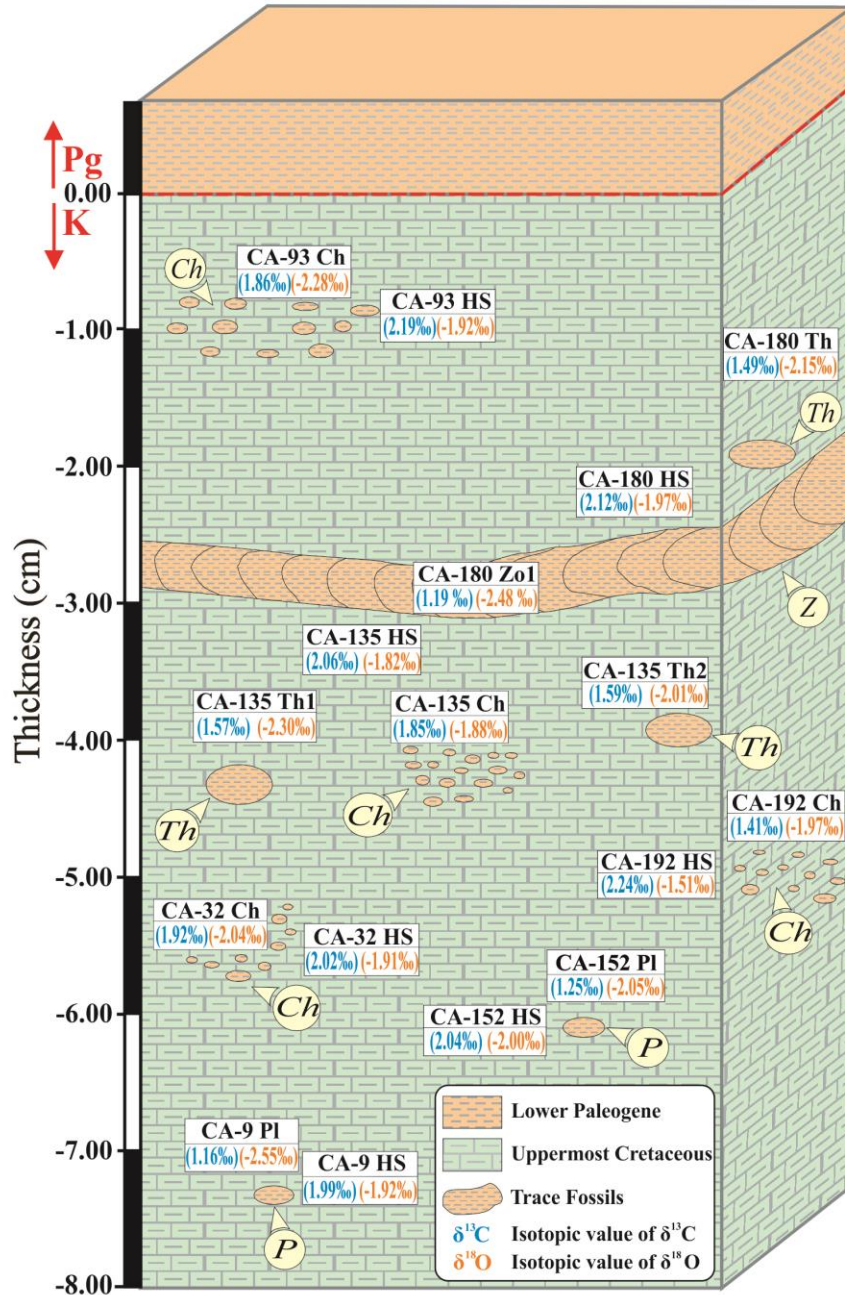
Fig. 3.4. Isotopic results. Comparison of the isotopic composition of carbonate ($\delta^{13}C$, $\delta^{18}O$) on the trace fossils infilling material and in the Cretaceous host sediment close to each trace at the Caravaca section (Southeast of Spain).

3.4.2.2. Upper Maastrichtian

The infilling of large *Chondrites* located at 1.0-cm below the ejecta layer shows values of 1.86‰ for $\delta^{13}C$ and -2.08‰ for $\delta^{18}O$, while data from the uppermost Maastrichtian sediments nearby this trace are 2.19‰ for $\delta^{13}C$ and -1.92‰ for $\delta^{18}O$.

Infilling material of small *Chondrites* is in the range of 1.41‰-1.92‰ for $\delta^{13}C$ (mean 1.73‰) and -1.88‰ to -2.97‰ for $\delta^{18}O$ (mean -2.30‰). The host sediments from the

upper Maastrichtian near these small Chondrites are in the range of 2.02‰-2.24‰ for $\delta^{13}C$ (mean 2.11‰) and -1.51‰- -1.91‰ for $\delta^{18}O$ (mean -1.75‰).

Isotopic data pertaining to the infilling material of *Planolites* are 1.16‰-1.25‰ for $\delta^{13}C$ (mean 1.20‰) and -2.05‰ and -2.55‰ for $\delta^{18}O$ (mean -2.30‰). The upper Maastrichtian sediments hosting trace fossils present values of 1.99‰-2.04‰ for $\delta^{13}C$ (mean 2.01‰) and -1.92‰ and -2.00‰ for $\delta^{18}O$ (mean -1.96‰).

Infilling material of *Thalassinoides* is in the range of 1.49‰-1.67‰ for $\delta^{13}C$ (mean 1.58‰) and -2.01‰ to -2.30‰ for $\delta^{18}O$ (mean -2.15‰). The sediments hosting these trace fossils show values of 2.06‰-2.12‰ for the $\delta^{13}C$ (mean 2.09‰) and of -1.82‰ and -1.97‰ for $\delta^{18}O$ (mean -1.89‰).

Isotopic values of the infilling material of *Zoophycos* are in the range of 1.19‰-1.32‰ for $\delta^{13}C$ (mean 1.25‰) and -2.48‰ to -2.77‰ for $\delta^{18}O$ (mean -2.63‰). Isotopic values of the sediments hosting the analyzed *Zoophycos* are 2.12‰ for $\delta^{13}C$ and -1.97‰ for $\delta^{18}O$ (Fig. 3.4).

3.4.3. Comparative analysis

Comparative analysis of the obtained geochemical data reveals significant information:

- Infilling material of the studied trace fossils, with independence of the particular ichnotaxon, shows higher values that those corresponding to the hosting Maastrichtian sediments.

- Values of Cr/Al, Co/Al and Ni/Al ratios from the ejecta layer are significantly higher than those corresponding to the upper Maastrichtian and lower Danian sediments, and higher as well than the infilling material of any of the studied specimens.

- Values from the lower Danian sediments, both those corresponding to samples from the laminated unit and from the bioturbated interval, are lower than those from the infilling materials.

- Furthermore, the values of Cr/Al, Co/Al and Ni/Al ratios from the infilling trace fossils are higher than those from the upper Maastrichtian and lower Danian sediments, and significantly lower than those corresponding to the ejecta layer.

In terms of isotopic composition, regardless of the particular ichnotaxa, data for the $\delta^{13}C$ are lower in the infilling material than in the corresponding Maastrichtian host sediment surrounding the specimen. The opposite occurs regarding the $\delta^{18}O$ values, consistently higher in the infilling material.

- Values of $\delta^{13}C$ in the K/Pg boundary layer are lower than those from the upper Maastrichtian sediments and higher than those from the lower Danian.

- Values of $\delta^{18}O$ in the K/Pg boundary layer are slightly lower than those from the upper Maastrichtian sediments and higher than that from the lower Danian.

- The $\delta^{13}C$ and $\delta^{18}O$ values from the lower Danian sediments, both those corresponding to samples from the laminated unit and from the bioturbated interval, are lower than those corresponding to the infilling materials of trace fossils.

Thus, data for the $\delta^{13}C$ from the lower Danian sediments and the K/Pg boundary layer are always lower than those registered in the infilling material of trace fossils, the latter in turn being lower than the values corresponding to the surrounding upper Maastrichtian sediments. In the case of $\delta^{18}O$, values from lower Danian sediments and the K/Pg boundary layer are consistently lower than those from the infilling material; the latter are likewise higher than the values corresponding to the upper Maastrichtian sediments hosting the traces.

3.5. Discussion

As previously indicated, numerous paleontolological studies have been conducted on the K/Pg boundary at the Caravaca section in order to evaluate the effect of the K/Pg boundary event on the biota, in particular on the micropaleontological assemblages. Micropaleontological studies involving planktonic (i.e., Arenillas and Molina, 1997; Arz et al., 2000; Canudo et al., 1991; Kaiho and Lamolda, 1999; Molina et al., 2001, 1998; Smit, 1990) and benthic foraminifera (Coccioni et al., 1993; Coccioni and Galeotti, 1994; Kaiho et al., 1999; Keller, 1992; Smit, 1990; Widmark and Speijer, 1997a, 1997b), together with calcareous nannofossils (i.e., Gardin and Monechi, 1998; Molina et al., 2001; Romein, 1977) shed some light on the effects of the K/Pg boundary perturbations on the micropaleontological community. The sudden decrease in diversity in coincidence with the K/Pg boundary event led to variable strategies of the biota, depending on the particular micropaleontological group. Similarly, the recovery shows different patterns and duration depending on the assemblage.

Early work on trace fossils in the K/Pg boundary at the Caravaca section was not very detailed, mainly indicating the presence of burrows filled with dark material from the overlying dark boundary clay layer (i.e., Arinobu et al., 1999; Molina et al., 2001; Smit, 2004; Smit and Ten Kate, 1982). Later on, more detailed ichnological analyses revealed a well-developed dark-colored trace fossil assemblage, bioturbating continuously from several horizons in the lowermost Danian dark boundary layer to the uppermost Maastrichtian sediments, cross-cutting vertically and penetrating laterally the K/Pg boundary layer (Rodríguez-Tovar and Uchman, 2008, 2006). This fact was interpreted as revealing a minor incidence of the K/Pg boundary event on the tracemaker macroinfaunal community, as well as its relatively rapid recovery after the event. Moreover, these authors pointed out the possibility that Maastrichtian sediments could be contaminated with Danian microfossils due to bioturbation, and that the bioturbational disturbance of the rusty layer could induce erroneous interpretations (Rodríguez-Tovar and Uchman, 2008, 2006).The vertical displacement and taphonomical filtering of nannofossils due to bioturbation at the Caravaca K/Pg boundary was furthermore confirmed (Kędzierski et al., 2011).

3.5.1. Macrobenthic tracemakers after the K/Pg: recovery and bioturbational effects

The geochemical and isotopic information obtained in the present study is of special relevance in that it supports macrobenthic trace fossil activity after the K/Pg boundary event, including recovery and bioturbational effects.

The infilling material of the trace fossils shows values of Cr/Al, Co/Al and Ni/Al ratios roughly midway between the higher values registered in the ejecta layer and the lower values obtained from the upper Maastrichtian and lower Danian sediments. This fact supports the mixture of the infilling material of the trace fossils, consisting not only of dark clay layer sediment but also of ejecta layer material. However, neither red-colored particles nor spherules were observed in the infilling material. Rodríguez-Tovar (2005) registered Fe-oxide spherules in the infilling of *Thalassinoides* at the nearby Agost section (Alicante, Spain). This absence, especially of the red-colored particles from the ejecta layer, could be the consequence of a significant mixture of the material; an important redistribution would have caused the dilution of the comparatively scarce red boundary layer material into the dark upper Maastrichtian sediment. Such a total mixture is more likely to occur when the sediment is still unconsolidated and softground conditions prevail. This context also suggests a relatively rapid recovery of tracemakers during the first phases of deposition of the dark boundary clay layer when the ejecta layer material is still unconsolidated. Softground conditions can be corroborated considering that the registered mixture is independent of the type of trace fossils —it involves the actively filled (i.e., *Planolites*), the passively filled (i.e., *Thalassinoides*), and the ones having a controversial origin (i.e., *Chondrites* and *Zoophycos*).

However, such a sediment mixture is not evidenced by the isotope composition, showing different patterns for the δ^{13}C and the δ^{18}O; δ^{13}C values are lower in the infilling material than in the corresponding Maastrichtian sediment surrounding the specimen, while δ^{18}O values are consistently higher in the infilling material. A number of possibilities could be envisaged, for instance a mixture of the infilling material involving not only the lower Danian sediment and the K/Pg boundary layer material, but also the upper Maastrichtian host sediment; or it may be that the analyzed trace fossils came from one or several horizons above the analyzed lower Danian sediments. In the first case, a mixture including the upper Maastrichtian host sediments is less likely when taking into account that both passively and actively filled trace fossils present a similar pattern. Hence, the second hypothesis is more plausible.

Isotopic data of the K-Pg boundary transition at the nearby Agost section, obtained from Danian dark-trace fossil filling as well as from upper Maastrichtian and lower Danian sediments, revealed a good correspondence between data from the filling material and the data corresponding to different levels of the lower Danian sediments (Rodríguez-Tovar et al., 2006, 2004). This correlation allows for a precise characterization of different horizons of colonization in the dark boundary clay layer. Such is not the case for the Caravaca section, where it is difficult to propose concrete horizon(s) of colonization based on the geochemical and isotopic data. Still, the horizon(s) of bioturbation must be close to the

K/Pg boundary, taking into consideration the interpreted softground conditions for the ejecta layer. Accordingly, the first bioturbated horizon at 14 mm from the K/Pg boundary layer is the most plausible interval, confirming the rapid recovery proposed by Rodríguez-Tovar and Uchman (2008, 2006).

As interpreted from the geochemical and isotopic data, the macrobenthic tracemaker activity during the recovery is important, significantly affecting the K-Pg boundary transition sediments, including the ejecta layer. Trace fossil producers determine the bioturbational mixture of sediments, which conditions the geochemical and the isotope composition. This fact must be considered in order to arrive at a precise analysis of the K/Pg boundary materials and correct interpretations.

3.6. Conclusions

Geochemical and isotopic analyses conducted on the Cretaceous-Paleogene boundary transition at the Caravaca section have provided significant information on the macrobenthic tracemaker activity after the K/Pg boundary event.

In particular, the Cr/Al, Co/Al and Ni/Al ratios from the infilling of trace fossils are higher than those of the upper Maastrichtian and lower Danian sediments, but lower than those corresponding to the ejecta layer, indicating a mixture of the sediment material due to biological activity across the boundary. Regarding the isotope composition, the $\delta^{13}C$ values are lower in the infilling material that in the corresponding Maastrichtian host sediment surrounding the specimen, while the $\delta^{18}O$ values are higher in the infilling material.

These data support a significant mixture of the infilling material of trace fossils, with a dominance of dark lower Danian sediments and a scarce contribution of the ejecta layer material. The mixture occurred due to the unconsolidated character of the sediment, including the ejecta layer. Softground conditions associated with this unconsolidated sediment further support the relatively rapid recovery of the macrobenthic tracemaker community, within horizons a few millimeters above the K/Pg boundary event. The observed mixture of the infilling material in the different ichnotaxon also evidences a significant macrobenthic tracemaker activity across the K/Pg boundary sediments, which should be considered in order to interpret original signatures and to reconstruct paleoenvironmental conditions during the K-Pg transition.

Acknowledgments

Chapter 4

PALEOENVIRONMENTAL CONDITIONS ACROSS THE CRETACEOUS-PALEOGENE TRANSITION AT THE APENNINES SECTIONS (ITALY): AN INTEGRATED GEOCHEMICAL AND ICHNOLOGICAL APPROACH

Claudia Sosa-Montes de Oca [a,*], Francisco J. Rodríguez-Tovar [a], Francisca Martínez-Ruiz [b], Paolo Monaco [c]

[a] Departamento de Estratigrafía y Paleontología, Universidad de Granada, Avda. Fuentenueva s/n, 18002 Granada, Spain

[b] Instituto Andaluz de Ciencias de la Tierra, Consejo Superior de Investigaciones Científicas-Universidad de Granada, Avda. de las Palmeras n 4, 18100 Armilla, Granada, Spain

[c] Dipartimento di Fisica e Geologia, via Pascoli snc, 06123 Perugia, Italy
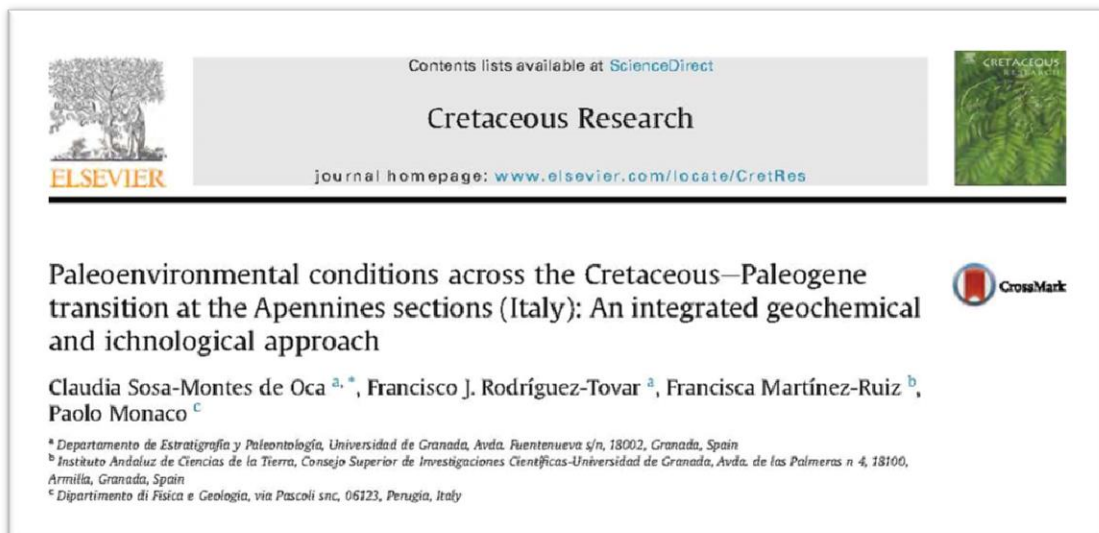
"Reserve your right to think, for even to think wrongly is better than not to think at all"

— Hypatia of Alejandria (370-416)

ABSTRACT

Two distal Cretaceous-Paleogene (K/Pg) boundary sections in the Central Apennine region (Italy) have been studied: Bottaccione Gorge and Contessa Highway. Geochemical and carbon isotope analyses on the infilling of trace fossils and on the host sedimentary rocks were performed to determine paleoenvironmental conditions during the Cretaceous-Paleogene transition. Major and trace element contents were measured in a 63 cm-thick interval at Bottaccione Gorge (from 22 cm below to 41 cm above the K/Pg boundary) and in a 72 cm-thick interval at Contessa Highway (from 43 cm below to 29 cm above the K/Pg boundary). Even though the K/Pg ejecta layer is now depleted at these sections due to continuous oversampling, the uppermost Maastrichtian and lowermost Danian deposits record the paleoenvironmental conditions prior to and after the K/Pg event. We used redox-sensitive element ratios (V/Al, Cr/Al, Co/Al, Ni/Al Cu/Al, Zn/Al, Mo/Al Pb/Al and U/Mo) and detrital element ratios (K/Al, Rb/Al, Zr/Al and ΣREE/Al) as proxies of certain environmental parameters, used for paleoenvironmental reconstruction. In general, similar values for elemental ratios are registered within Maastrichtian and Danian deposits, which supports similar paleoenvironmental conditions prior to and after the K/Pg event as well as the rapid reestablishment of the pre-impact conditions (i.e., oxygenation, nutrient availability, and/or sedimentary input). An enrichment in certain redox-sensitive elements above the K/Pg at the Bottaccione Gorge section suggests lower oxygenation, as also evidenced by the tracemaker community. Carbon isotope composition data from the infilling material of trace fossils furthermore reveals values similar to those of the host rocks at the corresponding depth, which supports an active infilling by nearly contemporaneous bioturbation during sediment deposition.

Keywords: K/Pg boundary, Gubbio sections, carbon isotopes, geochemical proxies, trace-fossils

4.1. Introduction

The boundary between the Cretaceous and the Paleogene (K/Pg boundary), recently dated at = 66.04 ± 0.02 Ma ago (Husson et al., 2014), is marked by one of the most devastating mass extinctions during the Phanerozoic (e.g., Koutsoukos, 2005; Schulte et al., 2010a). Since the early 1980s the origin of this extinction has been intensively debated, and several hypotheses were proposed at that time to explain the catastrophic event (e.g., Alvarez et al., 1980; Officer and Drake, 1985). The role of the Deccan Traps and how volcanism influenced the terrestrial and marine extinction are still matters of debate (e.g., Renne et al., 2015; Schoene et al., 2015; Stone, 2014; Tobin et al., 2016). The extraterrestrial hypothesis has been accepted in the wake of overwhelming evidences (e.g., Alvarez et al., 1980; Schulte et al., 2010a), and it is further supported by the synchronicity of the Chicxulub impact and the mass extinction (e.g., Molina, 2015; Pälike, 2013; Renne et al., 2013 and references therein).

The impact event was responsible for major environmental perturbations including nitric and sulfuric acid rain, widespread dust and blackout, destruction of the stratospheric ozone layer, and an enhancement of the greenhouse effect due to an increase in atmospheric concentrations of greenhouse gases (e.g., Kring, 2007 and references therein; Kaiho et al., 2016 for a recent hypothesis on the importance of latitude-dependent climate changes). These disturbances also led to secondary effects such as an increase in oceanic acidification (e.g., Alegret et al., 2012; Alegret and Thomas, 2005; Peryt et al., 2002) and a decrease in the sea surface temperature following the impact event (Galeotti et al., 2004a; Kaiho et al., 2016; Vellekoop et al., 2015, 2014). Such perturbations sharply transformed depositional and ecological conditions. Consequently, the reestablishment of these paleoenvironmental conditions after the K/Pg event has been of special interest in the context of evolutionary and ecological dynamics (e.g., Hull, 2015; Labandeira et al., 2016). Several proxies have been used to assess the reestablishment of the pre-impact conditions as well as the recovery of biota. Geochemical proxies, including major and trace elements distribution (e.g., Goderis et al., 2013; Smit, 1999, 1990), along with stable isotope composition (e.g., Arthur et al., 1987; Bojar and Smit, 2013; Kaiho et al., 1999; Zachos and Arthur, 1986) have been broadly used to assess paleoenvironmental conditions across the K-Pg boundary interval. The recovery of the biota has been intensively discussed, and diverse patterns have been proposed (e.g., Coxall et al., 2006; Esmeray-Senlet et al., 2015; Hull et al., 2011; Hull and Norris, 2011). Recent works provide new insights as to a more rapid productivity recovery than traditionally considered (e.g., Alegret et al., 2012; Alegret and Thomas, 2009; Birch et al., 2016). The analysis of trace fossils has also revealed a rapid recovery of the macrobenthic tracemaker community (e.g., Kędzierski et al., 2011; Rodríguez-Tovar, 2005; Rodríguez-Tovar and Uchman, 2008, 2006; Sosa-Montes de Oca et al., 2016). Within this context, the present paper aims to evaluate the evolution of paleoenvironmental conditions (i.e., rate of oxygenation, nutrient availability, and sedimentary input), and how these parameters affect the macrobenthic tracemaker community, across the K-Pg boundary interval at two of the classical K-Pg Gubbio sections in the Apennines, Central Italy —Bottaccione Gorge and Contessa Highway. These are reference sections of the K/Pg boundary since the discovery of the iridium

anomaly at Gubbio, which led Alvarez and co-workers to propose the extraterrestrial hypothesis underlying K/Pg mass extinction (Alvarez et al., 1980). Also, the K-Pg boundary was first defined biostratigraphically by Luterbacher and Premoli-Silva (1962) at the Bottaccione section. The K/Pg boundary from the Bottaccione Gorge and the Contessa Highway sections have been previously investigated in terms of geochemical composition (Alvarez et al., 1980, 1990; Alzeni et al., 1981; Ebihara and Miura, 1996), stable isotopes (Corfield et al., 1991; Voigt et al., 2012), magneto-bio-chronostratigraphy (Coccioni et al., 2016, 2013; Galeotti et al., 2015; Gardin et al., 2012; Husson et al., 2014; Lowrie et al., 1982), cyclostratigraphic analysis (Sinnesael et al., 2016) and trace fossil distribution (Monaco et al., 2015). However, integrative analyses involving different disciplines are scarce. The aim of this paper is to conduct the first high-resolution integrated geochemical and ichnological analysis in the K/Pg boundary from the Bottaccione Gorge and the Contessa Highway sections. We use the distribution of major and trace elements across the K-Pg transition and also compare the geochemical and carbon isotope composition from the infilling material of trace fossils with that of the host rocks to provide some new insights into paleoenvironmental changes associated with the K/Pg event and the reestablishment of pre-impact conditions.

4.2. Geological setting and the studied sections

The Gubbio region is located in the Umbria-Marche Basin, in the Apennines, central Italy. The K-Pg sediments at Gubbio (Fig. 4.1) have been widely studied at the Bottaccione Gorge (43º13´39.78´´N; 12º 20´14.28´´E) and the Contessa Highway (43º27´54.35´´N; 12º29´37.32´´E) sections. The Bottaccione Gorge section is located along state road SR298, from Gubbio to Scheggia, while the Contessa Highway section is located 2.5 km away from the latter, along state road SR452, running from Gubbio to Contessa (Coccioni et al., 2012). The sedimentary succession cropping out at the Bottaccione Gorge and the Contessa Highway sections belongs to the Scaglia Rossa Formation, which consists of a 400-m-thick sequence of pink -to -red pelagic limestones with a marl component and featuring chert bands or nodules. This formation corresponds to a time span of 80 Myr, between the Turonian and the early Eocene (Alvarez, 2009).

Fig. 4.1. Gubbio outcrops. Location and close-up photographs of the Cretaceous-Paleogene (K-Pg) transitions at Gubbio sections: Bottaccione Gorge and Contessa Highway (Umbrian-Marche Basin, central Italy).

The lithology of the K-Pg transition at these sections mainly consists of uppermost Maastrichtian white micritic limestone, with abundant planktonic foraminifera, and then lowermost Danian materials with the boundary clay marked by a 1.5-2.0-cm-thick dark red clay layer overlain by red micritic limestone (Fig. 4.2) (Coccioni et al., 2012). The ejecta layer is absent at these sections due to oversampling during the last few decades. Thus the well-known geochemical anomalies associated with the ejecta layer are not recorded in our sampling, though the boundary clay layer was sampled. Both sections are considered to represent an environment of continuous pelagic deposition (i.e., Alvarez, 2009; Coccioni et al., 2012, 2010; Gardin et al., 2012; Husson et al., 2014; Voigt et al., 2012). Although intrastratal folds and normal faults occur locally (Arthur and Fischer, 1977), these lie beyond our study intervals. Several estimations of the rate of sedimentation from the uppermost Maastrichtian to the lowermost Danian have recently been presented (i.e., (Gardin et al., 2012; Montanari and Koeberl, 2000; Mukhopadhyay et al., 2001; Sinnesael et al., 2016). In this high-resolution study, we consider those of Gardin et al. (2012) for the uppermost Maastrichtian, and Montanari and Koeberl (2000); Mukhopadhyay et al. (2001) for the lowermost Danian. Thus, we have a sedimentation rate of 1.23 cm kyr^{-1} for the Maastrichtian at the Bottaccione Gorge section and of 1.37 cm kyr^{-1} at the Contessa Highway section (Gardin et al., 2012). For the lowermost Danian, a sedimentation rate of 0.04 cm kyr^{-1} for the boundary clay layer interval at both sections is considered (Montanari and Koeberl, 2000), and of 0.2-0.3 cm kyr^{-1} for the red micritic limestones (Mukhopadhyay et al., 2001).
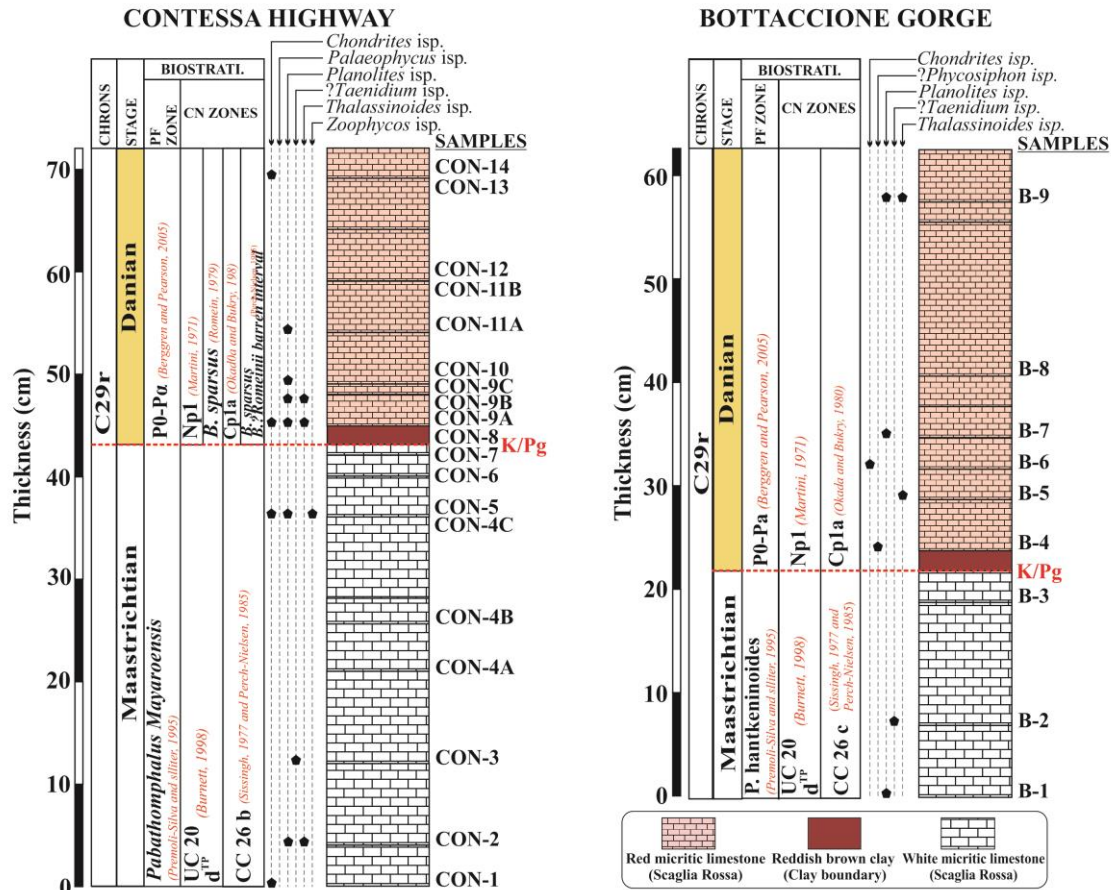
Fig. 4.2. Stratigraphic sections of Bottaccione Gorge and Contessa Highway. The biostratigraphy at the Contessa Highway section is based on Coccioni et al. (2010) for the lowermost Danian and on Gardin et al. (2012) for the uppermost Maastrichti. The biostratigraphy at the Bottaccione Gorge section is based on Galeotti et al. (2015) for the lowermost Danian and on Gardin et al. (2012) for the uppermost Maastrichti. The magnetostratigraphy of both sections is based on Lowrie et al. (1982).

These sedimentary rocks were deposited well above the carbonate compensation depth (CCD) at a middle-to-lower bathyal depth, between 1,500 and 2,500 m for the Bottaccione Gorge section (Coccioni et al., 2010; Galeotti et al., 2004b; Giusberti et al., 2009) and between 1,000 and 1,500 m for the Contessa Highway section (Coccioni et al., 2012), both at 30ºN paleoaltitude (van Hinsbergen et al., 2015).

4.3. Materials and methods

Geochemical and isotope analyses were conducted on samples from the K-Pg transition, including those from the infilling material of trace fossils and from the host rocks of these trace fossils. The sampling interval includes the white micritic limestone from the uppermost Maastrichtian, the red clay layer at the basal Danian and the red micritic limestone from the lowermost Danian (Fig. 4.2). At the Bottaccione Gorge a total of 16 samples along 63 cm of the K-Pg transition were analyzed (labeled B in Fig. 4.2 and Appendix A); of these, 4 samples correspond to the uppermost 22 cm of the white micritic limestone, 1 sample to the 2 cm of the red boundary clay layer, and 11 samples to the

lowermost 39 cm of the red micritic limestone (Fig. 4.2 and Appendix A). The studied stratigraphic interval spans a time period of approximately 233 kyrs, of which 18 kyrs correspond to Maastrichtian deposits and 215 kyrs correspond to Danian deposits (50 kyrs to the boundary clay layer, and 165 kyrs to the red micritic limestone) (Montanari and Koeberl, 2000; Mukhopadhyay et al., 2001). At the Contessa Highway a total of 41 samples were studied, along 72 cm of K-Pg transition (labeled CON in Fig. 2 and Appendix B); of these, 14 samples were selected from the uppermost 43 cm of the white micritic limestone, 10 samples are from the 2 cm-thick red boundary clay layer, and 17 samples are from the lowermost 27 cm of the red micritic limestone (Fig. 2 and Appendix B). This represents a time interval of approximately 201 kyrs, of which 31 kyrs correspond to Maastrichtian deposits and 170 kyrs correspond to Danian deposits (50 kyrs to the boundary clay layer and 120 kyrs to the red micritic limestone) (Gardin et al., 2012; Montanari and Koeberl, 2000; Mukhopadhyay et al., 2001). Bulk stable isotope analyses (δ^{18}O and δ^{13}C) were conducted on the samples from the host rocks at both sections (Appendix A and B), as well as on the infilling material of several specimens of trace fossils (Fig. 4.2 and Table 4.1). Due to the likely diagenetic alteration affecting the oxygen isotope signature the δ^{18}O data were discarded for this study and only the carbon isotope composition is considered for paleoenvironmental reconstruction. Regarding the host sedimentary rocks, 11 samples (4 from the white micritic limestone of the uppermost Maastrichtian, 1 from the boundary clay layer and 6 from the red micritic limestone) were studied in the Bottaccione section (Appendix A), and 20 samples (7 from the white micritic limestone from the uppermost Maastrichtian, 6 from the boundary clay layer and 7 from the red micritic limestone) in the Contessa Highway section (Appendix B). As for the infilling material of trace fossils, specimens were selected from the Maastrichtian and Danian deposits of both sections. Several ichnotaxa were studied, belonging to the ichnogenera *Chondrites*, *Planolites*, ?*Phycosiphon*, ?*Taenidium*, and *Thalassinoides*. In some cases, poor preservation impedes the ichnotaxonomical assignation of trace fossils (e.g., CON2Pl/Th-1, CON2Pl/Th-2, CON9ATF-6, CON9ACh/Pl-7, CON9BTF-2, and CON12TF-1). The Bottaccione section 11 samples were studied, including 3 specimens located in the Maastrichtian strata (*Planolites* and ?*Taenidium*) and 8 in the Danian strata (*Chondrites*, ?*Phycosiphon, Planolites* and *Thalassinoides*) (Table 4.1). At the Contessa Highway section 27 samples were studied, 8 specimens being from the Maastrichtian strata (*Chondrites*, *Planolites*, ?*Taenidium* and *Thalassinoides*), and 19 from the Danian strata (*Chondrites*, *Planolites*, ?*Taenidium* and *Thalassinoides*) (Table 4.1).

Table 4.1. Isotopic values of δ¹³C (‰VPDB) on the trace fossils found across the Cretaceous-Paleogene (K-Pg) transitions at Gubbio area: The Bottaccione Gorge and the Contessa Highway sections.

Trace Samples	Contessa	Distance (cm)	Stage	δ¹³C (‰ VPDB)
CON-14	CON14Ch-1	27.0		2.07
CON-12	CON12TF-1	18.0		2.10
CON-11	CON11APl-1	11.5		2.09
CON-10	CON10Pl-1	6.5		2.09
CON-9B	CON9BTF-2	4.5		2.01
	CON9BPl-3	4.5		2.01
	CON9BTh-1	4.0		1.93
	CON9APl-5	4.5	Danian	2.07
	CON9ATF-6	4.5		2.05
	CON9ATh-8	4.0		2.12
	CON9ACh-10	3.5		2.17
	CON9APl-11	3.5		2.29
CON-9A	CON9ATh-4	3.5		2.15
	CON9ATh-1	3.5		2.13
	CON9ATh-12	3.0		2.07
	CON9ACh/Pl-7	3.0		2.19
	CON9APl-9	2.5		2.21
	CON9ATh-2	2.5		2.04
	CON9ATh-3	2.5	K/Pg	2.09
CON-5	CON5Ch-2	−6.0		2.36
	CON5Pl-1	−7.0		2.39
	CON3Ta-1	−29.0		2.18
CON-3	CON3Ta-3	−30.0		2.28
	CON3Ta-2	−31.0	Maastrichtian	2.31
CON-2	CON2Pl/Th-1	−36.0		2.41
	CON2Pl/Th-2	−36.0		2.34
CON-1	CON1Ch-1	−42.0		2.36

Trace Samples	Bottaccione	Distance (cm)	Stage	δ¹³C (‰ VPDB)
	B9Th-1	38.0		1.84
B-9	B9Pl-2	38.0		2.03
	B9Th-3	38.0		1.74
B-7	B7Pl-1	12.0	Danian	1.94
B-6	B6Ch-2	11.0		2.10
B-5	B5Th-2	8.5		2.26
	B5Th-1	8.0		1.59
B-4	B4Ph-1	4.0	K/Pg	2.15
B-2	B2Ta-2	−12.0	Maastrichtian	2.59
	B2Ta-1	−14.0		2.31
B-1	B1Pl-1	−22.0		2.46

Samples were obtained using a Dremel tool fitted with a fine-tip diamond-studded drill bit; this tool allowed for sampling the infilling material of trace fossils, from even the smallest burrows, and for obtaining the host rocks from the Maastrichtian and Danian limestone.

For geochemical analysis, samples were crushed in an agate mortar and digested with HNO_3 + HF (Bea, 1996) in order to obtain the sample solution. Trace element concentrations were determined using an ICP-Mass Spectrometry (NEXION 300D). Results were calibrated using blanks and international standards, with analytical precision better than ± 2% for 50 ppm elemental concentrations and ± 5% for 5 ppm elemental concentrations. The concentrations of major elements (Al, Ca, Fe, K and Mn) were measured in the same samples solutions using an ICP-Optical Emission Spectroscope (Perkin-Elmer Optima 8300) with an Rh anode X-ray tube. Blanks and international standards were used for quality control and the analytical precision was better than ± 2.79% and 1.89% for 50 ppm elemental concentrations of Al and Ca, respectively, better than ± 0.52% for 20 ppm elemental concentrations of Fe, better than ± 0.44% for 5 ppm elemental concentrations of K, and better than ± 1.67% for 1 ppm elemental concentrations of Mn. Carbon isotope composition was obtained from powder samples using a Mass Spectrometer gas source (IRMS-GV INSTRUMENTS ltd. mod. Isoprime). Results are reported in conventional δ-notation relative to the Vienna Pee Dee Belemnite standard (VPDB) in ‰ units, with standard deviation obtained with NBS 19, NBS 18 ≤ 0.05‰ for δ¹³C. All the geochemical analyses were performed at the Center for Scientific Instrumentation (CIC), University of Granada, Spain.

The selected major and trace element concentrations used as proxies for oxygen conditions and detrital input were normalized to Al concentrations in order to avoid a lithological effect on element content (Calvert and Pedersen, 1993; Morford and Emerson, 1999; Tribovillard et al., 2006). In particular, K-Pg sediments display large oscillations in carbonate content, hence Al-normalized concentrations (Van der Weijden, 2002) or recalculation on a carbonate-free basis were needed to reflect oscillations in elemental content. The selected redox sensitive ratios were V/Al, Cr/Al, Co/Al, Ni/Al, Cu/Al, Zn/Al, Mo/Al, Pb/Al and U/Mo, which provided reliable information on oxygen content at the time of sediment deposition (e.g., Calvert and Pedersen, 2007; Tribovillard et al., 2006). Additionally, the abundance of U and Mo is a useful proxy for paleoredox conditions (Algeo and Tribovillard, 2009; Tribovillard et al., 2012), as are the enrichment factors (EFs) of U and Mo (Tribovillard et al., 2012; Zhou et al., 2012). Regarding detrital input proxies, we selected the K/Al, Rb/Al, Zr/Al and ΣREE/Al ratios.

4.4. Results

Geochemical and isotope data from the host rocks are presented in Appendix A for the Bottaccione Gorge section and in Appendix B for the Contessa Highway section, while Table 4.1 presents the isotopic data from the infilling material of trace fossils in both sections. In addition, comparison of geochemical and isotopic profiles from the host sedimentary rocks between the two sections is presented in Fig. 4.3, and comparison between isotopic data from the host rocks and infilling material is illustrated in Fig. 4.4 for both sections.

4.4.1. Elemental profiles

In general, enrichment/depletion profiles of redox and detrital elements from the host sedimentary rocks across the K-Pg transition reveal no significant changes from uppermost Maastrichtian to lowermost Danian deposits, except for the Zn/Al, Mo/Al and U/Mo ratios, which are used as redox proxies, and the REE/Al ratio, used as a detrital proxy.

4.4.1.1. The Bottaccione Gorge section

At the Bottaccione Gorge section, the most relevant variations across the K-Pg transition correspond to increases in Zn/Al, Mo/Al, and U/Mo ratios among the redox-sensitive ratios and in REE/Al ratio among the detrital proxies. Within the redox sensitive ratios, the Zn/Al ratio shows the highest values in samples B4HS-1 (193×10^{-4}), B5HS-1 (252×10^{-4}), B6HS-1 (111×10^{-4}), B7HS-2 (142×10^{-4}) and B7HS-1 (181×10^{-4}) within the 13 cm above the boundary clay layer, whereas the Mo/Al ratio shows the highest values in samples B6HS-1 (15.1×10^{-4}) and B7HS-1 (13.2×10^{-4}), respectively at 10 and 15 cm above the K/Pg boundary, and the U/Mo ratio in sample B3HS-3 reveals a peak (2.25) at the base of the clay layer. Of the detrital proxies, the REE/Al reveals a minimum (18.6×10^{-4}) in sample B3HS-3 at the base of the clay boundary layer, and then an increase in the lowermost Danian to values slightly higher (between 59.3 and 79.3×10^{-4}) than those registered within the uppermost Maastrichtian (from 42.1 to 51.7×10^{-4}).
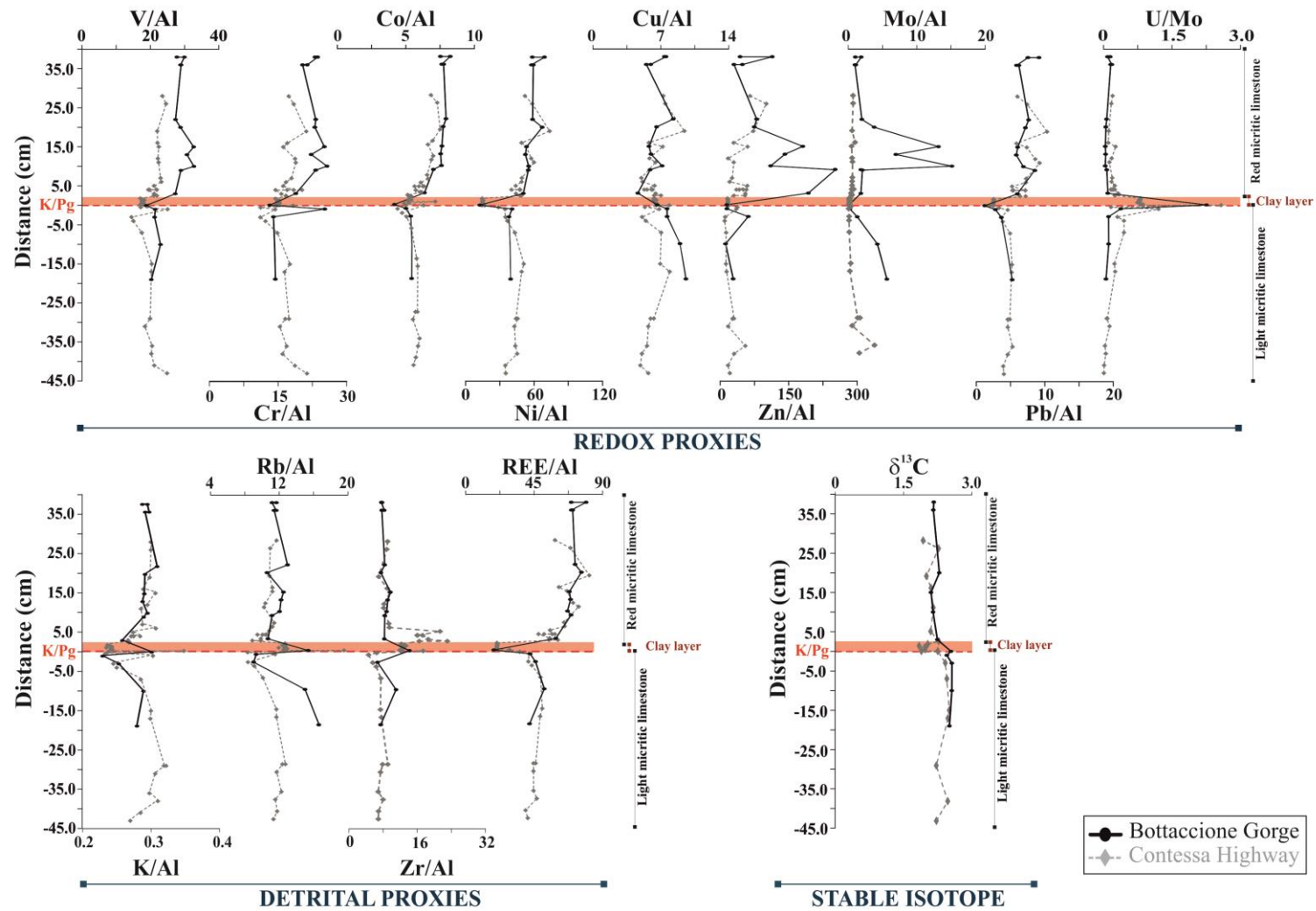
Fig. 4.3. Comparison of enrichment/depletion profiles at the Bottaccione Gorge and the Contessa Highway section of redox-sensitive element, detrital proxies, stable isotopes.

4.4.1.2. The Contessa Highway section

Remarkably, the normalized concentrations of redox-sensitive elements in the Contessa Highway section show even lesser fluctuations than those observed in the Bottaccione Gorge section. Among the redox sensitive ratios, the U/Mo ratio reveals a peak (2.57) in sample CON7HS-3 at the base of the clay layer. Regarding the detrital element ratios, a similar trend to that observed in the Bottaccione Gorge section is registered in REE/Al, having minimum values at the boundary clay (between 20.6 and $29.2x10^{-4}$) with respect to the uppermost Maastrichtian (between 35.9 and $50.6x10^{-4}$) and the lowermost Danian (between 48.2 and $81.4x10^{-4}$).

4.4.2. Stable isotope composition

Stable isotope data ($\delta^{13}C$) of the K-Pg transition sediments and infilling of the trace fossils are shown in Fig. 4.4, Table 1 and Appendix A, B.
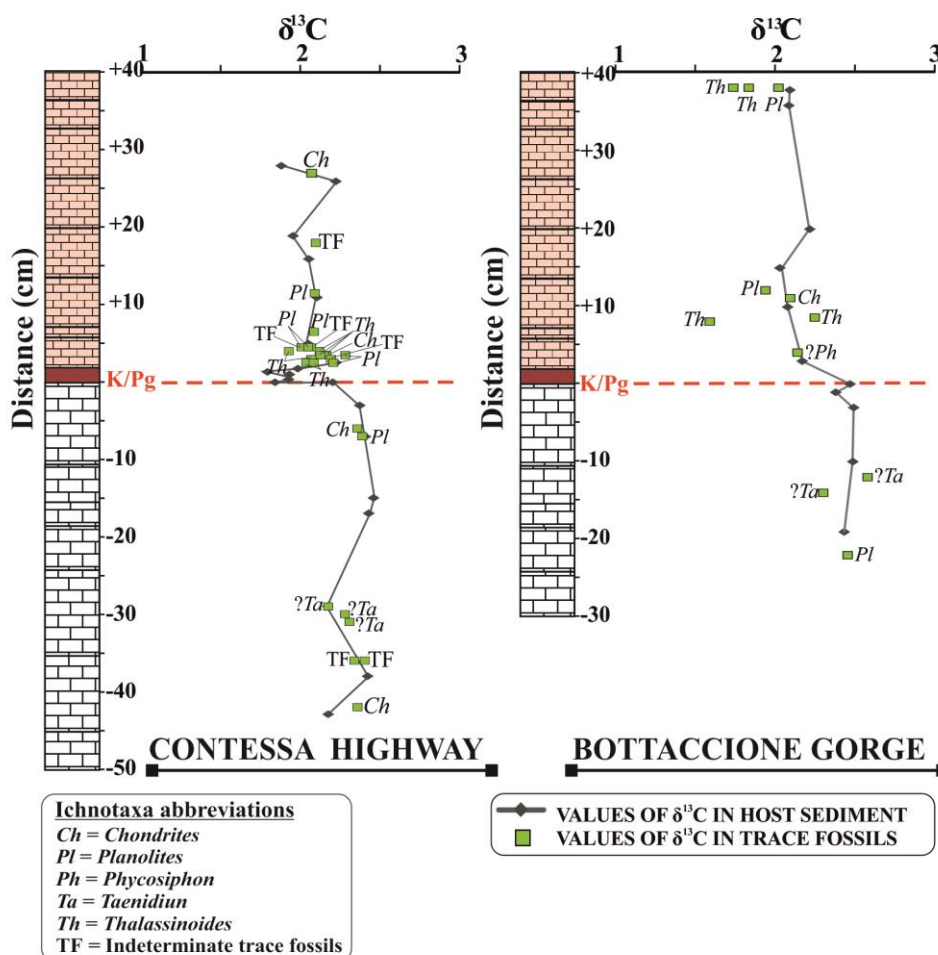
Fig. 4.4. Carbon isotopic composition of the Bottaccione Gorge and the Contessa Highway sections. Comparison of the carbon isotopic composition ($\delta^{13}C$) on trace fossil infilling material and on host sediment across the K/Pg transitions.

4.4.2.1. The Bottaccione Gorge section

As the ejecta layer has not been analyzed at these sections, the global carbon $\delta^{13}C$ decrease that characterizes the K/Pg boundary is not recorded, despite a similar isotope composition for the uppermost Maastrichtian and lowermost Danian deposits. The $\delta^{13}C$ values for the uppermost Maastrichtian rocks range from 2.40 to 2.51‰ (mean of 2.47‰), the sample analyzed at the base of the boundary clay layer shows a value of 2.49‰, and samples from the lowermost Paleogene show slightly lower $\delta^{13}C$ values, between 2.05‰ and 2.23‰ (mean 2.13‰) (Fig. 4.4 and Appendix A).

Isotopic data from the infilling of trace fossils, regardless of the particular ichnotaxon, are within the range of those from the host sedimentary rocks, with values similar to those of the host rocks at the depth where the trace fossils were (Fig. 4.4; Table 4.1 and Appendix A). Only certain values in $\delta^{13}C$ corresponding to the infilling of *Thalassinoides*, e.g., B5Th-1 (8 cm above the K/Pg boundary), B9Th-1 and B9Th-3 (both 38 cm above the K/Pg), show significant differences in comparison to those of the host rocks at the same depths (i.e., 1.59‰ *vs* a mean of 2.13‰, 1.84‰ *vs* a mean 2.13‰, and 1.74‰ *vs* a mean 2.13‰; for respective values of the infilling and host material).

4.4.2.2. The Contessa Highway section

Similarly to what occurs in the Bottaccione Gorge section, isotope values of $\delta^{13}C$ in the host sedimentary rocks across the K-Pg transition in the Contessa Highway section show no significant fluctuations from the uppermost Cretaceous (mean of 2.35‰) to the lowermost Paleogene, including the boundary clay layer (mean 1.94‰) and the red micritic limestone (mean 2.07‰).

The isotope data from the infilling material of trace fossils, regardless of the particular ichnotaxon, reveal values resembling those of the host rocks at the depth corresponding to trace fossil (Fig. 4.4, Table 4.1 and Appendix B).

4.5. Discussion

The geochemical composition of sedimentary rocks from the K-Pg transition at Gubbio (the Bottaccione Gorge and the Contessa Highway sections) has been profusely studied (see Alvarez, 2009 for a review). Alvarez et al. (1980) measured platinum group elements (PGE) at both sections, between 325 m below and immediately above the K/Pg boundary, reporting the Ir anomaly that led to the meteorite impact hypothesis. Alzeni et al. (1981) analyzed Si, Al, Fe, Mg, CaCO$_3$, Sr, Mn and clay minerals from Bottaccione Gorge at a metric resolution across the K-Pg transition, and reported some fluctuations in clay mineral associations and in the geochemical composition. Later on, Ebihara and Miura (1996) focused on the analysis of Pd, Ir, and Pt concentrations in both sections —mainly within the boundary clay layer, the upper Cretaceous and the lower Paleogene deposits— and suggested that the chemical composition did not significantly change across the K-Pg transition except for the PGE concentrations.

Despite significant diagenesis and potential remobilization of certain elements, it has been demonstrated that the K-Pg transitions preserved their original signatures within the ejecta layer, as evidenced by PGE anomalies (e.g., Martínez-Ruiz et al., 2006, 1999; Smit, 1990; Smit and Klaver, 1981) and also by the extraterrestrial nature of trace elements such as Cr (Shukolyukov and Lugmair, 1998). Therefore, major and trace element distribution across the K/Pg boundary has allowed for the reconstruction of the paleoenvironmental changes occurring at this time. In general, at distal sections considerable geochemical anomalies within the ejecta layer register a significant extraterrestrial contribution. However, the geochemical composition is quite similar above and below the ejecta layer, pointing to similar paleoenvironmental conditions pre- and post-impact event (e.g., Sosa-Montes de Oca et al., 2013). The absence of the ejecta layer at the studied sections impeded sampling of the deposits associated with the impact event, yet the lowermost Paleogene sediments (the boundary clay layer) register the post-impact conditions. The geochemical profiles obtained support a rapid recovery after the impact event, of the order of 10^2 years, which is almost instantly on a geological time scale. Redox-sensitive elements display low V/Al, Cr/Al, Co/Al, Ni/Al, Cu/Al, and Pb/Al ratios in both outcrops, which suggests oxygenated conditions prior to and immediately after the impact and the ejecta layer deposition. Such conditions are further supported by the increase in the U/Mo ratio. The abundance of U and Mo is a particularly useful proxy for paleoredox conditions (e.g., Tribovillard et al., 2012; Zhou et al., 2012). As the U and Mo enrichments in marine sediments are generally due to authigenic uptake from seawater in suboxic or euxinic conditions, respectively, the increase in the U/Mo ratio suggests oxic conditions. In addition, the U_{EF} vs Mo_{EF} covariation (Fig. 4.5A and B) indicates similarly oxic conditions during the uppermost Cretaceous and the lowermost Paleogene (including the boundary clay layer). Our data therefore further support a rapid reestablishment of oxygenated conditions after the deposition of the ejecta layer, which has been associated with anoxic deposition (Sosa-Montes de Oca et al., 2013).
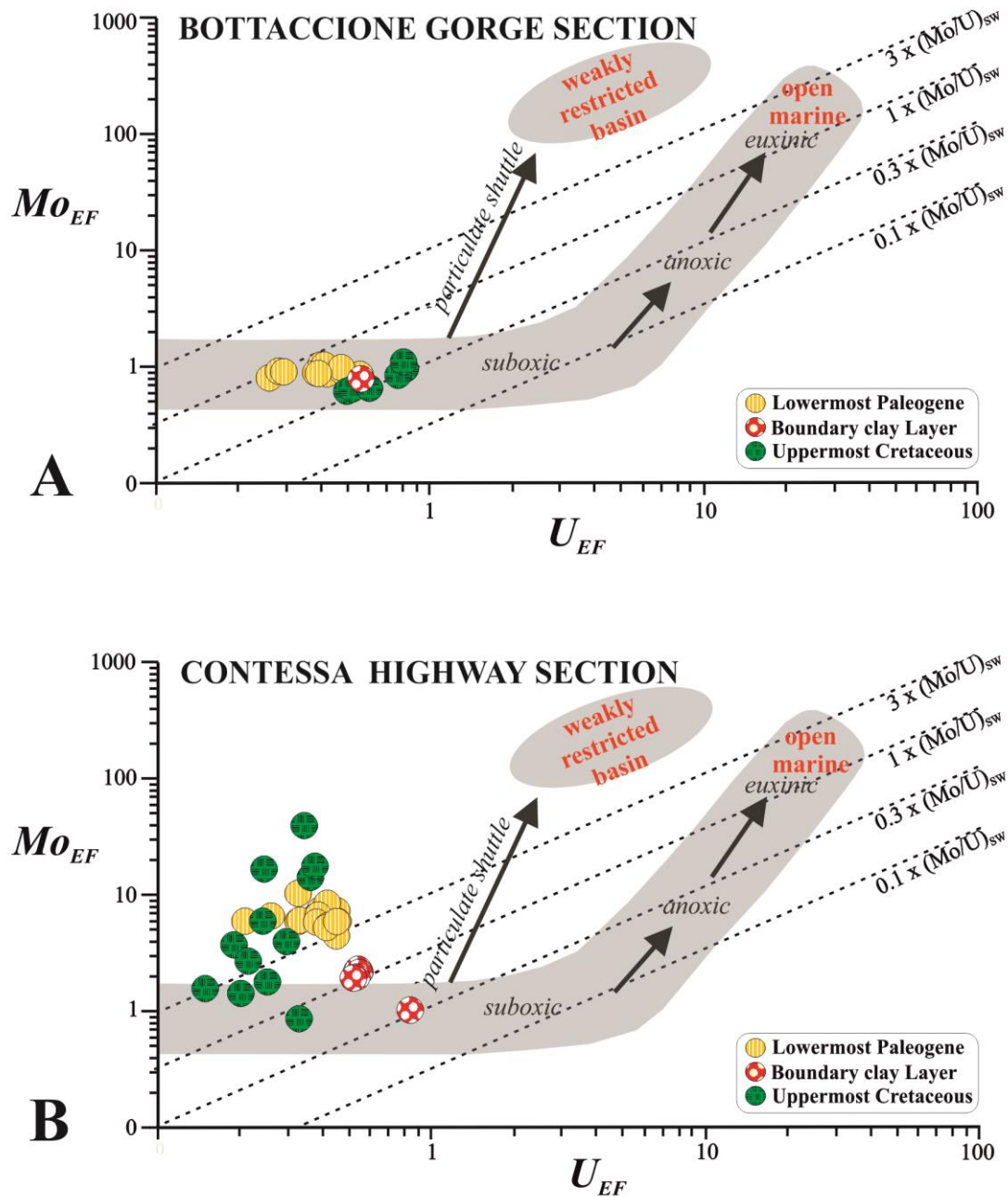
Fig. 4.5. Mo_{EF} vs U_{EF} covariation. Mo_{EF} vs U_{EF} covariation for the Cretaceous–Paleogene (K/Pg) boundary sections at the Bottaccione Gorge (A) and the Contessa Highway (B). Samples were normalized using post-Archean average shale (PAAS) compositions (Taylor and McLennan, 1985). Enrichment factors (EF) were calculated as:

$$X_{EF} = \left[\frac{\left(\frac{X}{Al} \right)_{sample}}{\left(\frac{X}{Al} \right)_{PAAS}} \right]$$

Where, X and Al represent the weight percentage concentrations of elements X and Al, respectively.

Only locally at the Bottaccione section, the slight enrichment of redox sensitive elements (V, Cr, Co) observed in the lowermost Paleogene points to less oxygenated conditions. Meanwhile, significant increases in the Zn/Al and Mo/Al ratios are observed in the first few centimeters of the lowermost Paleogene. According to their exclusive record in the Bottaccione section, such increases are interpreted as a consequence of local factors determining particular changes in oxygenation conditions, due to variations in ocean dynamics controlled by the paleogeography of the corresponding depositional settings — i.e., estimated paleodepth of 1,500-2,500 m at Bottaccione (Coccioni et al., 2010; Galeotti et al., 2004b; Giusberti et al., 2009), and 1,000-1,500 m at Contessa (Coccioni et al., 2012).

The benthic foraminifera also supports oxygenation prior to and immediately after the impact at different distal sections (i.e., Alegret, 2007; Alegret et al., 2003; Galeotti et al., 2004; Macleod et al., 1997). In fact, the benthic foraminifera did not suffer significant extinction (~10%) at the K/Pg boundary, but show transient assemblage changes and decreased diversity (Alegret and Thomas, 2013).

Regarding the detrital input, a slight enrichment in REE contents in the lowermost Paleogene points to a slight increase in detrital input after the impact that could be related with the greater chemical alteration of continental areas after the impact. Such changes are also indicated by magnetic susceptibility (MS) data, which support variations in the terrigenous dust input in the pelagic deep marine environment. The availability and transport of dust could have been influenced by variations in the vegetation cover on the Maastrichtian-Paleocene African or Asian zones as reported by Sinnesael et al. (2016).

With respect to the isotope composition, the $\delta^{13}C$ was not significantly affected by diagenetic overprint (Sprovieri et al., 2013), and except for the boundary excursion (Corfield et al., 1991; Voigt et al., 2012; Zachos and Arthur, 1986), it evidences minor changes across the K-Pg transition. The similar $\delta^{13}C$ values, with only minor changes from the uppermost Maastrichtian to the lowermost Paleogene materials (including the boundary clay layer and the red micritic limestone), also point to a rapid recovery of paleoenvironmental conditions. In fact, recent works provide evidence of a more rapid productivity recovery than traditionally considered, meaning the biological pump was less severely affected and for a shorter duration (Alegret et al., 2012; Alegret and Thomas, 2009; Birch et al., 2016; Esmeray-Senlet et al., 2015; Schueth et al., 2015; Sepúlveda et al., 2009).

Recent ichnological analysis reveals that the trace fossil assemblage shows no significant differences below and above the K/Pg boundary (Monaco et al., 2015). Dark sediment infilled traces registered in the white limestones of the uppermost Maastrichtian suggest tracemaker colonization from the Danian dark clay layer, cross-cutting the K/Pg boundary (Monaco et al., 2015).

Furthermore, the comparison of isotope data from the infilling material of trace fossils and the host sediment in the K-Pg transition at the Agost section (Spain) has shed light on the relationship between the isotopic values of the dark filling materials of traces registered in the uppermost Maastrichtian sediments and those corresponding to the lowermost Danian (Rodríguez-Tovar et al., 2006, 2004). Accordingly, distinct phases of colonization, pre-, syn-, and post-K/Pg boundary, were interpreted. Redistribution of material by

tracemakers throughout diverse distal sections of the K/Pg boundary at Bidart (France) and Caravaca (Spain), involving microfossils (calcareous nannoplankton, benthic foraminifera), has also been recognized (Alegret et al., 2015; Kędzierski et al., 2011; Rodriguez-Tovar et al., 2010; Rodríguez-Tovar and Uchman, 2008). At the studied sections, the comparison of the carbon isotope composition shows similar values for the infilling material of the trace fossils and for the host material in both the uppermost Maastrichtian and lowermost Danian deposits at the Contessa Highway section. This could point to nearly coetaneous bioturbation during sediment deposition. The similar isotopic composition agrees with the active infilling material (introduced by the tracemaker) of most of the studied traces from the uppermost Maastrichtian rocks (i.e., *Planolites*, *Taenidium*). The few exceptions, corresponding to the infilling of *Thalassinoides* registered in Danian rocks from the Bottaccione section (Fig. 4.4), agree with their passive infill (material entering the burrow gravitationally, without the active involvement of the tracemaker).

Therefore, our data support that the rate of oxygenation, nutrient availability and sedimentary input conditions are similar in the deposits from the uppermost Cretaceous and the lowermost Paleogene, so that the reestablishment of the oxygenated conditions and productivity would have occurred immediately after the deposit of the ejecta layer or instantly on a geological time scale (e.g., Sosa-Montes de Oca et al., 2013). Moreover, the paleoenvironmental reconstruction obtained from geochemical proxies fits the framework provided by ichnological data obtained from the Bottaccione Gorge section (Monaco et al., 2015). The sudden disappearance of the tracemaker community above the K/Pg boundary, between 6 and 9 cm, observed in the previous ichnological analysis (Monaco et al., 2015) was tentatively attributed to changes in the flux of food to the deep-sea floor and decreasing oxygenation. As indicated by the geochemical proxies studied here, this sudden disappearance of trace fossils is therefore most likely related to lower oxygenation and an increase in detrital input conditions.

4.6. Conclusions

Geochemical and isotopic analyses conducted on the infilling of trace fossils and the host sedimentary rocks in the Cretaceous-Paleogene boundary transitions at the Bottaccione Gorge and the Contessa Highway sections (Gubbio region, Italy) provide important information about the paleoenvironmental conditions after the K/Pg boundary event. Although the ejecta layer is absent at the studied sections due to oversampling during the last few decades, the preserved lowermost Danian recorded by the red boundary clay layer and the red micritic limestone still records the post-impact event conditions.

No major changes in the enrichment/depletion profiles of redox sensitive and detrital elements were registered in the uppermost Maastrichtian and lowermost Danian deposits. This can be interpreted as evidence of similar paleoenvironmental conditions (oxygenation, nutrient availability, and/or sedimentary input) prior to and after the K/Pg event, owing to a rapid reestablishment of environmental conditions (of the order of 10^2 years), almost instantly on a geological time scale.

Carbon isotope data show similar values for the infilling material of trace fossils and those of the host rocks at the corresponding depth. This is interpreted as revealing a nearly coetaneous bioturbation during sediment deposition. In general, the obtained data agree with a fast recovery of productivity patterns.

Acknowledgments

Chapter 5

APPLICATION OF LASER ABLATION-ICP-MS TO DETERMINE HIGH-RESOLUTION ELEMENTAL PROFILES ACROSS THE CRETACEOUS/PALEOGENE BOUNDARY AT AGOST (SPAIN)

Claudia Sosa-Montes de Oca [a]*, Gert J. de Lange [b], Francisca Martínez-Ruiz [c], Francisco J. Rodríguez-Tovar [a]

[a] Departamento de Estratigrafía y Paleontología, Universidad de Granada, Avda. Fuentenueva s/n, 18002 Granada, Spain

[b] Department of Earth Sciences–Geochemistry, Geosciences, Utrecht University, 3584 CD, Utrecht, The Netherlands

[c] Instituto Andaluz de Ciencias de la Tierra, IACT (CSIC-Universidad de Granada), Avda. Las Palmeras 4, 18100 Armilla, Granada, Spain

Contents lists available at ScienceDirect

Palaeogeography, Palaeoclimatology, Palaeoecology

journal homepage: www.elsevier.com/locate/palaeo

Application of laser ablation-ICP-MS to determine high-resolution elemental profiles across the Cretaceous/Paleogene boundary at Agost (Spain)

Claudia Sosa-Montes de Oca[a,*], Gert J. de Lange[b], Francisca Martínez-Ruiz[c], Francisco J. Rodríguez-Tovar[a]

[a] Departamento de Estratigrafía y Paleontología, Universidad de Granada, Avda. Fuentenueva s/n, 18002 Granada, Spain
[b] Department of Earth Sciences–Geochemistry, Geosciences, Utrecht University, 3584 CD, Utrecht, The Netherlands
[c] Instituto Andaluz de Ciencias de la Tierra, IACT (CSIC-Universidad de Granada), Avda. Las Palmeras 4, 18100 Armilla, Granada, Spain

"True wisdom comes to each of us when we realize how little we understand about life, ourselves and the world around us"

— Socrates (470-399 B.C)

ABSTRACT

A high-resolution analysis of the distribution of major and trace elements across a Cretaceous/Paleogene boundary (KPgB) was done using Laser Ablation-Inductivity Coupled Plasma-Mass Spectrometry (LA-ICP-MS) and was compared with traditional distinct sampling and analysis. At the Agost site (SE Spain) a 22-cm-long core containing the KPgB was recovered using a Rolatec RL-48L drill. Within this interval, the lowermost 5 cm correspond to the Maastrichtian and the uppermost 17 cm to the Danian. The core section was resin-embedded under O_2-free conditions, cut and polished for LA-ICP-MS continuous measurements with 10 μm increments and a laser-beam of 80 μm. Elemental concentrations in discrete samples taken prior to embedding from the same core interval were determined by Inductivity Coupled Plasma-Optical Emission Spectroscopy (ICP-OES). The LA-ICP-MS analyses in continuous mode considerably improve the resolution of geochemical profiles, allowing the compositional variability at a micrometer scale within the ejecta layer to be detected. In this study, we obtained profiles with 255 data points for the ejecta layer interval compared to 3 data points obtained by traditional manual sampling and ICP-OES analyses. Yet our recovered core section showed a rather limited preservation of the ejecta layer. This paper focuses on the presentation of LA-ICP-MS analysis as a particularly useful tool to investigate paleoenvironmental changes associated with bio-events. Additionally, the high-resolution of major and trace elemental distribution made it possible to study remobilization across thin but distinct boundaries such as the KPgB.

Keywords: LA-ICP-MS, resin-embedding, KPgB; ejecta layer, bio-events, trace-element remobilization

5.1. Introduction

Appropriate analytical resolution is crucial for paleoenvironmental studies based on geochemical proxies, in particular for those involving lithological boundaries as is the case of the KPgB. In general, data resolution has increased in recent decades in the wake of advanced capabilities and new analytical techniques. One of these new techniques is LA-ICP-MS (e.g., Sylvester and Jackson, 2016). This set-up combines novel developments over the past 30 years, involving laser ablation systems and elemental analytical methodologies at sub-mm resolution. As a result, LA-ICP-MS permits high-resolution elemental analysis including several continuous diagnostic trace elements at the sub-mm scale. LA-ICP-MS has been successfully applied in different scientific fields, such as: detailed analysis of natural rock systems (Jenner and Arevalo, 2016); microanalysis of fluid inclusions in hydrothermal systems (Wagner et al., 2016); and high-frequency variability in unconsolidated Holocene sediments (Jilbert et al., 2008).

The technique therefore allows high-resolution analyses within layers of sub-mm thickness, as is the case for the KPgB at distal sections (Urrutia-Fucugauchi and Pérez-Cruz, 2016). This boundary, dated at 66.04 ± 0.02 Ma (Renne et al., 2013), has been widely studied (Goderis et al., 2013; Schulte et al., 2010b), and its link to a meteorite impact broadly demonstrated (Alvarez et al., 1980; Schulte et al., 2010b; Smit and Hertogen, 1980). The impact caused major environmental changes (e.g., Kring, 2007; Wilf et al., 2003), including an impact winter (Brugger et al., 2017; Vellekoop et al., 2014; Woelders et al., 2017), followed by global warming (Vellekoop et al., 2016, 2014) and ocean acidification (e.g., Alegret et al., 2012; Alegret and Thomas, 2005; Peryt et al., 2002). In addition, it produced tsunamis and related deposits not only in the immediate vicinity of the Chicxulub impact area (Shonting and Ezrailson, 2017), but also at sites as distal as Argentina -(Scasso et al., 2005), Bulgaria -(Preisinger et al., 2002), Croatia -(Korbar et al., 2015), and The Netherlands -(Brinkhuis and Smit, 1996)

Major geochemical anomalies, recognized worldwide, characterize this boundary in both marine and continental depositional environments (Goderis et al., 2013). The extraterrestrial contribution is particularly evident in the ejecta layer of marine distal sites, located more than 4,000 km away from the Chicxulub impact crater (Goderis et al., 2013; Smit, 1999; Urrutia-Fucugauchi and Pérez-Cruz, 2016). In contrast, at marine proximal or intermediate sites, located closer to the impact site —such as Blake Nose (Martínez-Ruiz et al., 2001) or Demerara Rise (Berndt et al., 2011)— the extraterrestrial metal contribution is highly diluted by target rocks.

Recently, LA-ICP-MS analysis was used to studied the geochemistry and textural characteristics of glass spherules in proximal (Belza et al., 2015; Ritter et al., 2015) and distal sites (Belza et al., 2017) and LA-ICP-MS analyses have furthermore been undertaken in intermediate sites of KPgB (Berndt et al., 2011; Loroch et al., 2016), but merely oriented towards the analysis of individual spots, not in the continuous high-resolution laser mode as used here.

The Agost site (SE Spain) is one of the best-preserved and well-exposed marine distal settings of the KPgB (Macleod and Keller, 1991). It has been intensely studied because of its exceptional, expanded and continuous sedimentary record across the KPgB, i.e. without a hiatus (Molina, 2015; Rodríguez-Tovar et al., 2006). Hence, the Agost site is ideal for high resolution studies.

Nevertheless, appropriate high-resolution sampling is a challenge across the KPgB, due to the nature of the deposit, being a consolidated Maastrichtian gray calcareous marlstone and marlstone followed by the loose and unconsolidated ejecta layer and boundary clay, overlain by Danian light marly limestones. Furthermore, the thickness (millimetric scale) of the ejecta and boundary clay layers makes the in-tact sampling of a section containing all units extremely difficult. For this study, the KPgB at the Agost site was drilled using a Rolatec RL 48 L drilling machine.

We present here the first high-resolution continuous analysis (µm-scale) of Ca/Al, P/Al, Sr/Al, Ti/Al, Cr/Al, Co/Al, Cu/Al, Zr/Al, Pb/Al and U/Al ratios using LA-ICP-MS after resin embedding across the KPgB at Agost. The results of our novel methodology are compared with those obtained by means of traditional sampling and ICP-OES analysis, and show how sub-mm peaks remain undetected by traditional analysis. Such peaks are potentially diagnostic for diverse processes including diagenesis.

5.2. Geological setting

The KPgB distal section of Agost (38º27´3.31´N; 0º-38´-9.71´´E), located at km 9 on the west side of road CV-827, north of the town of Agost, Alicante (Spain), at 372.3 m altitude, was drilled for a high resolution study (Fig. 5.1).

The Agost site was at a distance of 5600 km from the Chicxulub impact structure at the time of deposition and is thus considered a distal section (e.g., Goderis et al., 2013; Urrutia-Fucugauchi and Pérez-Cruz, 2016); it is thought to represent a paleo-deposition depth of~600-1000 m (Alegret and Thomas, 2013; Smit, 1990), an upper-middle-bathyal environment similar to or slightly shallower than that proposed for the nearby Caravaca site.
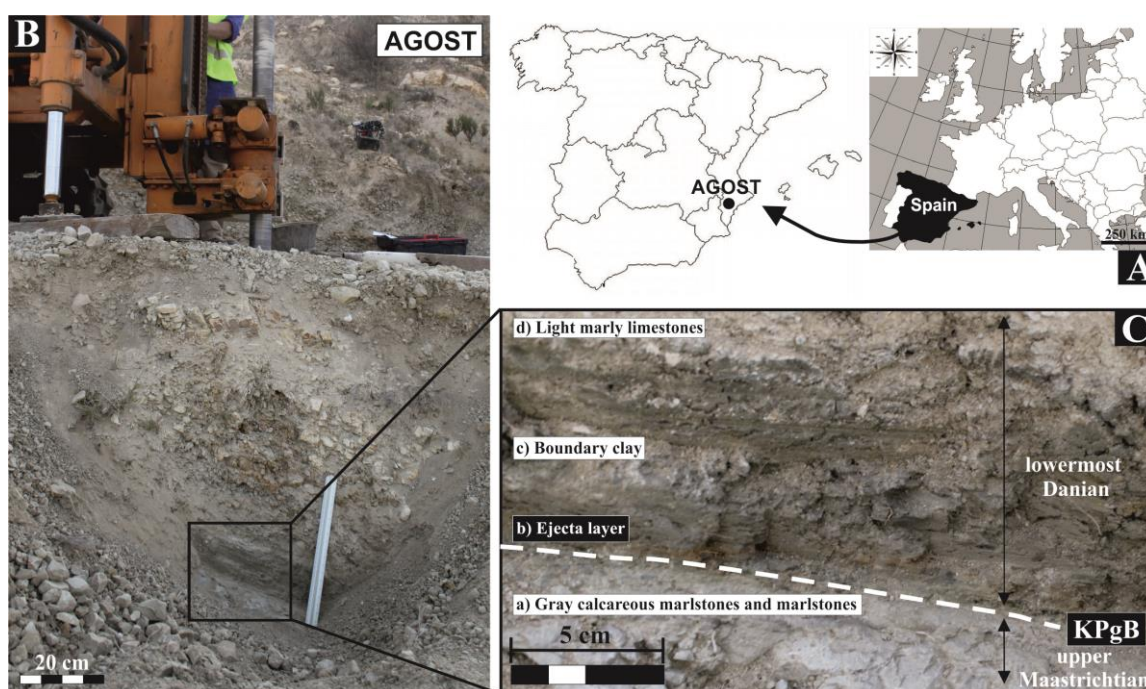
Fig. 5.1. Agost outcrop. A) Location of the Cretaceous-Paleogene transitions (KPgT) at Agost site (Alicante, Southeast Spain). B) Close photographs during drilling. C) The Agost KPgT comprises by: (a) gray calcareous marlstones and marlstones from the uppermost Maastrichtian, (b) 2-3 mm thick ejecta layer, (c) blackish-gray boundary clay layer and (d) the light marly limestones, the last three belonging to the lowermost Danian.

In ascending order, the Agost Cretaceous-Paleogene transition comprises: (a) the Cretaceous sediments that consist of gray calcareous marlstones and marlstones from uppermost Maastrichtian age, overlain by Paleogene sediments that include: (b) the 2-3-mm-thick red clay (the ejecta layer), (c) a blackish-gray clay layer (the boundary clay) that has gradually increasing carbonate contents, related with the recovery of biological productivity, giving way to the typical (d) light marly limestones from the lowermost Danian age (Fig. 5.1). The ejecta layer, marking the sharp contact between the Maastrichtian and Danian (KPgB), contains impact evidence such as spherules, Ir and other platinum-group element anomalies as well as enhanced concentrations of further trace elements such as Cr, Co, Ni, Cu, Zn, As and Sb. In addition, this interval registers a significant decline in planktonic $\delta^{13}C$ values, related to the decrease in primary productivity, and a decrease of $\delta^{18}O$ values related to Tª variations (Goderis et al., 2013; Schulte et al., 2010; Smit, 1990).

The Agost site has been broadly studied in terms of mineralogical (i.e. Ortega-Huertas et al., 2002, 1995), geochemical and isotopic composition (i.e. Ibáñez-Insa et al., 2017; Martínez-Ruiz et al., 1999; Ortega-Huertas et al., 1995, 1994, Rodríguez-Tovar et al., 2006, 2004), ichnological analysis (Laska et al., 2017; Rodríguez-Tovar, 2005; Rodríguez-Tovar and Uchman, 2004a, 2004b) and biostratigraphical studies, based on planktonic and benthic foraminifers (i.e. Arenillas et al., 2004; Arz et al., 2000; Canudo et al., 1991; Molina, 2015; Molina et al., 2005, 1998, 1996).

5.3. Materials and methods

5.3.1. Coring

Due to the difficulty in recovering a fresh/unexposed and in-tact sample of the full KPgB interval, containing the 4 parts mentioned above, from the uppermost Maastrictian to the lowermost Danian, a bore hole was drilled to obtain a core with the complete transition. It was recovered using a Rolatec RL 48 L drilling machine with rubber tracks from the Center for Scientific Instrumentation (CIC), University of Granada, Spain (Fig.1 in data in brief, Sosa-Montes de Oca et al., 2018).

From the platform for the drilling machine, the depth to the KPgB was estimated based on a nearby excavation. Subsequently drilled was till approximately 30 cm above the boundary, and an unaltered core sample was extracted by introducing an open thick-walled sampler, and hitting this with a mallet of 63.5 kg until a maximum of 75 cm penetration (size of walled sampler). Within this sampler a PVC tube is inserted, so that our targeted sediment interval was recovered inside the PVC tube (Fig. 5.2). Once obtained, the core was sealed and stored in a cold room.

From the platform for the drilling machine, the depth to the KPgB was estimated based on a nearby excavation. Subsequently drilled was till approximately 30 cm above the boundary, and an unaltered core sample was extracted by introducing an open thick-walled sampler, and hitting this with a mallet of 63.5 kg until a maximum of 75 cm penetration (size of walled sampler). Within this sampler a PVC tube is inserted, so that our targeted sediment interval was recovered inside the PVC tube (Fig. 5.2). Once obtained, the core was sealed and stored in a cold room.

5.3.2. Resin embedding of the KPgB interval

For resin-embedding, the PVC tube containing the partly unconsolidated material was placed horizontal, and a strip of the PVC was carefully cut and removed (Fig. 5.2A). Discrete samples were taken for ICP-OES analyses. As PVC does not resist the attack with acetone needed for the resin-embedding, the core was enforced using 0.2 mm aluminum foil. To do so, first the exposed sediment was covered with a teflon mesh (dimensions 240 x 30 mm) and perforated aluminum foil (dimensions 240 x 30 mm) (Fig. 5.2B), and finally all was covered with perforated aluminum foil (dimensions 240 x 190 mm), fixing it with wires (Fig. 5.2C).
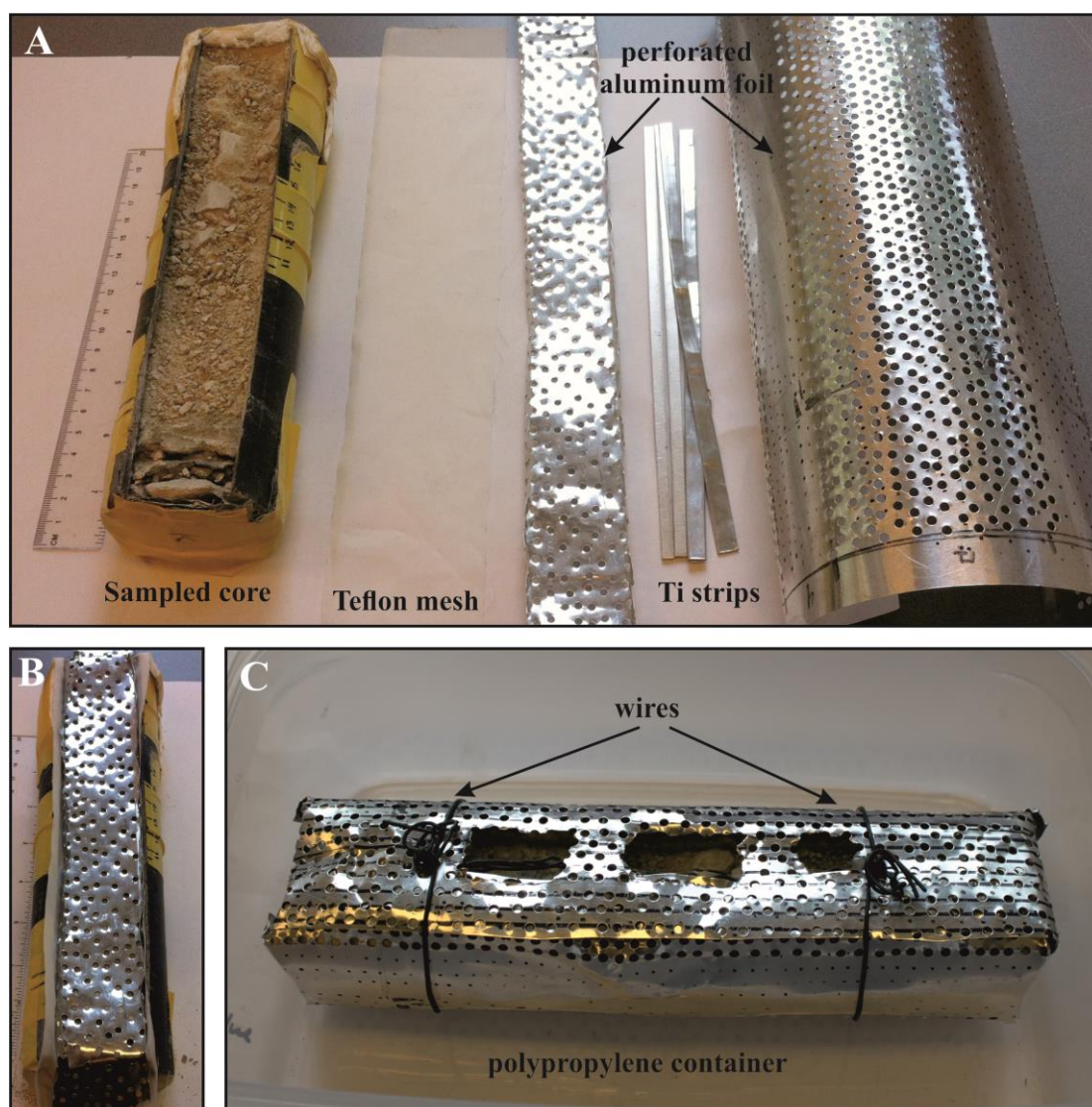
Fig. 5.2. Material used in the preparation of the core prior to the resin embedding process.

Spurr Epoxy Resin was used for resin embedding (see Jilbert et al., 2008), through which we not only preserve redox-sensitive elements, but also maintain the material structure. All the processes were performed in an argon-filled glove box during 32 days, in two different stages. The first was with acetone alone, for 5 consecutive days. To this end, 2 liters of oxygen-free acetone were used, changing them every 24 hours and keeping the core always submerged (Fig. 2 in data in brief, Sosa-Montes de Oca et al., 2018). At the same time and also inside the anoxic glove box, small pieces of PVC were immersed in a small batch of acetone to analyze the potential contamination this might produce. The contamination was tested with ICP-OES analyses, and appeared to be insignificant. The second stage entailed Spurr Epoxy Resin exchange (Table 5.1) during 27 days, in which 4 sub-steps were differentiated: Step 1: using a mixture of acetone and resin (3:1; 75% acetone: 25% resin) for 7 days. Step 2: using a mixture of acetone and resin (2:1; 66% acetone: 33% resin) for 7 days. Step 3: using a mixture of acetone and resin (1:1; 50% acetone: 50% resin) for 7 days. By last, step 4: using pure Spurr Epoxy Resin for 6 days. All exchanges were done using syringes with the core remaining undisturbed inside the bath.

Table 5.1. Components of formulations of Spurr epoxy resin and relative masses.

Spurr epoxy resin	Code	Relative mass
Cycloaliphatic epoxide resin	ERL 4221	16.4
Diglycidal ether of polypropyleneglycal	DER 736	5.72
Nonenyl succinic anhydride	NSA	23.6
Dimethylaminoethanol	DMAE	0.40

After that, the core was removed from the glove box, put into the oven for cure and drying during 48 hrs at 60º C, and finally the solid resin core was cut perpendicular to the sedimentation plane (Fig. 3 in data in brief, Sosa-Montes de Oca et al., 2018). The surface was polished and cut to form 5 overlapping arrays (~5 cm), which were analyzed using LA-ICP-MS line-scan analysis (see Fig. 5.3).
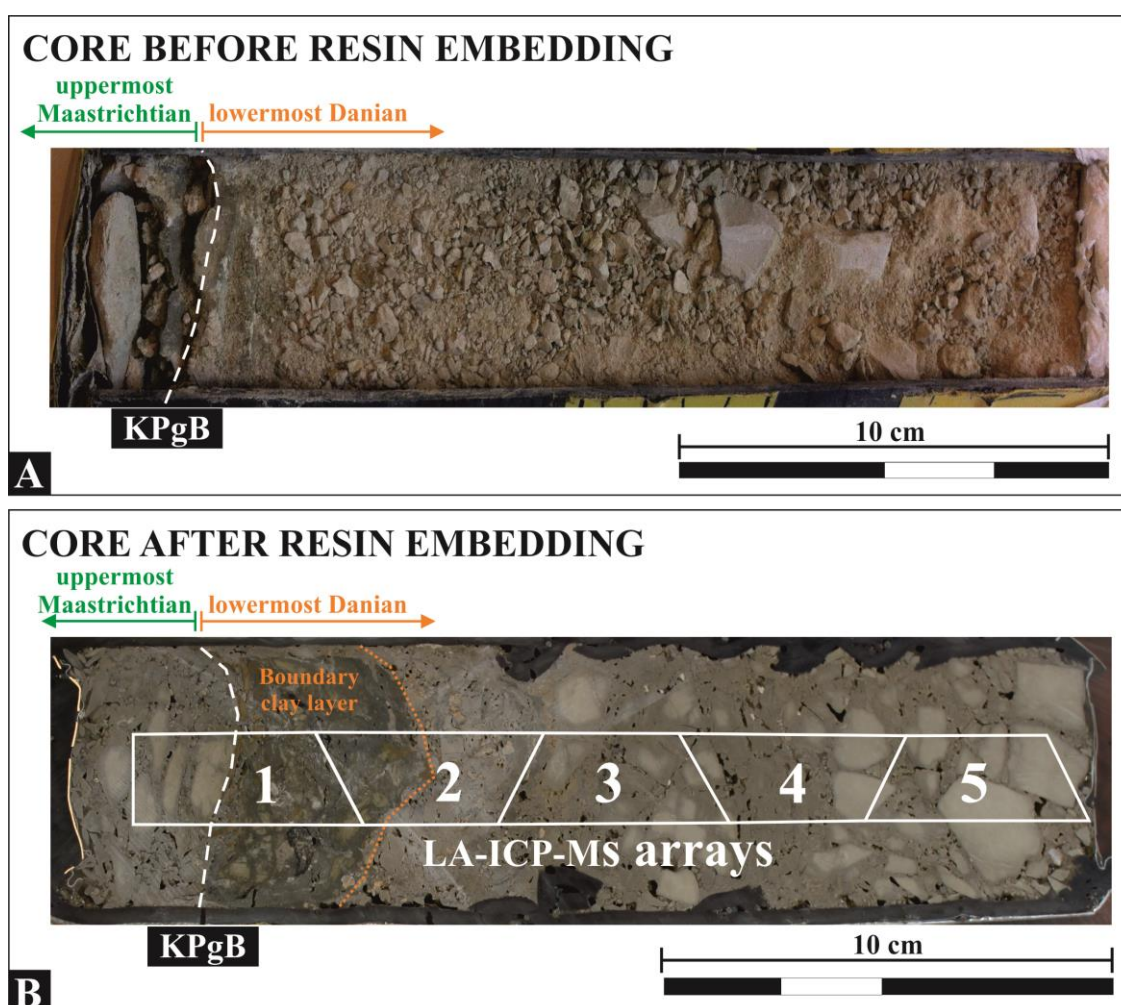
Fig. 5.3. Close photographs of studied core before and after resin embedding process. i) Core before resin embedding consolidation (Fig 5.3A). ii) Core after resin embedding consolidation where the arrays made for LA-ICP-MS measurements are marked (Fig. 5.3B).

5.3.3. LA-ICP-MS measurements and processing

Three line-scan analyses (a-b-c) for each of the arrays 1, 2, 3, 4 and 5 were performed. Exceptionally, for array 1, a total of 9 line-scan analyses (a-b-c-d-e-f-g-h-i) (see Fig. 5.4) were done. In this paper we report only the results from a line that includes the array 1 profile b and array 2 profile c, which was least affected by cracks. This line was of 84 mm and the measurements were taken at 10 μm steps. For that distance 4414 values were obtained, including 544 data points in the gray calcareous marlstones and marlstones from the uppermost Maastrichtian, and 3570 data points from the lowermost Danian sediments. The latter breaks down to 255 data points taken in the ejecta layer, 1827 data points taken in the boundary clay layer, and 1488 data points taken in the light marly limestones from Danian (Supplementary material in data in brief, Sosa-Montes de Oca et al., 2018).
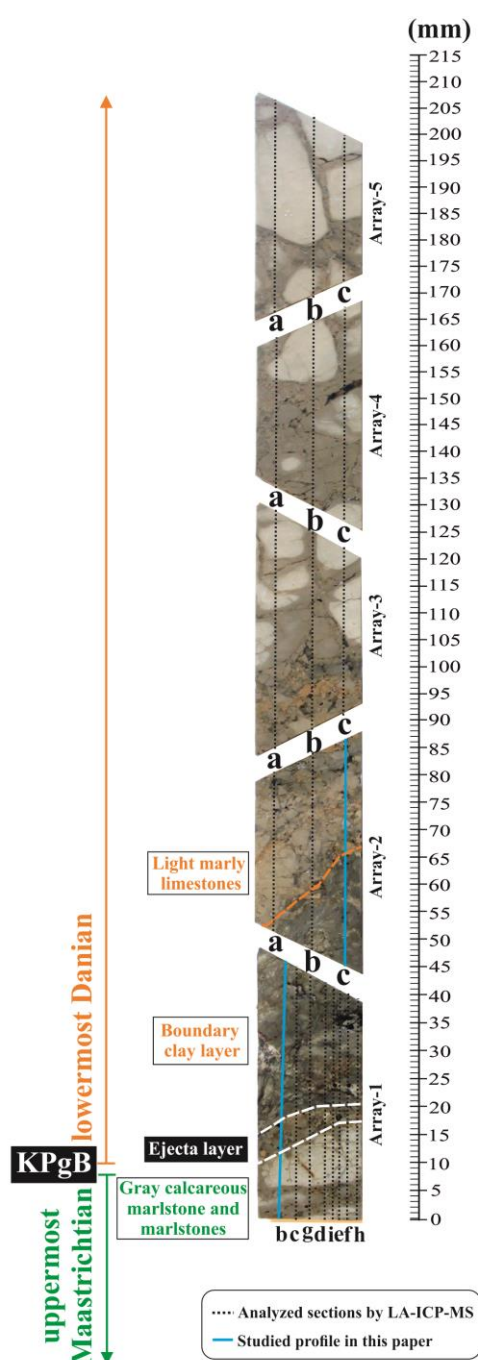
Fig. 5.4. LA-ICP-MS Profiles. Shown with dash line are all the profiles analyzed by LA-ICP-MS (Array-1, profiles b-c-d-e-f-g-h-I; array-2, profiles a-b-c; array-3, profiles a-b-c; array-4, profiles a-b-c and array-5, profiles a-b-c). With continuous blue line is the profile studied in this paper (array 1b-array 2c). (For interpretation of the references to color in this figure legend, the reader is referred to the web version of this article.).

A 193 nm wavelength COMPex 102 ArF excimer laser ablation system (Lambda Physik, Göttingen, Germany) connected to an Element 2 sector field ICP-MS (Thermo Scientific, Bremen, Germany) was used for all LA-ICP-MS analyses at the GML from Utrecht University (the Netherlands). The use of a deep ultra-violet (193 nm) laser beam has been proven to significantly reduce elemental fractionation effects during the ablation process when compared to infrared lasers (Günther et al., 1998). The ICP-MS was operated at low mass resolution ($M/\Delta M$=400) to provide optimal detection capability and sensitivity of the ICP-MS. The measurement frequency of the ICP-MS for all isotope spectra was ~2.5–3 Hz.

The 5 arrays obtained after resin embedding were analyzed and the data were processed following the procedure of Hennekam et al. (2015). In short, each array obtained was placed into a He-flushed ablation chamber for LA-ICP-MS analysis. For line-scanning the ablation chamber was moved perpendicular to the laminations of the resin-embedded arrays, at a speed of 0.0275 mm s^{-1}. The laser parameters were kept constant at a pulse repetition rate of 10 Hz, spot diameter of 80 µm, and energy density of ~8 J cm^{-2}. Laser input at the ablation site (fluence) was monitored daily before tuning the ICP-MS for optimal sensitivity following the procedure of Wang et al. (2006). The measurement frequency and scanning rate resulted in a constant shift increment of ~10 µm per measurement. When added to the laser spot diameter, this resulted in an overall sampled interval of ~90 µm per ICP-MS cycle, having 80 µm overlap with the previous and subsequent measurements.

The obtained counts were evaluated, corrected for background noise, and calibrated. First the mean background values, obtained from the mean intensities of an ~30 s interval before the start of the laser ablation measurement, were subtracted from the raw analyte intensities. Subsequently the background-corrected analyte intensities were corrected for the relative sensitivity of the specific isotope calculated by measurement of an external standard (NIST SRM610, Jochum et al., 2011), and also corrected for the natural abundance following Berglund and Wieser (2011). As the yield of ablated material varies during LA-ICP-MS, data are commonly reported as ratios of the analyzed element to an internal standard. In our case the internal standard was Al. It is important to note that LA-ICP-MS line-scanning gives qualitative data.

Final data are presented as ratios because on µm- to mm-scales no internal standard with a known concentration is available during LA-ICP-MS line-scanning of natural samples. The profiles were made with log-ratios to avoid the asymmetrical properties of normal ratios (Aitchison and Egozcue, 2005). Subsequently, data were plotted using a moving average with 5 data (in blue color) and also with 10 data (in black) (See Fig. 5.5).

As a summary, LA-ICP-MS specifications as well as elemental ratios used in this paper are indicated in Table 5.2.
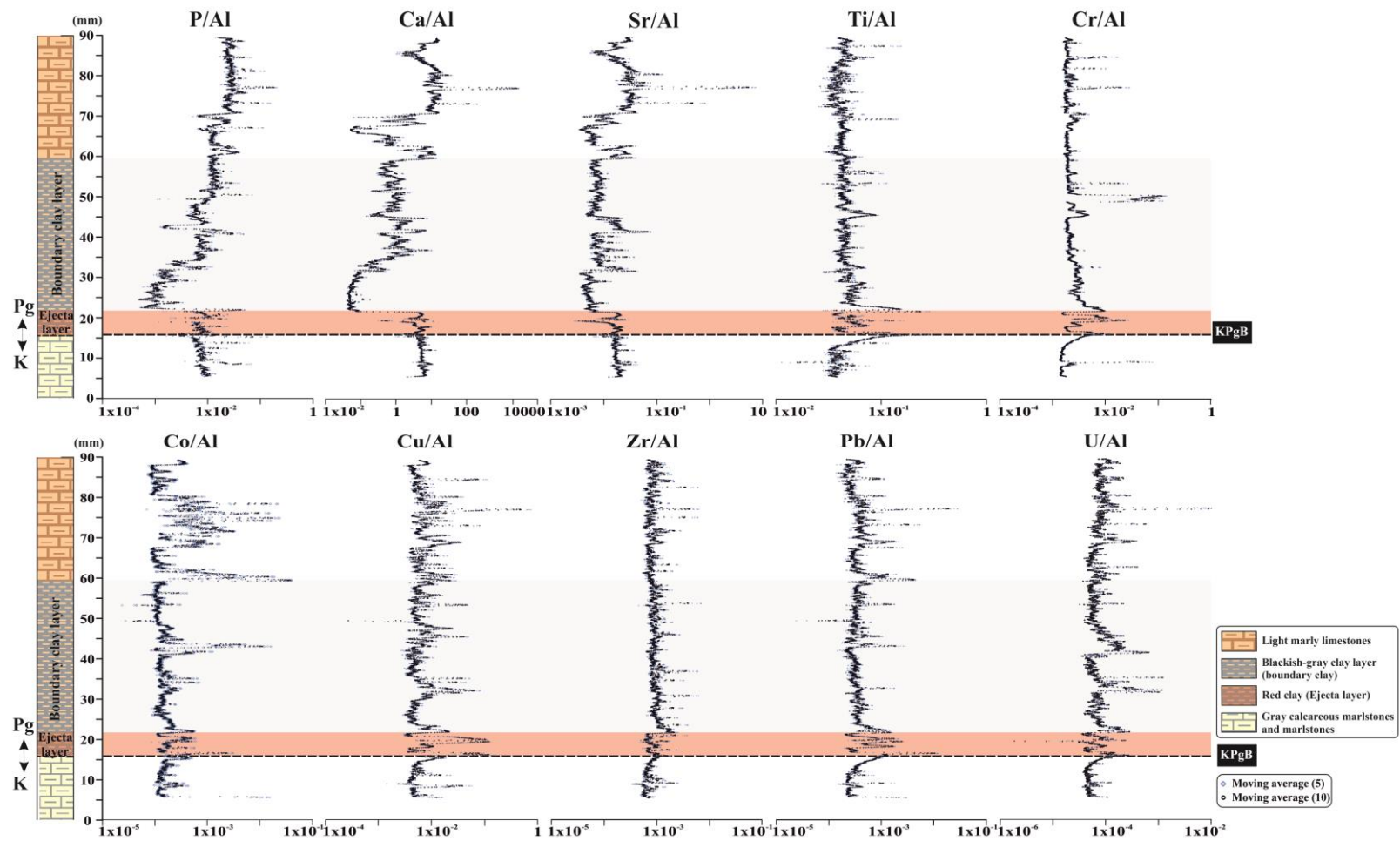
Fig. 5.5. Profiles by LA- ICP-MS. Elemental isotopic ratios measured by LA-ICP-MS across the KPgT at the Agost site. Ca/Al, P/Al, Sr/Al, Ti/Al, Cr/Al, Co/Al, Cu/Al, Zr/Al, Pb/Al and U/Al ratios; in i) the gray calcareous marlstones and marlstones from the uppermost Maastrichtian, ii) the ejecta layer, iii) the boundary clay layer and iv) the light marly limestones from the lowermost Danian.

Table 5.2. Typical LA-ICP-MS settings for measurements on resin embedded samples.

ICP-MS Type	Thermo Scientific Element 2
RF power	1300 W
Plasma gas	Ar (16.00 l min^{-1})
Auxiliary gas	Ar (0.85 l min^{-1})
Carrier gas	Ar (0.67 l min^{-1}) and He (0.75 l min^{-1})
Skimmer cone	Aluminum
Sampler cone	Nickel
Measurement frequency	~2.5–3 Hz
Resolution	Low (M/ΔM = 400)
Isotopes*	^{23}Na, ^{24}Mg, ^{25}Mg, ^{26}Mg, **^{27}Al**, ^{29}Si, **^{31}P**, **^{43}Ca**, ^{44}Ca, **^{49}Ti**, ^{51}V, **^{52}Cr**, ^{55}Mn, ^{57}Fe, **^{59}Co**, ^{60}Ni, **^{65}Cu**, ^{66}Zn, ^{75}As, ^{79}Br, ^{81}Br, **^{88}Sr**, ^{89}Y, **^{90}Zr**, ^{97}Mo, ^{98}Mo, ^{101}Ru, ^{103}Rh, **^{105}Pd**, ^{121}Sb, ^{137}Ba, ^{140}Ce, ^{185}Re, ^{193}Ir, ^{194}Pt, ^{195}Pt, **^{208}Pb**, ^{232}Th, **^{238}U**
Laser type	COMPex 102 (ArF Excimer, Lambda Physik)
Wavelength	193 nm
Fluence	8 J cm^{-2}
Spot size diameter	80 µm
Repetition rate	10 Hz
Scanning rate	0.0275 mm s^{-1}

*Elements used in this paper

5.3.4. ICP-OES analyses

Prior to resin embedding, discrete samples were taken for analysis by ICP-OES. Specifically, 55 samples were taken along 22 cm of the KPgB transition; they included 10 samples in the 5 cm of gray calcareous marlstone and marlstone from the uppermost Maastrichtian, and 45 samples in the 17 cm of the lowermost Danian sediments (Table 1 in data in brief, Sosa-Montes de Oca et al., 2018). Of the latter, 3 samples were taken in the 0.50 cm of the ejecta layer, 18 samples taken in the 4.50 cm of the boundary clay layer, and 24 samples taken in the 12.00 cm of light marly limestone. The sampling resolution rates were of 0.15 cm in the ejecta layer, 0.25 cm for the samples from the boundary clay layer, and 0.50 cm for calcareous marlstone and marlstone samples from the uppermost Maastrichtian and light marly limestone samples from the lowermost Danian.

Prior to ICP-OES analyses, samples were totally digested following routine procedures (Reitz et al., 2006). Major and minor elements were measured with a Spectro Ciros Vision ICP-OES at the Geolab of Utrecht University (the Netherlands). Analytical precision and accuracy for ICP-OES were better than 5% for the measured elements.

The sediments across the KPgB display large oscillations in carbonate content, hence Al-normalized concentrations or recalculation on a carbonate-free basis were needed to reflect oscillations in elemental content and to avoid such a 'closed sum' effect (e.g. Calvert and Pedersen, 1993; Tribovillard et al., 2006; van Os et al., 1991). The ratios analyzed using ICP-OES were P/Al, Ca/Al, Sr/Al, Ti/Al, Cr/Al, Co/Al, Cu/Al, Zr/Al, and Pb/Al (Table 1 in data in brief, Sosa-Montes de Oca et al., 2018).

5.3.5. High Resolution Scanning Electron Microscopy (HRSEM)

Textural and compositional information was also obtained from High Resolution Scanning Field Scanning Electron Microscope (HRSEM), the AURIGA from Carl Zeiss SMT. The HRSEM is located at the Center for Scientific Instrumentation (CIC), University of Granada (Spain).

The analysis by HRSEM was focused on the KPgB, explicitly on the boundary between the gray calcareous marlstone and marlstone from the uppermost Maastrichtian and the ejecta layer from the lowermost Danian.

5.4. Results and discussion

5.4.1. Technical analytical results

Geochemical data and profiles of the line (Array1b-Array2c) analyzed by LA-ICP-MS are represented in supplementary material (in data in brief, Sosa-Montes de Oca et al., 2018) and Fig. 5.5 respectively.

Geochemical data and profiles of the same core section but analyzed by ICP-OES on discrete samples are presented in Table 1 (in data in brief, Sosa-Montes de Oca et al., 2018) and Fig. 5.6 respectively.
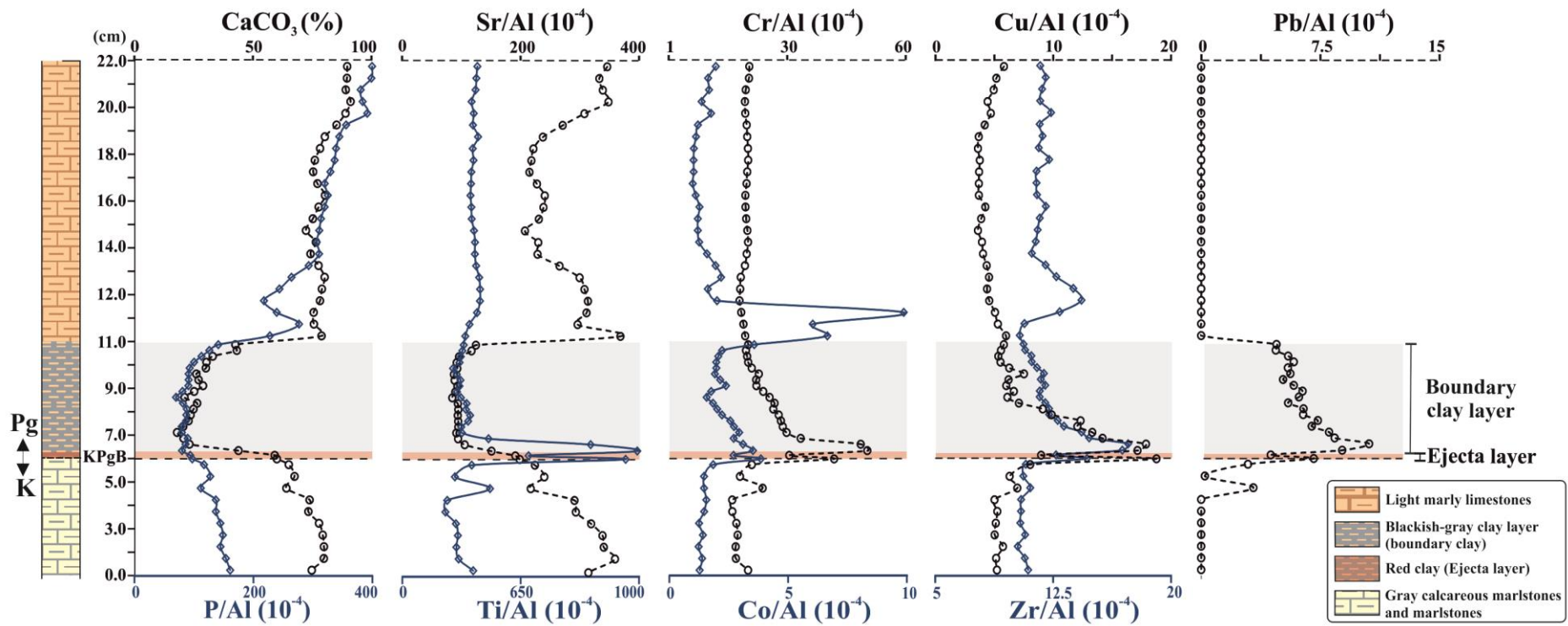
Fig. 5.6. Profiles by ICP-OES. Elemental content (major and trace) and elemental ratios, measured by ICP-OES across the KPgT at the Agost site. Al, Ca, CaO, CaCO$_3$, concentrations (%); Ca/Al and Fe/Al ratios; P/Al, Sr/Al, Ti/Al, Cr/Al, Co/Al, Cu/Al, Zr/Al and Pb/Al ratios (x 10^{-4}), in i) the gray calcareous marlstones and marlstones from the uppermost Maastrichtian, ii) the ejecta layer, iii) the boundary clay layer and iv) the light marly limestones from the lowermost Danian.

5.4.2. Comparing discrete-samples ICP-OES vs continuous LA-ICP-MS analyses

The shared interval covered by discrete sampling/ICP-OES and by continuous/LA-ICP-MS analyses is 84 mm, including 10 mm of Maastrichtian gray calcareous marlstone and marlstone, 5 mm of the ejecta layer, 38 mm of the boundary clay, and 31 mm of light marly limestone from the lowermost Danian.

The ejecta layer is commonly 0.2-0.3 mm thick at distal sections and has low carbonate content (Smit, 1999). Yet our recovered core section showed a rather limited preservation of the ejecta layer. This core disturbance became evident in the secondary electron images obtained with HRSEM (Fig. 5.7). The ejecta layer appears irregular and poorly preserved, and it contains small unaltered Maastrichtian limestone fragments. Although tsunami-generated disturbances have been reported in many distal sites (Brinkhuis and Smit, 1996; Korbar et al., 2015; Scasso et al., 2005), the consistently reported undisturbed sections at Agost do not support such process.
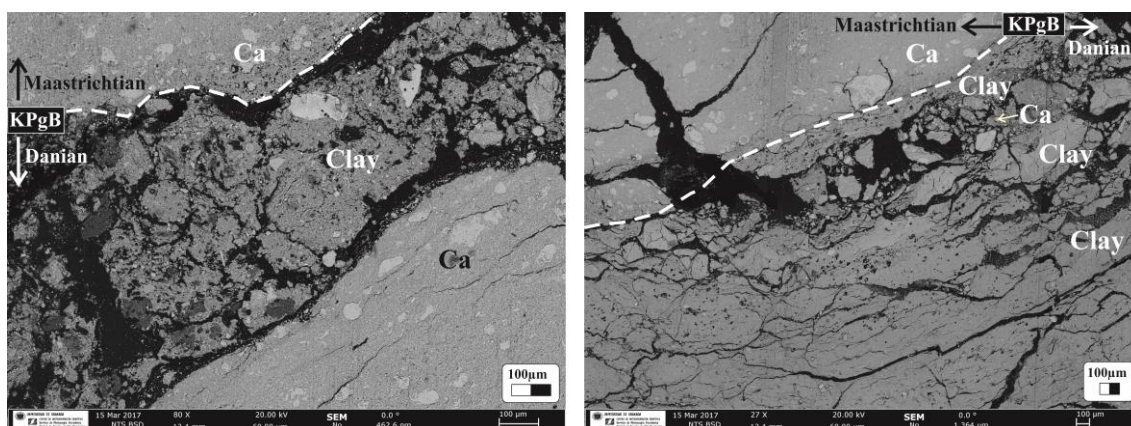
Fig. 5.7. Secondary electron images made by High Resolution Scanning Electron Microscopy (HRSEM).Visible is the fractured contact the between the gray calcareous marlstones and marlstones from the uppermost Maastrichtian and the ejecta layer from the lowermost Danian.

In the profiles of Ca/Al, P/Al and Sr/Al, a significant decrease after the ejecta layer is observed, then a slight recovery along the boundary clay, reaching values similar to those of the uppermost Maastrichtian in the light marls from the lowermost Danian. In contrast, elemental ratios as Ti/Al, Cr/Al, Co/Al, Cu/Al, Zr/Al, Pb/Al and U/Al show a clear peak at the KPgB (Fig. 5.5 and Fig. 5.6).

Specifically, when comparing the profiles obtained by both techniques (Fig. 5.8), we observe, for $CaCO_3$ (from ICP-OES Ca data) and the Ca/Al ratio analyzed by LA-ICP-MS, a maximum value of 75% $CaCO_3$ and 13 for Ca/Al ratio in the gray calcareous marlstone and marlstone from the uppermost Maastrichtian and in the light marly limestone from the lower Danian. Minimum values are observed for $CaCO_3$ (25%) and the Ca/Al ratio (0.05) at the base of the clay boundary, which gradually increases its carbonate content. Discordant data may at first sight be attributed to the difference in resolution between the two methods (Fig. 5.8).

Comparing the Ti/Al profile from ICP-OES and that from LA-ICP-MS, a large peak at the base of the ejecta layer (KPgB) was observed, but more peaks are also observed in the rest of the ejecta layer (Fig. 5.8).
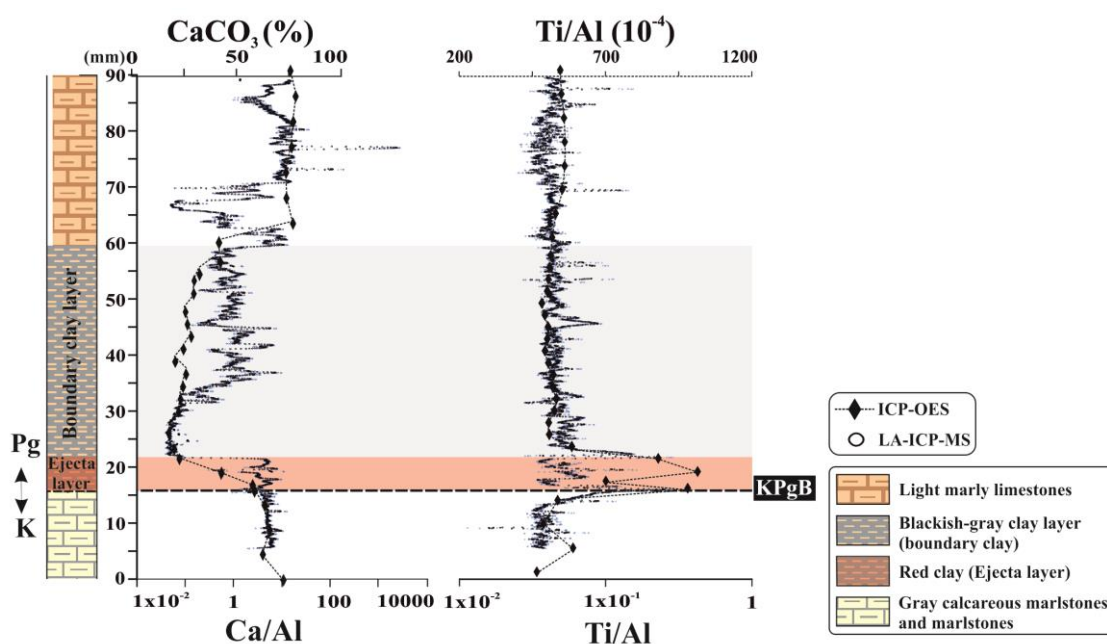
Fig. 5.8. Comparison of CaCO3 (%) analyzed by ICP-OES vs Ca/Al ratio analyzed by LA-CP-MS, and Ti/Al (10-4) analyzed by ICP-OES vs Ti/Al ratio analyzed by LA-CP-MS, both in a 9 mm interval, including: i) in the gray calcareous marlstones and marlstones from the uppermost Maastrichtian, ii) the ejecta layer, iii) the boundary clay layer and iv) the light marly limestones from the lowermost Danian.

No major changes in the profiles of redox sensitive elements such as Cr/Al, Co/Al, Cu/Al, Pb/Al and U/Al or in the profiles of detrital elements as Zr/Al were registered for the calcareous marlstone from uppermost Maastrichtian or the clay boundary from lowermost Danian. This is interpreted as evidence of similar paleoenvironmental conditions (oxygenation and/or sedimentary input) prior to and after the KPgB, owing to a rapid re-establishment of environmental conditions (Sosa-Montes de Oca et al., 2017, 2016, 2013).

Within the ejecta layer, due to its poor preservation, no clear correlation between the observed changes and the paleoenvironmental or diagenetic conditions is possible. Nevertheless, different peaks show the enormous potential of the applied methodology (LA-ICP-MS analyses in continuous mode after resin embedding) to investigate major and trace element distribution and remobilization (at sub-mm scale) across abrupt boundaries like the KPgB.

First, we compare the Cr/Al, Co/Al, Cu/Al, Zn/Al, Pb/Al and Ti/Al profiles obtained using the two techniques (ICP-OES and LA-ICP-MS), in a 3 mm interval (Fig. 5.9). Although Ni is also a typical meteorite-related element, we neither display nor discuss the Ni/Al profile, as it did not show clear peaks in this interval. Using discrete samples and the resulting limitations in sample resolution across an abrupt interval, commonly peaks of Cr,

Co, Cu, Zn, Pb and Ti are reported to occur simultaneously. This is also observed for our discrete samples analyzed by ICP-OES. However, using LA-ICP-MS analysis several peaks are observed in a sub-mm scale. Titanium is an element usually taken to be immobile, whereas elements as Pb, Cr, Cu, Co and Zn may be mobile under different redox conditions. Such fractional deposition or diagenetic mobilization of elements could be studied in the case of better preserved core material (Fig. 5.9).

The initial aim of this study was not only to demonstrate the novel high-resolution approach but also to apply this in a detailed reconstruction so as to assess the evolution of paleoenvironmental conditions (i.e., rate of oxygenation, nutrient availability, and sedimentary input). Unfortunately, an in-depth paleoceanographic interpretation of our data is not warranted. Consequently, this MS predominantly demonstrates that the applied methodology (LA-ICP-MS analyses in continuous mode after resin embedding) is adequate for advanced studies of abrupt boundaries such as the KPgB.
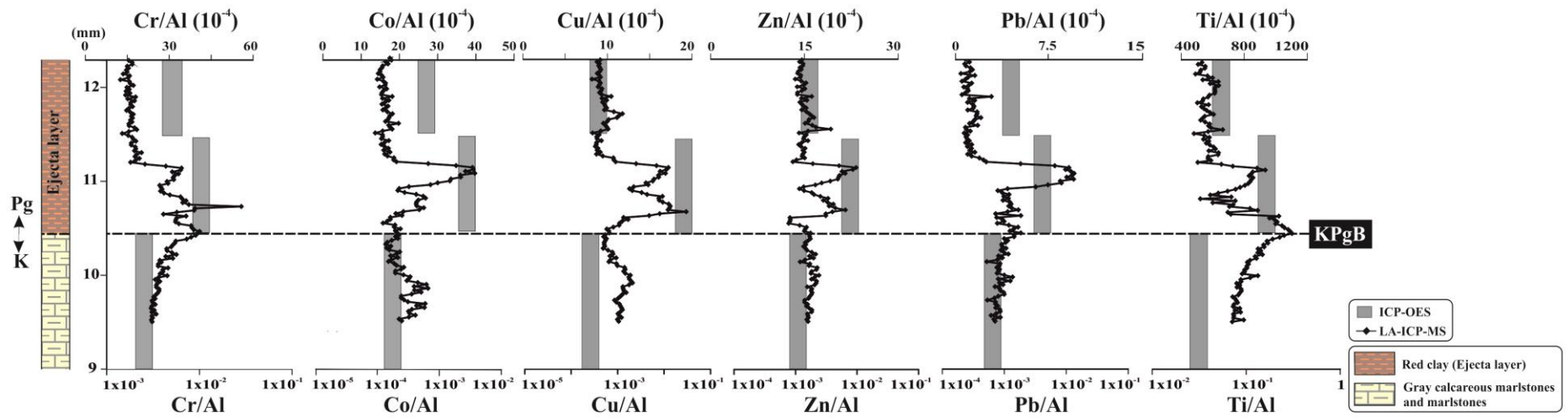
Fig. 5.9. Comparison of Cr/Al, Co/Al, Cu/Al, Zn/Al, Pb/Al and Ti/Al (10^{-4}) analyzed by ICP-OES vs the same ratios ratios analyzed by LA-ICP-MS, in a 3 mm interval, including: i) the gray calcareous marlstones and marlstones from the uppermost Maastrichtian and ii) the ejecta layer from the lowermost Danian.

The first important observation is that peaks for different elements commonly coinciding in traditional mm/cm-resolution sampling, clearly do not all coincide at μm-sample resolution. This is essential for unravelling depositional versus diagenetic processes. Impact(s) may have resulted in the sequential deposition of typical impact-related material, whereas subsequent diagenetic processes may have resulted in the mobilization and sequential deposition of certain trace elements. Such sequential (re)deposition at abrupt boundaries like the KPgB is probably limited to the sub-mm scale, for which reason high resolution tools are required to detect these processes.

5.4.3. Technical advantages provided by LA-ICP-MS

The obtained Ti-profile provides a clear example of the different capabilities of the two methodologies used here, i.e. discrete sampling followed by ICP-OES and continuous sub-mm scale analysis using LA-ICPMS. The Ti profile has a peak with a width of 1 mm by LA-ICP-MS (Fig. 5.5), while the same peak seems to cover 10 mm by ICP-OES (Fig. 5.6). Furthermore, at a sub-mm scale, the multiple peaks observed in the detailed profiles of Fig. 5.10 occur within a 1 mm interval. This can only be adequately detected using LA-ICP-MS, not using traditional discrete sampling. The obvious, main difference is the analytical resolution, being ~1 mm versus 0.09 mm. This represents, for the ~5 mm thick ejecta layer, that the amount of analytical data by LA-ICP-MS is much larger than by discrete sampling and ICP-OES: 255 versus 3 (Figs. 5.5 and 5.6). The low resolution obtained with traditional sampling, commonly limited to a resolution of 1 mm at best, could easily lead to missed or coinciding elemental peaks or other features. In contrast, the high resolution obtained with the continuous LA-ICP-MS analysis may lead to advanced and better interpretations, proving a particularly useful tool to investigate element distribution and remobilization at a sub-mm scale.

Another useful and relevant example of high resolution results by LA-ICP-MS is observed in the Pd/Al profile (Fig. 5.11). Although the detection of Pd may be influenced by some isobaric interferences, several peaks are observed within a 3 mm interval. Hence, a distinct pattern with rapid sub-mm changes can be detected at the sub-mm resolution but cannot be observed by traditional discrete sampling and subsequent analysis by ICP-OES.
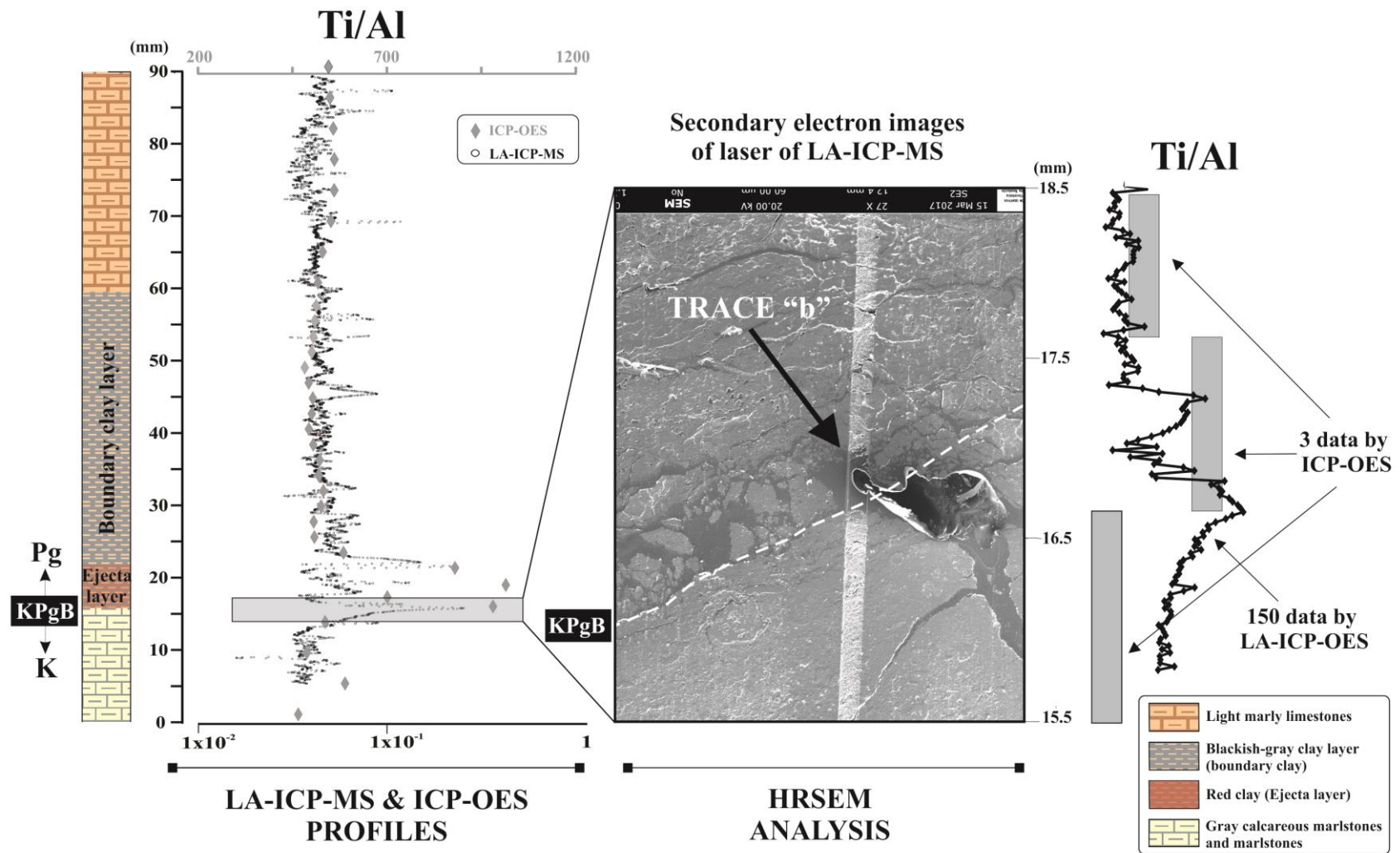
Fig. 5.10. Comparison of ICP-OES, LA-CP-MS and HRSEM.

Other interesting elements in particular for the KPgB are Pt and Ir. Yet due to their low sensitivity and the poor preservation of the ejecta layer in our core, both elements remained unquantified. The slightly enhanced level of Ir observed at the KPgB does, however, demonstrate the potential of our approach for Ir, and even more so if applied to an undisturbed KPgB with a thin but potentially more concentrated Ir-horizon. Alternatively, if remobilization of Ir, Pt, Pd or other PGE has occurred at this boundary, not only the peaks of these elements could be underestimated but also all calculation results derived from them. They include asteroid size, amount and nature of debris ejected, as well as the severe environmental effects produced. The high-resolution detection of these elements would therefore be advantageous for an adequate interpretation of all processes at the KPgB.
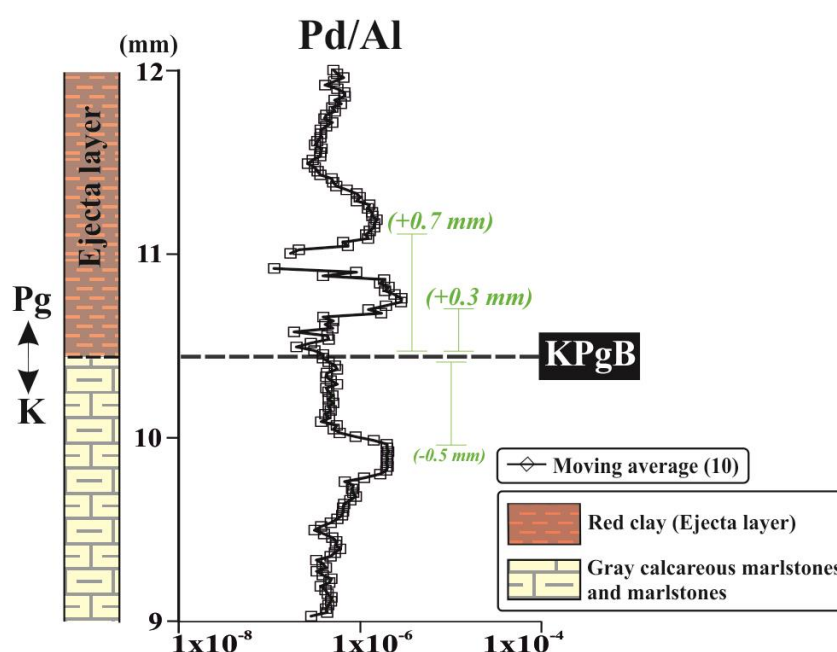
Fig. 5.11. Profile of Pd/Al ratio analyzed by LA-ICP-MS, in a 3 mm interval included in i) the gray calcareous marlstones and marlstones from the uppermost Maastrichtian and ii) the ejecta layer from the lowermost Danian.

5.4.4. Application of LA-ICP-MS to the KPgB

Despite significant diagenesis and potential remobilization of certain elements, it has been demonstrated that the KPgB preserved the original signature for a range of elements within the ejecta layer, as evidenced by PGE anomalies (e.g., Martínez-Ruiz et al., 1999; Rodríguez-Tovar et al., 2006; Smit, 1990; Smit and Klaver, 1981) and also by the extraterrestrial nature of trace elements such as Cr (Shukolyukov and Lugmair, 1998). Furthermore, as documented by previous environmental studies carried out at this boundary, the impact event was responsible for main environmental perturbations including nitric and sulfuric acid rain, widespread dust and blackout, destruction of the stratospheric ozone layer, and an enhancement of the greenhouse effect (e.g., Kring, 2007). It also led to secondary effects such as an increase in oceanic acidification (e.g., Alegret et

al., 2012; Alegret and Thomas, 2005; Peryt et al., 2002) and a decrease in the sea surface temperature (Galeotti et al., 2004a; Kaiho et al., 2016; Vellekoop et al., 2015, 2014). Because such perturbations sharply transformed depositional and ecological conditions, the reestablishment of paleoenvironmental conditions after the KPgB is of special interest in the context of evolutionary and ecological dynamics (e.g., Hull, 2015)

In general, the high resolution approach provided by LA-ICP-MS analyses, as opposed to ICP-OES (Fig. 5.10), enables researchers to verify the above information and moreover to reconstruct in detail the environmental changes associated with the recovery time of oxic conditions and productivity (Alegret et al., 2012; Alegret and Thomas, 2009; Birch et al., 2016; Esmeray-Senlet et al., 2015; Schueth et al., 2015; Sepúlveda et al., 2009; Sosa-Montes de Oca et al., 2017, 2016).

Comparing the traditional sampling done with ICP-OES analyses and the advanced approach with LA-ICP-MS, the major advance using the latter becomes evident: values for the transition from typical Maastrichtian to ejecta level are 10 mm for ICP-OES and 1 mm using LA-ICP-MS methodology. Expressed in time, and taking into account that the ejecta layer was deposited within a few days (up to a couple of weeks for the finest fractions) after the impact (Artemieva and Morgan, 2009), and that the lowermost Danian sedimentation rate is of 0.83 cm/ka (Groot et al., 1989), the 10 vs 1 mm results could indicate a somewhat different post-impact recovery time to oxic conditions (1200 versus <1 year).

In sum, analyzing an adequate and well-preserved KPgB using the high-resolution LA-ICP-MS methodology described here will help improve our knowledge of the recovery time of oxic conditions and therefore biological productivity, while also shedding new light on depositional and diagenetic processes such as the remobilization of trace elements that are potentially associated with such an abrupt boundary.

5.5. Conclusions

High resolution analyses were performed on a distal section from the KPgB at the Agost site, southeastern Spain. Results obtained by traditional sampling and ICP-OES analysis were compared with a novel methodology, using resin-embedded sediment and LA-ICP-MS continuous measurements with 10 μm increments and a laser-beam of 80 μm. Due to the largely improved analytical resolution, sub-mm variability was observed that remained undetected while using traditional discrete sampling and ICP-OES analysis. Traditional sampling may easily lead to missed or coinciding elemental peaks, whereas the high resolution obtained with continuous LA-ICP-MS analysis permits advanced interpretations. The latter is particularly useful for investigating element distribution and remobilization (at sub-mm scale) across abrupt boundaries such as the Cretaceous-Paleogene boundary (KPgB). This will not only improve our knowledge surrounding the recovery time of oxic conditions thus biological productivity, but will also be instructive about the trace-element remobilization potentially associated with an abrupt boundary. Consequently, the applied methodology (LA-ICP-MS analyses in continuous mode after resin embedding) is adequate for advanced studies of abrupt boundaries such as the KPgB,

enhancing time resolution while also detecting the distinctly different pacing of elemental peaks.

Acknowledgments

Chapter 6

MICROSCALE TRACE ELEMENT DISTRIBUTION ACROSS THE CRETACEOUS/PALAEOGENE EJECTA LAYER AT AGOST SECTION: CONSTRAINING THE RECOVERY OF PREIMPACT CONDITIONS

Claudia Sosa-Montes de Oca [a], Gert J. de Lange [b], Francisca Martínez-Ruiz [c], Francisco J. Rodríguez-Tovar [a]*

[a] Departamento de Estratigrafía y Paleontología, Universidad de Granada, Avda. Fuentenueva s/n, 18002 Granada, Spain

[b] Department of Earth Sciences–Geochemistry, Geosciences, Utrecht University, 3584 CD, Utrecht, The Netherlands

[c] Instituto Andaluz de Ciencias de la Tierra, IACT (CSIC-Universidad de Granada), Avda. Las Palmeras 4, 18100 Armilla, Granada, Spain

"Science and everyday life cannot and should not be separated"

— Rosalind Franklin. (1920-1958)

ABSTRACT

A high-resolution analysis (at sub-mm scale) of the distribution of major and trace elements across the ejecta layer marking the Cretaceous/Palaeogene boundary (KPgB) at the Agost section (SE Spain) was performed using Laser Ablation-Inductivity Coupled Plasma-Mass Spectrometry (LA-ICP-MS). The KPgB interval studied was 18 mm thick, and included calcareous marlstones from the uppermost Cretaceous, 2-mm-thick red clay (the ejecta layer) and blackish-gray clay (boundary clay layer) from the lowermost Palaeogene. The unconsolidated sediments were resin-embedded under O_2-free conditions and analyzed by LA-ICP-MS line continuous scan measurements at 10 μm increments and a laser-beam of 80 μm. LA-ICP-MS analyses at the micron scale show that the anomalous contents of trace and major elements in this boundary are restricted to the ejecta layer, which displays a relatively uniform distribution over the ≈2 mm of thickness. Trace and major elements ratios show similar values below and above the ejecta layer, supporting similar palaeoenvironmental conditions. Such an element distribution points to anomalies and anoxic conditions exclusively restricted to the ejecta deposition, hence a nearly instantaneous re-establishment of pre-impact conditions right after the impact event.

6.1. Introduction

The link between the major mass extinction associated with Cretaceous/Palaeogene boundary (KPgB) and a meteorite impact has been broadly demonstrated (Pälike, 2013; Schulte et al., 2010a). Even though a consensus now exists as to the fact that this impact entailed important short and long paleoenvironmental worldwide changes (Kring, 2007 and reference therein), questions about the timing of the re-establishment of pre-impact conditions and the recovery of biological productivity are still subjected to debate (e.g., Lowery et al., 2018; Sosa-Montes de Oca et al., 2017, 2016, 2013).

Major geochemical anomalies, recognized worldwide, characterize this boundary in both marine and continental depositional environments (Goderis et al., 2013), but the extraterrestrial contribution is particularly evident in the ejecta layer of marine distal sites, located more than 5,000 km from the Chicxulub impact crater (Goderis et al., 2013; Smit, 1999; Urrutia-Fucugauchi and Pérez-Cruz, 2016). The KPgB distal section of Agost (SE Spain) is one of the best exposed and most representative of marine sedimentation in distal areas to the Chicxulub impact site (Molina, 2015; Rodríguez-Tovar et al., 2006). This section has been broadly studied, and an exceptional KPgB section was focused on to approach high-resolution analyses.

The distribution of trace elements is crucial for any reconstruction of the palaeoenvironmental parameters associated with the impact, and especially to approach oxigenation conditions before, during and after the KPgB event. Thus, appropriate high-resolution sampling across the KPgB is a challenge, due to the different lithologies of the transition and the thickness (millimetric scale) of the ejecta and boundary clay layers.

Sosa-Montes de Oca et al. (2018) applied a novel methodology in KPgB sediment at the Agost section (Southeast Spain), which enables high-resolution LA-ICP-MS analyses in continuous mode after resin embedding, allowing preliminary conclusions about the recovery time of oxic conditions and biological productivity.

In this study, we used LA-ICP-MS in continuous high-resolution laser mode (µm-scale) after resin embedding across an intact sample of the KPgB at Agost, to obtain, for the first time, a high-resolution elemental analysis of Ca/Al, Mn/Al, Ti/Al, Cr/Al, Fe/Al, Cu/Al, Ni/Al, Zn/Al, As/Al and Sb/Al ratios within the thin ejecta layer, improving characterization of oxygen conditions related to the impact event.

6.2. Geological setting

The KPgB distal section of Agost (38º27´3.31´N; 0º-38´-9.71´´E) is located at km 9 on the west side of road CV-827, north of the town of Agost, Alicante (Southeast Spain) (Fig. 6.1). At the time of the KPgB impact, the Agost site was located in a upper-bathyal setting (~600 to 1000 m depth) (Schulte et al., 2010b), at around 27-30° N palaeolatitude (Smith et al., 1981).
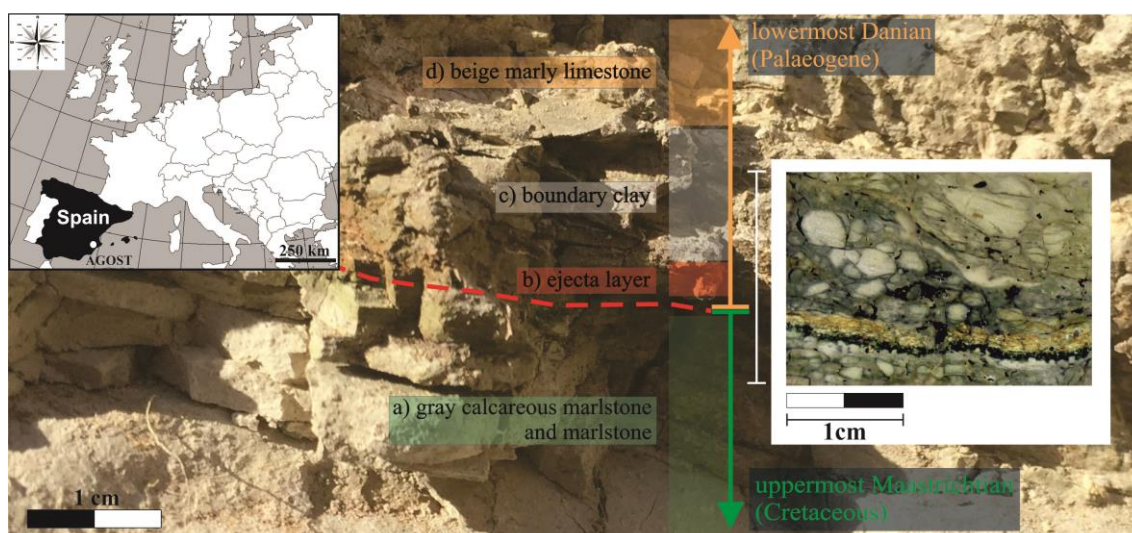
Fig. 6.1. Agost outcrop. Location of the Cretaceous-Palaeogene transitions (KPgT) at Agost site (Alicante, Southeast Spain). The studied Agost KPgT interval comprises: (a) gray calcareous marlstones and marlstones from the uppermost Maastrichtian, (b) 2-3-mm-thick ejecta layer, and (c) blackish-gray boundary clay layer from the lowermost Danian. Close photographs of the Agost resin embedding sample.

Lithologically, the Agost section comprises: (a) Cretaceous sediments consisting of gray calcareous marlstones and marlstones of late Maastrichtian age, overlain by lowermost Palaeogene sediments, including (b) the 2-mm-thick red clay (the ejecta layer), and (c) a blackish-gray clay layer (the boundary clay) (Fig. 6.1). The ejecta layer marks the sharp contact between the Maastrichtian and Danian, and contains impact evidence such as spherules, Iridium and other platinum-group element anomalies as well as enhanced concentrations of Cr, Fe, Ni, Cu, Zn, along with a significant decrease of Ca (Goderis et al., 2013; Smit, 1999).

The study focused on an 18 mm-thick interval, from which seven samples were obtained. According to the sedimentation rates of 1.98 cm Kyr^{-1} estimated for the uppermost Maastrichtian sediments, and that of 0.83 cm Kyr^{-1} calculated for the lowermost Danian sediments (Groot et al., 1989), the studied material would span a time interval from 240 years prior to the KPgB to 1300 years afterward. The deposition of the ejecta layer settled down instantly on a geological time scale, in the order of days to months (Artemieva and Morgan, 2009).

6.3. Materials and methods

6.3.1. Resin embedding Cretaceous-Palaeogene interval

The collected KPgB samples were divided in two parts; one part was reserved for ICP-OES and ICP-MS analyses, while with the other part, resin embedding treatments were conducted. For the resin embedding process, a previous reinforcement of the samples using aluminum foil (0.2 mm thickness) and Teflon mesh was undertaken. To do so, we first cut the sample edges as straight as possible and covered the bottom of the samples with Teflon mesh and perforated aluminum foil, fixing both with wires on each interval (Fig. 6.2).

Spurr Epoxy Resin for resin embedding was used (see Jilbert et al., 2008; Sosa-Montes de Oca et al., 2018a, 2018b). The duration of resin embedding depends on the dimensions of the samples. In the case study, all the processes were done in an argon-filled glove box during 26 days. The process is as follows: a) firstly, samples are treated with acetone exchange during four consecutive days; for this, 1 liter of oxygen-free acetone was used, changing every 24 hours and keeping the samples always submerged, b) secondly, samples are treated with Spurr Epoxy Resin exchange during 22 days, in which four sub-steps were differentiated: sub-step 1: using a mixture of acetone and resin 3:1 (75% acetone: 25% resin) during four days, sub-step 2: using a mixture of acetone and resin 2:1 (66% acetone: 33% resin) during four days, sub-step 3: using a mixture of acetone and resin 1:1 (50% acetone: 50% resin) during four days, and sub-step 4: using pure spurr epoxy resin during 10 days. All exchanges were done using syringes with the different intervals remaining undisturbed inside the bath, and all handling was done inside the anoxic glove box.

After that, the different samples treated were removed from the glove box and put into the oven for curing during 48 hrs at 60º C. The solid resin KPgB samples were then cut perpendicular to the bedding plane. Sample surfaces were polished and the two best samples, in which the ejecta layer is better preserved, were analyzed by LA-ICP-MS line-scan (see Fig. 6.2)
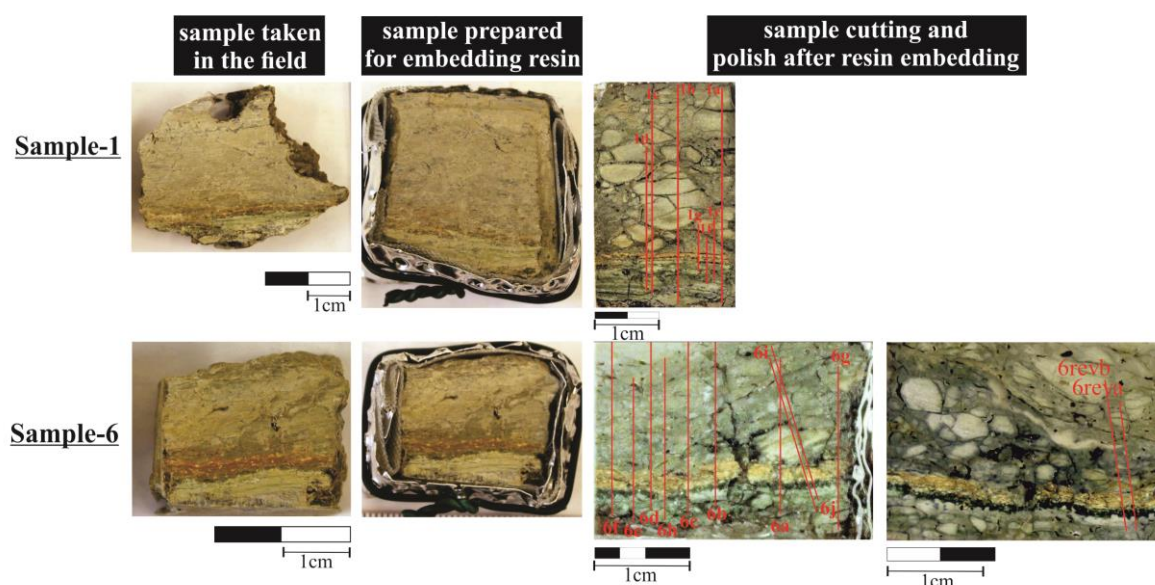
Fig. 6.2. Evolution of samples during the resin embedding process. The profiles studied in each sample (continuous red lines) are indicated in the selected resin embedding samples.

6.3.2. LA-ICP-MS measurements and processing

Samples 1 and 6 were selected for line scan analyses, because of better preservation of the ejecta layer. Therefore, 7 and 12 lines scan were respectively conducted in samples 1 and 6 (see Fig. 6.2). Each profile was between 9.20 and 14.30 mm long, and the analytical sampling was done at 10 µm steps. Between 451 and 700 values were thus obtained, including between 69 and 233 data from the gray marly limestone (uppermost

Maastrichtian), between 91 and 107 data from the ejecta layer, and between 127 and 526 data from the boundary clay layer (lowermost Danian).

A 193 nm wavelength COMPex 102 ArF excimer laser ablation system (Lambda Physik, Göttingen, Germany) connected to an Element 2 sector field ICP-MS (Thermo Scientific, Bremen, Germany) was used for all LA-ICP-MS analyses at the GML of Utrecht University (The Netherlands). The use of a deep ultra-violet (193 nm) laser beam proved to significantly reduce elemental fractionation effects during the ablation process compared to infrared lasers (Günther et al., 1998). The ICP-MS was operated at low resolution (M/ΔM=400) to provide optimal detection capability and sensitivity of the ICP-MS. The measurement frequency of the ICP-MS for all isotope spectra was ~2.5–3 Hz.

After resin embedding, samples 1 and 6 were analysed and the data were processed following the procedure of Sosa-Montes de Oca et al. (2018a, 2018b). In short, each array obtained was placed into a He-flushed ablation chamber for LA-ICPMS analysis. For line-scanning the ablation chamber was moved perpendicular to the laminations of the resin-embedded arrays, at a speed of 0.0275 mm s^{-1}. The laser parameters were kept constant at a pulse repetition rate of 10 Hz, spot diameter of 80 µm, and energy density of ~8 J cm^{-2}. Laser input at the ablation site (fluence) was daily monitored before tuning the ICP-MS for optimal sensitivity following the procedure of Wang et al. (2006). The measurement frequency and scanning rate resulted in a constant shift increment of ~10 µm per measurement. When added to the laser spot diameter, this resulted in an overall sampled interval of ~90 µm per ICP-MS cycle, having 80 µm overlap with the previous and subsequent measurement.

The mean background values were obtained from the mean intensities of a ~30 s interval before the start of the laser ablation measurement. These values were subtracted from the raw analytical intensities. The sensitivities of the isotopes were calculated by measurement of an external standard (NIST SRM 610), reference values being taken from Jochum et al. (2011); for the Au, Pd, Pt, Ir Rh, Ru, Os, we used an specific external standard (WPR-1). Subsequently, the background-corrected analytical intensities were also modified for the relative sensitivity of the specific isotope and its natural abundance taken from Berglund and Wieser (2011). Because the yield of ablated material varies during LA-ICP-MS, data are commonly reported as ratios of the analyzed element to an internal standard, in our case Al. The data are present as ratios because on µm- to mm-scales no internal standard with a known concentration is available during LA-ICP-MS line-scanning of natural samples. The final profiles were presented with log-ratios to avoid the asymmetrical properties of normal ratios (Aitchison and Egozcue, 2005). As a summary, LA-ICP-MS specifications as well as elemental ratios used in this paper are indicated in Table 6.1.

Table 6.1. Typical LA-ICP-MS settings for measurements on resin embedded samples

ICP-Ms Type	Thermo Scientific Element 2
RF power	1300 W
Plasma gas	Ar (16.00 l min^{-1})
Auxiliary gas	Ar (0.85 l min^{-1})
Carrier gas	Ar (0.67 l min^{-1}) and He (0.75 l min^{-1})
Skimmer cone	Aluminum
Sampler cone	Nickel
Measurement frequency	~2.5–3 Hz
Resolution	Low (M/ΔM = 400)
Isotopes*	^{23}Na, ^{24}Mg, ^{25}Mg, ^{26}Mg, **^{27}Al,** ^{29}Si, ^{31}P, **^{43}Ca, ^{44}Ca, ^{49}Ti**, ^{51}V, **^{52}Cr**, **^{55}Mn**, **^{57}Fe**, ^{59}Co, **^{60}Ni**, **^{65}Cu**, **^{66}Zn**, **^{75}As**, ^{88}Sr, ^{89}Y, ^{90}Zr, ^{97}Mo, ^{98}Mo, ^{103}Rh, ^{105}Pd, **^{121}Sb**, ^{137}Ba, ^{140}Ce, ^{185}Re, ^{193}Ir, ^{194}Pt, ^{195}Pt, ^{208}Pb, ^{232}Th, ^{238}U
Laser type	COMPex 102 (ArF Excimer, Lambda Physik)
Wavelength	193 nm
Fluence	8 J cm^{-2}
Spot size diameter	80 μm
Repetition rate	10 Hz
Scanning rate	0.0275 mm s^{-1}

***Elements used in this paper**

6.3.3. ICP-OES and ICP-MS analyses

Discrete samples were analyzed by ICP-OES and ICP-MS. Specifically, nine samples were taken along 2.2 cm of sample 1, and six samples were taken along 1.7 cm of sample 6.

For the geochemical analysis, samples were crushed in an agate mortar and digested with HNO3 + HF in order to obtain the sample solution. Trace element concentrations were determined using an ICP-Mass Spectrometry (NEXION 300D). Results were calibrated using blanks and international standards, with analytical precision better than ± 2% for 50 ppm elemental concentrations and ± 5% for 5 ppm elemental concentrations. The concentrations of major elements (Al, Ca, Fe, K and Mg) were measured in the same sample solutions using an ICP-Optical Emission Spectroscope (Perkin-Elmer Optima 8300) with an Rh anode X-ray tube. Blanks and international standards were used for quality control and the analytical precision was better than ± 2.76% and 1.89% for 50 ppm elemental concentrations of Al and Ca, respectively; better than ± 0.52% for 20 ppm elemental concentrations of Fe; better than ± 0.44% for 5 ppm elemental concentrations of K; and better than ± 1.48% for 2.5 ppm elemental concentrations of Mg. All the geochemical analyses were performed at the Center for Scientific Instrumentation (CIC), University of Granada, Spain.

The selected major and trace elements were normalized to Al concentrations in order to avoid a lithological effect on element content (Calvert and Pedersen, 1993; Morford and Emerson, 1999; Tribovillard et al., 2006). In particular, the KPgB sediments display large oscillations in carbonate content, hence Al-normalized concentrations (Van der Weijden, 2002) or recalculation on a carbonate-free basis were needed to reflect oscillations in elemental content. The ratios analyzed in this paper were Ca/Al, Cr/Al, Fe/Al, Ni/Al, Cu/Al, and Zn/Al.

6.3.4. High-Resolution Scanning Electron Microscopy (HRSEM)

Textural and compositional information was obtained from High-Resolution Scanning Field Scanning Electron Microscope (HRSEM), the AURIGA from Carl Zeiss SMT (Center for Scientific Instrumentation, University of Granada, Spain).

The analysis by HRSEM focused on the boundary between the gray calcareous marlstone and marlstone from the uppermost Maastrichtian and the ejecta layer from the lowermost Danian.

6.4. Results and discussion

6.4.1. Analytical results

After LA-ICP-MS measurements, all profiles were processed for both samples (seven profiles for sample 1 and 12 profiles for sample 6). Those profiles in which the ejecta layer is unaffected by cracks were selected (e.g., profile 1f in sample 1, and profiles 6reva and 6revb for sample 6). Statistic treatments were applied; syntetic average with a moving average (10) and also a composite graph (with an error of 15%) were made. Geochemical data for Ca/Al, Mn/Al, Ti/Al, Cr/Al, Fe/Al, Ni/Al, Cu/Al, Zn/Al, As/Al, and Sb/Al ratios measured by LA-ICP-MS are given in Appendix A from supplementary material and profiles for each element are represented in Figure 6.3 for a studied interval ≈18 mm long and in Figure 6.4 for a 5 mm-long studied interval.

Geochemical data and profiles on discrete samples 1 and 6 by ICP-OES and ICP-MS are presented in Table 6.2 and Figure 6.5.
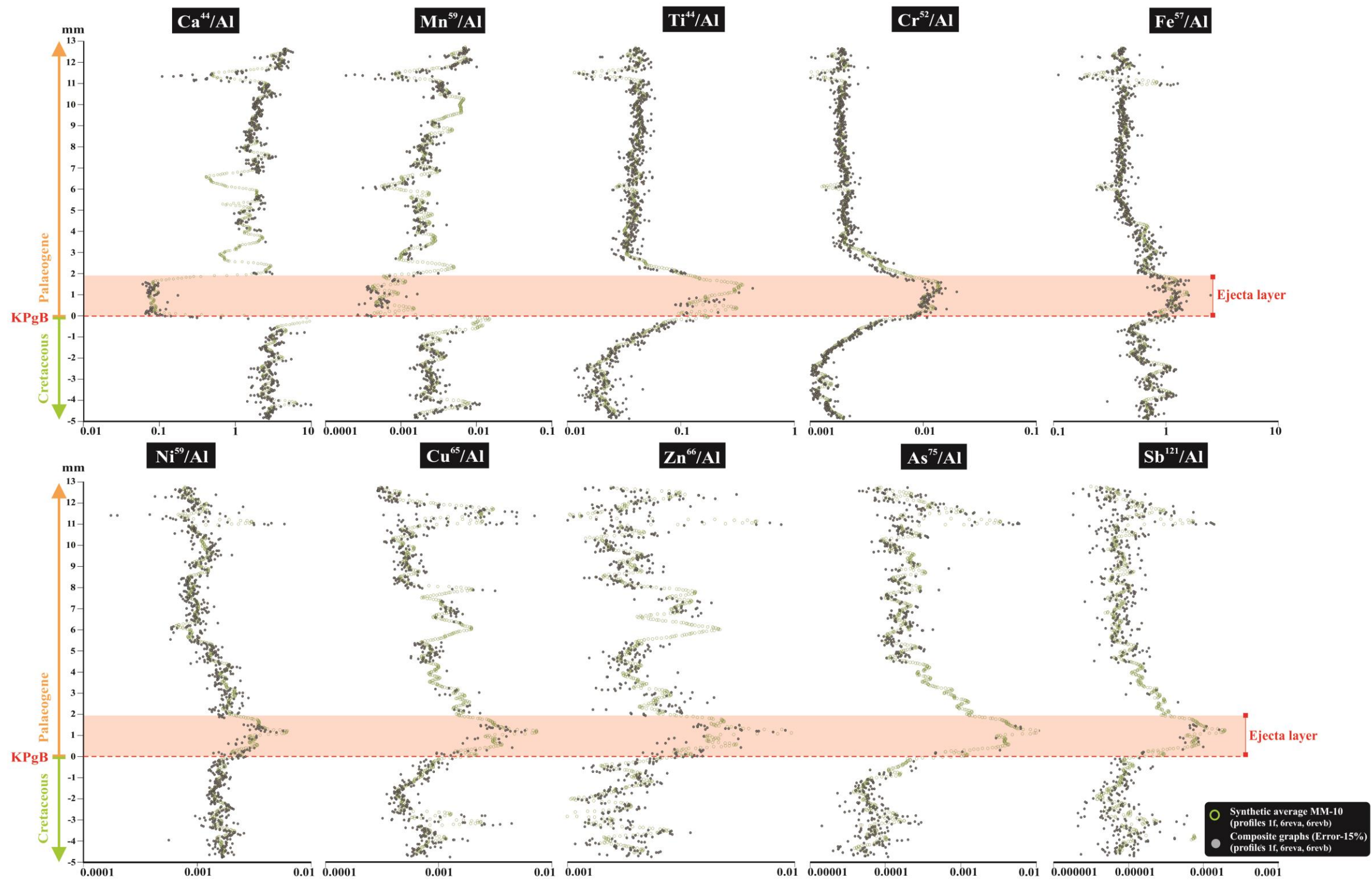
Fig 6.3. Profiles by LA-ICP-MS in an 18 mm-long interval. Elemental isotopic ratios (Ca/Al, Mn/Al, Ti/Al, Cr/Al, Fe/Al, Ni/Al, Cu/Al, Zn/Al, As/Al and Sb/Al) measured by LA-ICP-MS across the KPgT at the Agost, corresponding to i) the gray calcareous marlstones and marlstones from the uppermost Maastrichtian (from -5 to 0 mm), ii) the ejecta layer (0 mm) and iii) the boundary clay layer from the lowermost Danian (from 0 to 13 mm).
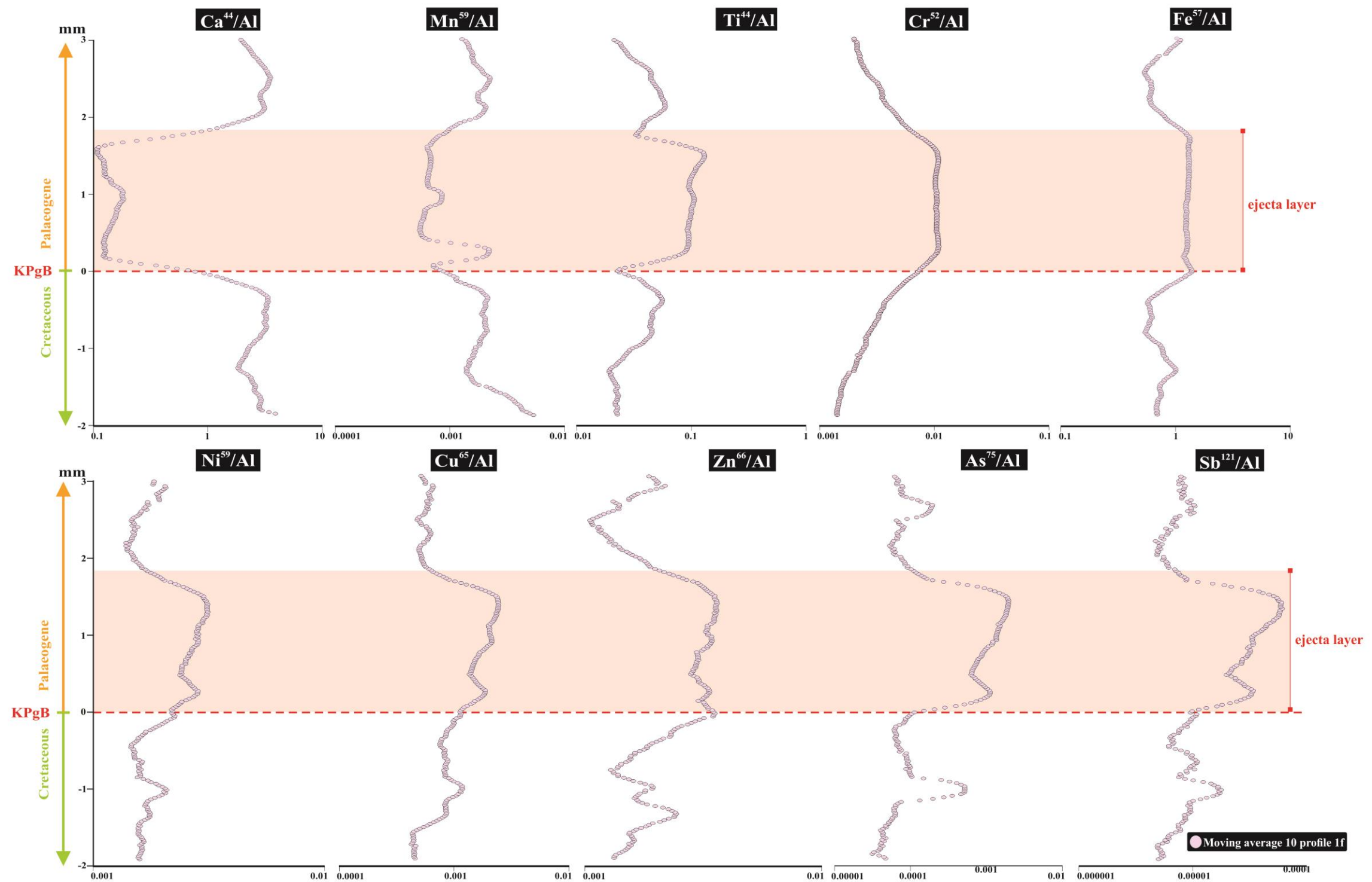
Fig 6.4. Profile 1f by LA- ICP-MS within 5 mm-long interval. Elemental isotopic ratios (Ca/Al, Mn/Al, Ti/Al, Cr/Al, Fe/Al, Ni/Al, Cu/Al, Zn/Al, As/Al and Sb/Al) measured by LA-ICP-MS across the KPgT at the Agost, corresponding to i) the gray calcareous marlstones and marlstones from the uppermost Maastrichtian (from -2 to 0 mm), ii) the ejecta layer (0 mm) and iii) the boundary clay layer from the lowermost Danian (from 0 to 3 mm).

Table 6.2. Table with the elemental content (major) and elemental ratios, measured by ICP-OES and ICP-MS across a 2.0 cm-long interval (from -0.5 to 1.5 cm) from the sample 6 and a 2.2 cm-interval (from -0.2 to 2.0 cm) from the sample 1 in the KPgB at the Agost section, inlcuing the gray calcareous marlstones and malstones from the uppermost Maastrichtian, the ejecta layer (red color) and the boundary clay layer from the lowermost Danian. Al, Ca, CaO, CaCO3, concentrations (%); Ca/Al and Fe/Al ratios; Cr/Al, Cu/Al, Ni/Al, and Zn/Al ratios (x 10^{-4}).

Samples Agost		Distance KPgB(cm)		Major elements					Geochemical proxies					
				Al	Ca	CaO	CaCO$_3$	Fe	Fe/Al	Ca/Al	Cr/Al	Cu/Al	Ni/Al	Zn/Al
Sample-1	Ag-1.9	(+2.0)	2	6.084	11.860	16.604	29.650	2.476	0.407	1.949	15.643	4.612	10.485	11.637
	Ag-1.8	(+1.5)	1.5	6.326	11.320	15.848	28.300	2.527	0.399	1.789	16.016	4.734	10.631	12.390
	Ag-1.7	(+1.0)	1	6.933	11.280	15.792	28.200	2.684	0.387	1.627	14.996	5.061	10.348	11.229
	Ag-1.6	(+0.5)	0.3	7.306	9.346	13.084	23.365	3.094	0.423	1.279	18.349	6.574	11.588	12.276
	Ag-1.5	(0,1, 0,2)	0.15	6.538	6.913	9.678	17.283	4.792	0.733	1.057	72.972	16.552	21.139	24.576
	Ag-1.4	(0,0, 0,1)	0.05	5.466	11.120	15.568	27.800	4.373	0.8	2.034	56.293	12.214	18.941	20.578
	Ag-1.3	(-0.1, 0.0)	-0.05	4.632	13.920	19.488	34.800	3.621	0.782	3.005	12.021	5.715	13.983	12.951
	Ag-1.2	(-0.2, -0.1)	-0.1	4.350	15.360	21.504	38.400	3.288	0.756	3.531	10.014	6.131	13.336	12.793
	Ag-1.1	(-0.2, -0.1)	-0.2	3.783	18.940	26.515	47.350	2.217	0.586	5.007	9.950	7.335	11.813	13.875
Sample-6	Ag-6.6	(+1.5)	1.50	4.945	16.530	23.142	41.325	2.012	0.41	3.34	15.14	4.32	8.57	11.18
	Ag-6.5	(+1.0)	1.00	5.883	14.000	19.600	35.000	2.384	0.41	2.38	15.12	4.15	8.59	11.47
	Ag-6.4	(+0.5)	0.50	6.559	9.059	12.682	22.648	2.842	0.43	1.38	19.41	5.81	10.65	12.28
	Ag-6.3	(0,0, 0,2)	0.10	7.499	2.197	3.076	5.493	6.650	0.89	0.29	91.29	25.26	27.89	36.98
	Ag-6.2	(-0.1)	-0.10	4.702	15.210	21.294	38.025	3.218	0.68	3.23	25.96	8.68	16.06	14.67
	Ag-6.1	(-0.5, -0.2)	-0.35	4.850	16.020	22.428	40.050	2.606	0.54	3.30	15.25	5.89	12.73	13.37
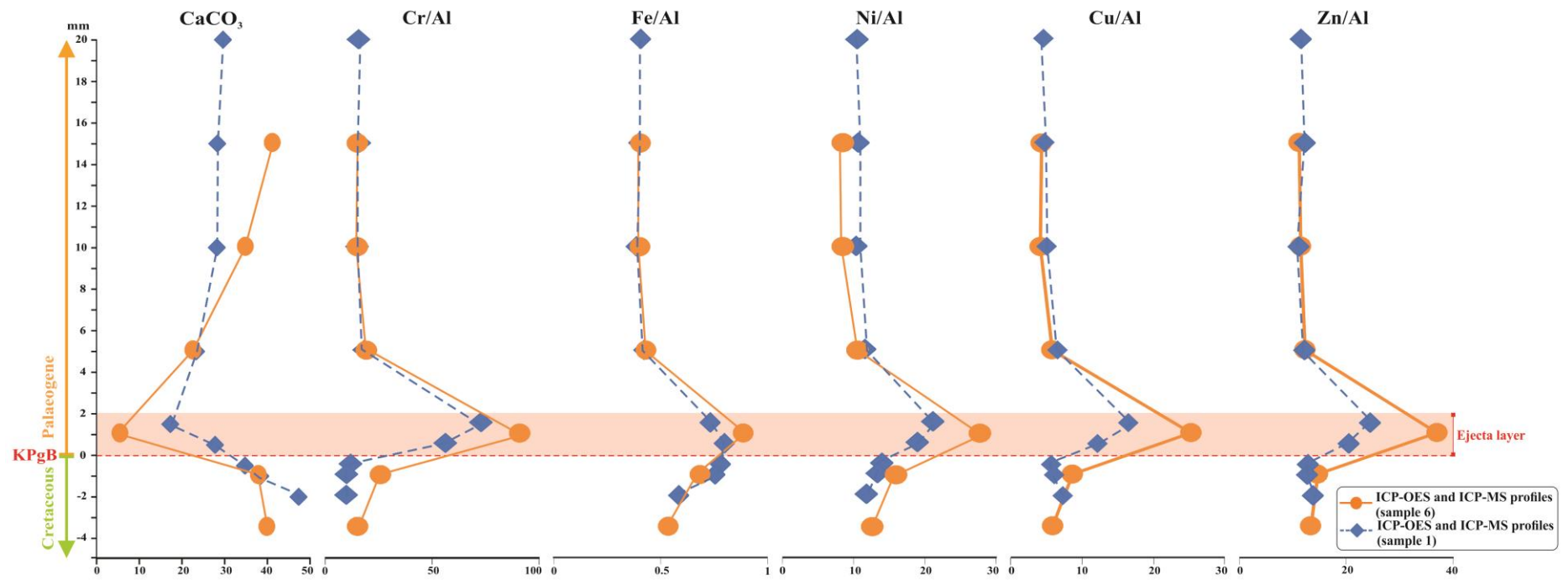
Fig. 6.5. Geochemical analysis conducted in discrete samples 1 and 6 from the KPgB at Agost. Trace element concentrations were determined using an Inductivity Coupled Plasma-Mass Spectrometry (ICP-MS), while the concentrations of major elements (Al, Ca, Fe) were measured using an Inductivity Coupled Plasma-Optical Emission Spectroscopy (ICP-OES).

6.4.2. Comparing discrete-samples ICP-OES and ICP-MS vs continuous LA-ICP-MS analyses

When comparing discrete-samples ICP-OES-MS vs continuous LA-ICP-MS analyses, the shared interval covered by both discrete sampling/ICP-OES-MS and by continuous/LA-ICP-MS analyses is 17.57 mm, including 4.75 mm of uppermost Maastrichtian gray calcareous marlstone and marlstone, 2.05 mm of the ejecta layer, and 10.77 mm of the boundary clay layer from the lowermost Danian (Fig. 6.6).
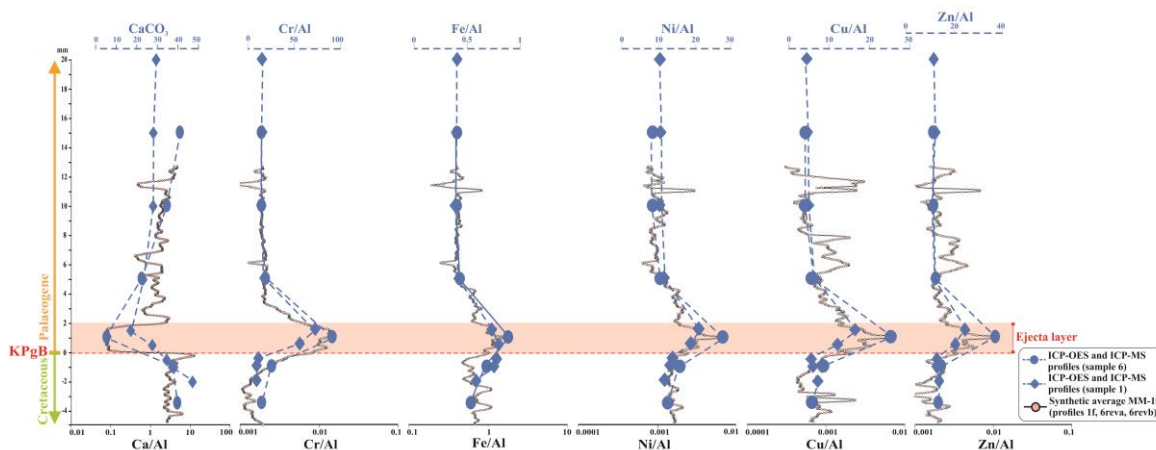
Fig. 6.6. Comparison of CaCO$_3$, Cr/Al, Fe/Al, Ni/Al, Cu/Al and Zn/Al (10^{-4}) analyzed by ICP-OES-MS vs Ca/Al, Cr/Al, Fe/Al, Ni/Al, Cu/Al and Zn/Al ratios analyzed by LA-ICP-MS, in a shared 17.57 mm interval, including the gray calcareous marlstones and marlstones from the uppermost Maastrichtian, the ejecta layer, and the boundary clay layer from the lowermost Danian.

At this 17.57 mm interval, maximum values of ≈50% in CaCO$_3$ and ≈4 for Ca/Al ratio are registered in both, the gray calcareous marlstone and marlstone from the uppermost Maastrichtian and in the light marly limestone from the lower Danian, while the ejecta layer is characterizaed by minimum values for CaCO$_3$ (between 10-20%) and the Ca/Al ratio (0.09).

In contrast, significant increases in Cr/Al, Fe/Al, Cu/Al, Ni/Al, Zn/Al ratios are exclusively observed within the ejecta layer, while in all the profiles similar values are observed in the uppermost Maastrichtian and lowermost Danian sediments (Fig. 6.6).

Specifically, when comparing the element profiles obtained for sample 1 profile f (1f) by LA-ICP-MS and profiles obtained for sample 1 by ICP-OES-MS, but within just a 5 mm interval (Fig. 6.7), the main difference observed is the analytical resolution, it being ~1 mm versus 0.09 mm. This represents, for the ~2.05 mm thick ejecta layer, that the amount of analytical data by LA-ICP-MS is much larger than by discrete sampling and ICP-OES-MS (101 versus 1). So, while a single peak is observed in ICP-OES-MS analyses, constant values are obtained by LA-ICP-MS linked to the ejecta layer (Fig. 6.7). This stands as proof of the rapid deposition of the ejecta layer, in the order or days or months (Artemieva and Morgan, 2009).

The conducted high-resolution analysis of the ejecta layer (mean of 2.05 mm) at the Agost section leads one to interpret similar oxygen conditions prior to and after the KPgB, with anoxic environments restricted only to the time of ejecta layer deposition.
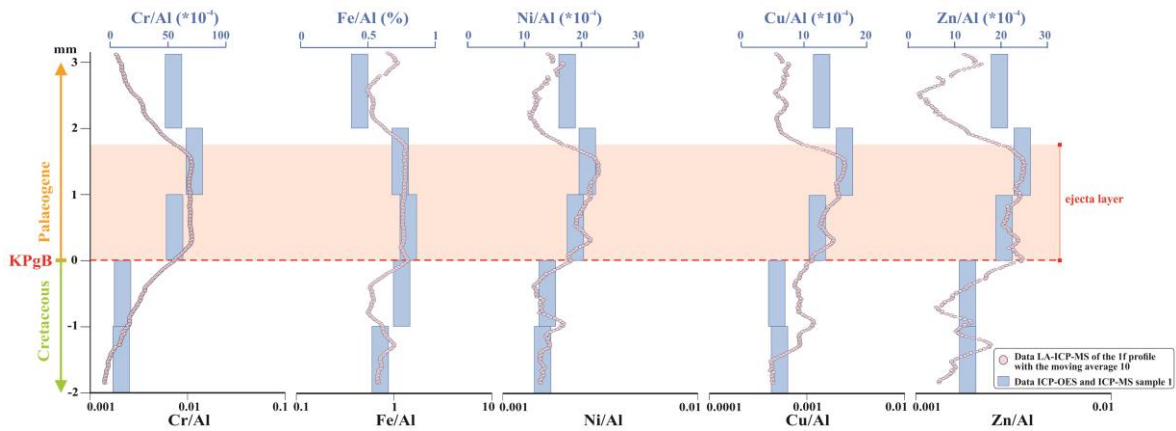
Fig. 6.7. Comparison of Cr/Al, Fe/Al, Ni/Al, Cu/Al and Zn/Al (10⁻⁴) analyzed by ICP-OES-MS vs the same ratios ratios analyzed by LA-ICP-MS, in a 5 mm interval, including the gray calcareous marlstones and marlstones from the uppermost Maastrichtian and the ejecta layer and the boundary clay layer from the lowermost Danian.

Lowery et al. (2018) have recently shown that the recovery of productivity in the Chicxulub structure is faster than that at many other sites. They find that proximity to the impact was not a control on recovery in marine ecosystems, and linked it with the recovery of environmental conditions (e.g. oxygenation conditions). In this paper we demonstrate that at the Agost distal section (≥5000 km from impact site), the recovery of the oxic conditions was instantaneous (in the range of days), which could also bring on a quick recovery of the macrobenthic tracemaker community.

Comparison between LA-CP-MS profile of Ca/Al and the photo by HRSEM (See Fig. 6.8) also illustrates how the decrease of the Ca/Al ratio is mainly associated with the ejecta layer, maintaining constant concentrations in all ejecta layer deposited.

Finally, at this scale resolution, using the high-resolution LA-ICP-MS methodology also serves to evidence the scarce remobilization of the trace elements at this section, whose element peaks are exclusively restricted to the ejecta layer.
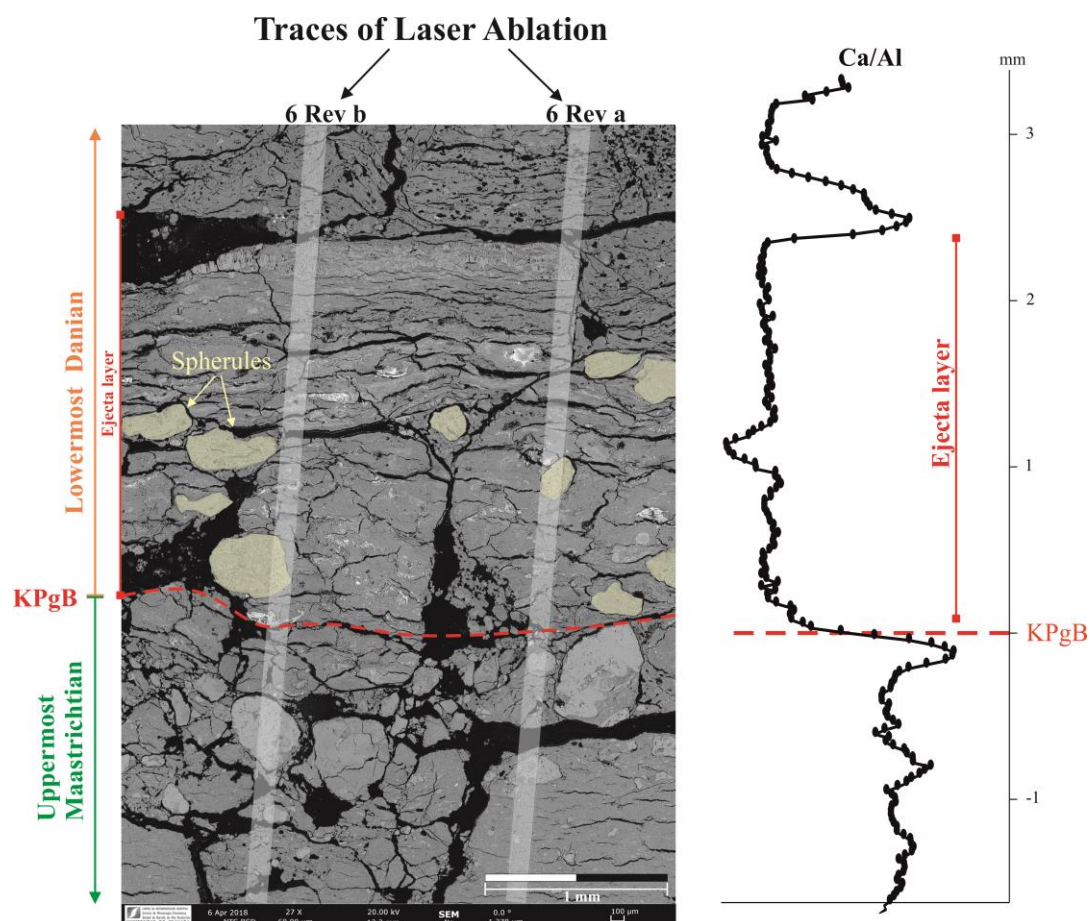
Fig. 6.8. Comparison between LA-CP-MS traces (Ca/Al Ratio) and secondary electron images made by High-Resolution Scanning Electron Microscopy (HRSEM). In the photo are the traces of LA-ICP-MS (Trace 6Reva and 6Revb), in red dash line the KPgB that marks the sharp contact the between the gray calcareous marlstones and marlstones from the uppermost Maastrichtian and the ejecta layer from the lowermost Danian, where numerous spherules are observed (in yellow).

6.5. Conclusions

High-resolution analyses performed in the distal section of Agost by ICP-OES and a novel methodology, using resin-embedded sediment and LA-ICP-MS continuous measurements with 10 μm increments, provide evidence that sediments from the uppermost Maastrichtian, the ejecta layer and the lowermost Danian record an instantaneous recovery of the pre-impact conditions, also supporting the fast recovery of productivity patterns across this boundary as reported in diverse KPg sections.

LA-ICP-MS continuous measurements further indicated that remobilization (at sub-mm scale) across KPgB is not significant, the peaks of different elements being restricted to the ejecta layer containing the impact evidence.

Acknowledgments

Chapter 7

CONCLUSIONS

CONCLUSIONES

"The only way to do great work is to love what you do"

— Steve Jobs (1955-2011)

7.1. Conclusions

The main objective of the present PhD Thesis was to characterize the palaeoenvironmental conditions (oxygenation and productivity), before, during and after the KPgB impact, based on a detailed and integrative geochemical and ichnological analysis in several KPgB distal sections. One novel aspect of this Thesis is the ultra high-resolution analysis conduted at the Agost section by means of resin-embedded tecniques and LA-ICP-MS continuous measurements, allowing for micron-resolution. Such ultra-high resolution analyses have proven to be a useful tool to investigate abrupt bio-events and associated palaeoenvironmental changes.

The general conclusions of this PhD are:

1. **Caravaca section:** Geochemical analysis at mm-scale resolution evidences a rapid return to pre-impact conditions in terms of oxygenation. Oxygen levels at bottom and intermediate waters recovered very quickly, in the range of a few hundred years after the KPgB event. Conditions during deposition of the ejecta layer were highly anoxic as a consequence of the enhanced contribution of metals to the basins and enhanced terrestrial and marine organic material input. Shortly after the impact, oxygen levels were rapidly re-established, permitting a prompt recovery of the macrobenthic tracemaker community, in turn favoured by the opportunistic behaviour of some organisms. This is supported by geochemical and isotopic analyses conducted on the infilling material of trace fossils and the host sediment.

   Geochemical and isotopic data from trace fossil infilling and host sediments support a significant mixture of the infilling material, which occurred due to the unconsolidated character of the sediment, including the ejecta layer. Softground conditions associated with this unconsolidated sediment further support the relatively rapid recovery of the macrobenthic tracemaker community within horizons a few millimeters above the KPgB event. The observed mixture of the infilling material in the ichnotaxa also evidences a significant macrobenthic tracemaker activity across the KPgB sediments, which should be considered in order to interpret original signatures and to reconstruct palaeoenvironmental conditions during the KPgB.

2. **Gubbio Sections**: Geochemical and isotopic analyses conducted at mm-cm scale resolution, both on the infilling of trace fossils and the host rocks of the KPgB at the Bottaccione Gorge and the Contessa Highway sections, provide important information about the paleoenvironmental conditions after the KPgB event. Although the ejecta layer is not well presented at these sections due to oversampling, the preserved lowermost Danian red boundary clay layer and the red micritic limestone still record the post-impact event conditions. No major changes in the enrichment/depletion profiles of redox sensitive and detrital elements were registered in the uppermost Maastrichtian and lowermost Danian deposits. This can be interpreted as evidence of similar paleoenvironmental conditions (oxygenation, nutrient availability and/or sedimentary input) prior to and after the KPgB, due to a rapid reestablishment of pre-impact environmental conditions. Carbon isotope data

also show similar values for the infilling material of trace fossils and the host rocks, which is interpreted as revealing a nearly coetaneous bioturbation during sediment deposition. In general, the obtained results agree with a fast recovery of productivity patterns.

3. **Agost section**: Results obtained by traditional sampling and ICP-OES analysis were compared with a novel technique using resin-embedded sediment and LA-ICP-MS continuous measurements with 10 μm increments and a laser-beam of 80 μm. Due to the largely improved analytical resolution, sub-mm variability was for the first time observed, undetected while using traditional discrete sampling. This technique has revealed particularly useful for investigating element distribution and remobilization (at sub-mm scale) across abrupt boundaries such as the KPgB.

In adition, a high-resolution elemental analysis (μm-scale) of Ca/Al, Mn/Al, Ti/Al, Cr/Al, Fe/Al, Cu/Al, Ni/Al, Zn/Al As/Al and Sb/Al ratios in an intact sample of the KPgB at after resin embedding were made. The results of this analysis support, for first time, that the anoxic conditions are exclusively restricted to the ejecta deposition, thus a near instantaneous reestablishment of pre-impact oxygenation conditions ocurred just after the impact event which could bring on the quick recovery of the macrobenthic tracemaker community.

7.2. Conclusiones

El objetivo principal de esta Tesis Doctoral es caracterizar las condiciones paleoambientales (oxigenación y productividad), antes, durante y después del impacto de KPgB, sobre la base de un análisis geoquímico e icnológico detallado e integrador en varias secciones distales de KPgB. Un aspecto novedoso de esta Tesis son los análisis de ultra-alta resolución realizados en la sección Agost, previa consolidación con resina en una cámara de vacío y posterior análisis en continuo mediante LA-ICP-MS, los cuales alcanzan una resolución micrométrica. Dichos análisis de resolución ultra-alta han demostrado ser una herramienta útil para investigar abruptos bio-eventos así como cambios paleoambientales asociados.

La investigación llevada a cabo en esta Tesis permite concluir:

1. **Sección de Caravaca:** el análisis geoquímico a una resolución mm evidencian una rápida recuperación de las condiciones pre-impacto en términos de oxigenación. Los niveles de oxígeno en las aguas profundas e intermedias se recuperaron muy rápidamente, en el rango de algunos cientos de años después del evento del KPgB. Las condiciones durante el depósito de la capa del impacto (ejecta layer) eran anóxicas como consecuencia del importante aporte de metales a las cuencas y sumado al incremento en el aporte de materia orgánica, tanto terrestre como marína. Rápidamente tras el impacto, los niveles de oxígeno se restablecieron, lo que facilitó la rápida colonización del sustrato por la comunidad macrobentónica, favorecida, a su vez por el comportamiento oportunista de algunos organismos. Esto último se demuestra a partir de los análisis geoquímicos e isotópicos realizados en el material de relleno de las trazas fósiles y en la roca encajante.

   Los datos geoquímicos e isotópicos confirman una mezcla en el material de relleno de las trazas fósiles, que se produjo debido al carácter no consolidado del sedimento, incluida la capa de impacto. Las condiciones de suelo blando asociadas con el sedimento no consolidado respaldan la recuperación relativamente rápida de la comunidad macrobentónicos generadora de trazas a pocos milímetros por encima del KPgB. La mezcla observada en el material de relleno en los diferentes ichnotaxones evidencia asu vez una importante actividad de organismos bioturbadores a través de los sedimentos de KPgB, que debe de tenerse en cuenta, para evitar interpretaciones erróneas de las señales originales asi como para reconstruir las condiciones paleoambientales durante el KPgB.

2. **Secciones de Gubbio:** los análisis geoquímicos e isotópicos realizados a una escala milimétrica y centimétrica, tanto en el relleno de las trazas fosiles como de las rocas del KPgB en las secciones de Bottaccione Gorge y Contessa Highway, aportan importante información acerca del restablecimiento de las condiciones paleoambientales después del KPgB. Aunque la capa del impacto está ausente en estas secciones debido al intenso muestreo, el Daniense inferior, constituido tanto por la capa de arcilla roja como por la caliza micrítica rojiza, registra las condiciones paleoambientales posteriores al avento de impacto.

No se han registrado cambios importantes en los perfiles de los elementos indicadores del aporte detrítico o redox en el Maastrichtiense superior y en el Daniense inferior. Este hecho se interpreta como una evidencia del rapido restablecimiento de las condiciones ambientales (oxigenación, disponibilidad de nutrientes y/o aporte sedimentario) después del KPgB. Los datos de isótopos de carbono muestran valores similares en el material de relleno de las trazas fósiles y en las rocas encajantes, lo que nos permite inferir una bioturbación casi coetánea durante el depósito de los sedimentos. En conclusión, los datos obtenidos concuerdan con una recuperación rápida de los patrones de productividad.

3. **Sección de Agost:** los resultados obtenidos mediante muestreo tradicional y análisis de ICP-OES se compararon con una novedosa metodología que consiste en la consolidación precvia con resina de los sedimentos y un posterior análisis en continuo mediante LA-ICP-MS (que presente incrementos de 10 μm y un haz láser de 80 μm). Debido a la importante mejora de la resolución analítica, se observo por por primera vez la variabilidad por debajo del milímetro, que sin embargo no podía ser detectada durante el muestreo discreto tradicional. En consecuencia la metodología aplicada es adecuada para investigar la distribución y removilización de elementos (en escala sub-mm) a través de límites abruptos tales como el KPgB.

Además, se ha realizado un análisis elemental de alta resolución (escala μm) de Ca/Al, Mn/Al, Ti/Al, Cr/Al, Fe/Al, Cu/Al, Ni/Al, Zn/Al, As/Al y Sb/Al en una muestra intacta del KPgB previa consolidación en resina de resina. Los resultados obtenidos demuestran, por primera vez, que las condiciones anóxicas están exclusivamente relacionadas con el depósito de la capa del impacto pero además este restablecimiento casi instantáneo de las condiciones de oxigenación podría favorecer la rápida recuperación de la comunidad macrobentónica generadora de trazas.

Chapter 8

FORTHCOMING RESEARCH

INVESTIGACIONES FUTURAS

"What we know is a drop, what we don´t know is an ocean"

— Isaac Newton (1642-1727)

8.1. Forthcoming research

The geochemical and ichnological data obtained and described here support that oxygenation conditions were re-established almost instantaneously following the ejecta layer deposition and that the macrobentic tracemaker community quickly colonized the substrate. Within this context, new analyses are foreseen for future research:

- Of special interest is the analysis of further sections (distal, intermediate, proximal) of the KPgB using the metodology developed in this thesis (continuous analysis at high resolution, previous consolidation with resin in a vacuum chamber).

- A detailed study of biomarkers in the KPgB interval at Agost and Caravaca sections, which has already been successfully performed in other proximal (e.g., Vellekoop et al., 2016, 2014) and distal (Vellekoop et al., 2015) sections, holds particular interest. The marine fossil record contains a wide variety of organic molecules —both marine (marine algae, cyanobacteria and archaea) and terrestrial organisms that lived at the time of deposition. The study of biomarkers will allow us to further understand changes in environmental conditions linked to temperature variations (Uk37, LDI and TEX86) and palaeoxygenation (BIT index and diols).

- A detailed geochemical analysis to constrain trace element sources is also of particular interest. In the KPgB ejecta, along with elements deriving from extraterrestrial contamination, the typically-derived terrestrial elements are also enriched. Processes leading to such enrichment are still poorly understood.

- Diagenetic processes giving rise to trace element remobilization are likewise relevant, especially in the case of extraterrestrial elements such as the PGEs used for reconstructing the impactor contribution at different KPgB sections. Further aspects to explore are the alteration of the original composition of spherules, not yet well understood, and the diagenetic processes behind the current compositions of such spherules.

8.2. Investigaciones futuras

Los análisis geoquímicos e icnológicos han demostrado como la oxigenación se restableció de manera instantánea una vez depositada la capa del impacto, pero además, una vez restablecidas las condiciones de oxigenación, la comunidad bioturbadora macrobentónica rápidamente colonizó el sustrato. En este contexto, se prevén nuevos análisis para futuras investigaciones:

- De especial interes sería el análisis de otras secciones del KPgB (distales, intermedias y proximales) utilizando la metodología desarrollada en esta tesis (análisis continuo y a alta resolución, previa consolidación en resina en una cámara de vacío), para así poder verificar los resultados obtenidos, y alcanzar interpretaciones sobre el KPgB de carácter global.

- Sobre la base del estudio geoquímico de alta resolución ya realizado, consideramos interesante el estudio detallado de los biomarcadores en los afloramientos de Agost y Caravaca, realizado con éxito en otras secciones proximales (e.g., Vellekoop et al., 2014, 2016) e incluso distales (Vellekoop et al., 2015) del KPgB. El registro fósil marino contiene una gran variedad de moléculas orgánicas, tanto de organismos marinos (algas marinas, cianobacterias y arqueas) como terrestres, que vivierón en el momento del depósito. El estudio de biomarcadores nos permitirá avanzar en el conocimiento de los cambios de las condiciones ambientales, como las variaciones de la temperatura (Uk37, LDI y TEX86) y la paleoxigenación (índice BIT y dioles).

- Un análisis detallado del análisis geoquímico ya realizado, para conocer las fuentes u origen de los diferentes elementos traza, también sería de particular interés. En la capa que forma el limite (ejectea layer), además del típico enriquecimiento en los elementos de origen extraterrestre, también se enriquecen ciertos elementos de origen terrestres. Los procesos que conducen a tal enriquecimiento aún son poco conocidos.

- Finalmente, el estudio de los procesos diagenéticos que conducen a la removilización de los elementos traza también son de especial relevancia, particularmente en el caso de los elementos extraterrestres del PGE que se han utilizado para reconstruir la contribución del meteorito en diferentes secciones de KPgB. Además, la alteración de la composición original de las esferulas aún no se comprende bien, ya que tampoco los procesos diagenéticos conducen a las composiciones que actualmente presentan tales esférulas.

REFERENCES

Abrajevitch, A., Kodama, K., 2009. Biochemical vs. detrital mechanism of remanence acquisition in marine carbonates: A lesson from the K–T boundary interval. Earth Planet. Sci. Lett. 286, 269–277.

Adams, J.B., 2004. The Cretaceous-Tertiary extinction: Modeling carbon flux and ecological response. Paleoceanography 19, 1–13. doi:10.1029/2002PA000849

Aitchison, J., Egozcue, J.J., 2005. Compositional data analysis: where are we and where should we be heading? Math. Geol. 37, 829–850. doi:10.1007/s11004-005-7383-7

Alegret, L., 2007. Recovery of the deep-sea floor after the Cretaceous-Paleogene boundary event: The benthic foraminiferal record in the Basque-Cantabrian basin and in South-eastern Spain. Palaeogeogr. Palaeoclimatol. Palaeoecol. 255, 181–194. doi:10.1016/j.palaeo.2007.02.047

Alegret, L., Arenillas, I., Arz, J.A., Díaz, C., Grajales-Nishimura, J.M., Meléndez, A., Molina, E., Rojas, R., Soria, A.R., 2005. Cretaceous-Paleogene boundary deposits at Loma Capiro, central Cuba: Evidence for the Chicxulub impact. Geology 33, 721–724. doi:10.1130/G21573.1

Alegret, L., Arenillas, I., Arz, J.A., Liesa, C., Meléndez, A., Molina, E., Soria, A.R., Thomas, E., 2002. The Cretaceous/Tertiary boundary: Sedimentology and micropalaeontology at El Mulato section, NE Mexico. Terra Nov. 14, 330–336. doi:10.1046/j.1365-3121.2002.00425.x

Alegret, L., Kaminski, M.A., Molina, E., 2004. Paleoenvironmental recovery after the Cretaceous/Paleogene boundary crisis: Evidence from the marine Bidart section (SW France). Palaios 19, 574–586. doi:10.1669/0883-1351(2004)019<0574:PRATPB>2.0.CO;2

Alegret, L., Molina, E., Thomas, E., 2003. Benthic foraminiferal turnover across the Cretaceous/Paleogene boundary at Agost (southeastern Spain): Paleoenvironmental inferences. Mar. Micropaleontol. 48, 251–279. doi:10.1016/S0377-8398(03)00022-7

Alegret, L., Molina, E., Thomas, E., 2001. Benthic foraminifera at the Cretaceous-Tertiary boundary around the Gulf of Mexico. Geology 29, 891–894.

Alegret, L., Rodríguez-Tovar, F.J., Uchman, A., 2015. How bioturbation obscured the Cretaceous-Palaeogene boundary record. Terra Nov. 27, 225–230. doi:10.1111/ter.12151

Alegret, L., Thomas, E., 2013. Benthic foraminifera across the Cretaceous/Paleogene boundary in the southern ocean (ODP Site 690): Diversity, food and carbonate saturation. Mar. Micropaleontol. 105, 40–51. doi:10.1016/j.marmicro.2013.10.003

Alegret, L., Thomas, E., 2009. Food

supply to the seafloor in the Pacific Ocean after the Cretaceous/Paleogene boundary event. Mar. Micropaleontol. 73, 105–116. doi:10.1016/j.marmicro.2009.07.005

Alegret, L., Thomas, E., 2007. Deep-Sea environments across the Cretaceous/Paleogene boundary in the eastern South Atlantic Ocean (ODP Leg 208, Walvis Ridge). Mar. Micropaleontol. 64, 1–17. doi:10.1016/j.marmicro.2006.12.003

Alegret, L., Thomas, E., 2005. Cretaceous/Paleogene boundary bathyal paleo-environments in the central North Pacific (DSDP Site 465), the Northwestern Atlantic (ODP Site 1049), the Gulf of Mexico and the Tethys: The benthic foraminiferal record. Palaeogeogr. Palaeoclimatol. Palaeoecol. 224, 53–82. doi:10.1016/j.palaeo.2005.03.031

Alegret, L., Thomas, E., Lohmann, K.C., 2012. End-Cretaceous marine mass extinction not caused by productivity collapse. Proc. Natl. Acad. Sci. U. S. A. 109, 728–32. doi:10.1073/pnas.1110601109

Algeo, T.J., Tribovillard, N., 2009. Environmental analysis of paleoceanographic systems based on molybdenum-uranium covariation. Chem. Geol. 268, 211–225. doi:10.1016/j.chemgeo.2009.09.001

Alvarez, L.W., Alvarez, W., Asaro, F., Michel, H.V., 1980. Extraterrestrial cause for the Cretaceous-Tertiary extinction. Science (80-.). 208, 1095–1108.

Alvarez, W., 2009. The historical record

in the Scaglia limestone at Gubbio: Magnetic reversals and the Cretaceous-Tertiary mass extinction. Sedimentology 56, 137–148. doi:10.1111/j.1365-3091.2008.01010.x

Alvarez, W., Asaro, F., Montanari, A., 1990. Iridium profile for 10 million years across the Cretaceous-Tertiary boundary at Gubbio (Italy). Science 250, 1700–1702.

Alzeni, F., Cipriani, N., Malesani, P., Monechi, S., 1981. Geochemistry at the Cretaceous-Tertiery boundary in the Bottaccione section (Italy). Riv. Ital. Paleont. 86, 845–854.

Arenillas, I., Arz, J., Molina, E., 2004. A new high-resolution planktic foraminiferal zonation and subzonation for the lower Danian. Lethaia 37, 79–95. doi:10.1080/00241160310005097

Arenillas, I., Arz, J.A., Grajales-Nishimura, J.M., Murillo-Muñetón, G., Alvarez, W., Camargo-Zanoguera, A., Molina, E., Rosales-Domínguez, C., 2006. Chicxulub impact event is Cretaceous/Paleogene boundary in age: New micropaleontological evidence. Earth Planet. Sci. Lett. 249, 241–257. doi:10.1016/j.epsl.2006.07.020

Arenillas, I., Molina, E., 1997. Análisis cuantitativo de los foraminíferos planctónidos del Paleoceno de Caravaca (Cordillera Bética): bioestratigrafía y evolución de las asociaciones. Rev. Española Paleontol. 12, 207–232.

Arinobu, T., Ishiwatari, R., Kaiho, K.,

Lamolda, M.A., 1999. Spike of pyrosynthetic polycyclic aromatic hydrocarbons associated with an abrupt decrease in δ13C of a terrestrial biomarker at the Cretaceous-Tertiary boundary at Caravaca, Spain. Geology 27, 723–726. doi:10.1130/0091-7613(1999)027<0723

Artemieva, N., Morgan, J., 2009. Modeling the formation of the K-Pg boundary layer. Icarus 201, 768–780. doi:10.1016/j.icarus.2009.01.021

Arthur, M.A., Fischer, A.G., 1977. Upper Cretaceous-Paleocene magnetic stratigraphy at Gubbio, Italy I. Lithostratigraphy and sedimentology. Bull. Geol. Soc. Am. 88, 367–371. doi:10.1130/0016-7606(1977)88<367:UCMSAG>2.0. CO;2

Arthur, M.A., Zachos, J.C., Jones, D.S., 1987. Primary productivity and the Cretaceousl Tertiary boundary event in the oceans. Cretac. Res. 8, 43–54.

Arz, J.A., Arenillas, I., Molina, E., Sepulveda, R., 2000. La estabilidad evolutiva de los foraminíferos planctónicos en el Maastrichtiense Superior y su extinción en el límite Cretácico/Terciario de Caravaca, España. Rev. Geol. Chile 27. doi:http://dx.doi.org/10.4067/S0716-02082000000100003

Aschoff, J.L., Giles, K.A., 2005. Salt diapir-influenced, shallow-marine sediment dispersal patterns: Insights from outcrop analogs. Am. Assoc. Pet. Geol. Bull. 89, 447–469. doi:10.1306/10260404016

Bambach, R.K., 2006. Phanerozoic Biodiversity Mass Extinctions. Annu. Rev. Earth Planet. Sci. 34, 127–155. doi:10.1146/annurev.earth.33.092203.122654

Barclay, R.S., Johnson, K.R., 2002. West Bijou site Cretaceous-Tertiary boundary, Denver BAsin, Colorado. Geol. Soc. Am. F. Guid. 5, 59–68.

Bea, F., 1996. Residence of REE, Y, Th and U in granites and crustal protoliths; implications for the chemistry of crustal melts. J. Petrol. 37, 521–552. doi:10.1093/petrology/37.3.521

Belza, J., Goderis, S., Montanari, A., Vanhaecke, F., Claeys, P., 2017. Petrography and geochemistry of distal spherules from the K–Pg boundary in the Umbria–Marche region (Italy) and their origin as fractional condensates and melts in the Chicxulub impact plume. Geochim. Cosmochim. Acta 202, 231–263. doi:10.1016/j.gca.2016.12.018

Belza, J., Goderis, S., Smit, J., Vanhaecke, F., Baert, K., Terryn, H., Claeys, P., 2015. High spatial resolution geochemistry and textural characteristics of "microtektite" glass spherules in proximal Cretaceous-Paleogene sections: Insights into glass alteration patterns and precursor melt lithologies. Geochim. Cosmochim. Acta 152, 1–38. doi:10.1016/j.gca.2014.12.013

Berglund, M., Wieser, M.E., 2011. Isotopic compositions of the elements 2009 (IUPAC Technical Report). Pure Appl. Chem. 83, 397–410. doi:10.1351/PAC-REP-10-06-

02

Berndt, J., Deutsch, A., Schulte, P., Mezger, K., 2011. The Chicxulub ejecta deposit at Demerara Rise (western Atlantic): Dissecting the geochemical anomaly using laser ablation-mass spectrometry. Geology 39, 279–282. doi:10.1130/G31599.1

Birch, H.S., Coxall, H.K., Pearson, P.N., Kroon, D., Schmidt, D.N., 2016. Partial collapse of the marine carbon pump after the Cretaceous-Paleogene boundary. Geology 44, 287–290. doi:10.1130/G37581.1

Blum, J.D., Chamberlain, C.P., Hingston, M.P., Koeberl, C., Marin, L.E., Schuraytzs, B.C., Sharptons, V.L., 1993. Isotopic comparison of K/T boundary impact glass with melt rock from the chicxulub and Manson impact structures. Nature 364, 325–327.

Bohor, B.F., 1990. Shock-induced microdeformations in quartz and other mineralogical indications of an impact event at the Cretaceous-Tertiary boundary. Tectonophysics 171, 359–372.

Bohor, B.F., Foord, E.E., Modreski, P.J., Triplehorn, D.M., 1984. Mineralogic evidence for an impact event at the Cretaceous-Tertiary boundary. Science (80-.). 224, 867–869.

Bohor, B.F., Glass, B.P., 1995. Origin and diagenesis of K/T impact spherules-From Haiti to Wyoming and beyond. Meteoritics 30, 182–198.

Bohor, B.F., Izett, G.A., 1986. Worldwide size distribution of shocked quartz at the K/T boundary: Evidence for a North American impact site, in: Lunar and Planetary Science Conference. pp. 68–69.

Bohor, B.F., Modreski, P.J., Foord, E.E., 1987. Shocked Quartz in the Cretaceous-Tertiary Boundary Clays: Evidence for a Global Distribution. Science (80-.). 236, 705–709. doi:10.1126/science.236.4802.705

Bohor, B.F., Triplehorn, D.M., Nichols, D.J., Millard Jr, H.T., 1987. Dinosaurs, spherules, and the "magic" layer: A new KT boundary clay site in Wyoming. Geology 15, 896–899.

Bojar, A.V., Smit, J., 2013. Isotopic studies in Cretaceous research: an introduction. Geol. Soc. London, Spec. Publ. 382, 1–4. doi:10.1144/SP382.12

Bostwick, J.A., Kyte, F.T., 1996. The size and abundance of shocked quartz in Cretaceous-Tertiary boundary sediments from the Pacific basin. Cretaceous-Tertiary event other catastrophes Earth Hist. Geol. Soc. Am. Spec. Pap. 307, 403–415.

Bottke, W.F., Vokrouhlický, D., Nesvorný, D., 2007. An asteroid breakup 160 Myr ago as the probable source of the K/T impactor. Nature 449, 48–53. doi:10.1038/nature06070

Bralower, T., Eccles, L., Kutz, J., Yancey, T., Schueth, J., Arthur, M., Bice, D., 2010. Grain size of Cretaceous-Paleogene boundary sediments from

Chicxulub to the open ocean: Implications for interpretation of the mass extinction event. Geology 38, 199–202. doi:10.1130/G30513.1

Brinkhuis, H., Smit, J., 1996. The Geulbemmerberg Cretaceous/Tertiary boundary section (Maastrichtian type area, SE Netherlands); an introduction. Geol. en Mijnb. 75, 101–106.

Bromley, R.G., 1996. Trace fossils: Biology, taphonomy and application. London: Chapman and Hall.

Brooks, R.R., Hoek, P.L., Reeves, R.D., Wallace, R.C., Johnston, J.H., Ryan, D.E., Holzbecher, J., Collen, J.D., 1985. Weathered spheroids in a Cretaceous/Tertiary boundary shale at Woodside Creek, New Zealand. Geology 13, 738–740.

Brooks, R.R., Reeves, R.D., Yang, X.-H., Ryan, D.E., Holzbecher, J., Collen, J.D., Neall, V.E., Lee, J., 1984. Elemental anomalies at the Cretaceous-Tertiary boundary, Woodside Creek, New Zealand. Science (80-.). 226, 539–542.

Brooks, R.R., Strong, C.P., Lee, J., Orth, C.J., Gilmore, J.S., Ryan, D.E., Holzbecher, J., 1986. Stratigraphic occurrences of iridium anomalies at four Cretaceous/Tertiary boundary sites in New Zealand. Geology 14, 727–729.

Brugger, J., Feulner, G., Petri, S., 2017. Baby, it's cold outside: Climate model simulations of the effects of the asteroid impact at the end of the Cretaceous. Geophys. Res. Lett. 44, 419–427.

doi:10.1002/2016GL072241

Calvert, S.E., Pedersen, T.F., 2007. Elemental proxies for palaeoclimatic and palaeoceanographic variability in marine sediments: Interpretation and application, Developments in Marine Geology, Developments in Marine Geology. Elsevier. doi:10.1016/S1572-5480(07)01019-6

Calvert, S.E., Pedersen, T.F., 1993. Geochemistry of Recent oxic and anoxic marine sediments: Implications for the geological record. Mar. Geol. 113, 67–88.

Campbell, C.E., Oboh-Ikuenobe, F.E., Eifert, T.L., 2007. Megatsunami deposit in Cretaceous-Paleogene boundary interval of southeastern Missouri, in: Evans, K.R., Horton, J., Wright, J., King, D.T., Morrow, J., Jared, R. (Eds.), The Sedimentary Record of Meteorite Impacts. Geological Society of America.

Canudo, J.I., Keller, G., Molina, E., 1991. Cretaceous / Tertiary boundary extinction pattern and fauna1 turnover at Agost and Caravaca , S . E . Spain. Mar. Micropaleontol. 17, 319–341.

Chen, C., Sun, W., 2017. Tracing the origin of peak rings at Chicxulub. Solid Earth Sci. 2, 63–64. doi:10.1016/j.sesci.2017.08.001

Chenet, A.L., Courtillot, V., Fluteau, F., Gerard, M., Quidelleur, X., Khadri, S.F.R., Subbarao, K. V., Thordarson, T., 2009. Determination of rapid Deccan eruptions across the Cretaceous-Tertiary boundary using paleomagnetic secular variation: 2.

Constraints from analysis of eight new sections and synthesis for a 3500-m-thick composite section. J. Geophys. Res. B Solid Earth 114, B06103. doi:10.1029/2008JB005644

Coccioni, R., Catanzariti, R., Frontalini, F., Galbrun, B., Jovane, L., Montanari, A., Savian, J.F., Sideri, M., 2016. Integrated magnetostratigraphy, biostratigraphy, and chronostratigraphy of the Paleogene pelagic succession at Gubbio (central Italy). Geol. Soc. Am. Spec. Pap. 524, 139–160.

Coccioni, R., Fabbrucci, L., Galeotti, S., 1993. Terminal Cretaceous deep-water benthic foraminiferal decimation, survivorship and recovery at Caravaca (SE Spain). Paleopelagos 3, 7–28.

Coccioni, R., Frontalini, F., Bancalà, G., Fornaciari, E., Jovane, L., Sprovieri, M., 2010. The Dan-C2 hyperthermal event at Gubbio (Italy): Global implications, environmental effects, and cause(s). Earth Planet. Sci. Lett. 297, 298–305. doi:10.1016/j.epsl.2010.06.031

Coccioni, R., Galeotti, S., 1994. K-T boundary extinction: Geologically instantaneous or gradual event? Evidence from deep-sea benthic foraminifera. Geology 22, 779–782. doi:10.1130/0091-7613(1994)022<0779

Coccioni, R., Menichetti, M., Montarani, A., 2012. GeoHistories from Gubbio Apennines, in: Guide to Field Trip: The Contessa Valley and the Bottaccione Gorge. p. 30.

Coccioni, R., Sideri, M., Bancala, G., Catanzariti, R., Frontalini, F., Jovane, L., Montanari, A., Savian, J., 2013. Integrated stratigraphy (Magneto-, bio-, and chronostratigraphy) and geochronology of the Palaeogene pelagic succession of the Umbria–Marche Basin (central Italy). Geol. Soc. London, Spec. Publ. 373, 111–131.

Corfield, R.M., Cartlidge, J.E., 1993. Oxygen and carbon isotope stratigraphy of the middle Miocene, Holes 805B and 806B, in: Proceedings of the Ocean Drilling Program. Scientific Results. pp. 307–322.

Corfield, R.M., Cartlidge, J.E., Premoli-Silva, I., Housley, R.A., 1991. Oxygen and carbon isotope stratigraphy of the Paleogene and Cretaceous limestones in the Bottaccione Gorge and the Contessa Highway sections, Umbria, Italy. Terra Res. 3, 414–422.

Courtillot, V., Besse, J., Vandamme, D., Montlgny, R., Jaeger, J.J., Cappetta, H., 1986. Deccan flood basalts at the Cretaceous/Tertiary boundary? Earth Planet. Sctence Lett. 80, 361–374. doi:10.1016/0009-2541(88)90533-5

Courtillot, V., Jaupart, C., Manighetti, I., Tapponnier, P., Besse, J., 1999. On causal links between flood basalts and continental breakup. Earth Planet. Sci. Lett. 166, 177–195.

Coxall, H.K., D'Hondt, S., Zachos, J.C., 2006. Pelagic evolution and environmental recovery after the Cretaceous-Paleogene mass

extinction. Geology 34, 297–300. doi:10.1130/G21702.1

Culver, S.J., 2003. Benthic foraminifera across the Cretaceous-Tertiary (K-T) boundary: A review. Mar. Micropaleontol. 47, 177–226.

D'Hondt, S., 2005. Consequences of the Cretaceous/Paleogene Mass extinction for marine ecosystems. Annu. Rev. Ecol. Evol. Syst. 36, 295–317. doi:10.1146/annurev.ecolsys.35.021 103.105715

Donaldson, S., Hildebrand, A.R., 2001. The global fluence of iridium at the Cretaceous-Tertiary boundary. Meteorit. Planet. Sci. 36, A50.

Ebihara, M., Miura, T., 1996. Chemical characteristics of the Cretaceous-Tertiary boundary layer at Gubbio, Italy. Geochim. Cosmochim. Acta 60, 5133–5144.

Esmeray-Senlet, S., Wright, J.D., Olsson, R.K., Miller, K.G., Browning, J. V, Quan, T.M., 2015. The Cretaceous/Paleogene mass extinction. Paleoceanography 30, 718–738. doi:10.1002/2014PA002724.Receive d

Fouke, B.W., Zerkle, A.L., Alvarez, W., Pope, K.O., Ocampo, A.C., Wachtman, R.J., Nishimura, J.M.G., Claeys, P., Fischer, A.G., 2002. Cathodoluminescence petrography and isotope geochemistry of KT impact ejecta deposited 360 km from the Chicxulub crater, at Albion island, Belize. Sedimentology 49, 117–138. doi:10.1046/j.1365-3091.2002.00435.x

Frei, R., Frei, K.M., 2002. A multi-isotopic and trace element investigation of the Cretaceous–Tertiary boundary layer at Stevns Klint, Denmark–inferences for the origin and nature of siderophile and lithophile element geochemical anomalies. Earth Planet. Sci. Lett. 203, 691–708.

Galeotti, S., Brinkhuis, H., Huber, M., 2004a. Records of post-Cretaceous-Tertiary boundary millennial-scale cooling from the western Tethys: A smoking gun for the impact-winter hypothesis? Geology 32, 529–532. doi:10.1130/G20439.1

Galeotti, S., Kaminski, M.A., Coccioni, R., Speijer, R.P., 2004b. High-resolution deep-water agglutinated foraminiferal record across the Paleocene/Eocene transition in the Contessa Road section (Central Italy). Proc. Sixth Int. Work. Agglutinated Foraminifera. Grzyb. Found. Spetial Publ. 8, 83–103.

Galeotti, S., Moretti, M., Cappelli, C., Phillips, J., Lanci, L., Littler, K., Monechi, S., Petrizzo, M.R., Premoli-Silva, I., Zachos, J.C., 2015. The Bottaccione section at Gubbio, central Italy: a classical Paleocene Tethyan setting revisited. Newsletters Stratigr. 48, 325–339. doi:10.1127/nos/2015/0067

Gallala, N., Zaghbib-Turki, D., Arenillas, I., Arz, J.A., Molina, E., 2009. Catastrophic mass extinction and assemblage evolution in planktic foraminifera across the Cretaceous/Paleogene (K/Pg) boundary at Bidart (SW France). Mar. Micropaleontol. 72, 196–209. doi:10.1016/j.marmicro.2009.05.001

Gardin, S., Galbrun, B., Thibault, N., Coccioni, R., Premoli-Silva, I., 2012. Bio-magnetochronalogy for the upper Campanian- Maastrichtian from the Gubbio area, Italy: New results from the Contessa Highway and Bottaccione sections. newsletters Stratigr. 45, 75–103.

Gardin, S., Monechi, S., 1998. Palaeoecological change in middle to low latitude calcareous nannoplankton at the Cretaceous/Tertiary boundary. Bull. la Société géologique Fr. 169, 709–723.

Giusberti, L., Coccioni, R., Sprovieri, M., Tateo, F., 2009. Perturbation at the sea floor during the Paleocene-Eocene Thermal Maximum: Evidence from benthic foraminifera at Contessa Road, Italy. Mar. Micropaleontol. 70, 102–119. doi:10.1016/j.marmicro.2008.11.003

Glass, B. p., Burns, C.A., 1987. Late Eocene Crystal-Bearing Spherules - 2 Layers or One - a Reply. Meteoritics 23, 265–279.

Goderis, S., Tagle, R., Belza, J., Smit, J., Montanari, A., Vanhaecke, F., Erzinger, J., Claeys, P., 2013. Reevaluation of siderophile element abundances and ratios across the Cretaceous-Paleogene (K-Pg) boundary: Implications for the nature of the projectile. Geochim. Cosmochim. Acta 120, 417–446. doi:10.1016/j.gca.2013.06.010

Goto, K., Tada, R., Tajika, E., Iturralde-Vinent, M.A., Matsui, T., Yamamoto, S., Nakano, Y., Oji, T., Kiyokawa, S., García Delgado, D.E., Díaz Otero, C., Rojas Consuegra, R.,

2008. Lateral lithological and compositional variations of the Cretaceous/Tertiary deep-sea tsunami deposits in northwestern Cuba. Cretac. Res. 29, 217–236. doi:10.1016/j.cretres.2007.04.004

Grajales-Nishimura, J.M., Murillo-Muetn, G., Rosales-Domnguez, C., Cedillo-Pardo, E., Garca-Hernndez, J., 2003. Heterogeneity of lithoclast composition in the deep-water carbonate breccias of the K/T boundary sedimentary succession, southeastern Mexico and offshore Campeche. AAPG Special Volumes.

Groot, J.J., de Jonge, R.B.G., Langereis, C.G., ten Kate, W.G.H.Z., Smit, J., 1989. Magnetostratigraphy of the Cretaceous-Tertiary boundary at Agost (Spain). Earth Planet. Sci. Lett. 94, 385–397. doi:10.1016/0012-821X(89)90155-6

Günther, D., Audétat, A., Frischknecht, R., Heinrich, C.A., 1998. Quantitative analysis of major , minor and trace elements in fluid inclusions using laser ablation – inductively coupled plasma mass spectrometry. J. Anal. At. Spectrom. 13, 263–270.

Hennekam, R., Jilbert, T., Mason, P.R.D., de Lange, G.J., Reichart, G.J., 2015. High-resolution line-scan analysis of resin-embedded sediments using laser ablation-inductively coupled plasma-mass spectrometry (LA-ICP-MS). Chem. Geol. 403, 42–51. doi:10.1016/j.chemgeo.2015.03.004

Hildebrand, A.R., Penfield, G.T., Kring, D.A., Pilkington, M., A., C.Z., Jacobsen, S.B., Boynton, W.V., 1991. Chicxulub Crater: A possible

Cretaceous/Tertiary boundary impact crater on the Yucatán Peninsula, Mexico. Geology 19, 867. doi:10.1130/0091-7613(1991)019<0867:CCAPCT>2.3.CO;2

Hollis, C.J., Strong, C.P., 2003. Biostratigraphic review of the Cretaceous/Tertiary boundary transition, mid-Waipara River section, North Canterbury, New Zealand. New Zeal. J. Geol. Geophys. 46, 243–253. doi:10.1080/00288306.2003.9515007

Hollis, C.J., Strong, C.P., Rodgers, K.A., Rogers, K.M., 2003. Paleoenvironmental changes across the Cretaceous/Tertiary boundary at Flaxbourne River and Woodside Creek, eastern Marlborough, New Zealand. New Zeal. J. Geol. Geophys. 46, 177–197. doi:10.1080/00288306.2003.9515003

Hough, R.M., Gilmour, I., Pillinger, C.T., Langenhorst, F., Montanari, A., 1997. Diamonds from the iridium-rich K-T boundary layer at Arroyo el Mimbral, Tamaulipas, Mexico. Geology 25, 1019–1022. doi:10.1130/0091-7613(1997)025<1019:DFTIRK>2.3.CO

Hsü, K.J., 1980. Terretrial catastrophe caused by cometary Impact at the end of Cretaceous. Nature 285, 201–203.

Hsü, K.J., He, Q., McKenzie, J.A., Weissert, H., Perch-Nielsen, K., Oberhänsli, H., Kelts, K., LaBrecque, J., Tauxe, L.,

Krähenbühl, U., 1982. Mass mortality and its environmental and evolutionary consequences. Science (80-.). 216, 249–256.

Hsü, K.J., McKenzie, J.A., 1985. A "Strangelove" ocean in the earliest Tertiary. Carbon Cycle Atmos. CO Nat. Var. Archean to Present 487–492.

Hull, P., 2015. Life in the aftermath of mass extinctions. Curr. Biol. 25, R941–R952. doi:10.1016/j.cub.2015.08.053

Hull, P.M., Norris, R.D., 2011. Diverse patterns of ocean export productivity change across the Cretaceous-Paleogene boundary: New insights from biogenic barium. Paleoceanography 26, PA3205. doi:10.1029/2010PA002082

Hull, P.M., Norris, R.D., Bralower, T.J., Schueth, J.D., 2011. A role for chance in marine recovery from the end-Cretaceous extinction. Nat. Geosci. 4, 856–860. doi:10.1038/ngeo1302

Husson, D., Galbrun, B., Gardin, S., Thibault, N., 2014. Tempo and duration of short-term environmental perturbations across the Cretaceous-Paleogene boundary. Stratigraphy 11, 159–171.

Ibáñez-Insa, J., Pérez-Cano, J., Fondevilla, V., Oms, O., Rejas, M., Fernández-Turiel, J.L., Anadon, P., 2017. Portable X-ray fluorescence identification of the Cretaceous/Paleogene boundary: Application to the Agost and Caravaca sections, SE Spain. Cretac. Res.

doi:10.1016/j.cretres.2017.06.004

Ingram, B.L., 1992. Ichthyolith strontium isotopic stratigraphy of deep-sea clays: Sites 885 and 886 (North Pacific transect), in: Proceedings-Ocean Drilling Program Scientific Results. National Science Foundation, pp. 399–412.

Ivany, L.C., Salawitch, R.J., 1993. Carbon isotopic evidence for biomass burning at the K-T boundary. Geology 21, 487–490.

Izett, G.A., 1991. Tektites in Cretaceous-Tertiary Boundary Rocks on Haiti and Their Bearing on the Alvarez Impact Extinction Hypothesis. J. Geophys. Res. 96, 20879–20905. doi:10.1029/91je02249

Izett, G.A., 1990. The Cretaceous/Tertiary boundary interval, Raton Basin, Colorado and New Mexico. Geol. Soc. Am. Spec. Pap. 249, 100.

Jenner, F.E., Arevalo, R.D., 2016. Major and trace elerment analysis of natural and experimental igneous systems using LA-ICP-MS. Elements 12, 311–316. doi:10.2113/gselements.12.5.311

Jilbert, T., de Lange, G.J., Reichart, G.J., 2008. Fluid displacive resin embedding of laminated sediments: preserving trace metals for high-resolution paleoclimate investigations. Limnol. Oceanogr. Methods 6, 16–22. doi:10.4319/lom.2008.6.16

Jochum, K.P., Weis, U., Stoll, B., Kuzmin, D., Yang, Q., Raczek, I.,

Jacob, D.E., Stracke, A., Birbaum, K., Frick, D.A., Günther, D., Enzweiler, J., 2011. Determination of reference values for NIST SRM 610-617 glasses following ISO guidelines. Geostand. Geoanalytical Res. 35, 397–429. doi:10.1111/j.1751-908X.2011.00120.x

Kaiho, K., Kajiwara, Y., Tazaki, K., Ueshima, M., Takeda, N., Kawahata, H., Arinobu, T., Ishiwatari, R., Akio, H., Lamolda, M.A., 1999. Ocenic primary productivity and dissolved oxygen levels at the Cretaceous/Tertiary boundary: their decrease, subsequent warming, ahd recovery. Paleoceanography 14, 511–524.

Kaiho, K., Lamolda, M.A., 1999. Catastrophic extinction of planktonic foraminifera at the Cretaceous-Tertiary boundary evidenced by stable isotopes and foraminiferal abundance at Caravaca, Spain. Geology 27, 355–358.

Kaiho, K., Oshima, N., Adachi, K., Adachi, Y., Mizukami, T., Fujibayashi, M., Saito, R., 2016. Global climate change driven by soot at the K-Pg boundary as the cause of the mass extinction. Sci. Rep. 6, 28427. doi:10.1038/srep28427

Kędzierski, M., Rodríguez-Tovar, F.J., Uchman, A., 2011. Vertical displacement and taphonomic filtering of nannofossils by bioturbation in the Cretaceous-Palaeogene boundary section at Caravaca, SE Spain. Lethaia 44, 321–328. doi:10.1111/j.1502-3931.2010.00244.x

Keller, G., 2013. Exploring the Causes of Mass Extinction Events. Eos (Washington. DC). 94, 200.

Keller, G., 1992. Paleoecologic response of Tethyan benthic foraminifera to the Cretaceous-Tertiary boundary transition. Stud. Benthic Foraminifera. Tokai Univ. Press. Tokyo 77–91.

Keller, G., Bhowmick, P.K., Upadhyay, H., Dave, A., Reddy, A.N., Jaiprakash, B.C., Adatte, T., 2011. Deccan volcanism linked to the Cretaceous-Tertiary boundary mass extinction: New evidence from ONGC wells in the Krishna-Godavari Basin. J. Geol. Soc. India 78, 399–428. doi:10.1007/s12594-011-0107-3

Keller, G., Stinnesbeck, W., Adatte, T., Holland, B., Stüben, D., Harting, M., De Leon, C., de la Cruz, J., 2003. Spherule deposits in Cretaceous–Tertiary boundary sediments in Belize and Guatemala. Geol. Soc. 160, 783–795.

King, D.T., Petruny, L.W., Neathery, T.L., 2007. Ecosystem perturbation caused by a small Late Cretaceous marine impact, Gulf Coastal Plain, USA. Geol. Soc. Am. Spec. Pap. 424, 97–107. doi:10.1130/2007.2424(06)

Kiyokawa, S., Tada, R., Iturralde-Vinent, M.A., Tajika, E., Yamamoto, S., Oji, T., Nakano, Y., Goto, K., Takayama, H., Garcia Delgado, D., Diaz Otero, C., Rojas-Consuegra, R., Matsui, T., 2002. Cretaceous-Tertiary boundary sequence in the Cacarajicara Formation, western Cuba: An impact-related, high-

energy, gravity-flow deposit, in: Koeberl, C., MacLeod, K.G. (Eds.), Catastrophic Events and Mass Extinctions: Impacts and Beyond. Geological Society of America.

Klaver, G.T., Van Kempen, T.M.G., Bianchi, F.R., Van Der Gaast, S.J., 1987. The Green spherules as indicators of the Cretaceous/Tertiary boundary in Deep Sea Drilling Project Hole 603B. Initial reports DSDP, Leg 93, Norfolk, Virginia to Norfolk, Virginia Part 2 1039–1056.

Koeberl, C., Sigurdsson, H., 1992. Geochemistry of impact glasses from the K/T boundary in Haiti: Relation to smectites and a new type of glass. Geochim. Cosmochim. Acta 56, 2113–2129. doi:10.1016/0016-7037(92)90333-E

Korbar, T., Montanari, A., Fucek, V.P., Fucek, L., Coccioni, R., McDonald, I., Claeys, P., Schulz, T., Koeberl, C., 2015. Potential Cretaceous-Paleogene boundary tsunami deposit in the intra-Tethyan Adriatic carbonate platform section of Hvar (Croatia). Bull. Geol. Soc. Am. 127, 1666–1680. doi:10.1130/B31084.1

Koutsoukos, E.A.M., 2005. The K-T Boundary, in: Koutsoukos, E.A.. (Ed.), Applied Stratigraphy: Topics in Geobiology. Springer, Dordrecht 23, pp. 147–161.

Kring, D.A., 2007. The Chicxulub impact event and its environmental consequences at the Cretaceous-Tertiary boundary. Palaeogeogr. Palaeoclimatol. Palaeoecol. 255, 4–21. doi:10.1016/j.palaeo.2007.02.037

Kring, D.A., 1995. The dimensions of the Chicxulub impact crater and impact melt sheet. J. Geophys. Res. 100, 16979–16986.

Kring, D.A., Claeys, P., Gulick, S.P.S., Morgan, J. V, Collins, G.S., Party, I.-I.E. 364 S., 2017. Chicxulub and the Exploration of Large Peak- Ring Impact Craters through Scientific Drilling. GSA Today 27. doi:10.1130/GSATG352A.1.

Kring, D.A., Durda, D.D., 2002. Trajectories and distribution of material ejected from the Chicxulub impact crater: Implications for postimpact wildfires. J. Geophys. Res. Planets 107.

Kyte, F.T., 1998. A meteorite from the Cretaceous/Tertiary boundary. Nature 396, 237–239.

Kyte, F.T., Bostwick, J.A., Zhou, L., 1996. The Cretaceous-Tertiary boundary on the Pacific plate: Composition and distribution of impact debris. Cretaceous-Tertiary event other catastrophes Earth Hist. Geol. Soc. Am. Spec. Pap. 307, 389–401.

Kyte, F.T., Smit, J., 1986. Regional variations in spinel composition: an important key to the Cretaceous/Tertiary event. Geology 14, 485–487. doi:10.1130/0091-7613(1986)14<485:RVISCA>2.0.C O

Kyte, F.T., Wasson, J.T., 1982. Geochemical constraints on the nature of large accretionary events. Geol. Soc. Am. Spec. Pap. 190, 235–242.

Kyte, F.T., Zhou, Z., Wasson, J.T., 1980. Siderophile-enriched sediments from the Cretaceous–Tertiary boundary. Nature 288, 651–656.

Labandeira, C.C., Rodríguez-Tovar, F.J., Uchman, A., 2016. The End-Cretaceous Extinction and Ecosystem Change, in: Mángano, M.G., Buatois, L.A. (Eds.), The Trace-Fossil Record of Major Evolutionary Events. pp. 265–300. doi:10.1007/978-94-017-9597-5_5

Laska, W., Rodríguez-Tovar, F.J., Uchman, A., 2017. Evaluating macrobenthic response to the Cretaceous–Palaeogene event: A high-resolution ichnological approach at the Agost section (SE Spain). Cretac. Res. 70, 96–110. doi:10.1016/j.cretres.2016.10.003

Lawton, T.F., Shipley, K.W., Aschoff, J.L., Giles, K.A., Vega, F.J., 2005. Basinward transport of Chicxulub ejecta by tsunami-induced backflow, La Popa basin, northeastern Mexico, and its implications for distribution of impact-related deposits flanking the Gulf of Mexico. Geology 33, 81–84. doi:10.1130/G21057.1

Leroux, H., Rocchia, R., Froget, L., Orue-etxebarria, X., Doukhan, J., Robin, E., 1995. The K/T boundary at Beloc (Haiti): Compared stratigraphic distributions of the boundary markers. Earth Planet. Sci. Lett. 131, 255–268.

Locklair, R.E., Savrda, C.E., 1998. Ichnology of rhythmically bedded Demopolis Chalk (Upper Cretaceous, Alabama): implications for paleoenvironment, depositional cycle origins, and tracemaker

behavior. Palaios 13, 423–438.

Loroch, D., Deutsch, A., Berndt, J., Bornemann, A., 2016. The Cretaceous/Paleogene (K-Pg) boundary at the J Anomaly Ridge, Newfoundland (IODP Expedition 342, Hole U1403B). Meteorit. Planet. Sci. 51, 1370–1385. doi:10.1111/maps.12667

Lowery, C.M., Bralower, T.J., Owens, J.D., Rodríguez-tovar, F.J., Jones, H., Smit, J., Gulick, S., Joanna, V., Green, S., Chenot, E., Whalen, M.T., Claeys, P., Farley, K., Sean, P., 2018. Rapid recovery of life at ground zero of the end-Cretaceous mass extinction. Nature. doi:10.1038/s41586-018-0163-6

Lowrie, W., Alvarez, W., 1977. Late Cretaceous geomagnetic polarity sequence: detailed rock and palaeomagnetic studies of the Scaglia Rossa limestone at Gubbio, Italy. Geophys. J. R. Astron. Soc. 51, 561–581. doi:10.1111/j.1365-246X.1977.tb04207.x

Lowrie, W., Alvarez, W., Napoleone, G., Perch-Nielsen, K., Premoli-Silva, I., Toumarkine, M., 1982. Paleogene magnetic stratigraphy in Umbrian pelagic carbonate rocks: The Contessa sections, Gubbio. Geol. Soc. Am. Bull. 93, 414–432. doi:10.1130/0016-7606(1982)93<414:PMSIUP>2.0.CO;2

Luterbacher, H.P., Premoli-Silva, I., 1962. Note préliminaire sur une révision du profil de Gubbio, Italie. Riv. Ital. di Paleontol. e Stratigr. 68, 253–288.

MacLeod, K.G., Whitney, D.L., Huber,

B.T., Koeberl, C., 2007. Impact and extinction in remarkably complete Cretaceous-Tertiary boundary sections from Demerara Rise, tropical western North Atlantic. Bull. Geol. Soc. Am. 119, 101–115. doi:10.1130/B25955.1

Macleod, N., Keller, G., 1994. Comparative biogeographic analysis of planktic foraminiferal survivorship across the Cretaceous/Tertiary (K/T) boundary. Paleobiology 20, 143–177.

Macleod, N., Keller, G., 1991. Hiatus distributions and mass extinctions at the Cretaceous/Tertiary boundary. Geology 19, 497–501. doi:10.1130/0091-7613(1991)019<0497:HDAMEA>2.3.CO

MacLeod, N., Keller, G., 1991. How complete are Cretaceous/tertiary boundary sections?A chronostratigraphic estimate based on graphic correlation. Geol. Soc. Am. Bull. 103, 1439–1457. doi:10.1130/0016-7606(1991)103<1439

Macleod, N., Rawson, P.F., Forey, P.L., Banner, F.T., 1997. The Cretaceous–Tertiary biotic transition. J. Geol. Soc. 154, 265–292.

Martínez-Ruiz, F., 1994. Geoquímica y mineralogía del tránsito Cretácico-Terciario en las Cordilleras Béticas y en la Cuenca Vasco-Cantábrica. Universidad de Granada.

Martínez-Ruiz, F., Ortega-Huertas, M., Kroon, D., Smit, J., Palomo-

Delgado, I., Rocchia, R., 2001. Geochemistry of the Cretaceous-Tertiary boundary at Blake Nose (ODP Leg 171B). Geol. Soc. London, Spec. Publ. 183, 131–148.

Martínez-Ruiz, F., Ortega-Huertas, M., Palomo, I., 1999. Positive Eu anomaly development during diagenesis of the K/T boundary ejecta layer in the Agost section (SE Spain): Implications for trace-element remobilization. Terra Nov. 11, 290–296.

Martínez-Ruiz, F., Ortega-Huertas, M., Palomo, I., Acquafredda, P., 1997. Quench textures in altered spherules from the Cretaceous-Tertiary boundary layer at Agost and Caravaca, SE Spain. Sediment. Geol. 113, 137–147. doi:10.1016/S0037-0738(97)00057-2

Martínez-Ruiz, F., Ortega-Huertas, M., Palomo, I., Barbieri, M., 1992. The geochemistry and mineralogy of the Cretaceous-Tertiary boundary at Agost (southeast Spain). Chem. Geol. 95, 265–281. doi:10.1016/0009-2541(92)90016-X

Martínez-Ruiz, F., Ortega-Huertas, M., Palomo, I., Smit, J., 2002. Cretaceous-Tertiary boundary at Blake Nose (Ocean Drilling Program Leg 171B): A record of the Chicxulub impact ejecta. Spec. Pap. Geol. Soc. Am. 356, Pages 189-199. doi:10.1130/0-8137-2356-6.189

Martínez-Ruiz, F., Ortega-Huertas, M., Rivas, P., 2006. Rare earth element composition as evidence of the precursor material of Cretaceous-Tertiary boundary sediments at distal sections. Chem. Geol. 232, 1–11. doi:10.1016/j.chemgeo.2006.02.013

Michel, H.V., Asaro, F., Alvarez, W., Alvarez, L.W., 1990. Geochemical studies of the Cretaceous-Tertiary boundary in ODP Holes 689B and 690C, in: Barker P.F., K.J.P. (Ed.), Proc., Scientific Results, ODP, Leg 113, Weddell Sea, Antarctica. ODP, Texas A&M University, College Station; UK distributors, IPOD Committee, NERC, Swindon, pp. 159–168.

Mizukami, T., Kaiho, K., Oba, M., 2014. A spike of woody plant biomarkers in the deep-sea iridium layer at the Cretaceous/Paleogene boundary. Palaeogeogr. Palaeoclimatol. Palaeoecol. 412, 241–248. doi:10.1016/j.palaeo.2014.07.041

Mizukami, T., Kaiho, K., Oba, M., 2013. Significant changes in land vegetation and oceanic redox across the Cretaceous/Paleogene boundary. Palaeogeogr. Palaeoclimatol. Palaeoecol. 369, 41–47. doi:10.1016/j.palaeo.2012.09.020

Molina, E., 2015. Evidence and causes of the main extinction events in the Paleogene based on extinction and survival patterns of foraminifera. Earth-Science Rev. 140, 166–181. doi:10.1016/j.earscirev.2014.11.008

Molina, E., Alegret, L., Arenillas, I., 2004. The Cretaceous/Paleogene boundary at the Agost section revisited: paleoenvironmental reconstruction and mass extinction pattern. J. Iber. Geol. 31, 135–148.

Molina, E., Alegret, L., Arenillas, I., Arz, J.A., 2005. The

Cretaceous/Paleogene boundary at the Agost section revisited: paleoenvironmental reconstruction and mass extinction pattern. J. Iber. Geol. 31, 135–148.

Molina, E., Alegret, L., Arenillas, I., Arz, J.A., Gallala, N., Grajales-Nishimura, J.M., Murillo-Muñetón, G., Zaghbib-Turki, D., 2009. The Global Boundary Stratotype Section and Point for the base of the Danian Stage (Paleocene, Paleogene, "Tertiary", Cenozoic): auxiliary sections and correlation. Episodes 32, 84–95.

Molina, E., Alegret, L., Arenillas, I., Arz, J.A., Gallala, N., Hardenbol, J., Von Salis, K., Steurbaut, E., Vandenberghe, N., Zaghbib-Turki, D., 2006. The Global Boundary Stratotype Section and Point for the base of the Danian Stage (Paleocene, Paleogene, "Tertiery", Cenozoic) at El Kef , Tunisia-Original definition and revision. Episodes 29, 265–273.

Molina, E., Arenillas, I., Arz, J.A., 1998. Mass extinction in planktic foraminifera at the Cretaceous/Tertiary boundary in subtropical and temperate latitudes. Bull. la Soc. Geol. Fr. 169, 351–363.

Molina, E., Arenillas, I., Arz, J.A., 1996. The Cretaceous/Tertiary boundary mass extinction in planktic foraminifera at Agost, Spain. Rev. Micropaleontol. 39, 225–243.

Molina, E., Arenillas, J., Arz, J.A., 2001. Micropaleontology, in: Martínez-Ruiz, F., Molina, E., Rodríguez-Tovar, F.J. (Eds.), Fieldtrip Guide to the Agost and Caravaca Sections (Betic Cordillera, Spain). pp. 40–45.

Monaco, P., Rodríguez-Tovar, F.J., Uchman, A., 2015. A delayed response of the trace fossil community at the Cretaceous-Paleogene boundary in the Bottaccione section, Gubbio, Central Italy. Geobios 48, 137–145. doi:10.1016/j.geobios.2015.02.001

Montanari, A., 1991. Authigenesis of impact spheroids in the K/T boundary clay from Italy: New constraints for high-resolution stratigraphy of terminal Cretaceous events. J. Sediment. Res. 61.

Montanari, A., Koeberl, C., 2000. Impact stratigraphy—The Italian Extraterrestrial chromite in latest Maastrichtian and Paleocene pelagic limestone 2109 record, in: Lecture Notes in Earth Sciences, Vol 93. Springer, Heidelberg, p. 364.

Morford, J.L., Emerson, S., 1999. The geochemistry of redox sensitive trace metals in sediments. Geochim. Cosmochim. Acta 63, 1735–1750. doi:10.1016/S0016-7037(99)00126-X

Morgan, J., Lana, C., Kearsley, A., Coles, B., Belcher, C., Montanari, S., Díaz-Martínez, E., Barbosa, A., Neumann, V., 2006. Analyses of shocked quartz at the global KP boundary indicate an origin from a single, high-angle, oblique impact at Chicxulub. Earth Planet. Sci. Lett. 251, 264–279.

Morgan, J.V., Gulick, S.P.S., Bralower, T., Chenot, E., Christeson, G., Claeys, P., Cockell, C., Collins, G.., Coolen, M.J.L., Ferrière, L., Gebhardt, C.,

Goto, K., 2016. Impact Craters. Science (80-.). 354, 878–883.

Mukhopadhyay, S., Farley, K.A., Montanari, A., 2001. A short duration of the Cretaceous-Tertiary boundary event: Evidence from Extraterrestrial Helium-3. Science (80-.). 291, 1952–1954. doi:10.1126/science.291.5510.1952

Murillo-Muñeton, G., Dorobek, S.L., 2003. Controls on the evolution of carbonate mud mounds in the Lower Cretaceous Cupido Formation, Northeastern Mexico. J. Sediment. Res. 73, 869–886. doi:10.1306/043003730869

Nichols, D., Johnson, K., 2008. Plants and the K-T Boundary., Cambridge: ed. doi:10.1017/CBO9780511535536

Nichols, D.J., Brown, J.L., Attrep Jr, M., Orth, C.J., 1992. A new Cretaceous-Tertiary boundary locality in the western Powder River basin, Wyoming: biological and geological implications. Cretac. Res. 13, 3–30.

Nichols, D.J., Hartman, J.H., Johnson, K.R., 2002. Palynology and palynostratigraphy of the Hell Creek Formation in North Dakota: a microfossil record of plants at the end of Cretaceous time. Geol. Soc. Am. Spec. Pap 361, 393–456.

Nichols, D.J., Jarzen, D.M., Orth, C.J., Oliver, P.Q., 1986. Palynological and iridium anomalies at Cretaceous-Tertiary boundary, south-central Saskatchewan. Science (80-.). 231, 714–717.

Officer, C.B., Drake, C.L., 1985. Terminal Cretaceous environmental events. Science (80-.). 227, 1161–1167.

Olsson, R.K., Miller, K.G., Browning, J.V., Habib, D., Sugarman, P.J., 1997. Ejecta layer at the Cretaceous-Tertiary boundary, Bass River, New Jersey (Ocean Drilling Program Leg 174AX). Geology 25, 759–762.

Ortega-Huertas, M., Martínez-Ruiz, F., Acquafredda, P., Palomo, I., 1994. Platinum-group elements in the cores of potessium feldspar spherules from the cretaceous-tertiary boundary at caravaca (Spain). Estud. Geol 50, 3–7.

Ortega-Huertas, M., Martínez-Ruiz, F., Palomo, I., Chamley, H., 2002. Review of the mineralogy ot the Cretaceous-Tertiary boundary clay: evidence supporting a major extraterrestrial catastrophic event. Clay Miner. 37, 395–411. doi:10.1180/0009855023730054

Ortega-Huertas, M., Martínez-Ruiz, F., Palomo, I., Charnley, H., 1995. Comparative mineralogical and geochemical clay sedimentation in the Betic Cordilleras and Basque-Cantabrian Basin areas at the Cretaceous-Tertiary boundary. Sediment. Geol. 94, 209–227.

Ortega-Huertas, M., Palomo, I., Martínez-Ruiz, F., González, I., 1998. Geological factors controlling clay mineral patterns across the Cretaceous-Tertiary boundary in Mediterranean and Atlantic sections. Clay Miner. 33, 483–500.

Pälike, H., 2013. Impact and Extinction.

Science (80-.). 339, 655–656.

Peryt, D., Alegret, L., Molina, E., 2002. The Cretaceous/Palaeogene (K/P) boundary at Aïn Settara, Tunisia: Restructuring of benthic foraminiferal assemblages. Terra Nov. 14, 101–107.

Pillmore, C.L., Tschudy, R.H., Orth, C.J., Gilmore, J.S., Knight, J.D., 1984. Geologic framework of nonmarine Cretaceous-Tertiary boundary sites, Raton basin, New Mexico and Colorado. Science (80-.). 223, 1180–1183.

Pope, K.O., Ocampo, A.C., Fischer, A.G., Alvarez, W., Fouke, B.W., Webster, C.L., Vega, F.J., Smit, J., Fritsche, A.E., Claeys, P., 1999. Chicxulub impact ejects from Albion Island, Belize. Earth Planet. Sci. Lett. 170, 351–364. doi:10.1016/s0012-821x(99)00123-5

Pope, K.O., Ocampo, A.C., Fischer, A.G., Vega, F.J., Ames, D.E., King Jr, D.T., Fouke, B.W., Wachtman, R.J., Kletetschka, G., 2005. Chicxulub impact ejecta deposits in southern Quintana Roo, México, and central Belize, in: Kenkmann, T., Hörz, F., Deutsch, A. (Eds.), Large Meteorite Impacts III. Geological Society of America.

Powell, M.., Macgregor, J., 2011. A geographic test of species selection using planktonic foraminifera during the Cretaceous/Paleogene mass extinction foraminifera during the Cretaceous/Paleogene mass extinction 37, 426–437.

Preisinger, A., Aslanian, S., Brandstatter, F., Grass, F., Stradner, H.,

Summesberger, H., 2002. Cretaceous-Tertiary profile, rhythmic deposition, and geomagnetic polarity reversals of marine sediments near Bjala, Bulgaria. Spec. Pap. Soc. Am. 356, 213–230.

Raup, D.M., Sepkoski, J.J., 1982. Mass extinctions in marine fossil record. Science (80-.). 215, 1501–1503.

Reitz, A., Thomson, J., de Lange, G.J., Hensen, C., 2006. Source and development of large manganese enrichments above eastern Mediterranean sapropel S1. Paleoceanography 21, 1–17. doi:10.1029/2005PA001169

Renne, P.R., Deino, A.L., Hilgen, F.J., Kuiper, K.F., Mark, D.F., Mitchell, W.S., Morgan, L.E., Mundil, R., Smit, J., 2013. Time scales of critical events around the Cretaceous-Paleogene boundary. Science 339, 684–687. doi:10.1126/science.1230492

Renne, P.R., Sprain, C.J., Richards, M.A., Self, S., Vanderkluysen, L., Pande, K., 2015. Possibly Induced By Impact. Science (80-.). 350, 76–78. doi:10.1126/science.aac7549

Ritter, X., Deutsch, A., Berndt, J., Robin, E., 2015. Impact glass spherules in the Chicxulub K-Pg event bed at Beloc, Haiti: Alteration patterns. Meteorit. Planet. Sci. 50, 418–432. doi:10.1111/maps.12432

Rodríguez-Tovar, F.J., 2005. Fe-oxide spherules infilling Thalassinoides burrows at the Cretaceous-Paleogene (K-P) boundary: Evidence of a near-

contemporaneous macrobenthic colonization during the K-P event. Geology 33, 585–588. doi:10.1130/G21527.1

Rodríguez-Tovar, F.J., Martín-Peinado, F.J., 2011. Colonization of contaminated sediments: Implications in recovery of mass extinctions events, in: Goldschmidt Conference Abstracts. p. 1742.

Rodríguez-Tovar, F.J., Martín-Peinado, F.J., 2009. The environmental disaster of Aznalcollar (southern Spain) as an approach to the Cretaceous-Palaeogene mass extinction event. Geobiology 7, 533–543. doi:10.1111/j.1472-4669.2009.00213.x

Rodríguez-Tovar, F.J., Martínez-Ruiz, F., Bernasconi, S.M., 2006. Use of high-resolution ichnological and stable isotope data for assessing completeness of a K-P boundary section, Agost, Spain. Palaeogeogr. Palaeoclimatol. Palaeoecol. 237, 137–146. doi:10.1016/j.palaeo.2005.11.019

Rodríguez-Tovar, F.J., Martínez-Ruiz, F., Bernasconi, S.M., 2004. Carbon isotope evidence for the timing of the Cretaceous-Palaeogene macrobenthic colonisation at the Agost section (southeast Spain). Palaeogeogr. Palaeoclimatol. Palaeoecol. 203, 65–72. doi:10.1016/S0031-0182(03)00660-6

Rodríguez-Tovar, F.J., Uchman, A., 2008. Bioturbational disturbance of the Cretaceous-Palaeogene (K-Pg) boundary layer: Implications for the interpretation of the K-Pg boundary impact event. Geobios 41, 661–667.

doi:10.1016/j.geobios.2008.01.003

Rodríguez-Tovar, F.J., Uchman, A., 2006. Ichnological analysis of the Cretaceous-Palaeogene boundary interval at the Caravaca section, SE Spain. Palaeogeogr. Palaeoclimatol. Palaeoecol. 242, 313–325. doi:10.1016/j.palaeo.2006.06.006

Rodríguez-Tovar, F.J., Uchman, A., 2004a. Ichnotaxonomic analysis of the Cretaceous/Palaeogene boundary interval in the Agost section, south-east Spain. Cretac. Res. 25, 635–647. doi:10.1016/j.cretres.2004.06.003

Rodríguez-Tovar, F.J., Uchman, A., 2004b. Trace fossils after the KT boundary event from the Agost section, SE Spain. Geol. Mag. 141, 429–440. doi:10.1017/S0016756804009410

Rodriguez-Tovar, F.J., Uchman, A., Molina, E., Monechi, S., 2010. Bioturbational redistribution of Danian calcareous nannofossils in the uppermost Maastrichtian across the K-Pg boundary at Bidart, SW France. Geobios 43, 569–579. doi:10.1016/j.geobios.2010.03.002

Rodríguez-Tovar, F.J., Uchman, A., Orue-Etxebarria, X., Apellaniz, E., Baceta, J.I., 2011. Ichnological analysis of the Bidart and Sopelana Cretaceous/Paleogene (K/Pg) boundary sections (Basque Basin, W Pyrenees): Refining eco-sedimentary environment. Sediment. Geol. 234, 42–55. doi:10.1016/j.sedgeo.2010.11.004

Rohde, R.A., Muller, R.A., 2005. Cycles in fossil diversity. Nature 434, 208–

210. doi:10.1029/2000JB00033

Romein, A.J.T., 1977. Calcareous nannofossils from Cretaceous-Tertiary boundary interval in Barranco del Gredero (Caravaca, Prov-Murcia, SE Spain). Proc. K. Ned. Akad. VAN Wet. Ser. B-PALAEONTOLOGY Geol. Phys. Chem. Anthropol. 80, 256.

Scasso, R.A., Concheyro, A., Aberhan, M., Hecht, L., Medina, F.A., Tagle, R., 2005. A tsunami deposit at the Cretaceous/Paleogene boundary in the Neuquén Basin of Argentina. Cretac. Res. 26, 283–297. doi:10.1016/j.cretres.2004.12.003

Schmitz, B., Andersson, P., Dahl, J., 1988. Iridium, sulfur isotopes and rare earth elements in the Cretaceous-Tertiary boundary clay at Stevns Klint, Denmark. Geochim. Cosmochim. Acta 52, 229–236.

Schmitz, B., Asaro, F., Michel, H.V., Thierstein, H.R., Huber, B.T., 1991. Element stratigraphy across the Cretaceous/Tertiary boundary in Hole 738C, in: Barron J., L.B. (Ed.), Proc., Scientific Results, ODP, Leg 119, Kerguelen Plateau-Prydz Bay. ODP, Texas A&M University, College Station, pp. 719–730.

Schoene, B., Samperton, K.M., Eddy, M.P., Keller, G., Adatte, T., Bowring, S.A., Khadri, S.F.R., Gertsch, B., 2015. U-Pb geochronology of the Deccan Traps and relation to the end-Cretaceous mass extinction. Science (80-.). 347, 182–184. doi:10.1126/science.aaa0118

Schueth, J.D., Bralower, T.J., Jiang, S.,

Patzkowsky, M.E., 2015. The role of regional survivor incumbency in the evolutionary recovery of calcareous nannoplankton from the Cretaceous/Paleogene (K/Pg) mass extinction. Paleobiology 41, 661–679. doi:10.1017/pab.2015.28

Schulte, P., Alegret, L., Arenillas, I., Arz, J.A., Barton, P.., Paul, R., Bralower, T.J., Christeson, G.L., Claeys, P., Cockell, C.S., Collins, G.S., Deutsch, A., Goldin, T.J., Goto, K., José, M., Grieve, R.A.F., Gulick, S.P.S., Johnson, K.R., Koeberl, C., Kring, D.A., Macleod, K.G., Matsui, T., Melosh, J., Montanari, A., Morgan, J.V., Neal, C.R., Douglas, J., Norris, R.D., Pierazzo, E., Ravizza, G., Rebolledo-vieyra, M., Reimold, W.U., Robin, E., Salge, T., Speijer, R.P., Sweet, A.R., Vajda, V., Whalen, M.T., Willumsen, P.S., 2010a. Supporting Online Material for The Chicxulub Asteroid Impact and Mass Extinction at the Cretaceous- Paleogene Boundary. Science (80-.). 327, 1214–1218. doi:10.1126/science.1177265

Schulte, P., Alegret, L., Arenillas, I., Arz, J.A., Barton, P.J., Bown, P.R., Bralower, T.J., Christeson, G.L., Claeys, P., Cockell, C.S., Collins, G.S., Deutsch, A., Goldin, T.J., Goto, K., Grajales-Nishimura, J.M., Grieve, R.A.F., Gulick, S.P.S., Johnson, K.R., Kiessling, W., Koeberl, C., Kring, D.A., MacLeod, K.G., Matsui, T., Melosh, J., Montanari, A., Morgan, J.V., Neal, C.R., Nichols, D.J., Norris, R.D., Pierazzo, E., Ravizza, G., Rebolledo-Vieyra, M., Reimold, W.U., Robin, E., Salge, T., Speijer, R.P., Sweet, A.R., Urrutia-Fucugauchi, J., Vajda, V., Whalen, M.T., Willumsen, P.S., 2010b. The chicxulub asteroid impact and mass extinction at the cretaceous-

paleogene boundary. Science (80-.). 327, 1214–1218. doi:10.1126/science.1177265

Schulte, P., Kontny, A., 2005. Chicxulub impact ejecta from the Cretaceous-Paleogene (K-P) boundary in northeastern Mexico. Spec. Pap. - Geol. Soc. Am. 384, 191–221. doi:10.1130/0-8137-2384-1.191

Schulte, P., Speijer, R., Mai, H., Kontny, A., 2006. The Cretaceous-Paleogene (K-P) boundary at Brazos, Texas: Sequence stratigraphy, depositional events and the Chicxulub impact. Sediment. Geol. 184, 77–109. doi:10.1016/j.sedgeo.2005.09.021

Schulte, P., Speijer, R.P., 2009. Late Maastrichtian-early paleocene sea level and climate changes in the Antioch Church Core (Alabama, Gulf of Mexico margin, USA): A multi-proxy approach. Geol. Acta 7, 11–34. doi:10.1344/105.000000279

Sepkoski, J.J., 1996. Patterns of Phanerozoic Extinction: a Perspective from Global Data Bases, in: Global Events and Event Stratigraphy in the Phanerozoic. pp. 35–51. doi:10.1007/978-3-642-79634-0_4

Sepúlveda, J., Wendler, J.E., Summons, R.E., Hinrichs, K.-U., 2009. Rapid Resurgence of Marine Productivity After the Cretaceous-Paleogene Mass Extinction. Science (80-.). 326, 129–132. doi:10.1126/science.1176233

Shonting, D., Ezrailson, C., 2017. The Chicxulub Tsunami, in: Chicxulub: The Impact and Tsunami. Springer, pp. 69–106.

Shukolyukov, A., Lugmair, G.W., 1998. All use subject to JSTOR Terms and Conditions isotopic evidence for the Cretaceous-Tertiary impactor and Its Type. Science (80-.). 282, 927–929.

Sigurdsson, H., D´Hondt, S., Arthur, M.A., Bralower, T.J., Zachos, J.C., van Fossen, M., Channell, L.E.T., 1991. Glass from the Cretaceous/Tertiary boundary in Haiti. Nature 349, 482–487. doi:10.1038/353737a0

Sigurdsson, H., Leckie, R.M., 1997. Caribbean Volcanism , Cretaceous/Tertiary Impact , and Ocean-Climate History: Synthesis of Leg 165. Proc. Ocean Drill. Progr. 165, 377–400.

Sinnesael, M., De Vleeschouwer, D., Coccioni, R., Claeys, P., Frontalini, F., Jovane, L., Savian, J.F., Montanari, A., 2016. High-resolution multiproxy cyclostratigraphic analysis of environmental and climatic events acros the Cretaceous-Paleogene boundary in the classic pelagic succession of Gubbio (Italy). Geol. Soc. Am. Spec. Pap. 524 2524, 115–137. doi:10.1130/2016.2524(09).

Smit, J., 2004. The section of the Barranco del Gredero (Caravaca, SE Spain): A crucial section for the Cretaceous/Tertiary boundary impact extinction hypothesis. J. Iber. Geol. 31, 179–191.

Smit, J., 1999. The global stratigraphy of the Cretaceous-Tertiary boundary impact ejecta. Annu. Rev. Earth Planet. Sci. 27, 75–113.

Smit, J., 1990. Meteorite impact, extinctions and the Cretaceous-Tertiary boundary. Geol. en Mijnb. 69, 187–204.

Smit, J., 1982. Extinction and evolution of planktonic foraminifera after a major impact at the Cretaceous/Tertiary boundary, in: The Cretaceous/Tertiary Boundary Event. Geological society of America. Spetial Paper 190, pp. 329–352.

Smit, J., Hertogen, J., 1980. An extraterrestrial event at the Cretaceous-Tertiary boundary. Nature 285, 198–200.

Smit, J., Klaver, G., 1981. Sanidine spherules at the Cretaceous-Tertiary boundary indicate a large impact event. Nature 292, 47–49.

Smit, J., Roep, T.B., Alvarez, W., Montanari, A., Claeys, P., Grajales-Nishimura, J.M., Bermudez, J., 1996. Coarse-grained, clastic sandstone complex at the K/T boundary around the Gulf of Mexico: Deposition by tsunami waves induced by the Chicxulub impact?, in: Ryder, G., Fastovsky, D.E., Gartner, S. (Eds.), The Cretaceous-Tertiary Event and Other Catastrophes in Earth History . Geological Society of America.

Smit, J., Ten Kate, W.G.H.Z., 1982. Trace-element patterns at the Cretaceous-Tertiary boundary— Consequences of a large impact. Cretac. Res. 3, 307–332.

Smith, A.G., Hurley, A.M., Briden, J.C., 1981. Phanerozoic paleocontinental world maps. CUP Archive.

Soria, A.R., Liesa, C.L., Mata, M.P., Arz, J.A., Alegret, L., Arenillas, I., Meléndez, A., 2001. Slumping and a sandbar deposit at the Cretaceous-Tertiary boundary in the El Tecolote section (northeastern Mexico): An impact-induced sediment gravity flow. Geology 29, 231–234.

Sosa-Montes de Oca, C., de Lange, G.J., Martínez-Ruiz, F., Rodriguez-Tovar, F.J., 2018a. High-resolution data from Laser Ablation-ICP-MS and by ICP-OES analyses at the Cretaceous/Paleogene boundary section at Agost (SE Spain). Data Br. doi:10.1016/j.dib.2018.04.118

Sosa-Montes de Oca, C., de Lange, G.J., Martínez-Ruiz, F., Rodríguez-Tovar, F.J., 2018b. Application of laser ablation-ICP-MS to determine high-resolution elemental profiles across the Cretaceous/Paleogene boundary at Agost (Spain). Palaeogeogr. Palaeoclimatol. Palaeoecol. 497, 128–138. doi:10.1016/j.palaeo.2018.02.012

Sosa-Montes de Oca, C., Martínez-Ruiz, F., Rodríguez-Tovar, F.J., 2013. Bottom-water conditions in a marine basin after the Cretaceous-Paleogene impact event: Timing the recovery of oxygen levels and productivity. PLoS One 8, e82242. doi:10.1371/journal.pone.0082242

Sosa-Montes de Oca, C., Rodríguez-Tovar, F.J., Martínez-Ruiz, F., 2016. Geochemical and isotopic characterization of trace fossil infillings: New insights on tracemaker activity after the K/Pg impact event. Cretac. Res. 57, 391–401. doi:10.1016/j.cretres.2015.03.003

Sosa-Montes de Oca, C., Rodríguez-Tovar, F.J., Martínez-Ruiz, F., Monaco, P., 2017. Paleoenvironmental conditions across the Cretaceous–Paleogene transition at the Apennines sections (Italy): An integrated geochemical and ichnological approach. Cretac. Res. 71. doi:10.1016/j.cretres.2016.11.005

Sprovieri, M., Sabatino, N., Pelosi, N., Batenburg, S.J., Coccioni, R., Iavarone, M., Mazzola, S., 2013. Late Cretaceous orbitally-paced carbon isotope stratigraphy from the Bottaccione Gorge (Italy). Palaeogeogr. Palaeoclimatol. Palaeoecol. 379–380, 81–94. doi:10.1016/j.palaeo.2013.04.006

Stone, R., 2014. Back from the dead:The once-moribund idea that volcanism helped kill off the dinosaurs gains new credibility. Science (80-.). 346, 1281–1283.

Stott, L.D., Kennett, J.P., 1989. New constraints on early Tertiary palaeoproductivity from carbon isotopes in foraminifera. Nature 342, 526.

Sweet, A.R., Braman, D.R., 1992. The KT boundary and contiguous strata in western Canada: interactions between paleoenvironments and palynological assemblages. Cretac. Res. 13, 31–79.

Sweet, A.R., Braman, D.R., Lerbekmo, J.F., 1999. Sequential palynological changes across the composite Cretaceous-Tertiary (KT) boundary claystone and contiguous strata, western Canada and Montana, USA. Can. J. Earth Sci. 36, 743–768.

Sylvester, P.J., Jackson, S.E., 2016. A brief history of laser ablation inductively coupled plasma mass spectrometry (LA-ICP-MS). Elements 12, 307–310. doi:10.2113/gselements.12.5.307

Tada, R., Nakano, Y., Iturralde-Vinent, M.A., Yamamoto, S., Kamata, T., Tajika, E., Toyoda, K., Kiyokawa, S., Garcia Delgado, D., Oji, T., Goto, K., Takayama, H., Rojas-Consuegra, R., Matsui, T., 2002. Complex tsunami waves suggested by the Cretaceous-Tertiary boundary deposit at the Moncada section, western Cuba, in: Koeberl, C., MacLeod, K.G. (Eds.), Catastrophic Events and Mass Extinctions: Impacts and Beyond. Geological Society of America.

Taylor, S.R., McLennan, S.M., 1985. The Continental Crust: Its Composition and Evolution. Oxford: Blackwell Scientific.

Tobin, T.S., Bitz, C.M., Archer, D., 2016. Modeling climatic effects of carbon dioxide emissions from Deccan Traps Volcanic Eruptions around the Cretaceous-Paleogene boundary. Palaeogeogr. Palaeoclimatol. Palaeoecol. 478, 139–148. doi:10.1016/j.palaeo.2016.05.028

Tribovillard, N., Algeo, T.J., Baudin, F., Riboulleau, A., 2012. Analysis of marine environmental conditions based onmolybdenum-uranium covariation-Applications to Mesozoic paleoceanography. Chem. Geol. 324–325, 46–58. doi:10.1016/j.chemgeo.2011.09.009

Tribovillard, N., Algeo, T.J., Lyons, T., Riboulleau, A., 2006. Trace metals

as paleoredox and paleoproductivity proxies: An update. Chem. Geol. 232, 12–32. doi:10.1016/j.chemgeo.2006.02.012

Trinquier, A., Birck, J.L., Allègre, C.J., 2006. The nature of the KT impactor. A 54Cr reappraisal. Earth Planet. Sci. Lett. 241, 780–788.

Tschudy, R.H., Pillmore, C.L., Orth, C.J., Gilmore, J.S., Knight, J.D., 1984. Disruption of the terrestrial plant ecosystem at the Cretaceous-Tertiary boundary, Western Interior. Science (80-.). 225, 1030–1032.

Urrutia-Fucugauchi, J., Pérez-Cruz, L., 2016. Planetary sciences, geodynamics, impacts, mass extinctions, and evolution: Developments and interconnections. Int. J. Geophys. 2016. doi:10.1155/2016/4703168

Vajda, V., Raine, I., Hollis, C., 2003. Global effects of the Chicxulub asteroid impact on terrestrial vegetation-the palynological record from New Zealand KT boundary. Impact Ser. Cratering, 0–57.

Vajda, V., Raine, J.I., 2003. Pollen and spores in marine Cretaceous/Tertiary boundary sediments at mid-Waipara River, North Canterbury, New Zealand. New Zeal. J. Geol. Geophys. 46, 255–273. doi:10.1080/00288306.2003.9515008

Van der Weijden, C.H., 2002. Pitfalls of normalization of marine geochemical data using a common divisor. Mar. Geol. 184, 167–187.

van Hinsbergen, D.J.J., de Groot, L.V., van Schaik, S.J., Spakman, W., Bijl, P.K., Sluijs, A., Langereis, C.G., Brinkhuis, H., 2015. A paleolatitude calculator for paleoclimate studies. PLoS One 10, e0126946.

Van Morkhoven, F.P.C.M., Berggren, W.A., Edwards, A.S., Oertli, H.J., 1986. Cenozoic cosmopolitan deep-water benthic foraminifera. Elf Aquitaine.

van Os, B.J.H., Middelburg, J.J., de Lange, G.J., 1991. Possible diagenetic mobilization of barium in sapropelic sediment from the eastern Mediterranean. Mar. Geol. 100, 125–136. doi:10.1016/0025-3227(91)90229-W

Vandenberghe, N., Hilgen, F.J., Speijer, R.P., 2012. The Paleogene Period, in: The Geologic Time Scale 2012. Elsevier, pp. 855–921. doi:10.1016/B978-0-444-59425-9.00028-7

Vellekoop, J., Esmeray-Senlet, S., Miller, K.G., Browning, J. V., Sluijs, A., van de Schootbrugge, B., Sinninghe Damste, J.S., Brinkhuis, H., 2016. Evidence for Cretaceous-Paleogene boundary bolide "impact winter" conditions from New Jersey, USA. Geology 44, 619–622. doi:10.1130/G37961.1

Vellekoop, J., Sluijs, A., Smit, J., Schouten, S., Weijers, J.W.H., Sinninghe Damste, J.S., Brinkhuis, H., 2014. Rapid short-term cooling following the Chicxulub impact at the Cretaceous-Paleogene boundary. Proc. Natl. Acad. Sci. U. S. A. 1–5. doi:10.1073/pnas.1319253111

Vellekoop, J., Smit, J., van de Schootbrugge, B., Weijers, J.W.H., Galeotti, S., Sinninghe Damste, J.S., Brinkhuis, H., 2015. Palynological evidence for prolonged cooling along the Tunisian continental shelf following the K-Pg boundary impact. Palaeogeogr. Palaeoclimatol. Palaeoecol. 426, 216–228. doi:10.1016/j.palaeo.2015.03.021

Voigt, S., Gale, A.S., Jung, C., Jenkyns, H.C., 2012. Global correlation of Upper Campanian-Maastrichtian successions using carbon-isotope stratigraphy: develoment of a new Maastrichtian timescale. newsletters Stratigr. 45, 25–53.

Wagner, T., Fusswinkel, T., Wälle, M., Heinrich, C.A., 2016. Microanalysis of fluid inclusions in crustal hydrothermal systems using laser ablation methods. Elements 12, 323–328.

Wang, Z., Hattendorf, B., Günther, D., 2006. Analyte Response in Laser Ablation Inductively Coupled Plasma Mass Spectrometry. J. Am. Soc. Mass Spectrom. 17, 641–651. doi:10.1016/j.jasms.2006.01.005

Ward, W.., Keller, G., Stinnesbeck, W., Adatte, T., 1995. Yucatán subsurface stratigraphy: Implications and constraints for the Chicxulub impact. Geology 23, 873–876. doi:10.1130/0091-7613(1995)023<0873

Widmark, J.G.V., Speijer, R.P., 1997. Benthic foraminiferal faunas and trophic regimes at the terminal Cretaceous Tethyan seafloor. Palaios 12, 354–371.

Widmark, J.G. V., Speijer, R.P., 1997. Benthic foraminiferal ecomarker species of the terminal Cretaceous (late Maastrichtian) deep-sea Tethys. Mar. Micropaleontol. 31, 135–155. doi:10.1016/S0377-8398(97)00008-X

Wilf, P., Johnson, K.R., Huber, B.T., 2003. Correlated terrestrial and marine evidence for global climate changes before mass extinction at the Cretaceous-Paleogene boundary. Proc. Natl. Acad. Sci. 100, 599–604. doi:10.1073/pnas.0234701100

Willumsen, P., 2004. Taxonomy and biostratigraphy of two new species of Carpatella Grigorovich 1969 (Dinophyceae) from the Cretaceous-Tertiary boundary in New Zealand. J. Micropalaeontology 23, 119–125.

Willumsen, P.S., 2012. Three new species of dinoflagellate cyst from Cretaceous–Paleogene (K-Pg) boundary sections at mid- Waipara River and Fairfield Quarry, South Island, New Zealand. Palynology 36, 48–62.

Willumsen, P.S., 2000. Late Cretaceous to early Paleocene palynological changes in midlatitude Southern Hemisphere, New Zealand. GFF 122, 180–181.

Woelders, L., Vellekoop, J., Kroon, D., Smit, J., Casadío, S., Prámparo, M.B., Dinarès-Turell, J., Peterse, F., Sluijs, A., Lenaerts, J.T.M., Speijer, R.P., 2017. Latest Cretaceous climatic and environmental change in the South Atlantic region. Paleoceanography. doi:10.1002/2016PA003007

Wolfe, J.A., 1991. Palaeobotanical evidence for a June "impact winter" at the Cretaceous/Tertiary boundary. Nature 352, 420.

Yancey, T.E., Guillemette, R.N., 2008. Carbonate accretionary lapilli in distal deposits of the Chicxulub impact event. Bull. Geol. Soc. Am. 120, 1105–1118. doi:10.1130/B26146.1

Zachos, J.C., Arthur, M.A., 1986. Paleoceanography of the Cretaceous/Tertiary boundary event: Inferences from stable isotopic and other data. Paleoceanography 1, 5–26.

Zhou, L., Wignall, P.B., Su, J., Feng, Q., Xie, S., Zhao, L., Huang, J., 2012. U/Mo ratios and $\delta 95/95$Mo as local and global redox proxies during mass extinction events. Chem. Geol. 324–325, 99–107. doi:10.1016/j.chemgeo.2012.03.020

Appendix

HIGH-RESOLUTION DATA FROM LASER ABLATION-ICP-MS AND BY ICP-OES ANALYSES AT THE CRETACEOUS/PALEOGENE BOUNDARY SECTION AT AGOST (SE SPAIN)

Claudia Sosa-Montes de Oca [a], Gert J. de Lange [b], Francisca Martínez-Ruiz [c], Francisco J. Rodríguez-Tovar [a]*

a Departamento de Estratigrafía y Paleontología, Universidad de Granada, Avda. Fuentenueva s/n, 18002 Granada, Spain

b Department of Earth Sciences–Geochemistry, Geosciences, Utrecht University, 3584 CD, Utrecht, The Netherlands

c Instituto Andaluz de Ciencias de la Tierra, IACT (CSIC-Universidad de Granada), Avda. Las Palmeras 4, 18100 Armilla, Granada, Spain

Contents lists available at ScienceDirect

Data in Brief

journal homepage: www.elsevier.com/locate/dib

ELSEVIER

Data Article

High-resolution data from Laser Ablation-ICP-MS and by ICP-OES analyses at the Cretaceous/Paleogene boundary section at Agost (SE Spain)

Claudia Sosa-Montes de Oca [a,*], Gert J. de Lange [b], Francisca Martínez-Ruiz [c], Francisco J. Rodríguez-Tovar [a]

[a] *Departamento de Estratigrafía y Paleontología, Universidad de Granada, Avda. Fuentenueva s/n, 18002 Granada, Spain*
[b] *Department of Earth Sciences–Geochemistry, Utrecht University, 3584 CD Utrecht, The Netherlands*
[c] *Instituto Andaluz de Ciencias de la Tierra, IACT (CSIC-Universidad de Granada), Avda. Las Palmeras 4, 18100 Armilla, Granada, Spain*

ARTICLE INFO

ABSTRACT

A high-resolution analysis of the distribution of major and trace elements across the Cretaceous/Paleogene boundary (KPgB) in the distal section of Agost (SE Spain) was performed. The KPgB sediments were drilled to recover a 22 cm-long core; the lower 5 cm corresponding to the uppermost Maastrichtian and the upper 17 cm to the lowermost Danian. The unconsolidated sediments were resin-embedded under O_2-free conditions, cut and polished. Laser Ablation-Inductivity Coupled Plasma-Mass Spectrometry (LA-ICP-MS) analyses were conducted at 10 μm increments and a laser-beam of 80 μm. Discrete samples were taken immediately prior to the resin-embedding and analyzed by Inductivity Coupled Plasma-Optical Emission Spectroscopy (ICP-OES). Results obtained by both analytical methods (LA-ICP-MS and ICP-OES) are presented. (Further interpretations and discussion are included in Sosa-Montes de Oca et al., 2018 [6]).

Specifications table

Subject area	*Sedimentary geochemistry*
More specific subject area	*Paleoenvironmental changes across KPgB*
Type of data	*Figures, Excel file, Table*
How data was acquired	– COMPex 102 ArF excimer laser ablation system (Lambda Physik, Göttingen, Germany) connected to an Element 2 sector field ICP-MS (Thermo Scientific, Bremen, Germany) was used for LA-ICP-MS analyses at the GML from Utrecht University (the Netherlands)
	– Spectro Ciros Vision ICP-OES at the Geolab from Utrecht University (The Netherlands)
Data format	*Analyzed*
Experimental factors	*Previously resin embedding processes*
Experimental features	*High resolution profiles across the KPgB sediments*
Data source location	*Agost, Alicante (Spain)*
	Latitude: 38°27′3.31″N; Longitude: 0°-38′-9.71″E
Data accessibility	*Data are included in this article*

Value of the data

- Data show continuous high-resolution element profiles across the KPgB.
- Data reveal significant changes in elemental ratios as Ca/Al, P/Al, Sr/Al, Ti/Al, Cr/Al, Co/Al, Cu/Al, Zr/Al, Pb/Al and U/Al within the $\approx$ 2 mm-thick KPg ejecta layer.
- Data contribute to improve the characterization of major and trace element distribution. This high-resolution approach is found to as reliable tool to evaluate rapid paleoenvironmental changes associated with bio-events.

1. Data

The boundary between the Cretaceous and Paleogene periods has been widely investigated [1–3]. Numerous KPgB sections are known worldwide [4], the Agost site (SE, Spain) being a very well-preserved and well-exposed marine distal section [5]. This section has been profusely studied, due to its exceptionally, expansive and continuous sedimentary record, making the Agost site ideal for high-resolution analyses [6].

The KPgB was drilled using a Rolatec RL 48L drilling machine from the Center for Scientific Instrumentation (CIC), University of Granada, Spain (Fig. 1). A platform was built for the drilling machine and an unaltered core was extracted (Fig. 1). The core was sealed and stored in a cold room.

2. Experimental design, materials and methods

Discrete samples were taken for ICP-OES analysis (Table 1). Next, the core was prepared for resin embedding in order to preserve redox-sensitive elements while maintaining the material structure. All the resin embedding processes were done in an argon-filled glove box for 32 days, in two different stages: First, with acetone exchange during five days (Fig. 2), and secondly with Spurr Epoxy Resin exchange for 27 days (Fig. 3). Afterwards, the core was removed from the glove box and put into the oven for curing and drying 48 h at 60 °C. The embedded core was cut perpendicular to the bedding plane (Fig. 3), polished, and then cut to obtain 2 overlapping arrays (~5 cm each one), which were analyzed by means of a LA-ICP-MS line-scan.

Here we present the geochemical data obtained using both techniques across the KPgB, including the ejecta layer. In the LA-ICP-MS profiles, 4114 data points were obtained in a 9 mm studied interval

Fig. 1. Photographs of the Agost site, during the drilling and unaltered sampling.

specifically, 544 data points in the gray calcareous marlstones and marlstones from the uppermost Maastrichtian, and 3570 data points from the lowermost Danian sediments. Among the latter, 255 data points were taken in the ejecta layer, 1827 data points in the boundary clay layer and 1488 data points in the light marly limestones (Excel file 1 from Supplementary material). In turn, the ICP-OES profiles include only 31 data points in a 21.50 cm studied interval, four of which correspond to the gray calcareous marlstones and marlstones from the uppermost Maastrichtian and 27 to the lowermost Danian sediments. Of these 27, three data points were taken in the ejecta layer, 16 in the boundary clay layer and 8 data points in the light marly limestones (Table 1).

The counts obtained through LA-ICP-MS analysis were interpreted, corrected for background noise, and calibrated. First, the relative ionization factors of the NIST610 standards were calculated. To this end, a NIST610 standard was tested between each sample line-scan analysis and the measurement counts are associated with concentrations by using ratios relative to Al (ppm/counts ratio relative to Al=1) (Excel file 2 from Supplementary material). Then the LA-ICP-MS line-scans obtained for the different isotopes were also: i) corrected for background, subtracting the mean background values obtained from the average intensities of a ~30 s interval before starting the laser ablation measurement; ii) the background-corrected analyte intensities were corrected for the relative sensitivity of the specific isotope calculated by measuring an external standard (using the NIST610 values previously calculated) [7]; iii) the natural abundance of each isotope was corrected [8]; iv) lastly, data were reported as ratios of an internal standard (in this case Al) because the yield of ablated material varies during LA-ICP-MS.

The profiles are presented as (log-) ratios, since they are statistically more informative//precise than normal ratios; in addition, on µm- to mm-scales no internal standard with a known concentration is available during LA-ICP-MS line-scanning of natural samples (Excel file 3 from Supplementary material).

The ICP-OES data are furthermore used as an extra calibration step by means of simple regression, so that both data sets can be compared for the same interval.

Table 1

Table with the elemental content (major and trace) and elemental ratios, measured by ICP-OES across a 21.5 cm interval of the KPgB at the Agost section. Al, Ca, CaO, CaCO3, concentrations (%); Ca/Al and Fe/Al ratios; P/Al, Sr/Al, Ti/Al, Cr/Al, Co/Al, Cu/Al, Zr/Al and Pb/Al ratios (×10⁻⁴), in: i) gray calcareous marlstones and malstones from the uppermost Maastrichtian, ii) ejecta layer, iii) boundary clay layer and iv) light marly limestones from the lowermost Danian.

Samples	Distance K/Pg (cm)	Stage	Lithology	Dilution	Geochemical proxies													
					(%)						(10^{-4})							
					Al	Ca	CaO	CaCO₃	Ca/Al	Fe/Al	P/Al	Sr/Al	Ti/Al	Cr/Al	Co/Al	Cu/Al	Zr/Al	Pb/Al
1	16.75		Light marly limestones	202.10	1.68	35.66	49.94	89.15	21.17	0.51	398.75	346.19	521.87	20.26	1.96	5.76	11.62	0.00
2	16.25			206.90	1.78	35.61	49.88	89.03	20.06	0.51	397.71	332.79	518.82	20.17	1.63	5.11	11.96	0.00
3	15.75			237.10	1.70	35.42	49.60	88.54	20.81	0.50	379.76	338.81	516.70	19.37	1.67	4.89	11.73	0.00
4	15.25			194.40	1.63	36.21	50.72	90.53	22.17	0.50	383.00	348.24	504.99	19.15	1.36	4.37	11.61	0.00
5	14.75			206.40	1.91	35.37	49.54	88.43	18.57	0.50	390.80	307.70	511.28	19.24	1.75	4.65	12.30	0.00
6	14.25			193.00	2.23	33.87	47.44	84.68	15.22	0.47	355.15	270.94	508.91	19.60	1.21	4.13	11.58	0.00
7	13.75			236.00	2.57	31.91	44.69	79.78	12.41	0.45	343.84	237.45	524.10	19.75	1.13	3.62	11.77	0.00
8	13.25			200.60	2.79	31.10	43.56	77.75	11.15	0.44	338.31	221.49	508.37	19.91	1.04	3.55	11.52	0.00
9	12.75			244.60	2.84	30.22	42.33	75.56	10.66	0.44	335.90	218.27	510.53	19.99	1.02	3.71	12.18	0.00
10	12.25			226.40	2.87	29.96	41.96	74.89	10.45	0.43	328.96	214.86	504.26	19.74	1.03	3.65	11.39	0.00
11	11.75			193.20	2.70	30.66	42.94	76.65	11.34	0.43	319.30	227.52	503.14	19.56	0.99	3.63	11.38	0.00
12	11.25			202.10	2.58	31.93	44.73	79.84	12.37	0.44	324.56	240.72	501.64	19.28	1.11	3.63	11.41	0.00
13	10.75			243.00	2.68	30.87	43.23	77.16	11.52	0.44	319.09	238.43	504.08	19.32	1.27	4.18	11.97	0.00
14	10.25			232.80	2.78	29.90	41.87	74.74	10.74	0.44	313.01	230.64	505.10	19.47	1.20	3.82	11.59	0.00
15	9.75			239.30	3.13	28.75	40.27	71.88	9.18	0.43	310.19	207.23	511.91	19.78	1.20	3.55	11.45	0.00
16	9.25			202.30	2.91	30.42	42.60	76.04	10.47	0.43	305.80	229.76	514.81	19.94	1.26	3.89	11.34	0.00
17	8.75			223.10	2.87	29.50	41.31	73.75	10.28	0.44	309.70	228.52	514.59	19.60	1.59	3.98	11.09	0.00
18	8.25			223.20	2.50	30.86	43.22	77.14	12.33	0.48	292.41	265.57	518.21	19.17	1.95	4.29	11.95	0.00
19	7.75			238.10	2.23	31.86	44.62	79.65	14.32	0.47	263.61	299.56	527.33	18.11	2.18	4.49	12.63	0.00
20	7.25			233.70	2.17	31.41	43.99	78.52	14.49	0.44	243.38	307.65	530.01	17.98	1.62	4.32	13.70	0.00
21	6.75			229.30	2.18	31.09	43.55	77.74	14.24	0.45	217.36	313.54	529.64	17.80	2.01	4.51	14.21	0.00
22	6.25	Danian		236.10	2.49	30.02	42.05	75.06	12.06	0.44	238.68	311.23	521.08	18.24	9.84	4.99	12.84	0.00
23	5.75			257.90	2.90	30.07	42.11	75.17	10.37	0.45	276.10	296.11	498.49	18.78	6.02	5.24	10.63	0.00
24	5.25			233.00	2.62	31.35	43.91	78.38	11.98	0.50	227.18	368.52	486.07	19.23	6.64	5.93	10.33	0.00
25	4.875		Boundary clay layer	227.50	6.58	16.92	23.70	42.31	2.57	0.42	140.80	124.41	481.49	19.99	3.57	5.75	10.57	4.69
26	4.625			218.30	6.51	17.16	24.04	42.90	2.64	0.41	125.55	117.04	477.42	19.42	2.22	5.50	10.67	4.65
27	4.375			208.60	7.53	13.12	18.37	32.79	1.74	0.41	112.49	95.77	472.94	19.71	2.06	5.29	11.06	5.42
28	4.125			201.00	7.75	12.07	16.91	30.18	1.56	0.42	100.11	91.93	469.09	19.97	1.98	5.46	11.08	5.77
29	3.875			207.70	7.75	11.98	16.78	29.95	1.55	0.40	92.62	92.97	450.06	20.89	1.98	6.21	11.41	5.40
30	3.625			230.50	8.15	10.37	14.53	25.94	1.27	0.40	90.83	87.18	460.77	22.66	1.92	7.46	11.85	5.55
31	3.375			241.80	7.84	10.76	15.07	26.89	1.37	0.40	90.90	88.38	472.00	21.98	2.14	6.15	11.65	5.10
32	3.125			211.80	7.66	11.50	16.11	28.76	1.50	0.41	90.49	93.11	468.99	22.04	2.38	5.95	11.93	5.77

Table 1 (*continued*)

| Samples	Distance K/Pg (cm)	Stage	Lithology	Dilution	Geochemical proxies (%)						(10^{-4})							
					Al	Ca	CaO	CaCO$_3$	Ca/Al	Fe/Al	P/Al	Sr/Al	Ti/Al	Cr/Al	Co/Al	Cu/Al	Zr/Al	Pb/Al
33	2.875			197.60	8.05	10.02	14.03	25.05	1.24	0.43	80.61	89.52	461.46	23.76	1.76	6.60	11.59	6.32
34	2.625			222.10	8.69	8.40	11.77	21.01	0.97	0.43	69.60	84.55	473.17	25.35	1.57	6.05	11.58	6.09
35	2.375			250.80	8.02	10.52	14.73	26.29	1.31	0.45	81.34	93.84	490.22	26.60	1.84	7.02	11.94	5.41
36	2.125			212.00	7.66	9.90	13.87	24.76	1.29	0.49	87.75	94.61	488.33	26.30	2.01	9.06	12.17	6.38
37	1.875			234.80	7.94	9.42	13.20	23.56	1.19	0.49	87.02	93.77	500.66	27.66	2.21	9.82	12.18	6.35
38	1.625			223.20	7.95	9.08	12.72	22.70	1.14	0.56	86.63	94.58	494.52	28.22	2.56	12.27	12.72	7.27
39	1.375			238.20	7.85	8.17	11.45	20.43	1.04	0.62	79.13	94.60	474.29	28.67	2.72	11.99	13.11	6.89
40	1.125			218.60	8.06	7.16	10.03	17.90	0.89	0.69	79.40	91.32	476.25	29.63	2.94	13.27	14.22	7.96
41	0.875			223.30	7.83	8.24	11.53	20.59	1.05	0.66	89.23	94.34	554.95	33.19	2.70	14.13	14.70	8.32
42	0.625			234.60	7.32	9.22	12.92	23.06	1.26	0.76	85.71	105.52	857.39	48.29	3.10	17.82	17.15	10.46
43	0.35	KPgB	Ejecta layer	254.30	5.47	17.43	24.41	43.58	3.19	0.75	79.67	150.69	995.28	49.95	3.52	17.10	16.78	8.78
44	0.15			236.40	4.57	23.50	32.92	58.76	5.14	0.52	93.61	190.95	673.70	30.30	2.70	8.91	12.61	4.33
45	0			242.20	4.46	23.87	33.43	59.66	5.35	0.59	96.98	198.41	960.64	41.60	3.85	18.71	14.56	7.01
46	−0.25	Maastrichtian	Calcareous marlstones and marlstones	203.50	3.98	25.86	36.22	64.65	6.50	0.41	116.58	224.05	505.28	20.89	1.85	7.99	10.71	2.91
47	−0.75			224.00	3.73	26.82	37.56	67.04	7.19	0.37	127.08	239.79	455.49	17.90	1.46	6.24	10.55	0.22
48	−1.25			206.80	4.08	25.47	35.67	63.66	6.24	0.40	111.37	217.01	559.27	23.63	1.46	6.90	10.99	3.25
49	−1.75			224.60	3.12	29.34	41.10	73.36	9.42	0.36	136.43	290.95	432.65	15.96	1.56	4.96	10.41	0.00
50	−2.25			217.80	3.08	29.14	40.81	72.85	9.47	0.36	136.55	293.20	427.42	15.99	1.47	5.19	10.41	0.00
51	−2.75			210.50	2.88	30.93	43.32	77.33	10.76	0.37	144.07	318.96	458.63	17.01	1.25	5.07	10.36	0.00
52	−3.25			193.50	2.76	31.56	44.20	78.89	11.44	0.38	148.41	338.23	464.05	17.32	1.41	4.97	10.67	0.00
53	−3.75			196.10	2.77	31.76	44.48	79.39	11.46	0.38	144.27	340.32	459.90	16.84	1.24	5.67	10.20	0.00
54	−4.25			211.50	2.61	31.73	44.44	79.33	12.14	0.38	153.29	359.35	466.51	16.88	1.38	5.09	10.65	0.00
55	−4.75			204.40	2.89	29.70	41.60	74.26	10.27	0.40	160.49	319.98	509.64	19.94	1.28	5.16	10.86	0.00
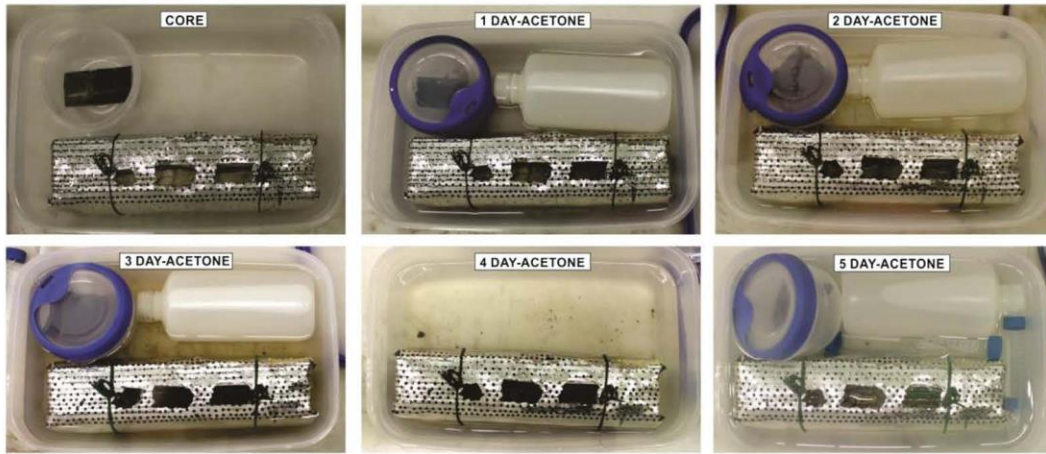
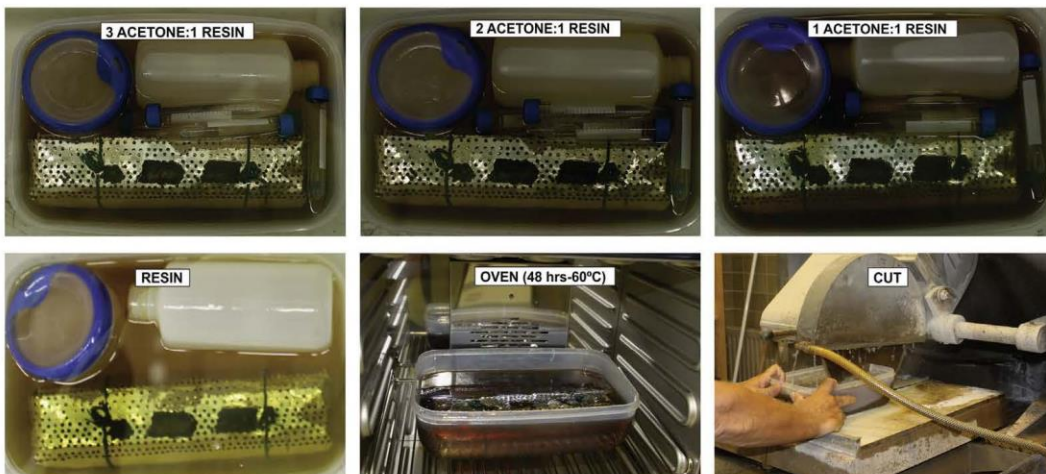**Fig. 2.** Photographs during acetone stage of resin embedding process, inside the glove box.

Fig. 3. Photographs during resin stage of resin embedding process, in the oven (at 60° for 48 h) for curing and drying and while cutting the arrays for LA-ICP-MS analysis.

Acknowledgements

Transparency document. Supporting information

Supplementary data associated with this article can be found in the online version at https://doi.org/10.1016/j.dib.2018.04.118.

C

Appendix A. Supporting information

Supplementary data associated with this article can be found in the online version at https://doi.org/10.1016/j.dib.2018.04.118.

References

[1] L.W. Alvarez, W. Alvarez, F. Asaro, H.V. Michel, Extraterrestrial cause for the Cretaceous-Tertiary extinction, Science 208 (1980) 1095–1108.

[2] J. Smit, J. Hertogen, An extraterrestrial event at the Cretaceous-Tertiary boundary, Nat. Geosci. 285 (1980) 198–200.

[3] P. Schulte, L. Alegret, I. Arenillas, J.A. Arz, P.J. Barton, P.R. Bown, T.J. Bralower, G.L. Christeson, P. Claeys, C.S. Cockell, G. S. Collins, A. Deutsch, T.J. Goldin, K. Goto, J.M. Grajales-Nishimura, R.A.F. Grieve, S.P.S. Gulick, K.R. Johnson, W. Kiessling, C. Koeberl, D.A. Kring, K.G. MacLeod, T. Matsui, J. Melosh, A. Montanari, J.V. Morgan, C.R. Neal, D.J. Nichols, R.D. Norris, E. Pierazzo, G. Ravizza, M. Rebolledo-Vieyra, W.U. Reimold, E. Robin, T. Salge, R.P. Speijer, A.R. Sweet, J. Urrutia-Fucugauchi, V. Vajda, M.T. Whalen, P.S. Willumsen, The Chicxulub asteroid impact and mass extinction at the Cretaceous-Paleogene boundary, Science 327 (2010) 1214–1218. http://dx.doi.org/10.1126/science.1177265.

[4] S. Goderis, R. Tagle, J. Belza, J. Smit, A. Montanari, F. Vanhaecke, J. Erzinger, P. Claeys, Reevaluation of siderophile element abundances and ratios across the Cretaceous-Paleogene (K-Pg) boundary: implications for the nature of the projectile, Geochim. Cosmochim. Acta 120 (2013) 417–446. http://dx.doi.org/10.1016/j.gca.2013.06.010.

[5] N. Macleod, G. Keller, Hiatus distributions and mass extinctions at the Cretaceous/Tertiary boundary, Geology 19 (1991) 497–501. http://dx.doi.org/10.1130/0091-7613(1991)019 < 0497:HDAMEA > 2.3.CO.

[6] C. Sosa-Montes de Oca, G.J. de Lange, F. Martínez-Ruiz, F.J. Rodríguez-Tovar, Application of laser ablation-ICP-MS to determine high-resolution elemental profiles across the Cretaceous/Paleogene boundary at Agost (Spain), Palaeogeogr. Palaeoclimatol. Palaeoecol. (2018), http://dx.doi.org/10.1016/j.palaeo.2018.02.012.

[7] K.P. Jochum, U. Weis, B. Stoll, D. Kuzmin, Q. Yang, I. Raczek, D.E. Jacob, A. Stracke, K. Birbaum, D.A. Frick, D. Günther, J. Enzweiler, Determination of reference values for NIST SRM 610-617 glasses following ISO guidelines, Geostand. Geoanalytical Res. 35 (2011) 397–429. http://dx.doi.org/10.1111/j.1751-908X.2011.00120.x.

[8] M. Berglund, M.E. Wieser, Isotopic compositions of the elements 2009 (IUPAC Technical Report), Pure Appl. Chem. 83 (2011) 397–410. http://dx.doi.org/10.1351/PAC-REP-10-06-02.

CURRICULUM VITAE

Claudia Sosa Montes de Oca was born in Montevideo (Uruguay). She obtained her bachelor´s degree in Geology in 1999. Her last year at university was made in Naples University (Italy). From 2003 to 2010 she worked in several private geotechnical consulting companies (G2G, Conanma and Vorsevi), preparing geotechnical reports for both building and civil engineering. In the 2010-2011 academic year, she enrolled in the official Master of Geology at the University of Granada, and in the second year of this master she started a research project titled: "Distribution of trace elements in sediments of the Cretaceous-Palaeogene boundary: geochemical anomalies and conditions of oxygenation" under the supervision of Dr. Francisca Martínez Ruiz, obtaining her Master´s degree in December of 2011. Since January of 2014 Claudia is a PhD candidate in the department of Stratigraphy and Palaeontology at the University of Granada, under the supervision of Dr. Francisco Javier Rodríguez Tovar and Dr. Francisca Martínez Ruiz, leading to this dissertation.

1.- Peer-reviewed articles – JCR (SCI) – indexed journal papers

Published:

- **Sosa-Montes de Oca, C.**, de Lange, G.J., Martínez-Ruiz, F., Rodríguez-Tovar, F.J., (2018). High-resolution data from Laser Ablation-ICP-MS and by ICP-OES analyses at the Cretaceous/Paleogene boundary section at Agost (SE Spain). Data in Brief 18, 1900–1906. *doi: 10.1016/j.dib.2018.04.118.*

- **Sosa-Montes de Oca, C.**, de Lange, G.J., Martínez-Ruiz, F., Rodríguez-Tovar, F.J., (2018). Application of Laser Ablation-ICP-MS to determine high-resolution elemental profiles across the Cretaceous/Paleogene boundary at Agost (Spain). Palaeogeography, Palaeoclimatology, Palaeoecology 497, 128–138. *doi:10.1016/j.palaeo.2018.02.012*

- **Sosa-Montes de Oca, C.**, Rodríguez-Tovar, F.J., Martínez-Ruiz, F., Monaco, P. (2017). Paleoenvironmental conditions across the Cretaceous-Paleogene transition at the Apennines sections (Italy): An Integrated geochemical and ichnological approach. Cretaceous Research 71, 1–13. *doi: 10.1016/j.cretres.2016.11.005*

- **Sosa-Montes de Oca, C.**, Rodríguez-Tovar, F.J., Martínez-Ruiz, F., (2016). Geochemical and isotopic characterization of trace fossil infillings: New insights on tracemaker activity after the K-Pg impact event. Cretaceous Research 57, 391–401. *doi:10.1016/j.cretres.2015.03.003.*

- **Sosa-Montes de Oca, C.**, Martínez-Ruiz, F., Rodríguez-Tovar, F.J., (2013). Bottom-water conditions in marine basins after the Cretaceous-Paleogene impact event: Timing the recovery of oxygen levels and productivity. Plos One 8 (12), e82242. *doi:10.1371/journal.pone.0082242.*

To be submitted:

- **Sosa-Montes de Oca, C.**, de Lange, G.J., Martínez-Ruiz, F., Rodríguez-Tovar, F.J. Microscale trace element distribution across the Cretaceous/Palaeogene ejecta layer at Agost section: Constraining the recovery of preimpact conditions.

2.- Other peer-reviewed articles - in non JCR(SCI) indexed journals.

- **Sosa-Montes de Oca, C.**, Rodríguez-Tovar, F.J., Martínez-Ruiz, F., 2014. Distribución de metales traza en sedimentos del límite Cretácico/Paleógeno: Implicaciones paleoambientales. MACLA 19.

- **Sosa-Montes de Oca, C.**, Rodríguez-Tovar, F.J., Martínez-Ruiz, F., 2015. Análisis geoquímico e isotópico del material de relleno de trazas fósiles en el tránsito Cretácico-Paleógeno (K-Pg): recuperación de la biota tras el evento del impacto. XIII EJIP Conference Proceedings, 250–252.